

INAUGURAL - DISSERTATION  
zur  
Erlangung der Doktorwürde  
der  
Naturwissenschaftlich-Mathematischen  
Gesamtfakultät  
der  
Ruprecht-Karls-Universität  
Heidelberg

Vorgelegt von  
Diplom-Geoökologin Uta Beyersdorf-Kuis  
aus Hildburghausen

Tag der mündlichen Prüfung: 2014







## Table of contents

<b>List of figures</b> .....	<b>iii</b>
<b>List of tables</b> .....	<b>vi</b>
<b>Abbreviations and symbols</b> .....	<b>viii</b>
<b>Abstract</b> .....	<b>ix</b>
<b>Kurzfassung</b> .....	<b>xi</b>
<b>1 Introduction</b> .....	<b>1</b>
<b>2 Fundamentals</b> .....	<b>4</b>
<b>2.1 Meteorite components</b> .....	<b>4</b>
2.1.1 Chondrites and their components.....	4
2.1.2 Formation and alteration of chondritic components .....	7
2.1.3 Matrix .....	10
<b>2.2 Chondrules</b> .....	<b>11</b>
2.2.1 Definition of chondrules .....	11
2.2.2 Classification of chondrules.....	13
2.2.3 Chondrule formation .....	19
2.2.3.1 Chondrule precursors .....	19
2.2.3.2 Open or closed system behavior during chondrule formation? .....	21
2.2.3.3 Chondrule heating event(s) .....	21
2.2.3.4 Cooling of the chondrule droplet.....	23
2.2.3.5 Different chondrule types and their formation .....	25
2.2.3.6 Setting of chondrule formation.....	26
2.2.3.7 Timing of chondrule formation .....	26
2.2.3.8 Processes after chondrule formation.....	29
2.2.3.9 Primary properties of chondrules.....	29
<b>2.3 Cosmogenic noble gases in meteorites</b> .....	<b>29</b>
2.3.1 Cosmic radiation .....	29
2.3.1.1 Solar cosmic rays (SCR) .....	30
2.3.1.2 Galactic cosmic rays (GCR) .....	31
2.3.2 Cosmogenic nuclides.....	32
2.3.3 Noble gases in chondrules .....	36
<b>2.4 Pre-irradiation</b> .....	<b>37</b>
2.4.1 Definition of pre-irradiation .....	37
2.4.2 Settings of pre-irradiation .....	37
2.4.3 Pre-irradiation of chondrules .....	38
2.4.3.1 Previous analyses of pre-irradiation effects in chondrules .....	38
2.4.3.2 Difficulties concerning the analysis and interpretation of pre-irradiation effects in chondrules .....	41
2.4.4 Pre-irradiation of other meteorite components .....	42
<b>3 Motivation</b> .....	<b>44</b>
<b>4 Materials and methods</b> .....	<b>45</b>
<b>4.1 Sample selection</b> .....	<b>45</b>
4.1.1 Selection criteria .....	45
4.1.2 Sample description .....	46

4.1.2.1	CV chondrites .....	47
4.1.2.2	CR chondrites .....	49
4.1.2.3	Ungrouped Acfer 094.....	54
<b>4.2</b>	<b>Separation of chondrules.....</b>	<b>55</b>
<b>4.3</b>	<b>Determination of target elements .....</b>	<b>57</b>
4.3.1	INAA analysis .....	58
4.3.2	SEM analysis .....	58
<b>4.4</b>	<b>Mineralogical analysis.....</b>	<b>59</b>
<b>4.5</b>	<b>Noble gas measurements.....</b>	<b>59</b>
<b>4.6</b>	<b>Production rate of cosmogenic noble gases.....</b>	<b>61</b>
<b>4.7</b>	<b>Calculation of cosmic ray exposure ages.....</b>	<b>62</b>
<b>4.8</b>	<b>Calculation of <math>^{40}\text{K}</math>-<math>^{40}\text{Ar}</math> ages .....</b>	<b>62</b>
<b>5</b>	<b>Results and discussion .....</b>	<b>64</b>
<b>5.1</b>	<b>Target elements .....</b>	<b>64</b>
5.1.1	INAA analysis .....	64
5.1.2	SEM analysis .....	76
<b>5.2</b>	<b>Mineralogy.....</b>	<b>77</b>
<b>5.3</b>	<b>Noble gases in chondrules and matrix.....</b>	<b>82</b>
5.3.1	Concentrations.....	82
5.3.2	Neon isotopes.....	87
5.3.3	Production rates.....	92
<b>5.4</b>	<b>Cosmic ray exposure ages of chondrules and matrix .....</b>	<b>97</b>
5.4.1	Shielding-corrected ages .....	97
5.4.1.1	This study .....	97
5.4.1.2	Comparison with literature data.....	100
5.4.1.3	Reliability of shielding-corrected CRE ages .....	101
5.4.2	Shielding-uncorrected (“nominal”) ages.....	102
5.4.3	Noble gas loss .....	105
<b>5.5</b>	<b><math>^{40}\text{K}</math>-<math>^{40}\text{Ar}</math> ages of chondrules and matrix .....</b>	<b>106</b>
<b>5.6</b>	<b>Pre-irradiation of chondrules.....</b>	<b>108</b>
5.6.1	Samples with potentially pre-irradiated chondrules.....	108
5.6.2	Difficulties concerning the interpretation of pre-irradiation effects, arguments for a pre-irradiation of chondrules and this study’s limitation.....	112
5.6.2.1	Difficulties concerning the interpretation of pre-irradiation effects in chondrules.....	112
5.6.2.2	General arguments for a pre-irradiation of chondrules.....	118
5.6.2.3	Limitation of this study .....	120
5.6.3	Settings of pre-irradiation of chondrules.....	120
<b>6</b>	<b>Summary and future work.....</b>	<b>124</b>
<b>7</b>	<b>References.....</b>	<b>127</b>
	<b>Appendix .....</b>	<b>144</b>
	<b>Danksagung.....</b>	<b>151</b>

## List of figures

Figure 2-1: Classification of meteorites showing the major meteorite divisions, classes, clans and groups and relationships among meteorite groups (adapted after Weisberg et al. 2006) .....	5
Figure 2-2: Petrologic types of each chondrite group (adapted after Weisberg et al. 2006) .....	7
Figure 2-3: Average chondrule diameter (a) and chondrule abundance (b) for major chondrite groups. <i>Data are from Scott (2007)</i> .....	12
Figure 2-4: Different classification schemes of chondrules (adapted after Sears 2004).....	14
Figure 2-5: Photomicrographs of textures from selected Dhajala (H3) chondrules according to Gooding and Keil (1981) .....	16
Figure 2-6: Non-porphyrific macrochondrules in chondrites (adapted after Weyrauch and Bischoff 2012).....	16
Figure 2-9: Formation of a chondrule (adapted after Jones et al. 2005).....	20
Figure 2-10: Chondrule thermal histories inferred from experimental constraints and predicted by different models (Desch et al. 2012).....	22
Figure 2-11: Sketch showing the processes involved in chondrule formation (adapted after Scott 2007) .....	24
Figure 2-12: Formation ages of chondrules from ordinary and carbonaceous chondrites relative to CAIs (adapted after Scott 2007) .....	27
Figure 2-13: Time scales of solid formation and disk evolution based on Pb-Pb dating of CAIs and chondrules from carbonaceous chondrites (adapted after Connelly et al. 2012).....	28
Figure 2-14: Spectra of solar and galactic cosmic ray protons at 1 AU (Michel et al. 1996) .....	31
Figure 2-15: Sketch showing a typical spallation of $^{24}\text{Mg}$ .....	32
Figure 2-16: Sketch showing the pre-irradiation of single meteorite components as free-floating objects in the solar nebula (a) and in the parent body regolith (b). .....	38
Figure 2-17: Sketch showing the pre-irradiation of primary rock fragments (PRF) in the solar nebula by the early active sun before parent body accretion (a) or in the parent body regolith (b) (adapted after Huber et al. 2012).....	41
Figure 4-1: Freeze-thaw technique similar to Grossman (2010a) for chondrule separation.....	56
Figure 4-2: Special teflon vials used for chondrule separation. ....	56
Figure 5-1: Selected target element abundances from ALH 81032 aliquots determined with INAA ....	65
Figure 5-2: Relative abundances of Ni versus Fe of all chondrule (ch) and matrix (mat) samples (a) and an inset of the left corner (b).....	69
Figure 5-3: Relative abundances of Fe, Si and Mg of chondrules (ch) and matrix (mat) from (a) CR2 chondrites, (b) CR3 chondrites and Acfer 094 and (c) CV3 chondrites (adapted after Jones et al. 2005).....	70
Figure 5-4: Relative abundances of Fe vs. Mg for all chondrules (ch) and matrix (mat) samples relative to CI (adapted after Jones et al. 2005).....	71
Figure 5-5: Elemental abundances for chondrules (ch) and matrix (mat) of all samples relative to CI and Mg (adapted after Abreu and Brearley 2010, Jones et al. 2005, Wasson et al. 2000) .....	72
Figure 5-6: Selected abundances of target elements in two halves of one El Djouf 001 chondrule (El-ch11) determined with INAA.....	74
Figure 5-7: Classification of all analyzed chondrules (a), CV chondrite chondrules (b), and chondrules from CR chondrites and Acfer 094 (c) according to Wood (1962) and McSween et al. (1977, 1983) and Scott and Taylor (1983), Jones and Scott (1989) and Jones (1990, 1994, 1996) .....	75

Figure 5-8: Selected abundances of target elements in one half of the EI Djouf 001 chondrule EI-ch11b determined by INAA and by SEM.....	77
Figure 5-9: Back scattered electron images of EI Djouf chondrule EI-ch11b (a) and intersects 3 (b) and 5 (c).....	78
Figure 5-10: Back scattered electron image of one MET 00426 chondrule (a) and intersects 2 (b) and 5 (c).....	80
Figure 5-11: Back scattered electron image of one QUE 99177 chondrule (a) and intersects 1 (b) and 2 (c).....	80
Figure 5-12: Back scattered electron image of one Acfer 082 chondrule (a) and intersects 2 (b) and 5 (c).....	81
Figure 5-13: Back scattered electron image of one Allende chondrule (a) and intersects 7 (b) and 12 (c).....	81
Figure 5-14: Three isotope plot of neon for CR2 chondrites NWA 852 (NWA), EI Djouf 001 (EI) and Renazzo (Re).....	87
Figure 5-15: Three isotope plot of neon for ungrouped Acfer 094 (A94) and CR3 chondrites QUE 99177 (QUE) and MET 00426 (MET).....	89
Figure 5-16: Three isotope plot of neon for CV3 chondrites Acfer 082 (A82), Vigarano (Vi) and Allende (Al).....	91
Figure 5-17: Three isotope plot of neon for CR2 chondrites NWA 852 (NWA), EI Djouf 001 (EI) and Renazzo (Re) released at 600°C and 1800°C.....	91
Figure 5-18: Uncorrected production rates for Ne (a), He (b) and Ar (c) of all chondrule (ch) and matrix (mat) samples.....	94
Figure 5-19: $P_{21-1.11}$ production rates of chondrules relative to those of the corresponding matrix samples.....	96
Figure 5-20: $T_{21-corr}$ CRE ages of chondrules (ch) and matrix (mat) from CR2 chondrites NWA 852 (NWA) (a), Renazzo (Re) (b) and EI Djouf 001 (EI) (c) calculated with $Si_{50}$ .....	98
Figure 5-21: $T_{21-corr}$ CRE ages of chondrules (ch) and matrix (mat) from CR3 chondrite QUE 99177 (QUE) calculated with $Si_{50}$ .....	99
Figure 5-22: $T_{21-corr}$ CRE ages of chondrules (ch) and matrix (mat) from CV3 chondrites Acfer 082 (A82) (a), Allende (Al) (b) and Vigarano (Vi) (c) calculated with $Si_{50}$ .....	99
Figure 5-23: $T_{21-corr}$ CRE ages of CR2 chondrites (a) and CV3 chondrites (b) analyzed in this study and previous studies.....	100
Figure 5-24: Shielding-corrected $T_3$ and $T_{21}$ CRE ages of all chondrule and matrix samples.....	101
Figure 5-25: $T_{21-1.11}$ CRE ages of chondrules (ch) and matrix (mat) from CR2 chondrites NWA 852 (NWA) (a), Renazzo (Re) (b) and EI Djouf 001 (EI) (c) calculated with $Si_{50}$ .....	103
Figure 5-26: $T_{21-1.11}$ CRE ages of chondrules (ch) and matrix (mat) from CR3 chondrite MET 00426 (MET) (a), QUE 99177 (QUE) (b) and ungrouped Acfer 094 (A94) (c) calculated with $Si_{50}$ .....	104
Figure 5-27: $T_{21-1.11}$ CRE ages of chondrules (ch) and matrix (mat) from CV3 chondrites Acfer 082 (A82) (a), Allende (Al) (b) and Vigarano (Vi) (c) calculated with $Si_{50}$ .....	104
Figure 5-28: Plot showing $(^3He/^{21}Ne)_c$ versus $(^{22}Ne/^{21}Ne)_c$ for all chondrule (ch) and matrix (mat) samples.....	106
Figure 5-29: $T_{21-1.11}$ CRE ages of chondrules from CR2 chondrites (a), CR3 chondrites (b), and CV3 chondrites (c).....	108
Figure 5-30: CRE ages of chondrules relative the respective matrix (a, b) and percentage (c) of pre-irradiated chondrules from this study based on $T_{21-1.11}$ CRE ages calculated with $Si_{50}$ abundances.....	110



Figure 5-31: $T_{21-1.11}$ CRE ages of all analyzed chondrules arranged according to their chondrule type .....	111
Figure 5-32: Sketch showing the apparent size sorting (Brazil-nut effect) on the meteorite parent body regolith (after Hörz and Schaal 1981) .....	117
Figure 5-33: $Mg/(Al+Si)$ vs. $(^{21}Ne/^{22}Ne)_c$ for selected chondrules and matrix samples from CR2 chondrites NWA 852 (NWA) and El Djouf 001 (El), CR3 chondrite QUE 99177 (QUE) and CV3 chondrites Acfer 082 (A82), Vigarano (Vi) and Allende (Al) relying on mineral separates from the Bruderheim meteorite (adapted after Das and Murty 2009).....	122
Figure 5-34: $Mg/(Al+Si)$ vs. $(^{21}Ne/^{22}Ne)_c$ for chondrules (ch) from QUE 99177 for meteoroids with 10 and 30 cm radius .....	123

## List of tables

Table 2-1: Progressive stages of shock metamorphism of ordinary (Stöffler et al. 1991) and enstatite chondrites (Rubin et al. 1997). .....	9
Table 2-2: Different weathering categories for meteorites. ....	9
Table 2-3: Matrix abundances in different chondrite groups (Scott 2007). ....	10
Table 2-4: Chondrule classification extended from McSween (1977a) and Jones (1994) applying composition names to all textural types (Hewins 1997). ....	17
Table 2-5: Different chondrule-forming models (Hewins 1997).....	22
Table 2-6: Nuclear particle effects in extraterrestrial materials (adapted after Caffee et al. 1988).....	30
Table 2-7: Cosmogenic radionuclides with half-lives above 1 month and stable cosmogenic nuclides frequently analyzed in meteorites (adapted after Michel et al. 1996).....	33
Table 2-8: Previous analyzed meteorites showing evidence for pre-irradiation effects in chondrules using noble gases analysis.....	39
Table 2-9: Previous analyzed meteorite separates showing evidence for pre-irradiation effects using noble gases analysis. ....	43
Table 4-1: Samples selected for analysis of pre-irradiation effects of chondrules in primitive meteorites. ....	46
Table 4-2: Features of the three CV subgroups (adapted after Weisberg et al. 1997). ....	47
Table 4-3: Detailed information about the selected meteorite samples (MetBase 7.1). ....	48
Table 4-4: Characteristics of CR3 chondrites MET 00426 and QUE 99177 according to Mittlefehldt (2001) .....	53
Table 4-5: Methods used for the determination of target elements in studies analyzing pre-irradiation effects of chondrules .....	57
Table 4-6: Equations used for calculating production rates of cosmogenic noble gases in studies analyzing pre-irradiation-effects in chondrules.....	61
Table 5-1: Elemental abundances of fine- and coarse-grained aliquots from L chondrite ALH 81032 determined using INAA.....	64
Table 5-2: Noble gas data for unirradiated and irradiated diorite samples. ....	66
Table 5-3: Reactions describing the production of nucleogenic Ne, He and Ar (Wetherill 1954) .....	66
Table 5-4: Influence of Mg abundance (factor a) and dosis (factor b) on the $^{21}\text{Ne}_n$ concentration in the irradiated diorite.....	67
Table 5-5: Ni/Fe ratios of all matrix (mat) and chondrules (ch) samples.....	69
Table 5-6: Tentative chondrule types according the schemes by Scott and Taylor (1983), Jones and Scott (1989) and Jones (1990, 1992a, b; 1994, 1996).....	75
Table 5-7: Elemental abundances for selected chondrules determined with SEM.....	76
Table 5-8: Concentrations of $^{21}\text{Ne}_c$ , shielding parameters ( $^{22}\text{Ne}/^{21}\text{Ne}$ ) <sub>c</sub> , production rates ( $P_{21\text{-corr}}$ , $P_{21-1.11}$ ), and CRE ages ( $T_{21\text{-corr}}$ , $T_{21-1.11}$ ) of all matrix (mat) and chondrule (ch) samples.....	83
Table 5-9: Concentrations of $^3\text{He}$ , production rates ( $P_{3\text{-corr}}$ , $P_{3-1.11}$ ), and CRE ages ( $T_{3\text{-corr}}$ , $T_{3-1.11}$ ) of all matrix (mat) and chondrule (ch) samples .....	85
Table 5-10: Concentrations of $^{38}\text{Ar}_c$ , production rates ( $P_{38\text{-corr}}$ , $P_{38-1.11}$ ), and CRE ages ( $T_{38\text{-corr}}$ , $T_{38-1.11}$ ) of all matrix (mat) and chondrule (ch) samples .....	86
Table 5-11: Uncertainty of $P_{21-1.11}$ due to minimal and maximal Si abundances relative to $P_{21-1.11}$ calculated with $\text{Si}_{50}$ .....	92
Table 5-12: Differences of production rates and CRE ages calculated with the formula by Eugster (1988) and Eugster and Michel (1995).....	95

---

Table 5-13: Production rates obtained using the formula by Eugster (1988) and the model by Leya and Masarik (2009).....	96
Table 5-14: Shielding-corrected $T_{21\text{-corr}}$ CRE ages of all matrix (mat) and chondrules (ch) samples calculated with $Si_{50}$ . ....	97
Table 5-15: Shielding-uncorrected $T_{21\text{-}1.11}$ CRE ages of all matrix (mat) and chondrule (ch) samples calculated with $Si_{50}$ abundances.....	102
Table 5-16: $^{40}\text{K}$ - $^{40}\text{Ar}$ ages of all matrix (mat) and chondrule (ch) samples. ....	107
Table 5-17: Pre-exposure and type of chondrules analyzed in this study and tracing pre-irradiation effects. ....	112
Table 5-18: Difficulties concerning the analysis of pre-irradiation effects in chondrules.....	119

## Abbreviations and symbols

ALH	Allan Hills, Far Western Icefield (Antarctic meteorite collection area)
amu	Unit of the mass number
AU	Astronomical unit (mean distance from Earth to Sun, $\sim 150 \cdot 10^6$ km)
CAI	Calcium-aluminium-rich inclusion
CC	Carbonaceous chondrite
CRE	Cosmic ray exposure
EET	Elephant Moraine (Antarctic meteorite collection area)
EMPA	Electron microprobe analysis
GCR	Galactic cosmic rays
GEMS	Glass with embedded metal and sulfides
GRA	Graves Nunataks (Antarctic meteorite collection area)
GRO	Grosvenor Mountains (Antarctic meteorite collection area)
GRV	Grove Mountains (Antarctic meteorite collection area)
HaH	Hammadah al Hamra (meteorite collection area in the Libyan Sahara desert)
IDP	Interplanetary dust particle
INAA	Instrumental neutron activation analysis
LEW	Lewis Cliff (Antarctic meteorite collection area)
MAC	MacAlpine Hills (Antarctic meteorite collection area)
MET	Meteorite Hills (Antarctic meteorite collection area)
NWA	Northwest Africa (meteorite collection area in the Sahara desert)
OC	Ordinary chondrite
PCA	Pecora Escarpment (Antarctic meteorite collection area)
QUE	Queen Alexandra Range (Antarctic meteorite collection area)
SAH	Sahara (meteorite collection area in the Sahara desert)
SCR	Solar cosmic rays
SEM	Scanning electron microscope
TIL	Thiel Mountains, Moulton Escarpment (Antarctic meteorite collection area)
UOC	Unequilibrated ordinary chondrite
Y	Yamato Mountains (Antarctic meteorite collection area)

## Abstract

Noble gases in meteorites contain a “cosmogenic” component which is due to their exposure to cosmic rays. Cosmogenic noble gases (like radionuclides) are generally produced during the time a meteoroid travels from its parent body to encounter with earth and define its cosmic ray exposure (CRE) age. However, cosmogenic noble gases may also be produced at an earlier stage (“pre-irradiation”). Noble gases in chondrules, in particular, may provide information about the energetic particle environment and the lifetime of chondrules as free-floating objects in the early solar system in case they were pre-irradiated in the solar nebula and about surface processes on asteroids in the case of a pre-irradiation in the parent body regolith. Therefore, in this study noble gases were determined to search for possible pre-irradiation effects in chondrules and matrix samples from nine carbonaceous chondrites, including the CR2 chondrites Renazzo, El Djouf 001 and NWA 852, the CR3 chondrites MET 00426 and QUE 99177, the CV3 chondrites Allende, Vigarano and Acfer 082 as well as ungrouped Acfer 094.

After the separation of chondrules from the bulk meteorites using a freeze-thaw technique, abundances of important target elements were determined using instrumental neutron activation analysis (INAA). Noble gas measurements (He, Ne, Ar) were performed on the same sample material, which eliminates problems of sample inhomogeneity which were a problem in other earlier studies. CRE ages were calculated with  $^{21}\text{Ne}_c$  production rates calculated following Eugster (1988). In addition, mineralogical analyses of chondrules using a scanning electron microscope (SEM) were performed, and  $^{40}\text{K}$ - $^{40}\text{Ar}$  ages of chondrules and matrix samples were determined. In this study so-called “nominal” CRE ages with the shielding parameter  $(^{22}\text{Ne}/^{21}\text{Ne})_c = 1.11$  were used. Although this “nominal” CRE ages are not accurate, this approach is most reliable for the *comparison* of the ages of different samples from the same location because uncertainties involved in the shielding correction were avoided. Ages were calculated using cosmogenic  $^{21}\text{Ne}$ .  $T_{21}$  CRE ages are most reliable because He is easily affected by gas loss and Ar is mostly influenced by trapped components in primitive meteorites. CRE ages for Ne with “normal” shielding are indicated as  $T_{21-1.11}$  CRE ages.

Strong evidence for pre-irradiation effects was found in all chondrules from El Djouf 001 and NWA 852, which have elevated  $T_{21-1.11}$  CRE ages relative to the matrix. While the age difference of El Djouf 001 chondrules ranges between 0.4 and 1.9 Ma relative to the matrix, the two analyzed NWA 852 chondrules have nominal CRE ages that are 27.1 and 32.9 Ma longer than the respective matrix age, which is comparable with values for Murchison (CM2) chondrules reported in the literature. However, only 20% of Murchison chondrules show pre-irradiation effects (Roth et al. 2011, Huber et al. 2012). The differences concerning the percentage of pre-irradiation and duration of pre-irradiation may suggest different processes in the respective parent body regoliths. However, while El Djouf 001 is clearly different, the situation for NWA 852 may be similar to Murchison based on the large  $T_{21-1.11}$  CRE differences. Although pre-irradiation was observed in all chondrules from NWA 852, no reliable conclusion can be drawn concerning the percentage of pre-irradiated chondrules because only a small number (2) was analyzed.

Some of the chondrules from MET 00426, QUE 99177, and Acfer 082 show apparent pre-irradiation effects since they have elevated  $T_{21-1.11}$  CRE ages relative to the matrix. Remarkably, however, since the MET 00426 and QUE 99177 matrices have elevated  $T_{21-1.11}$  CRE ages compared to at least one chondrule, not only chondrules, but also the matrix from MET 00426 and QUE 99177 appear to have been pre-irradiated. The indication for pre-

irradiation of matrix material is an important new finding of this work in terms of analyzing pre-irradiation effects in primitive meteorites.

Chondrules from Allende and Vigarano show no evidence for pre-irradiation since their  $T_{21-1.11}$  CRE ages are indistinguishable from the matrix. In the case of Allende chondrules this is in accordance with the results from previous studies.

For Renazzo and Acfer 094 no reliable conclusion concerning pre-irradiation can be reached, because only a small number of chondrules were analyzed, which show  $T_{21-1.11}$  CRE ages indistinguishable from the corresponding matrix.

General reasons why a pre-irradiation of chondrules (as a whole) are difficult to discern include i) no discernibility of pre-irradiation effects in meteorites with long CRE ages, ii) the dependency of the production rate of cosmogenic noble gas nuclides on chemistry and shielding, iii) lower CRE ages of the matrix due to recoil losses, iv) noble gas loss from the bulk meteorite/matrix due to thermal metamorphism or the lower retentivity for cosmogenic gases, and vi) the superimposition on pre-irradiation records in chondrules or in the matrix by records from single grains or clasts. In addition, pre-irradiation effects in chondrules might not be expected based on the following arguments: i) the impossibility of pre-irradiation of chondrules in the early solar system due to high dust densities, ii) the limited lifetime of small objects in the inner solar system, and iii) the impossibility of pre-irradiation of chondrules on parent body surfaces (regolith). All these general difficulties and arguments could be neutralized by methodical approaches (e.g., selection of meteorites with i) short CRE ages and iv) limited thermal metamorphism; ii) use of  $T_{21-1.11}$  “nominal” CRE ages without shielding correction) and/or theoretical considerations (e.g., i) redistribution of chondrules to the outer edges of the protoplanetary disk with lower dust densities, where an irradiation should have been possible; iii) possibility of size sorting in a granular medium due to the Brazil-nut effect). On the other hand, the observations clearly show that chondrules were pre-irradiated. These observations include i) elevated nominal CRE ages of some chondrules relative to the matrix in previous studies as well as in this study, which cannot be explained by different abundances of target elements or shielding; this pre-irradiation of chondrules is recorded by an excess of  $^{21}\text{Ne}_c$ ; ii) different CRE ages of chondrules within a single meteorite, which suggests either different irradiation environments or identical irradiation and subsequent gas loss affecting some chondrules. In addition, iii) locally different regions of chondrule formation and different irradiation histories can explain these observations.

Overall, pre-irradiation of all chondrules from NWA 852 and El Djouf 001 as well as some chondrules from MET 00426, QUE 99177, and Acfer 082 is indicated. In addition, the matrices of MET 00426 and QUE 99177 show also evidence for pre-irradiation.

This study, like previous studies analyzing pre-irradiation effects in chondrules, is limited since the setting of pre-irradiation cannot be determined with certainty. Parameters like the shielding parameter ( $^{22}\text{Ne}/^{21}\text{Ne}_c$ ), which may help to decide where the chondrules were pre-irradiated (in the regolith on the meteorite parent body vs. solar nebula setting), are not unequivocal. In case of NWA 852 and El Djouf 001 with dominant solar wind components in the matrices pre-irradiation in the parent body regolith is indicated. The considerably longer pre-irradiation and in most cases higher concentration of trapped (solar) gases of NWA 852 chondrules compared to El Djouf 001 chondrules may imply that NWA 852 chondrules resided in a near-surface position (up to 1 or 2 m depth) on the CR meteorite parent body, whereas El Djouf 001 chondrules were shielded from cosmic radiation in much deeper regions and spent less time in a near-surface position. On the other hand, the highly varying  $T_{21-1.11}$  CRE ages of MET 00426 and QUE 99177 chondrules may imply pre-irradiation as free-floating objects in the solar nebula. Especially for QUE 99177, which lacks solar wind gases, a pre-irradiation in the solar nebula appears highly likely.

## Kurzfassung

Edelgase in Meteoriten enthalten eine „kosmogene“ Komponente, die auf die Exposition gegenüber kosmischer Bestrahlung zurückzuführen ist. Kosmogene Edelgase (wie auch Radionuklide) werden generell in der Zeit produziert, die der Meteoroid benötigt, um von seinem Mutterkörper bis zur Erde zu gelangen. Diese Zeitspanne wird als Bestrahlungsalter (CRE-Alter) definiert. Kosmogene Edelgase können jedoch auch in einer früheren Phase („Vorbstrahlung“) produziert werden. Edelgase in Chondren können insbesondere Aufschluss über die Merkmale der energetischen Partikel und die Lebensdauer der Chondren als freifliegende Objekte im frühen Sonnensystem im Fall einer Vorbstrahlung im solaren Nebel als auch über Oberflächenprozesse auf Asteroiden im Fall einer Vorbstrahlung im Mutterkörperregolith geben. Daher werden in dieser Studie Edelgase untersucht, um mögliche Vorbstrahlungseffekte in Chondren- und Matrixproben von neun kohligem Chondriten zu analysieren. Die untersuchten Proben schließen die CR2-Chondrite Renazzo, El Djouf 001 und NWA 852, die CR3-Chondrite MET 00426 und QUE 99177, die CV3-Chondrite Allende, Vigarano und Acfer 082 sowie den ungruppierten Acfer 094 ein.

Nach der Separation der Chondren vom Gesamtmeteorit mit Hilfe von Frost-Tau-Zyklen wurden die Konzentrationen wichtiger Targetelemente mittels Instrumenteller Neutronenaktivierungsanalyse (INAA) bestimmt. Das identische Probenmaterial wurde für Edelgasmessungen (He, Ne, Ar) verwendet, was Probleme der Probeninhomogenität beseitigt, die in früheren Studien auftraten. Die Bestrahlungsalter wurden mit der Produktionsrate von  $^{21}\text{Ne}_c$  berechnet, wofür wiederum die Formel nach Eugster (1988) verwendet wurde. Zusätzlich wurden die Chondren mineralogisch mit dem Rasterelektronenmikroskop (SEM) analysiert, und  $^{40}\text{K}$ - $^{40}\text{Ar}$ -Alter von Chondren und Matrix wurden bestimmt. In dieser Studie werden sogenannte „nominale“ Bestrahlungsalter mit einem Abschirmungsparameter  $(^{22}\text{Ne}/^{21}\text{Ne})_c = 1.11$  verwendet. Obwohl diese „nominalen“ Bestrahlungsalter nicht exakt sind, ist dieser Ansatz für den Vergleich von Altern unterschiedlicher Proben aus gleicher Position am zuverlässigsten, da Unsicherheiten, die mit der Abschirmungskorrektur verbunden sind, vermieden werden. Die Alter wurden mit Hilfe des kosmogener  $^{21}\text{Ne}$  berechnet ( $T_{21}$ ). Die  $T_{21}$ -Alter sind am zuverlässigsten, da Helium leicht durch Gasverlust beeinflusst werden kann und Argon in den meisten primitiven Meteoriten durch primordiale (solare oder „planetare“) Komponenten dominiert ist. Die Bestrahlungsalter für Ne mit „normaler“ Abschirmung sind als  $T_{21-1.11}$  bezeichnet.

Überzeugende Belege für Vorbstrahlungseffekte wurde in allen Chondren von El Djouf 001 und NWA 852 gefunden, die erhöhte  $T_{21-1.11}$  CRE-Alter relativ zur Matrix aufweisen. Während der Altersunterschied der El Djouf 001-Chondren zwischen 0,4 und 1,9 Ma relativ zur Matrix liegt, sind die nominalen CRE-Alter der beiden NWA 852-Chondren 27,1 und 32,9 Ma höher als die der Matrix, was mit den Werten für Murchison-Chondren (CM2) aus der Literatur vergleichbar ist. Allerdings zeigen nur 20% der Murchison-Chondren Vorbstrahlungseffekte (Roth et al. 2011, Huber et al. 2012). Die Unterschiede bezüglich des Anteils der vorbestrahlten Chondren und der Dauer der Vorbstrahlung kann auf verschiedene Prozesse in den jeweiligen Mutterkörperregolithen hinweisen. Während die Situation für NWA 852 ähnlich der von Murchison sein kann ausgehend von den großen Unterschieden der  $T_{21-1.11}$  CRE-Alter, weicht El Djouf 001 eindeutig ab. Obwohl in allen Chondren von NWA 852 eine Vorbstrahlung bestimmt wurde, kann aufgrund der geringen Anzahl (2) keine zuverlässige Schlussfolgerung bezüglich des Anteils der vorbestrahlten Chondren gezogen werden.

Einige Chondren von MET 00426, QUE 99177 und Acfer 082 zeigen offensichtliche Vorbstrahlungseffekte, da ihre  $T_{21-1.11}$  CRE-Alter gegenüber dem der Matrix erhöht sind.

Bemerkenswert ist außerdem, dass die Matrixproben von MET 00426 und QUE 99177 erhöhte  $T_{21-1.11}$  CRE-Alter aufweisen gegenüber mindestens einer Chondre. Demnach scheinen nicht nur einige Chondren, sondern auch die Matrix von MET 00426 und QUE 99177 vorbestrahlt worden zu sein. Der Hinweis auf die Vorbestrahlung von Matrixmaterial stellt eine wichtige neue Erkenntnis dieser Arbeit im Bezug auf die Analyse von Vorbestrahlungseffekten in primitiven Meteoriten dar.

Chondren von Allende und Vigarano zeigen keine Hinweise auf Vorbestrahlung, da sich ihre  $T_{21-1.11}$  CRE-Alter nicht von denen der Matrix unterscheiden. Im Fall der Allende-Chondren stimmt dies mit den Ergebnissen früherer Studien überein.

Für Renazzo und Acfer 094 konnten keine zuverlässigen Schlussfolgerungen bezüglich der Vorbestrahlung gezogen werden, da nur eine kleine Anzahl von Chondren untersucht wurde, deren  $T_{21-1.11}$  CRE-Alter nicht von denen der Matrix zu unterscheiden ist.

Allgemeine Gründe, weswegen eine Vorbestrahlung von Chondren (als Ganzes) schwer messbar ist, sind: i) die schlechte Messbarkeit von Vorbestrahlungseffekten in Meteoriten mit langen CRE-Altern, ii) die Abhängigkeit der Produktionsrate der kosmogenen Edelgasnuklide von der Chemie und Abschirmung, iii) geringere CRE-Alter der Matrix aufgrund von Rückstoßverlusten aus der Matrix, iv) Edelgasverlust vom Gesamtmeteorit/der Matrix aufgrund von thermischem Metamorphismus oder einer geringeren Retentivität der Matrix gegenüber kosmogenen Gasen sowie v) die Überlagerung von Vorbestrahlungseffekten in Chondren oder der Matrix durch Vorbestrahlungseffekte in Einzelkörnern oder Klasten. Zudem könnte eine Vorbestrahlung von Chondren aufgrund folgender Argumente nicht zu erwarten sein: i) die Unmöglichkeit der Vorbestrahlung von Chondren im frühen Sonnensystem aufgrund von hohen Staubdichten, ii) die begrenzte Lebenszeit von kleinen Objekten im inneren Sonnensystem sowie iii) die Unmöglichkeit der Vorbestrahlung von Chondren auf Oberflächen von Mutterkörpern (Regolith). Alle diese Schwierigkeiten und Argumente können auf Grundlage von methodischen Ansätzen (wie etwa der Auswahl von Meteoriten mit i) kurzen CRE-Altern und iv) schwachem thermalem Metamorphismus; ii) der Verwendung von  $T_{21-1.11}$  nominaler CRE-Alter ohne Abschirmungskorrektur) und/oder theoretischen Überlegungen (wie etwa i) die Umverteilung der Chondren zu den äußeren Rändern der protoplanetaren Scheibe mit geringeren Staubdichten, wo eine Bestrahlung denkbar war; iii) Möglichkeit der Korngrößensortierung in einem granularen Medium aufgrund des Paranuss-Effektes) entkräftet werden.

Andererseits gibt es Beobachtungen, die eindeutig eine Vorbestrahlung von Chondren belegen. Diese Beobachtungen umfassen i) erhöhte nominale CRE-Alter von Chondren relativ zur Matrix in früheren Studien und in dieser Studie, die nicht durch unterschiedliche Konzentrationen der Targetelemente oder unterschiedliche Abschirmung erklärt werden können; diese Vorbestrahlung der Chondren ist in einem Überschuss an  $^{21}\text{Ne}_c$  gespeichert; ii) verschiedene CRE-Alter von Chondren in einem einzigen Meteorit deuten entweder auf verschiedene Bestrahlungsbedingungen oder identische Bestrahlung und anschließenden Gasverlust von einigen Chondren hin. Zudem können iii) lokal unterschiedliche Regionen der Chondrenbildung und eine unterschiedliche Bestrahlungsgeschichte diese Beobachtungen erklären.

Insgesamt zeigt sich eine Vorbestrahlung aller Chondren von NWA 852 und El Djouf 001 sowie einiger Chondren von MET 00426, QUE 99177 und Acfer 082. Zusätzlich zeigen die Matrixproben von MET 00426 und QUE 99177 ebenfalls Hinweise auf Vorbestrahlung.

Diese Studie ist jedoch begrenzt, ähnlich wie frühere Studien zur Analyse von Vorbestrahlungseffekten in Chondren, da der Ort der Vorbestrahlung nicht mit Sicherheit bestimmt werden kann. Parameter, wie etwa der Abschirmungsparameter ( $^{22}\text{Ne}/^{21}\text{Ne}_c$ ),



können helfen bei der Entscheidung, wo die Vorbestrahlung stattfand, sind jedoch nicht eindeutig.

Bei NWA 852 und El Djouf 001 lässt dominanter Sonnenwind in der Matrix auf eine Vorbestrahlung im Mutterkörperregolith schließen. Die erheblich längere Vorbestrahlung und die meist höheren Konzentrationen an implantierten (solaren) Gasen in NWA 852-Chondren im Vergleich zu El Djouf 001-Chondren können darauf schließen, dass sich die NWA 852-Chondren in einer oberflächennahen Position (bis zu 1 oder 2 m tief) im CR-Meteoritenmutterkörper befunden haben, während die El Djouf 001-Chondren wesentlich tiefer vor kosmischer Bestrahlung abgeschirmt waren und nur eine kürzere Zeit in einer oberflächennahen Position verbrachten. Dahingegen können die stark variierenden  $T_{21-1.11}$  CRE-Alter der MET 00426- und QUE 99177-Chondren auf eine Vorbestrahlung als freifliegende Objekte im solaren Nebel hindeuten. Besonders für QUE 99177, dem Sonnenwind-implantierte Edelgase fehlen, erscheint eine Vorbestrahlung im solaren Nebel als sehr wahrscheinlich.



## 1 Introduction

The time between chondrule formation and chondrite accretion (planetesimal formation) in the early solar system is not well determined (e.g., Metzler 2012). Chondrules and calcium-aluminium-rich inclusions (CAIs) are the first solid materials, which formed in the early solar system (e.g., Connelly et al. 2012). Besides the matrix and CAIs, chondrules are major compositional units of primitive meteorites (so-called chondrites), which experienced only minimal further alteration after accretion to asteroids / planetesimals. The analyses of chondrules can provide constraints on the conditions and processes in the early solar system, because chondrule properties should reflect the composition of and physical conditions in the solar nebula when the sun and the planets were forming (Okazaki et al. 2001).

A pre-irradiation (or pre-compaction exposure) is defined as the situation where certain parts of a meteorite only show an excess of cosmogenic nuclides, relative to other fractions of the meteorite, which cannot be explained by higher production rates due to higher concentrations of major target elements or favorable shielding during their recent cosmic ray exposure travelling from parent body to earth (Wieler 2002b). Instead, the pre-irradiated meteoritic component has been longer exposed to cosmic rays before the ejection from kilometer-sized parent body (Eugster et al. 2006).

The analyses of pre-irradiation effects in chondrules using noble gases may provide information about the energetic particle environment and the lifetime of chondrules in the early solar nebula as well as about surface processes on the parent body regolith depending on the setting of pre-irradiation.

Chondrules or other single meteorite components like single grains or clasts may have been pre-irradiated in different settings: On the meteorite parent body in the unconsolidated surface layer (regolith) or in the solar nebula as free-floating objects. As discussed below in detail, for the first scenario the evidence from previous work seems to be strong (e.g., Huber et al. 2012, Roth et al. 2011), while the latter one is still actively debated (e.g., Das and Murty 2009, Eugster et al. 2007, Polnau et al. 2001).

In the case of a pre-irradiation in the parent body regolith, small, independent meteorite grains or chondrules have been exposed to irradiation prior the compaction into the matter that became the studied meteorite. The presence of granular materials covering the surfaces of small bodies like asteroids or comets in our solar system has been shown by spacecraft images and also by in situ observations of the asteroids Eros and Itokawa. Additionally, there is strong evidence that small body regoliths are very complex and active (Murdoch et al. 2013 and references therein). Taking shaking-induced particle segregation into account, the so-called Brazil-nut effect (e.g., Shinbrot 2004, Kudrolli 2004, Rosato et al. 1987), which does likely occur even in low-gravity environments as on asteroid surfaces (Murdoch et al. 2013, Tancredi et al. 2012), a preferential exposure of chondrules in a meteorite parent body regolith seems well possible. Implanted solar wind (SW) gases and cosmogenic nuclides produced by solar cosmic rays (SCR) reside in the uppermost few mm of the exposed matter. Since inferred CRE ages for  $2\pi$  exposure in the asteroidal regolith have in some cases found to be too long and incompatible with the expected lifetime of asteroidal regoliths, an exposure to an enhanced flux of early SCRs by the active initial sun has been invoked (Chaussidon and Gournelle 2006).

On the other hand, concerning a pre-irradiation of chondrules in the solar nebula setting, an irradiation of chondrules as free-floating objects has often been considered as not possible due to high dust densities in the midplane of the protoplanetary disk, which would have shielded the chondrules from cosmic rays, and the limited lifetime of small objects in the early solar system. This is not necessarily so. With respect to the high dust densities, since

chondrules could also have been exposed to cosmic rays at the surface of the protoplanetary disk where dust/gas ratios were lower. This scenario is consistent with the formation of chondrules close to the sun and redistribution throughout the solar system (X-wind model by Shu et al. 2001, 1997, 1996, solar nebula jet flows by Liffman 2005). A redistribution of chondrules above the solar accretion disk may have allowed the irradiation of chondrules even if they were formed in regions with high dust densities like the midplane (e.g., Wasson 1993, Cuzzi and Alexander 2006). As for the argument of a limited lifetime of small particles in the early solar system caused by inward drift due to gas drag, this may have been counteracted by transport of chondrules to the periphery of the protoplanetary disk or outward radial diffusion in a weakly turbulent nebula (Scott 2007 and references therein). In addition, after sinking to the midplane of the protoplanetary disk chondrules may have been incorporated into planetesimals and thus be preserved (Weidenschilling 1977). Remote observations of protostellar disks indicate that at least in some cases these are sufficiently turbulent to have preserved small particles for several million years (Natta et al. 2006, Haisch et al. 2001).

While there is no cogent reason that pre-irradiation effects should be constrained to chondrules, the concentration on chondrules in this as well as in previous studies searching for pre-irradiation effects stems from the fact that chondrules are abundant (Roth et al. 2011) and are believed to have formed close to the sun (Shu et al. 2001, 1997, 1996) at high temperatures. The latter should have resulted in low abundances of primordial noble gases interfering in the analysis (Vogel et al. 2004) and should have led to loss of cosmogenic noble gas components that might have been present already in the precursor material (Roth et al. 2011).

Among the previous work, Polnau et al. (1999) found systematically higher concentrations of cosmogenic noble gases in a chondrule fragment relative to the matrix in the H6 chondrite ALH 76008. The authors interpreted the apparent enhanced CRE age of the chondrule fragment as due to precompaction exposure since preferential gas loss from the fine-grained matrix and systematic errors in the correction for variable target element chemistry were excluded. Polnau et al. (2001) later analyzed eight ordinary chondrites for pre-irradiation effects of chondrules and reported evidence for six of them. However, the excesses of cosmogenic nuclides in the chondrules analyzed by Polnau et al. (1999, 2001) were rather small. Intriguing evidence for pre-irradiation of Renazzo (CR2) chondrules is contained in the data reported by Vogel et al. (2003, 2004): In all their analyzed chondrules, cosmogenic neon  $^{21}\text{Ne}_c$  was roughly one order of magnitude more abundant than in the matrix. However, Vogel et al. (2003, 2004) did not assess their data for pre-irradiation. The authors noted that in chondrules the abundances of trapped gases were very low, which is in contrast to the typical situation for pre-irradiation in a parent body regolith, where SW gases are abundantly found (e.g., Pedroni 1991, Wieler et al. 1989). Eugster et al. (2007) analyzed 15 carbonaceous, ordinary and enstatite chondrites, and found equivocal results except for some chondrules from Dhajala (H3.8) for which their results may suggest some precompaction exposure. Clear evidence for pre-irradiation of chondrules was provided by Roth et al. (2008, 2009, 2011). Among 26 chondrules from Allende (CV3) and 38 chondrules from Murchison (CM2) seven Murchison chondrules showed a record of pre-compaction exposure corresponding to an irradiation of up to 30 Ma at present-day galactic cosmic rays (GCR) intensity in a  $4\pi$  geometry. The authors exclude the inheritance of cosmogenic noble gases from chondrule precursors, and prefer a scenario of pre-irradiation by GCR in the regolith of the Murchison parent body rather than an irradiation by an early intense flux of SCR. However, the data did not allow a firm conclusion, where the excess of cosmogenic noble gases in chondrules were acquired, and their preferred scenario does not explain the

pre-irradiation of chondrules in solar gas-free meteorites found in other work. Das and Murty (2009) reported higher CRE ages compared to the matrix samples for a few chondrules from Dhajala (H3.8), Bjurböle (L/LL4) and Murray (CM2), suggesting that the chondrule and/or chondrule precursors received cosmic irradiation in a solar nebula setting before the accretion into the parent body. Matsuda et al. (2010) reported enhanced  $T_3$  and  $T_{21}$  CRE ages of Parnallee (LL3.6) chondrules relative to the matrix, suggesting pre-irradiation of chondrules. However, the accuracy of their calculated CRE ages is questionable because they used identical production rates for all of the chondrules and also the matrix in spite of the likely differences in target element abundances. Das et al. (2010) reported higher CRE ages for chondrule fragments of Murchison (CM2), Dhajala (H3.8), Chainpur (LL4), Bjurböle (L/LL4) and Parsa (EH3) relative to the matrix, corresponding to pre-compaction exposure in the range from 5 to 35 Ma. For olivine or olivine-rich grains from the same meteorites Das et al. (2012) found similar CRE ages to those of the matrix with the exception of three individual olivine-rich grains from Dhajala (H3.8) and one grain each from Bjurböle (L/LL4) and Chainpur (LL4). Das et al. (2010, 2012) proposed that chondrules were exposed to enhanced SCR during or shortly after chondrule formation, however their target element concentrations were incorrectly determined leading to too low production rates of cosmogenic neon ( $^{21}\text{Ne}_c$ ) and hence too high  $T_{21}$  CRE ages (Ott et al. 2013). Huber et al. (2012) analyzed the irradiation history of individual Murchison (CM2) chondrules, combining their data with those of Roth et al. (2011) and Metzler (2004). According to Huber et al. (2012), chondrules in primary rock fragments (PRFs) show no evidence for pre-irradiation, whereas 20-30% of chondrules embedded in the clastic matrix experienced different degrees of pre-irradiation of up to 25 Ma (assuming a  $4\pi$  irradiation). This is in agreement with the results from Roth et al. (2011), and points towards a pre-irradiation in the parent body regolith. Strashnov and Gilmour (2012), finally, reported identical ages within uncertainties for H5 Allegan chondrules and matrix is based on the  $^{81}\text{Kr-Kr}$  method.

In this study chondrules and matrix samples of nine carbonaceous chondrites were analyzed for noble gases and abundances of important target elements in order to search for pre-irradiation effects. The project is embedded in the cooperation network SPP 1385 “The first 10 Million Years of the Solar System – a Planetary Materials Approach”.

## 2 Fundamentals

### 2.1 Meteorite components

#### 2.1.1 Chondrites and their components

##### ***Meteorite classification***

Meteorites are classified to sort these extraterrestrial rocks into similar types in order to better understand their origin and relationship (Bischoff 2001). The classification of meteorites is largely based on their bulk chemical composition, mineralogical properties, and oxygen isotopic composition (Scott 2007, Weisberg et al. 2006).

Meteorites are subdivided into the two main divisions “differentiated” and “undifferentiated” (**Figure 2-1**) considering their origin and evolution. However, this distinction does not rule out that the accreting starting materials of the parent bodies were similar; rather, it indicates different evolutions of the bodies (Bischoff 2001). Undifferentiated meteorites, unlike differentiated meteorites, have not been completely molten and they contain different components embedded in a fine-grained matrix.

Chondrites are primitive undifferentiated sedimentary rocks, which are principally composed of chondrules (silicate melt droplets), and represent extraordinary mixtures of presolar and solar nebula materials and asteroidal debris (Scott 2007) that escaped being incorporated into planets. Thus, chondrites provide unique insights into processes operating in the circumstellar disk from which the planets formed at the very start of the solar system (Zanda 2004). CI chondrites are closest to the solar chemical composition and lack chondrules.

The hierarchy of terms for chondrite classification (see **Figure 2-1**) is explained briefly as follows (Weisberg et al. 2006):

- A **class** consists of two or more groups sharing primary whole-rock chemical and oxygen isotopic properties. Chondrites within one class
  - have similar refractory lithophile-element abundances and
  - their oxygen isotopic compositions plot in the same general region.
- A **clan** is a relatively new term in chondrite classification, which is used to encompass chondrites that have chemical, mineralogical, and isotopic similarities and are thought to have formed in the same local region of the solar nebula in a narrow range of heliocentric distances. For chondrites within a clan a petrologic kinship was suggested, but the petrologic and/or bulk chemical characteristics preclude a group relationship. Chondrite groups within a clan
  - have closely similar refractory lithophile-element abundances,
  - plot on the same oxygen isotopic mixing line,
  - share an isotopic anomaly, or
  - have similar petrologic characteristics.
- **Group** is the most basic and significant unit, indicating meteorites from the same parent body. A group is defined as a minimum of five unpaired chondrites; for cases with less than five members, the term **grouplet** has been applied. Chondrites of a group or grouplet are characterized by
  - closely similar petrologic characteristics (chondrule size, modal abundances, mineral composition), and
  - closely similar whole-rock chemical and oxygen isotopic characteristics.
- **Subgroups** were introduced as systematic petrologic differences have been recognized in members of some chondrite groups like CV chondrites.

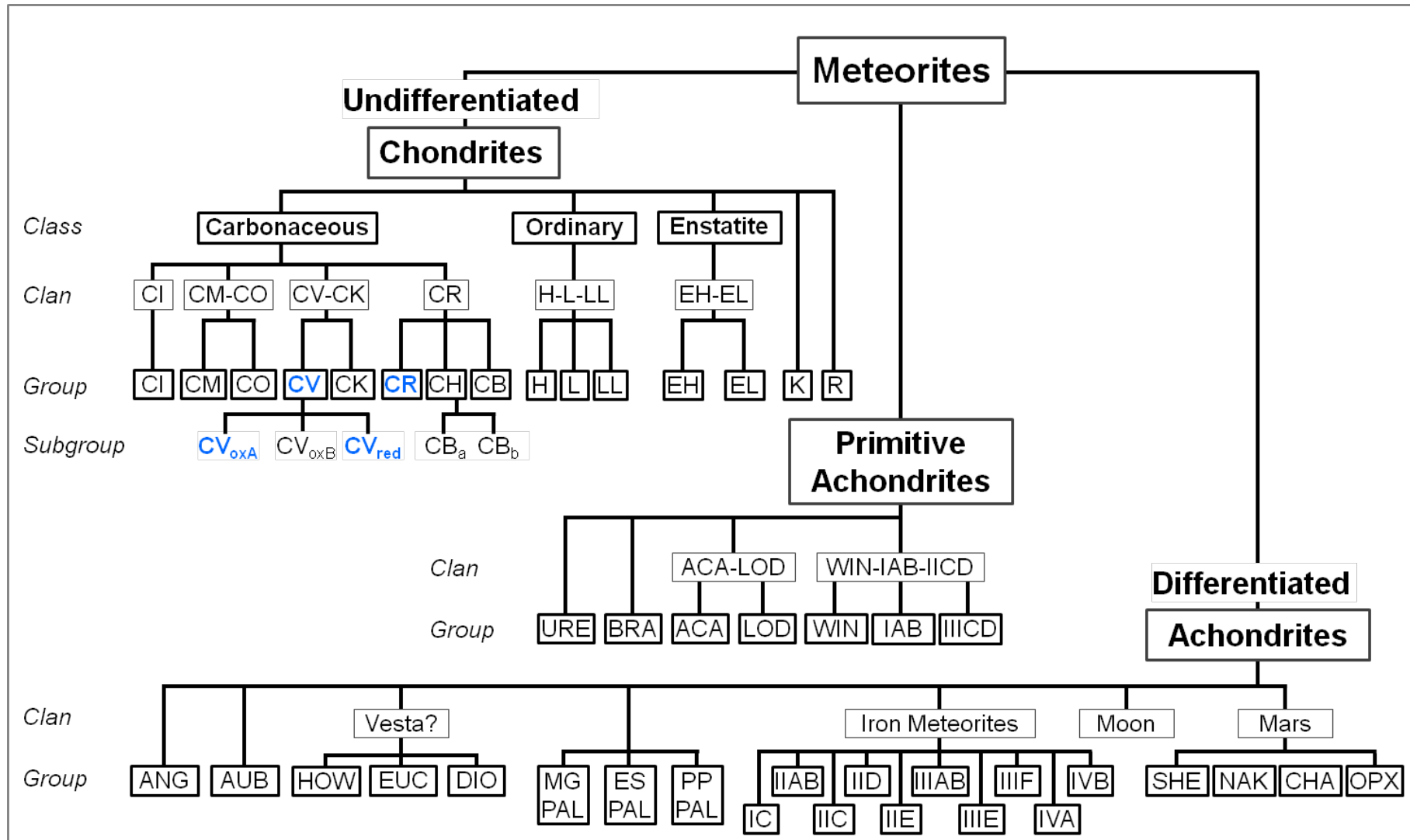


**Figure 2-1: Classification of meteorites showing the major meteorite divisions, classes, clans and groups and relationships among meteorite groups** (adapted after Weisberg et al. 2006). Unique and ungrouped meteorites are omitted. Blue colored chondrite groups were analyzed in this study. Abbreviations: URE-ureilite, BRA-brachinite, ACA-acapulcoite, LOD-Iodranite, WIN-winonaite, ANG-angrite, AUB-aubrite, HED-howardite-eucrite-diogenite, MES-mesosiderite, MG PAL-main-group pallasite, ES PAL-Eagle Station pallasite, PP PAL-pyroxene pallasite, SHE-shergottite, NAK-nakhlite, CHA-chassignite, OPX-orthopyroxenite. Some authors (McSween and Huss 2010, Weisberg et al. 2006) suggest that ureilites and brachinites belong to the primitive achondrites, while others (Krot et al. 2007a, Bischoff 2001) consider them differentiated (planetary).

Chondrites are divided into 15 defined groups (see **Figure 2-1**), and each group is believed to represent material from a single parent body. All chondrite groups except the K and R groups can be assigned to the carbonaceous (C), ordinary (O), and enstatite (E) chondrite classes. Each chondrite group appears to be composed of a unique mixture of materials that formed under diverse conditions and were mixed together and accreted from the solar nebula at a specific time and place (Scott 2007). Groups within the C-chondrite class are named with the letter C and a second letter that is usually the first initial of the type specimen: CI (Ivuna-like), CM (Mighei-like), CO (Ornans-like), CV (Vigarano-like), CK (Karoonda-like), CR (Renazzo-like), CB (Bencubbin-like), and CH (high Fe, ALH 85085-like) (Weisberg et al. 2006).

Additionally, there are some chondrites with mineralogical and/or chemically unique features that defy classification in existing chondrite groups; these chondrites are called ungrouped (Weisberg et al. 2006) and include for example Acfer 094.

Since meteorite searches in hot and cold deserts dramatically increased the number of meteorite finds, including rare samples, new additional meteorite groups or grouplets were defined (Bischoff 2001). K chondrites (after Kakangari) for example were introduced as a new “grouplet”, because there are only three members (Kakangari, Lewis Cliffs 87232 and presumably Lea County 002) (Weisberg et al. 2006).

Carbonaceous chondrites are among the most primitive materials (e.g., Stracke et al. 2012) in the solar system, although they have probably undergone physical alteration (see *chapter 2.1.2*) to some degree (Kallemeyn and Wasson 1981). However, despite this processing, the carbonaceous chondrites remain the single most important source of information available on early solar system evolution (McSween 1979). Carbonaceous chondrites are characterized by whole-rock refractory lithophile abundances  $\geq 1$  relative to CI and normalized to Mg, and their oxygen isotopic compositions plot near or below the terrestrial fractionation line (Weisberg et al. 2006). In this study we analyzed CV and CR chondrites (blue colored in **Figure 2-1**) and one ungrouped chondrite.

### **Components of chondrites**

Chondrites are composed of the following components (e.g. Stracke et al. 2012, Scott 2007):

- chondrules
- matrix
- refractory inclusions (calcium-aluminium-rich inclusions, CAIs)
- metallic Fe,Ni grains.

Chondritic components are believed to have formed in the solar nebula disk as their bulk chemical compositions matches that of the Sun’s (neglecting H, C, N, O, and inert gases). Furthermore, chondrite matrices contain small amounts of interstellar and circumstellar grains, and the mineralogical, chemical, and oxygen isotopic composition of chondritic components can be generally understood in terms of thermal processing over diverse temperatures in the solar nebula (Scott 2007).

### **Analyses of bulk meteorite vs. single components**

Analyses of bulk meteorites and single components have provided complementary datasets implying complex meteorite histories. While bulk analyses enable to recognize relationships between meteorites and to assign individual parent bodies, analysis of single components within a meteorite is required to provide more detailed and specific information about formation histories (Grady and Wright 2006). Analyses of chondrules for example can provide constrains on the conditions of the solar nebula, because chondrule properties should reflect the composition of and physical conditions in the solar nebula when the sun and the planets were forming (Okazaki et al. 2001).



### 2.1.2 Formation and alteration of chondritic components

Components separated from extraterrestrial material, tracing primary processes, are believed to have formed in the solar nebula. After the presolar epoch, during which nucleosynthesis occurred and interstellar chemistry formed molecules, the nebula epoch followed, including the formation of primary solids and processing into objects prior to accretion into planetesimals. CAIs and chondrules, representing the first solids, are believed to have formed in the nebula epoch (Grady and Wright 2006) with a time difference of approximately ~1 and ~3 Ma (e.g., Connelly et al. 2008, Amelin et al. 2002) (see *chapter 2.2.3.7*).

Chondritic material has been altered during and/or after the accretion in the solar nebula by several processes that modify its original nebula properties. The degree of alteration of chondrites by **secondary processes** is described using a petrologic type classification (**Figure 2-2**) based on petrologic, mineral and thermoluminescence properties (e. g., Van Schmus and Wood 1967, Sears and Dodd 1988, Brearley and Jones 1998, Weisberg et al. 2006). Secondary processes include alteration by water (aqueous alteration), alteration by heat (thermal metamorphism), shock processes resulting from impacts (which likely took place on the chondrite parent bodies), reaction of solids with surrounding gas possibly as a nebula or parent-body process as well as terrestrial weathering (Jones et al. 2005).

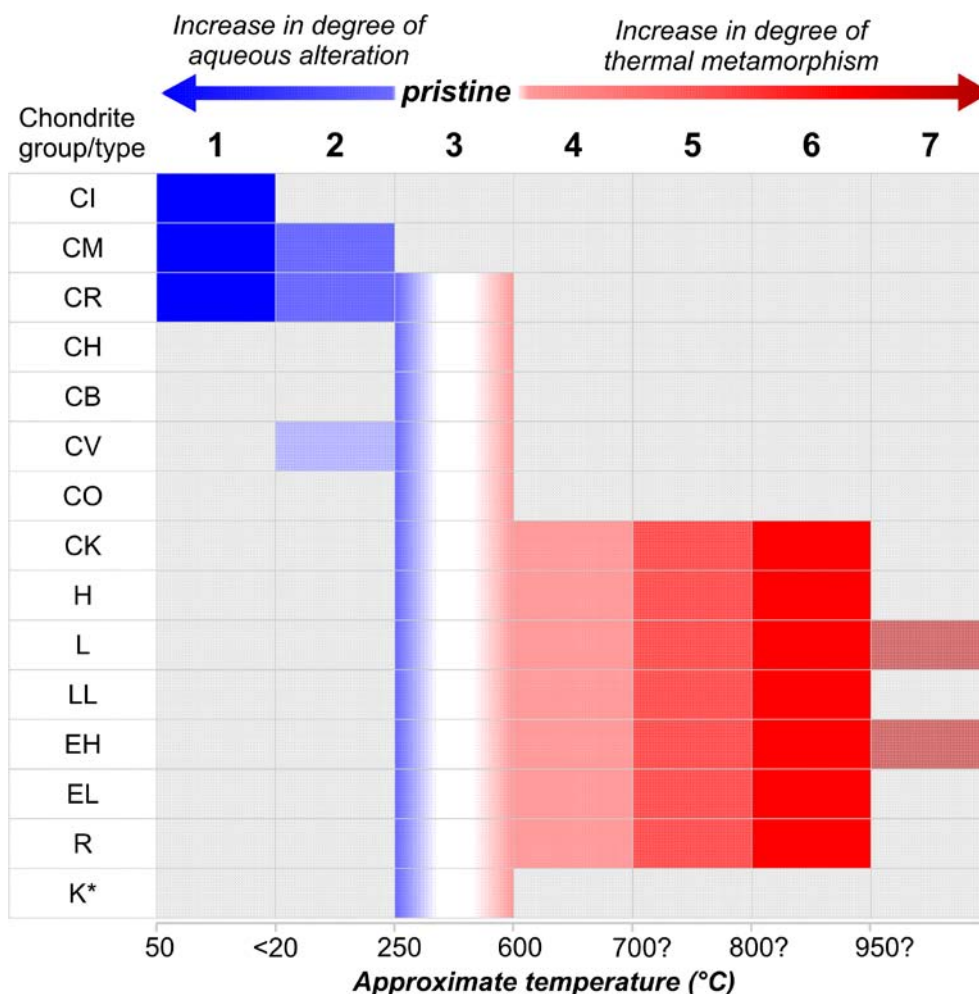


**Figure 2-2: Petrologic types of each chondrite group** (adapted after Weisberg et al. 2006). \*K chondrites represent a “grouplet” because only three members are known and a “group” requires five or more members. Temperatures are given according to McSween and Huss (2010).

**Aqueous alteration** results in the formation of hydrated phyllosilicates and biopyriboles, amphibole, talc, tochilinite and magnetite and a host of carbonates hydrated sulfates, occurring sometimes in veins (Keil 2000). With increasing temperatures in the parent body, some volatiles degassed and aqueous alteration was replaced by **thermal metamorphism**. Possible heat sources that caused melting, metamorphism, and alteration are shock heating (especially for ordinary chondrites), electromagnetic induction heating, and short-lived isotopes (primarily  $^{26}\text{Al}$  with a minor contribution from  $^{60}\text{Fe}$ ), where the latter seems more likely (Scott 2007). At the lower end of the temperature scale, metamorphism may have occurred in the presence of water derived from dehydration of hydrated minerals. At higher temperatures the water had already been driven off and this dry metamorphism resulted in the formation of new minerals, homogenization of originally zoned minerals, re-equilibration of elements between coexisting phases, and coarsening and recrystallization of the chondritic textures, possibly resulting in the loss of recognizable chondrules (Keil 2000).

The most pristine material is thought to be present in type 3 meteorites, while types 3 to 6 indicate increasing degree of petrologic equilibration and recrystallization, and types 2 and 1 indicate increasing degree of aqueous alteration (see **Figure 2-2**). Type 7 chondrites have been completely recrystallized or melted. Petrologic type 3 chondrites have been divided into 3.0 to 3.9 subtypes on the basis of thermoluminescence, which mostly depends on the degree of crystallization of chondrule mesostasis (Weisberg et al. 2006), and subtypes 3.0 and 3.1 have been further divided into 3.00 to 3.15 based on the Cr concentrations in olivine with  $>2$  wt% FeO (Scott 2007). However, some chondrites may have been aqueously altered and have been later thermally metamorphosed; there is no possibility to label this case with the commonly applied classification system (Weisberg et al. 2006). For CM chondrites representing the largest group of aqueously altered carbonaceous chondrites Rubin et al. (2007) and Browning et al. (1996) provide more detailed classification schemes. More recently a new classification scheme for aqueous alteration was applied to carbonaceous chondrites using the total phyllosilicate abundance; it improves the resolution of the traditional 1-3 scheme for aqueous alteration (Howard and Alexander 2013).

Assuming melting of the parent bodies of igneous meteorites by heat from  $^{26}\text{Al}$  and  $^{60}\text{Fe}$  and quick accretion after chondrule formation, formation ages of chondrules should correlate inversely with the thermal histories of their parent bodies: Metamorphosed samples may have resided deep in the parent body, whereas least metamorphosed samples were likely located in the cooler surface region. For example relatively old Allende chondrules (see *chapter 2.2.3.7*) experienced maximum metamorphic temperatures up to 550-600°C (Huss et al. 2006) in the CV parent body, whereas younger chondrules in CR chondrites reached no more than 225°C (Keil 2000) in the CR parent body (Scott 2007).

The degree of **shock** pressures that chondrites experienced is described by a shock stage classification, ranging from S1 (unshocked) to S6 (very strongly shocked) (**Table 2-1**) (Krot et al. 2007a). It is determined from various mineralogical and textural parameters and in case of ordinary chondrites is based on shock effects observed in olivine and plagioclase (Stöffler et al. 1991). For enstatite chondrites orthopyroxene is used instead (Rubin et al. 1997).

A further secondary process affecting chondritic material is **brecciation**. Impacts between solar-system objects (asteroids and comets) can result in the formation of breccias, rocks composed of fragments derived from previous generations of rocks, cemented together to form a new lithology. Concerning noble gases and pre-irradiation effects, it is important to realize that regolith breccias contain fragmental debris on the surface of the meteorite parent body, mixed by impact events and containing solar-wind gases (see *chapter 2.3.3*) (Krot et al. 2007a).

**Table 2-1: Progressive stages of shock metamorphism of ordinary (Stöffler et al. 1991) and enstatite chondrites (Rubin et al. 1997).**

Shock stage	Description	Shock pressure (GPa) <sup>a</sup>	Post-shock temperature increase (°C) <sup>b</sup>
S1	unshocked	<4-5	10-20
S2	very weakly shocked	5-10	20-50
S3	weakly shocked	10-15	100-150
S4	moderately shocked	25-30	250-350
S5	strongly shocked	45-60	600-850
S6	very strongly shocked shock melted	75-90	1500-1750

*\*Shock stage S6 has not yet been identified in enstatite chondrites. <sup>a</sup>Shock pressures are from Rubin et al. (1997) and references therein and are based on shock recovery experiments at 293 K on H6 Kernouve (9% porosity); less porous materials develop shock features at higher shock pressures. <sup>b</sup>Post-shock temperature ranges (i.e. shock-induced temperature increase relative to ambient temperature) are estimates based on extrapolated data (Stöffler et al. 1991 and references therein).*

**Terrestrial weathering** is an additional process affecting meteorites, which is usually used in the classification of meteorite finds. Weathering finally leads to the disintegration of the meteorite, and is important in connection with the terrestrial age and the estimate of the true fall rate of meteorites (Wlotzka 1993). There are two different classification schemes: One for hand specimen of Antarctic meteorites (commonly used) and another one for meteorites as they appear in polished thin sections (rarely used) (Krot et al. 2007a, Bland et al. 2006) (**Table 2-2**). For meteorite finds from Roosevelt Country, New Mexico, a correlation between weathering grades and terrestrial ages were found. In these climatic conditions weathering grades developed from W2 (5.000 to 15.000 a) up to W6 (30.000 to >45.000 a). For chondrites from the Lybian and Algerian Sahara similar terrestrial ages were found, whereas Antarctic meteorite finds weather much more slowly (Wlotzka 1993). Therefore, chondrites in hot deserts rarely have terrestrial ages >50 ka (Bland et al. 2006), whereas terrestrial ages of

**Table 2-2: Different weathering categories for meteorites.**

Hand specimen of Antarctic meteorites (Meteorite Working Group at the NASA Johnson Space Centre cited by Krot et al. 2007a)		Polished thin sections of meteorites (Wlotzka 1993)	
A	Minor rustiness	W0	No visible oxidation of metal or sulfides, typical for most fresh falls, although some are already W1
B	Moderate rustiness	W1	Minor oxide veins and rims around metal and troilite
C	Severe rustiness	W2	Moderate oxidation of ~20-60% metal
e	Evaporate minerals visible to the naked eye	W3	Heavy oxidation of metal and troilite, 60-95% being replaced
		W4	Complete (>95%) oxidation of metal and troilite, but no oxidation of silicates
		W5	Beginning alteration of mafic silicates, mainly along cracks
		W6	Massive replacement of silicates by clay minerals and oxides

Antarctica finds can be much higher, up to 2 Ma (H5 chondrite ALH 88019, Scherer et al. 1997b) and 2.35 Ma (L4 chondrite LEW 86360, Welten et al. 1997). Carbonaceous chondrites are more susceptible to terrestrial weathering than other meteorite types because of a larger proportion of fine-grained matrix (and a correspondingly larger surface area of reactant), higher abundances of volatile elements, and the presence of abundant organic compounds. The only CI1 chondrites in the Natural History Museum in London, for instance, are falls showing that CIs are not robust enough to last long in the terrestrial environment (Bland et al. 2006).

### 2.1.3 Matrix

Although matrix accounts for 30 to 70 vol% in most carbonaceous chondrites (**Table 2-3**) (Scott 2007), there is still no clear definition of what matrix really is.

#### **Definition**

McSween and Richardson (1977) operationally defined matrix as dark, aphanitic material free of coarse silicate grains, magnetite, sulfide, or metal optically discernible at 400x in a reflected light using a petrographic microscope. Scott (2007) designates matrix as fine-grained, silicate material with grain sizes of 10 nm to 5  $\mu\text{m}$  that coats chondrules and other coarse chondritic ingredients, which fills in some cases the interstices between them. Matrix material contain small amounts of presolar grains (up to 200 ppm of presolar silicate observed in CR3 QUE 99177 by Floss and Stademann 2009a), and it is mineralogically indistinguishable from rims on chondrules and CAIs, which have thicknesses of ~10-100  $\mu\text{m}$  (Scott 2007).

#### **Importance**

The matrix material of primitive chondrites is important because it can preserve the composition, heterogeneity, and chemical trends of fines (material smaller than approximately 1  $\mu\text{m}$ ) from the early solar nebula (Hurt et al. 2012). However, because of its fine-grained nature, matrix was especially susceptible to alteration during heating and aqueous alteration of asteroids (Scott 2007).

#### **Mineralogy**

Matrices of unaltered carbonaceous chondrites are mainly composed of crystalline Mg-rich silicates and amorphous Fe-rich silicates. Additionally they contain smaller amounts of Fe, Ni metal, sulfides, refractory oxides, carbonaceous material, up to ~200 ppm presolar silicates (Floss and Stademann 2009a) and other minerals. Organic matter in chondrite matrices is largely insoluble and may be partly or wholly interstellar (Scott 2007). The composition and nature of fine-grained matrix varies within an individual chondrite and from one chondrite to another (Zanda 2004).

**Table 2-3: Matrix abundances in different chondrite groups** (Scott 2007).

Group	Matrix (vol%) <sup>a</sup>
CI	95
CM	70
CO	30
CV	40
CK	75
CR	30-50
CH	5
CB <sub>a</sub>	<5
CB <sub>b</sub>	<5
H	10-15
L	10-15
LL	10-15
EH	<0.1-10
EL	<0.1-10
K	70
R <sup>b</sup>	35

<sup>a</sup>Includes matrix-rich rock fragments, which account for all the matrix in CH and CB chondrites. <sup>b</sup>“Grouplet”

### **Formation**

Matrix is a mixture of materials that formed in diverse locations in the solar nebula. Most crystalline silicates formed in the solar nebula as olivine or low-Ca pyroxene single crystals. Primitive chondrite matrices and cometary interplanetary dust particles (IDPs) are similar concerning their silicates, refractory grains, and organic material, suggesting that chondrite matrices formed from silicate dust that resembled the dust where comets formed and that the silicate and organic components at the two sites had closely related origins (Scott 2007).

It was inferred that matrix silicates like chondrules formed in relatively high-temperature events (*see chapter 2.2.3.3*) based on these features (Scott 2007): i) cooling of both matrix silicates and chondrules in hours from >1300 K, ii) matrix and chondrules are chemically complementary in carbonaceous chondrites (e.g., Hezel and Palme 2010, Bland et al. 2005), and iii) identical minerals in matrices and chondrules in K and EH3 chondrites. As forsterite and enstatite are the main constituents of igneous rims on type I chondrules, and they are also abundant in the matrix of K and EH3 chondrites, it was concluded that chondrite matrix may be a mixture of silicate dust grains from all the regions where the associated chondrules formed (Scott 2007).

## **2.2 Chondrules**

### **2.2.1 Definition of chondrules**

The word chondrule derives from the Greek χονδρός, which means grain. Chondrules were first described by Reichenbach (1860) as “geschiebeartige Knollen und Kugeln”. He proposed that chondrules are small independent meteorites, derived from the breaking up of preexisting stones, and forming a new meteorite. Rose (1864) described chondrules as small granules (“kleine Kugeln”) occurring in a class of stony meteorites.

#### ***Different chondrule definitions***

While Rose (1864), based on macroscopic analysis, did not define chondrules clearly, Tschermak (1885) described chondrules after microscopic analysis as “spheres and rounded bodies consisting of one or several single crystals or often several different minerals may form almost the whole of the stone (L5 Borkut); or they may lie, intact or fractured, in a friable or solid tuffaceous groundmass (L5 Ausson)”.

Chondrules are ferromagnesian silicate objects that show evidence for at least partial melting as a free-floating object before incorporation into meteorite parent bodies (e.g., Scott 2007, Jones et al. 2005, Zanda 2004, Hewins 1997, Grossman et al. 1988). This definition includes fragmented as well as complete spherules, and similar objects that lack droplet form because of incomplete melting, but excludes particles of other compositions like CAIs, basaltic fragments, and melt spherules found in impact and volcanic deposits (Hewins 1997). Chondrules are generally embedded in fine-grained matrix (Polnau et al. 2001). Ideal chondrules are spherical as they solidified from liquid droplets, but most chondrules are not spheres. A significant fraction is present as fragments, some are molded around one another and others are insufficiently melted for surface tension to make them round (Zanda 2004). Chondrules are believed to be derived from liquids crystallized in low gravity in the early solar system (Zanda 2004). Together with CAIs chondrules represent the oldest solids formed in the protoplanetary disk (Connelly et al. 2008).

### **Abundance and size of chondrules in different chondrite groups**

Chondrules are the major component of most chondritic meteorites (e.g., Hutcheon et al. 2009, Lauretta et al. 2006, Jones et al. 2005, Sears 2004, Wasson 1993), reaching up to 80 vol% in enstatite and ordinary chondrites (**Figure 2-3a**). Thus, chondrules account for many bulk properties of a chondrite. CI chondrites did not contain chondrules. It is estimated that  $\sim 10^{24}$  g of chondrules exist in the asteroid belt today. The asteroid belt has been depleted by a factor of  $\sim 1000$ , indicating that there may have been  $\sim 10^{27}$  g of chondrules in the primordial belt. This prevalence of chondrules suggests that chondrule-forming events were widespread in the solar nebula (Morris and Desch 2010).

In 1885 Tschermak described that chondrules vary in size, from as large as walnuts to as small as dust particles, with most about the size of millet grains. More recent studies showed that chondrules are usually sub-millimeter in size and that the average size varies among chondrite groups (e.g., Scott 2007, Weisberg et al. 2006, Jones et al. 2005, Zanda 2004, Hewins 1997) (**Figure 2-3b**). The distribution of chondrule sizes within each chondrite group is log normal, and about 90% of the chondrules have a diameter within a factor 2 of the mean group diameter (Jones et al. 2005), which may indicate aerodynamic size sorting (e.g., Jones et al. 2005, Liffman 2005, Cuzzi et al. 2001). This size sorting may have occurred differently: Chondrule precursors may have been physically sorted according size or already-formed chondrules may have been sorted in the protoplanetary disk or on parent bodies due to regolith mixing. Nevertheless, observed size distributions might also result from the process by which chondrules and their precursors formed in the nebula (Jones et al. 2005).

However, Rubin (2010) suggests that the abundance of dust and the number of chondrule remelting events in different chondrule-forming regions of the solar nebula may have been the most important factors controlling the chondrule size distribution in each chondrite group, and that size-sorting occurred during accretion.

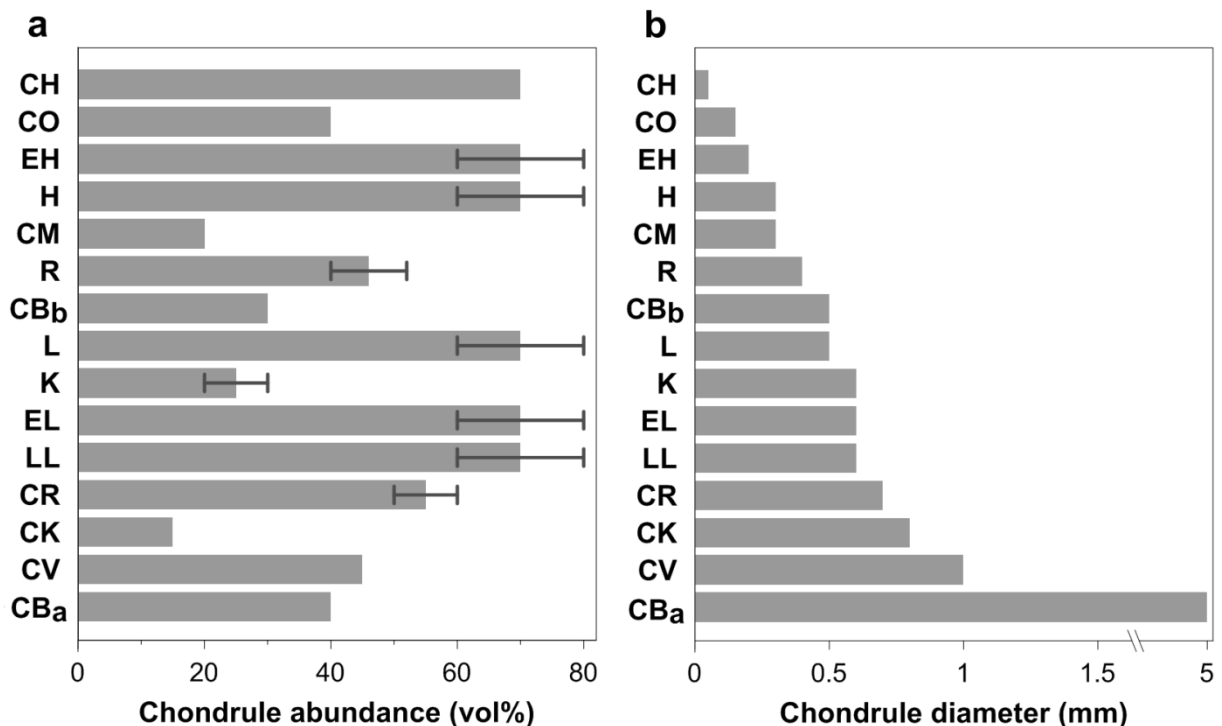


**Figure 2-3: Average chondrule diameter (a) and chondrule abundance (b) for major chondrite groups.** Data are from Scott (2007). Chondrule abundance includes lithic and mineral fragments. Chondrite groups are arranged in order of increasing chondrule diameter.

Based on characteristic properties of chondrules from different chondrite groups, Jones (2012) argued that each chondrite group sampled a unique chondrule reservoir, and that chondrite groups may represent fractions of larger reservoirs that are represented by chondrite classes.

Beside “normal-sized” chondrules there also exist microchondrules and macrochondrules. *Microchondrules* have diameters  $\leq 40 \mu\text{m}$  and occur in ordinary chondrites in fine-grained matrix rims around chondrules in type-3 ordinary chondrites (e.g., Bigolski et al. 2014, Krot et al. 1997) and in CR chondrites for example in dark inclusions (Weisberg et al. 1993). They represent the major chondrule type in CH chondrites with average diameters of  $20 \mu\text{m}$  (Bigolski et al. 2013). *Macrochondrules* having more than 5 mm in maximum dimensions are petrologically similar to average chondrules (Weisberg et al. 1988) and relatively rare (Weyrauch and Bischoff 2012).

### **Mineralogy of chondrules**

The most important minerals in chondrules are (composition of minerals refer to a solid solution) (Jones et al. 2005)

- olivine ( $(\text{Fe}, \text{Mg})_2\text{SiO}_4$ ) with the Mg end-member forsterite (Fo) and the Fe end-member fayalite (Fa)
- pyroxene ( $(\text{Fe}, \text{Mg}, \text{Ca})_2\text{Si}_2\text{O}_6$ ) with the Mg end-member enstatite (En), the Fe end-member ferrosilite (Fs) and the Ca content is given as the wollastonite (Wo) content
- plagioclase (feldspar) ( $\text{CaAl}_2\text{Si}_2\text{O}_8 - \text{NaAlSi}_3\text{O}_8$ ) with the Ca end-member anorthite (An) and the sodium end-member albite (Ab)
- spinel ( $\text{MgAl}_2\text{O}_4$ )
- chromite ( $\text{FeCr}_2\text{O}_4$ )
- troilite (FeS)
- kamacite (Fe-Ni)
- glass (Hewins et al. 2005)

Phenocrysts of aluminium-rich chondrules are typically plagioclase and spinel as well as olivine and pyroxene. The material between mineral grains in a chondrule is called mesostasis consisting of glass and/or very fine-grained crystals (Jones et al. 2005).

### **Diversity of chondrules**

Chondrules are highly diverse in their properties concerning size, texture (porphyritic or non-porphyritic), chemical and isotopic composition, and rims (presence or absence, thickness, composition). The nature and diversity of the chondrules can provide information about conditions in the early solar system and insights into their formation processes (Sears 2004).

## **2.2.2 Classification of chondrules**

Chondrules have been classified according to their texture and/or chemical composition or minor petrographic features of their major phases (**Figure 2-4**). While there has been a long-term trend of textural classification schemes, compositional-based schemes are favored nowadays, because with improved analytical instruments trends became clearer. Also, compositional-based schemes can be applied to a greater variety of chondrules and host chondrites, including metamorphosed chondrites (Sears 2004).

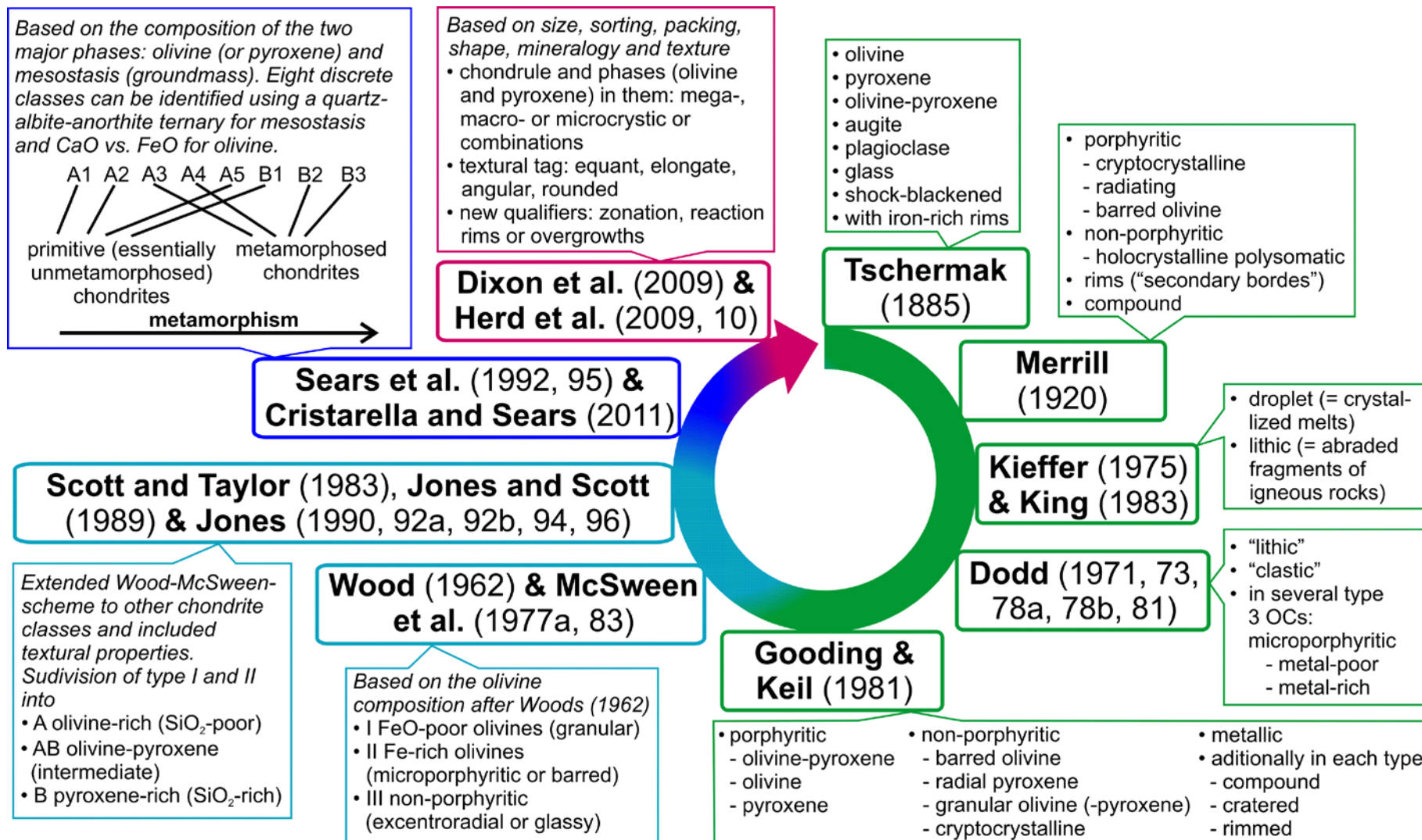


**Figure 2-4: Different classification schemes of chondrules** (adapted after Sears 2004). Textural classification schemes (indicated by green frames) giving way to schemes based on both textural and compositional characteristics (indicated by turquoise frames) and schemes based on the composition of the major phases only (indicated by a blue frame). The most recent classification scheme includes mineralogical, textural and further petrographic features (indicated by a purple frame).



The most often used mineralogical-textural classification scheme is that of Gooding and Keil (1981). Essential textural terms are explained as follows (**Figure 2-5**):

- **Porphyritic texture.** Phenocrysts of olivine and/or low Ca-pyroxene with accessory amounts of sulfides and Ni-Fe metal resides in a mesostasis of glassy to cryptocrystalline material of generally feldspathic bulk composition, which accounts for up to 30-50 vol%. Phenocryst size may range from more than 0.5 of the maximum chondrule diameter downward to nearly that of the larger microlites, which are distinctive components of the mesostasis.
  - *Porphyritic olivine (PO) chondrules (Figure 2-5a)* possess olivine/pyroxene modal ratios  $\geq 10/1$ .
  - *Porphyritic pyroxene (PP) chondrules (Figure 2-5b)* possess olivine/pyroxene modal ratios  $\leq 10/1$ .
  - *Porphyritic olivine-pyroxene (POP) chondrules (Figure 2-5c)* possess intermediate olivine/pyroxene modal ratios.
- **Nonporphyritic texture**
  - *Barred olivine (BO) chondrules* are composed of prismatic olivine crystals that are strongly elongated and occur in parallel orientation (**Figure 2-5d**).
  - *Radial pyroxene (RP) chondrules* consist of fan-like arrays of low Ca-pyroxene radiating from one or more points on the chondrule surface (**Figure 2-5e**).
  - *Granular chondrules* may consist of fine-grained pyroxene (GP) or olivine and pyroxene (GOP) and are characterized by their small grain size and anhedral crystals. Mesostasis occurs usually as patches.
  - *Cryptocrystalline (C) chondrules (Figure 2-5f)* are devoid of recognizable, systematic structure. They may exhibit a pyroxene-like bulk composition. Some C chondrules possess outer shells of very fine-grained silicate material like fine-grained RP chondrules.
  - *Metallic (M) chondrules* are the most rare types of chondrules and consist mostly of Ni,Fe metal, accessory sulfides, phosphates and/or phosphides and oxides and occasional fragments of silicate material. However, Gooding and Keil (1981) point out that the description as “chondrules”, implying a prior existence as self-contained droplet, is much less certain than for other chondrule types.
- **Additional chondrule surface features** can occur in each textural chondrule type.
  - *Compound chondrules (Figure 2-5a)* are attached or partly imbedded in chondrule-like objects of similar size. Mostly a small hemisphere is attached to a large sphere, however, two or more attached hemispheres are also observed sometimes.
  - *Cratered chondrules* exhibit circular, bowl-shaped depressions in their otherwise low-relief surfaces. Both chondrule surface features are believed to have formed by similar events (see *chapter 2.2.3.3*): Compound chondrules can evolve by collision of plastic chondrules, if chondrules partly coalesced, or cratered chondrules, if chondrules separate deflectively (Gooding and Keil 1981).
  - *Rimmed chondrules* are surrounded by distinctive shells or rinds. Concerning the origin of chondrule rims some authors (e.g., Bland et al. 2011, Ormel et al. 2008, Cuzzi 2004, Metzler et al. 1992, Allen et al. 1980) propose a pre-accretionary formation from dust particles, while others prefer a formation on the meteorite parent body (e.g., Trigo-Rodriguez et al. 2006) (*see chapter 2.2.3.3*).

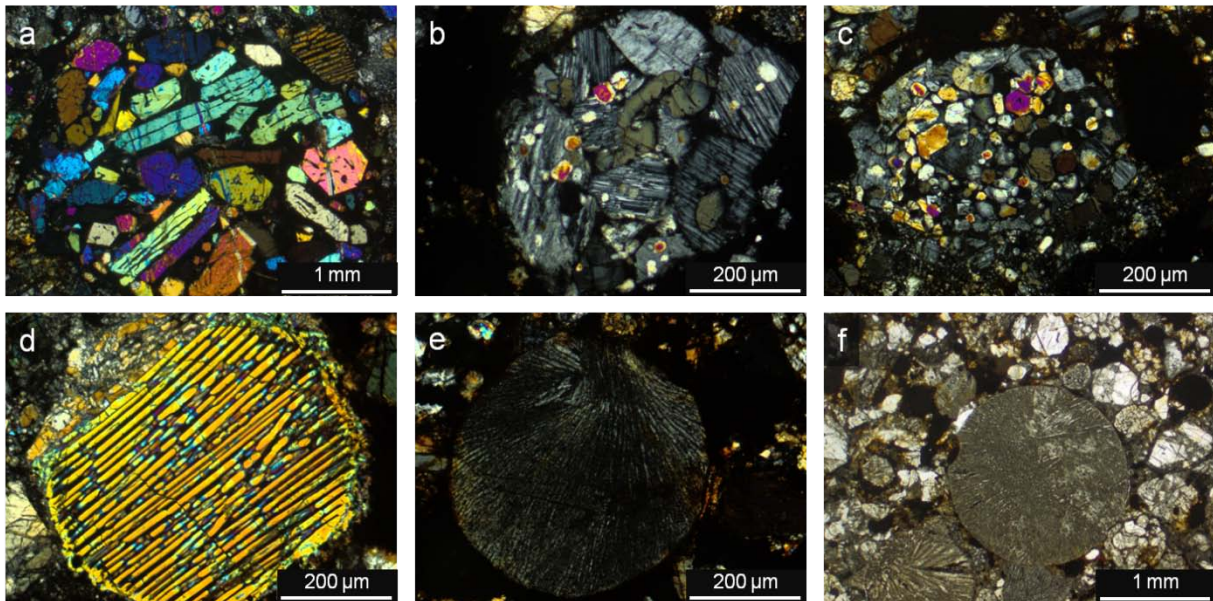
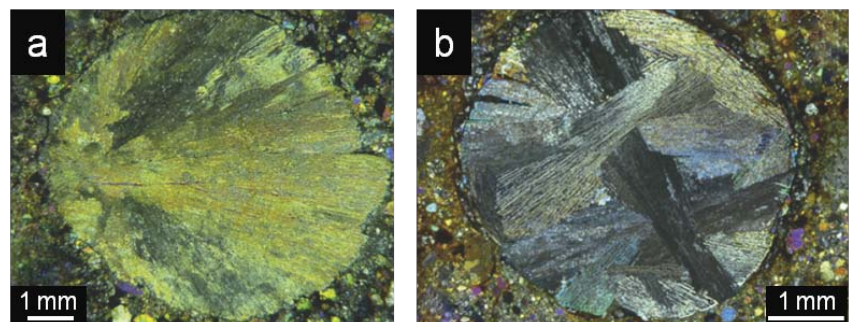


**Figure 2-5: Photomicrographs of textures from selected Dhajala (H3) chondrules according to Gooding and Keil (1981).** (a) – (c) *Porphyritic forms*. (d) – (f) *Non-porphyritic forms*. (a) *Porphyritic olivine chondrule (PO)*, in the upper right region a barred olivine chondrule is attached, thus both represent a compound chondrule, (b) *Porphyritic pyroxene chondrule (PP)*, (c) *Porphyritic olivine-pyroxene chondrule (POP)*, (d) *Barred olivine chondrule (BO)*, (e) *Radial pyroxene chondrule (RP)*, (f) *Cryptocrystalline chondrule (C)*. Transmitted light, crossed polars (a-e) and plain-polarized light (f). Photos were taken by J. Weinauer.

For normal-sized chondrules porphyritic textures (PO, PP, POP) are generally more common than non-porphyritic textures (BO, RP, GP, GOP, C, M). Both textural types seemed to have formed in different physical environments. Higher relative abundances of compound and cratered chondrules of non-porphyritic chondrules, for instance, have led to a (model-dependent) suggestion for higher number densities (chondrules per unit of space) during formation of non-porphyritic chondrules. Chondrule size and shape do not depend on textural type, supporting the inference that porphyritic and non-porphyritic chondrules originated as molten or partly molten droplets (Gooding and Keil 1981).

In contrast to normal-sized chondrules of most chondrite groups (except CH and CB chondrites), porphyritic textures are less abundant in macrochondrules. For a better description of large chondrules new textural subtypes were defined, including radial olivine-pyroxene (ROP) or multi-radial olivine-pyroxene (MROP) chondrules (**Figure 2-6**) (Weyrauch and Bischoff 2012).

**Figure 2-6: Non-porphyritic macrochondrules in chondrites** (adapted after Weyrauch and Bischoff 2012). (a) *Radial olivine-pyroxene chondrule (ROP)* within Bluff (L5). (b) *Multi-radial olivine-pyroxene chondrule (MROP)* within Hammadah al Hamra 093 (LL3). Transmitted light, crossed polarizers.



Textural properties can be used to draw constraints on the conditions of chondrule formation (Gooding and Keil 1981). From igneous textures it has been concluded that chondrules were “flash-heated” from low temperatures to above their liquidus and then cooled at a rate slow enough to allow crystals to form (Desch et al. 2012). Droplet chondrules (Kieffer 1975) suggest a rapid or disequilibrium crystallization of free-floating droplets, whereas less perfect circular objects with more porphyritic texture (lithic chondrules, e.g., Kieffer 1975, Dodd 1978a, b, 1981) may have been mechanically derived from porphyritic or coarsely granular parent rock without passing through a liquid droplet stage (Dodd 1978a).

Rubin (2010) suggested that remelting processes would be responsible for reducing the proportion of radial pyroxene (RP) and cryptocrystalline (C) chondrules relative to porphyritic chondrules. Remelting of RP and C chondrules surrounded by dust would tend to produce porphyritic chondrules, because small dust particles mixed with the melt provide nuclei for crystallizing phenocrysts (Rubin 2010).

However, the majority of mineralogical-textural classifications (green highlighted in **Figure 2-4**) is based on the analysis of chondrules from ordinary chondrites of type 3 to 4, thus defining primary (formational) rather than secondary (recrystallization or alteration) textural types (Gooding and Keil 1981). As there are differences between chondrules of carbonaceous and ordinary chondrites (e.g., McSween 1977a), application of these mineralogical-textural classifications on chondrules of carbonaceous chondrites, especially metamorphosed (type >4) ones, is critical.

Wood (1962) and McSween et al. (1977a, 1983) introduced the first compositional-based classification scheme (see **Figure 2-4**), where chondrules were classified according to their olivine composition into types I to III. The scheme by Scott and Taylor (1983), Jones and Scott (1989) and Jones (1990, 1992a & b, 1994, 1996) (see **Figure 2-4, 2-7**) is based on compositional and textural features; adapted and extended the Wood-McSween-scheme by subdividing types I and II in A (SiO<sub>2</sub>-poor, i.e. olivine-rich), AB and B (SiO<sub>2</sub>-rich, i.e. pyroxene-rich). Types I and II were defined according to the olivine/pyroxene ratio, which depends on the SiO<sub>2</sub> content and the thermal history (Hewins et al. 2005), and according to the FeO contents in their olivines similar to McSween (1977a) and McSween et al. (1983) (**Table 2-4**). Type I (magnesian) chondrules are volatile-depleted, reduced and often metal-bearing, whereas metal is absent from volatile-rich type II (ferroan) chondrules in which Fe is oxidized within the silicates or in sulfides (Zanda 2004). More precisely, olivines in type I (low-FeO) chondrules contain <10% Fa, while much more zoned olivines in type II (high-FeO) chondrules contain >10% Fa. Furthermore, low-FeO porphyritic olivine chondrules have

**Table 2-4: Chondrule classification extended from McSween (1977a) and Jones (1994) applying composition names to all textural types** (Hewins 1997).

Type	Subtype		Textural varieties
I (FeO-poor, olivine Fa < 10%)	IA	ol > 80%*	(BO, PO), MPO, GO, DZ
	IAB	intermediate	RPO, POP, GOP, DZ
	IB	px > 80%	RP, PP, GP, DZ
II (FeO-rich, olivine Fa > 10%)	IIA	ol > 80%	BO, PO, (MPO, GO), DZ
	IIAB	intermediate	RPO, POP, GOP, DZ
	IIB	px > 80%	RP, PP, GP, DZ

*Textural varieties are given according to Gooding and Keil (1981). First letter: B - barred, R - radiating, P - porphyritic, MP - microporphyritic, G - granular, DZ - dark zoned. Second and third letter: O - olivine, P - pyroxene. Types in parentheses are less common. \* Olivine/(olivine+pyroxene) volume ratio.*

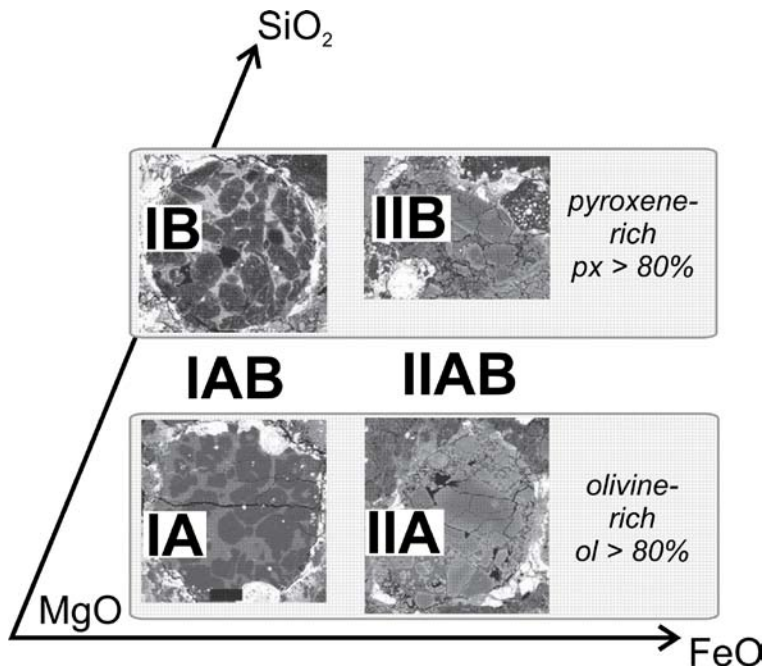
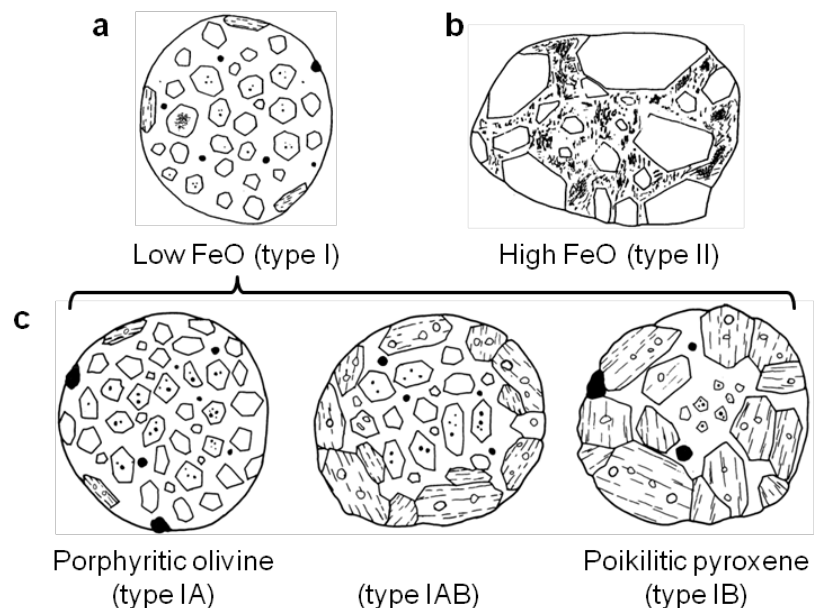


**Figure 2-7: Classification of chondrules according to Scott and Taylor (1983), Jones and Scott (1989) and Jones (1990, 1992a & b, 1994, 1996) placed in a  $\text{MgO-SiO}_2\text{-FeO}$  triangle showing the relative Mg, Fe and Si contents** (adapted after Hewins and Zanda 2012). *Back scattered electron images of Semarkona chondrules: IA and IB 0.7 mm wide, IIA 0.6 mm wide and IIB 0.8 mm wide. ol and px describe volume ratios according Hewins (1997).*

conventionally been called type IA, and poikilitic pyroxene chondrules type IB (Hewins 1997). Most chondrules in carbonaceous chondrites are type I chondrules, whereas ordinary chondrites are largely dominated by type II chondrules (Zanda 2004).

Type I chondrules (**Figure 2-8a**) tend to be more variable in their textural characteristics than type II chondrules (**Figure 2-8b**); they are usually rounder, contain smaller olivines, more Fe,Ni metal (opaque spherules), and clearer (sometimes sparse) mesostasis. Elongated low-Ca pyroxenes might occur at the periphery. Low-FeO chondrules range from porphyritic-olivine chondrules (type IA) with minor twinned clinopyroxenes on their rims to poikilitic pyroxene chondrules (type IB) with minor olivine as euhedral phenocrysts in their cores and chadocrysts in the twinned clinopyroxenes (**Figure 2-8c**); in many meteorites intermediate types (type IAB) are common (Scott and Taylor 1983).

**Figure 2-8: Schematic diagram showing petrographic distinctions between low-FeO (type I) (a) and high-FeO (type II) (b) porphyritic olivine chondrules and sequence of low-FeO chondrules ranging from porphyritic olivine chondrules (left, type IA) to poikilitic pyroxene chondrules (right, type IIB)** (adapted after Scott and Taylor 1983). *Transmitted light.*



The most recent classification scheme (see **Figure 2-4**) introduced by Dixon et al. (2009) and Herd et al. (2009, 2010) is based on size, sorting, packing, shape, mineralogy and textures of chondrules and phases within them. This classification was tested and extended on polished thin sections of Saratov (L4). It is proposed to be generally applicable to all ordinary chondrites with well preserved chondrules (i.e. type 3 and 4) and at least partially applicable or extendible to all chondrites and might discriminate among different textural types far better than the long-standing mineralogical-textural classifications.

### 2.2.3 Chondrule formation

Although chondrules were first described over 150 years ago (Reichenbach 1860) and extensive studies were performed on chondrules since then, different aspects of chondrule formation, including origin and properties of precursor material, chondrule-forming mechanism and behavior at crystallization (open or closed system), are still actively debated.

#### 2.2.3.1 Chondrule precursors

Chondrules are believed to have formed by rapid melting of pre-existing nebula materials (e.g., Wasson 1993), commonly called precursors or precursor aggregates (“dustball”) (**Figure 2-9a**) composed of anhydrous minerals, predominantly fine-grained olivine (<5  $\mu\text{m}$ ), and lesser amounts of pyroxene, feldspathic glass, chromite, metal, and sulfide (Lauretta et al. 2006). Hezel and Palme (2007) excluded the formation of chondrules from fine-grained “dustballs” and proposed that chondrules rather formed from coarse-grained precursor aggregates with variable amounts of  $\mu\text{m}$ -fine matrix material. Larger silicate grains in the precursor material are mostly derived from previous generations of chondrules and/or they are condensation grains (Jones et al. 2005).

The identification of the materials from which chondrules were made can provide information about nebula events and processes prior to chondrule melting (Hewins 1997). As the present chemical composition of chondrite matrix is too iron-rich, it is not considered as direct chondrule precursor material (Jones et al. 2005). Furthermore, chondrules in carbonaceous and ordinary chondrites are very diverse and could not have been formed simply by melting their bulk matrix material (Scott 2007). Hewins and Zanda (2012) proposed that chondrules could be made either by modifying a ferroan precursor primary by evaporation or reduction or a magnesian precursor primary by condensation given the dispersions of  $\text{MgO-SiO}_2\text{-FeO}$  composition (see **Figure 2-7**). Fine-grained material within the precursors of various chondrules as well as the properties of skeletal blebby (barred) olivine and cryptocrystalline chondrules in CH chondrites and the presence of granoblastic olivine aggregates suggest that chondrules are unlikely to have formed by a unique mechanism and from a single type of precursor. Additionally, it is likely that the precursors of ordinary chondrite chondrules contained sulfur (S), whereas most of those for chondrules in carbonaceous chondrites did not. Thus, for ordinary chondrites Hewins and Zanda (2012) deduced a mildly ferroan dustball precursor for many type I chondrules, and evaporation as a dominant process.

There was a great diversity in bulk chemical and oxygen isotopic composition of precursor aggregates, resulting in a wide range of compositions in a given region of the solar nebula. Differences among precursors may vary with time and/or space, and recycling of previous generations of chondrules may contribute to precursor heterogeneity (Jones et al. 2005).

Assuming closed system behavior of chondrules and mixing of heterogeneous precursor grains as only reason for the scatter in chondrule bulk chemical composition, Hezel and

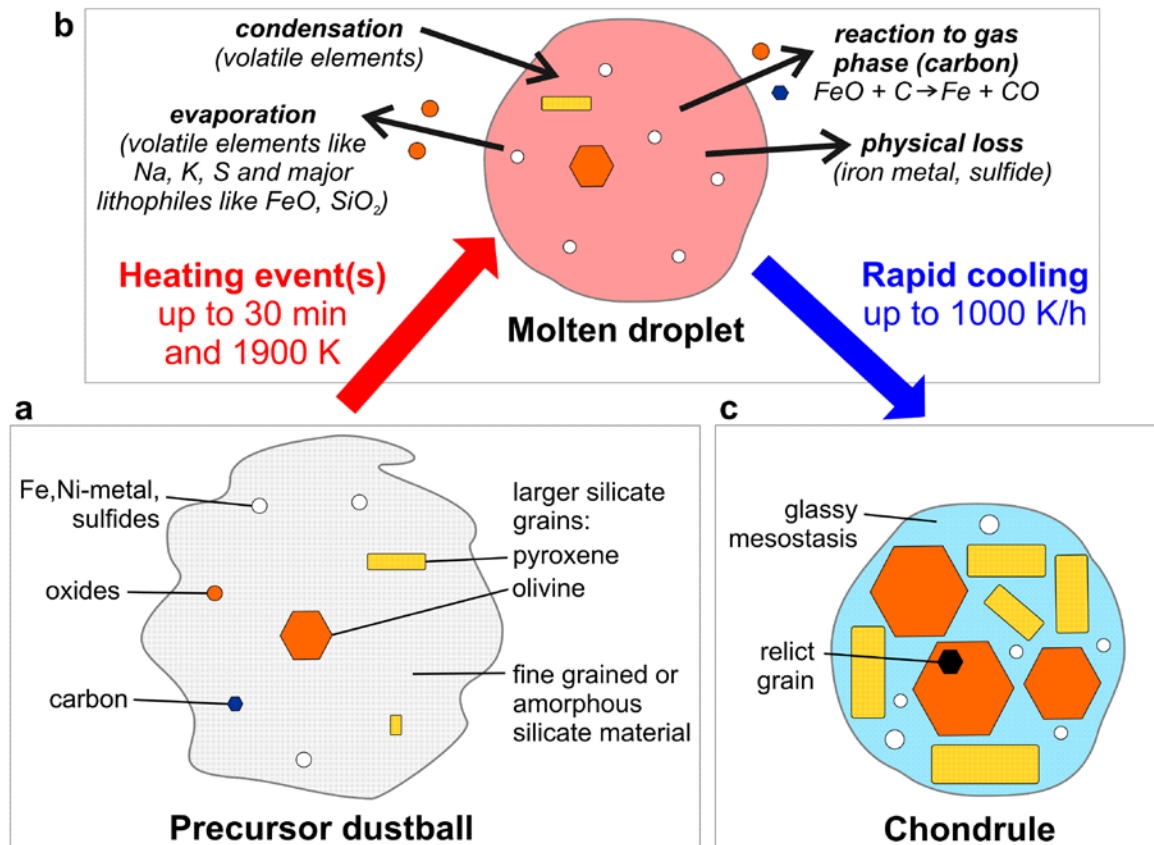


**Figure 2-7: Formation of a chondrule** (adapted after Jones et al. 2005). *The precursor aggregate (dustball) (a), consisting of different compositional features, is heated up to build a molten droplet (b) which might show open system behavior. Finally, by rapid cooling a chondrule solidifies (c).*

Palme (2007) concluded that not more than ~10 precursor grains each with 100 μm in diameter should contribute to a single chondrule.

When the precursor material melts, Fe-Ni-S droplets are immiscible in the silicate liquid and larger silicate grains are partly dissolved (Jones et al. 2005). The degree of melting mainly determines textural chondrule properties. Radial pyroxene (RP) or cryptocrystalline (C) chondrules for instance probably formed at superliquidus temperatures by complete melting from nuclei-free melts or in presence of a few small dust grains triggering rapid crystallization (Rubin 2010). In contrast, porphyritic chondrules require the presence of more heterogeneous nuclei in the liquids, and are thus possibly the result of incomplete melting and certainly of less superheating resulting in numerous relatively large crystals. However, for most easily melted chondrules (the most FeO- and SiO<sub>2</sub>-rich, i.e. type IIB) were probably superheated and crystals subsequently nucleated by collision with dust grains (Hewins 1997).

Alternatives to the formation of chondrules from precursor aggregates are

**i) Formation by *condensation of liquids* from a dust enriched gas.**

Ebel and Grossman (2000) noted that liquids with compositions close to those of chondrules could be stable in local environments with high total pressures or high partial pressures of the relevant elements, providing an explanation for the absence of Rayleigh distillation induced isotopic fractionations in chondrules. Additionally, the extreme variety of compositions of chondrules in CHs can apparently only be explained by fractional condensation (e.g., Varela et al. 2011, Krot et al. 2000a).

ii) Formation as frozen droplets of **spray from impact plumes** launched by collision of molten (due to intensive heating by  $^{26}\text{Al}$  decay) planetesimals (*splashing model*).

Sanders and Scott (2012) inferred that chondrule production by splashing would have continued as long as molten planetesimals with a thin crust were colliding and merging (~0.3 to ~2.5 Ma after CAI formation). They conclude that “splashing” is reconcilable with many features of chondrules.

### 2.2.3.2 Open or closed system behavior during chondrule formation?

To understand the origin and evolution of chondrules, it is necessary to separate the effects of initial crystallization and subsequent alteration within individual chondrules. Crystallization may have taken place in an open or closed system. In a closed system olivine and pyroxene crystallized in situ from a melt corresponding to the bulk composition of the chondrule without interaction with the surroundings, whereas in an open system the chondrule droplet may have interacted with the nebula gas and/or dust (Jones and Scott 1989). Hewins and Zanda (2012) noted that it is unlikely that chondrule melts behave as closed system in low pressure nebula gases, whereas this is more likely in planetary settings.

If a chondrule is molten and behaves as an open system, chemical and isotopic changes can take place as a result of interactions with the surroundings (*see chapter 5.1.1*), including condensation and evaporation of volatile elements, reaction with the gas phase as well as physical loss (**Figure 2-9b**) (Jones et al. 2005). In contrast, a closed system behavior of chondrules required a flash heating mechanism in order to avoid interactions with the nebula gas. The chondrule formation then would have little effect on the chondritic matter aside from textural properties, and no connection to the chemical and isotopic differences between CI meteorites and other chondrite classes. In the past, most researchers have assumed that chondrules formed as closed systems (e.g., Alexander et al. 2008), however recently a growing number are challenging this view and are arguing for open system behavior based on the comparison of chondrule chemistry and texture. For instance, in type I chondrules of ordinary chondrites an inverse correlation between grain size and volatile content was found: Finest (least melted) chondrules have Mg-normalized bulk compositions close to that of CIs and contain no metal but abundant Ni-bearing Fe-sulfide, whereas typical coarse-grained chondrules are volatile-depleted and metal-bearing (Zanda 2004). Furthermore, Schrader et al. (2013) proposed that type I and type II chondrules in CR chondrites experienced exchange with isotopically slightly distinct gaseous reservoirs.

### 2.2.3.3 Chondrule heating event(s)

#### **Temperature and duration**

Thermal histories of chondrules suggest rapid heating of chondrules, if the retention of volatiles is diagnostic of cooling rates, reaching peak temperatures between 1750-2370 K (1750-2100 K for porphyritic and 1820-2370 K for barred olivine and radial chondrules) (Desch et al. 2012). Assuming shocks as chondrule-forming mechanism it was proposed that solids will be pre-heated ahead of the shock in the pre-shock region due to the propagation of a radiation front originating in the hot post-shock region (**Figure 2-10**). Temperatures in the pre-shock region will exceed the liquidus temperatures of solids (~1400 K), and evaporation will occur. Models can be constructed that allow pre-heating to  $\geq 1300$  K to last less than 30 minutes, thus preventing isotopic fractionation of sulfur (Morris and Garvie 2013, Morris and Desch 2010).

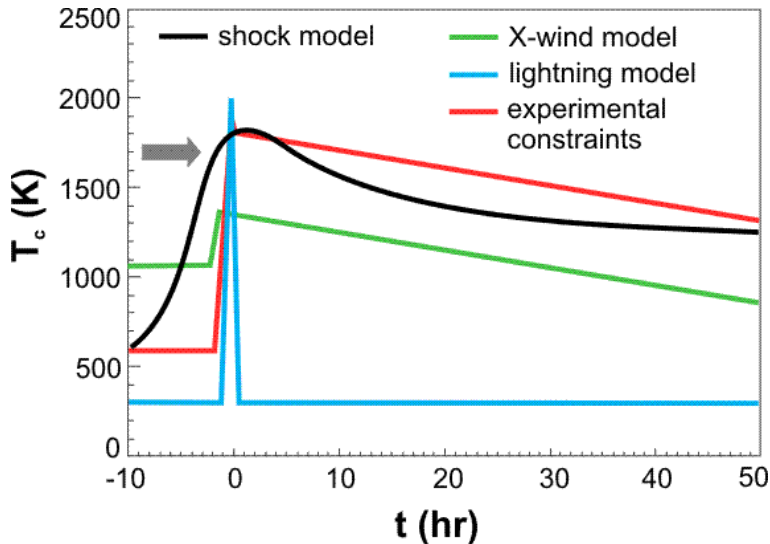


**Figure 2-8: Chondrule thermal histories inferred from experimental constraints and predicted by different models** (Desch et al. 2012). Sources: experimental constraints – Desch et al. (2012), shock model - Morris and Desch (2010), X-wind model – Shu et al. (2001, 1996), lightning model – e.g., Desch and Cuzzi (2000). The arrow indicates the region above with evaporation occurs.

### Energy sources

Concerning a possible energy source there is strong support for a flash heating origin of chondrules in the protoplanetary disk (Hewins 1997). Shocks in the solar nebula are the most generally accepted chondrule-forming model (e.g., Morris and Desch 2010, Alexander et al. 2008, Scott 2007), because it has been shown that millimeter-sized silicate grains in the nebula could have been heated during passage of a shock wave and cooled at the rate inferred from laboratory experiments. Furthermore, in the nebular shock model one expects most chondrules to have porphyritic textures as observed (Scott 2007). Nevertheless, there are a large number of other potential chondrule-forming mechanisms (**Table 2-5, Figure 2-10**) having all unresolved issues, however. Still, the driving force of shocks (e.g., spiral shock waves early and at large distances from the sun, mechanically dissipating solar energy or later shocks due to clump infall) is not clearly known (Hewins 1997). The generation of shocks in the nebula is possible in a variety of different ways, including gravitational instabilities in the disk, asteroids in eccentric orbits, proto-Jupiter, and planetary embryos (Scott 2007). Most recently nebula shocks driven by eccentric planetesimals and nebula shocks driven by diskwide gravitational instabilities have been noted as possible energy source for the chondrule forming process, the latter being somewhat favored (Morris and Desch 2014, Desch et al. 2012).

**Table 2-5: Different chondrule-forming models** (Hewins 1997).

Chondrule model	Arguments against
Hot inner nebula	Cooling time too long, chondrule movement too slow
Lightning	Ionization prevents charge build-up, dust reduces energy
Impact	Generates clasts, agglutinates, not rims; high relative velocities too low
Meteor ablation	Atmospheres hard to retain on asteroids, high relative velocity needed
Magnetic fields	Ionization too low for field generation, precursors have to be lofted very high
Fu Orionis events	Cooling over months, very close to sun
Bipolar overflows	T = 10,000 K; droplets would hover very close to sun
Accretion shocks	Grain aggregates in interstellar medium, very high accretion rates needed
Nebular shocks	Caused by clumps, outbursts, or spiral?



### **Multiple heating events**

There is widespread evidence for multiple heating events and recycling, especially in porphyritic chondrules, including relict grains, igneous rims and arguably enveloping compound chondrules (Jones et al. 2005) (**Figure 2-11**). All these features likely result from collisions involving chondrules that were molten or partly molten. Half of CV chondrite chondrules and more than 10% of ordinary chondrite (OC) chondrules have igneous rims, and about 15% of chondrules have relict grains (Scott 2007).

Many chondrule rims have materials that are distinct from the chondrule host. There are two main types of rims, depending on the size and composition of their grains (Jones et al. 2005):

- *Fine-grained rims* are composed of aggregates of (sub-)micrometer grains of FeO-rich, silicate minerals, Fe,Ni metal, and sulfides. Their size and composition is similar to fine-grained chondrule matrix and they are common in CM, CO and CV chondrites (Jones et al. 2005).
- *Coarse-grained igneous rims* are composed of material that was heated and melted after melting of the host chondrule. These rims are generally more FeO-rich than the host chondrule, and are common in CV and CR chondrites (Jones et al. 2005) as well as H-L-LL3 and CO3 chondrites (Rubin 1984).

Most authors conclude that chondrule rims were acquired in the nebula (e.g., Bland et al. 2011, Ormel et al. 2008, Cuzzi 2004, Metzler et al. 1992, Allen et al. 1980). Fine-grained rims may have formed from highly porous, low-temperature, FeO-rich dust, in which the chondrule became embedded in the nebula after cooling. Afterwards, the dust was most likely compacted around the chondrule to become a rim after accretion to the parent asteroid (Jones et al. 2005). For igneous rims, however, Trigo-Rodriguez et al. (2006) proposed an asteroidal formation. Scott (2007) notes that the truth in all likelihood lies between these extremes: Transient fluffy rims may have been formed in the nebula, whereas permanent rims were likely formed during the earliest stages of planetesimal growth from chondritic materials.

Morris and Garvie (2013) concluded that a minimum particle size (core plus dust rim) of ~200  $\mu\text{m}$  is required to retain an igneous rim upon subsequent heating; dust rims around smaller particles would evaporate completely. This calculation is based on modeling including petrographic measurements of chondrules and assuming chondrule forming conditions (Morris and Desch 2010, Tachibana and Huss 2005) with a beginning core and rim radius given by the relationship found by Paque and Cuzzi (1997). In the study by Krot and Wasson (1995) all chondrules were >450  $\mu\text{m}$  in diameter. Compound chondrules with igneous rims were over 200  $\mu\text{m}$  in radius, with one exception (175  $\mu\text{m}$  radius) (Wasson et al. 1995).

#### **2.2.3.4 Cooling of the chondrule droplet**

When the molten chondrule droplet cools (**Figure 2-9c**), silicate grains grow, grains that survived melting (relict grains) are incorporated into the melt-grown grains, and Fe-Ni-S melts solidify to metal and sulfide phases (Jones et al. 2005). The abundance of nuclei, acting as seeds for crystal growth, depends on the peak temperature and the duration of the heat pulse (Hewins et al. 2005).

In laboratory experiments cooling rates between 1°C/h (linear) and 5000 °C/h (exponential curve declining to 500°C/h) have been used to grow zoned olivine crystals, whereby olivine zonation is restricted to low cooling rates in bulk compositions, which permits pyroxene nucleation and growth (Hewins 1997). Zanda (2004) suggests cooling rates for chondrules

between 10 and 1000 °C/h, which is much slower than the radiative cooling of isolated spherules in free space, and much faster than global nebula cooling, which is considered as an evidence that chondrules were formed in large quantities embedded in hot gas. More recently Desch et al. (2012) proposed very rapid cooling rates at  $10^3$ - $10^4$  K/h from their shock model, whereby the chondrules spent no more than 10 minutes above their liquidus temperature. After they cooled several hundred K, chondrules crystallized over a range of temperatures  $\approx$ 1400-1800 K, at rates that were probably different for different texture types (BO chondrules  $\sim 10^3$  K/h, porphyritic chondrules  $10$ - $10^3$  K/h) (Desch et al. 2012).

To permit retention of most of the Na and of at least some S as observed in many chondrules, especially in type IIs, “almost quenching” was suggested (Wasson 1993). However, slow cooling rates might also be acceptable, if the chondrule melt became stabilized by local concentrations of dust in the nebula due to evaporation during heating, resulting in a liquid-gas equilibrium, as suggested by Wood (1996). In any case, heating and cooling during chondrule formation were probably rapid, because large relict grains were not dissolved in the melt (Hewins 1997).

Since the favored heating mechanism involves friction during the rapid passage of a shock wave (e.g., Morris and Desch 2010), the cooling rate represents a possible indicator of the scale of the heating event, or at least of the size of chondrule concentration heated in that event (Hewins 1997).

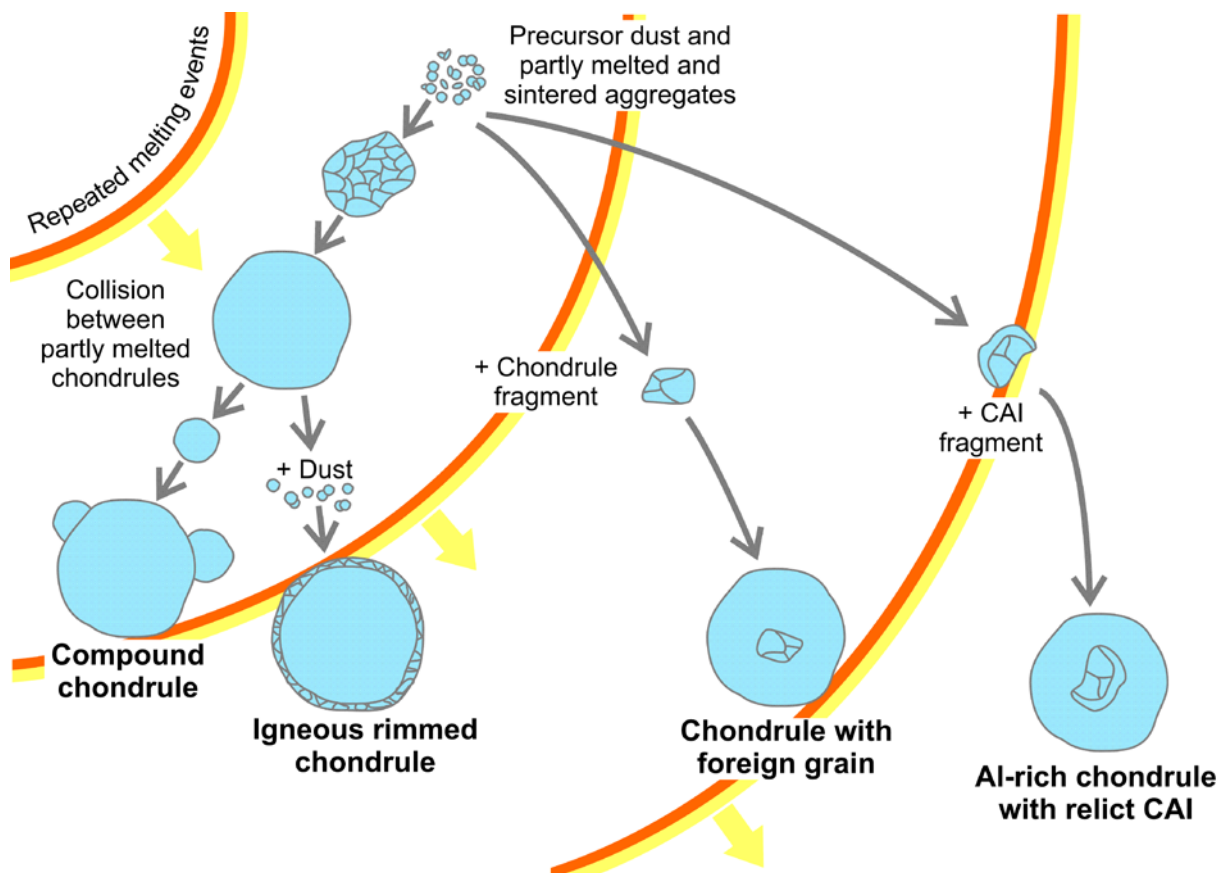


**Figure 2-9: Sketch showing the processes involved in chondrule formation** (adapted after Scott 2007). Heating and melting of dust as well as growth by collisions between solid particles and melted or partly melted objects are important processes causing the formation of compound chondrules, igneous rims, foreign grains in chondrules and relict CAIs in Al-rich chondrules.

### 2.2.3.5 Different chondrule types and their formation

Whether type I and type II chondrules were formed from different precursors in the solar nebula or from one precursor under changing conditions in the solar nebula is still a matter of debate.

On the one hand, Scott and Taylor (1983) suggested that type I (FeO-poor) and type II (FeO-rich) chondrules (see *chapter 2.2.2*) may have formed under different oxidation-reduction conditions based on the inverse relationship between the abundance of metallic Fe, Ni and FeO in porphyritic olivine chondrules. Both types could not have formed from one precursor material, because addition or subtraction of FeO would affect the olivine/pyroxene ratio. They suggest, therefore, that the precursor materials for type I and type II chondrules were sorted, producing regions in the solar nebula with materials of rather uniform composition. However, these regions were not large enough or far enough apart to preclude a few percent of hot colliding chondrules from having very different compositions (Scott and Taylor 1983). Hewins and Zanda (2012) proposed granoblastic olivine aggregates and fine-grained (dustball) precursors for type I chondrules, while, based on the presence of forsteritic relicts, they argue for polymict dustball precursors for type II chondrules. They inferred that the less abundant type II chondrules in carbonaceous chondrites were probably added late to batches of type I chondrules from different oxygen isotopic reservoirs.

If, in fact type I and II chondrules formed in different environments, this suggests that chondrule formation was a repetitive process, which involved mixing of materials from diverse sources (Scott 2007).

Some other researchers do not exclude the formation of both chondrule types from the same precursor material, however. Solid material condensing from the nebula gas would become more oxidized as the system cools as predicted by the condensation sequence: Early, high-temperature condensates are dominated by Fe metal and MgO-rich silicates, whereas lower-temperature condensates would include FeO-rich silicates (Jones et al. 2005). For example, the equilibrium Fa of olivine in contact with metal ( $\approx 90\%$  Fe,  $\approx 9\%$  Ni) is 4 mol% at 600 K and 15 mol% at 500 K, and kinetic effects will cause lower mean values at these temperatures (Wasson et al. 2000). Therefore, chondrule formation at temperatures above 500-600 K is expected to produce low FeO chondrules and chondrules with Fa > 9 mol% must have formed at temperatures below 500-550 K. While in addition some reduction of FeO may have occurred during chondrule formation, this has probably had only minor effect on the FeO/MgO ratio (Wasson et al. 2000). A progressive change in oxidation stage of chondrule precursors with time is considered to be consistent with some evidence that FeO-rich (type II) chondrules are younger than FeO-poor (type I) chondrules (Kunihiro et al. 2004) and that carbon (C) is an order of magnitude more abundant in FeO-poor chondrules than in FeO-rich ones (Hanon et al. 1998). However, evidence contradicting this scenario is provided by Semarkona type I chondrules, containing sulfur in the form of FeS, a low-temperature compound (Hewins et al. 1997).

Supporting the case for common precursors, Schrader et al. (2013) suggest that type II chondrule precursors may have consisted of a mixture of type I chondrules or chondrule fragments and finer-grained material of unknown oxygen-isotope composition. This suggestion is based on the observation of similar oxygen-isotope compositions in relict magnesian olivine grains in type II and type I CR chondrules, and the existence of type II-like ferroan igneous rims around some type I porphyritic chondrules in CR chondrites (Schrader et al. 2013).

### 2.2.3.6 Setting of chondrule formation

Chondrules may have formed either as “free-floating wanderer in the disk”, but they may also have been “by-product of collisions of early-formed planetesimals” (Connolly 2012). Both these hypotheses are currently viable (Connolly 2012). It is commonly believed that chondrules formed in the solar nebula rather than in a planetary / asteroidal environment (e.g., Hutcheon et al. 2009, Hewins 1997), although the latter idea is gaining more support now than 30 years ago (Connolly 2012). Assuming a formation in the solar nebula, chondrule formation in the dusty midplane seems indicated (e.g., Cuzzi and Alexander 2006, Alexander et al. 2008), because very little coarse dust is expected to reach levels high above this plane (Wasson 1993). This is not a safe assumption, however, since Cuzzi et al. (1996) argue that turbulence would have prevented settling of dust aggregates towards the midplane. Transformation of precursor dust aggregates into chondrules significantly changed their aerodynamic properties, resulting in concentration of chondrules in stagnant zones between eddies and sinking to the midplane (Cuzzi et al. 1996).

Bulk samples of carbonaceous chondrites have always CI chondritic Mg/Si ratios, whereby chondrules are having super CI chondritic and matrices are having sub CI chondritic ratios. Hezel and Palme (2010), who noted this complementarity, conclude that chondrules and matrix are chemically connected as both formed from the same chemical reservoir by similar processes. Separate origins of chondrules and later mixing of chondrules and matrix as well as redistribution of Mg and Fe between chondrules and matrix or leaching of Si from chondrule mesostasis into the matrix on the parent body were excluded by these authors. Instead, the Mg/Si complementarity was suggested to have been established in the nebula before parent body accretion by the extraction of a Mg-rich component from a CI chondritic component. This Mg-rich component then served as precursor for chondrules, leaving behind Mg-depleted material, the parent material of matrix (Hezel and Palme 2010).

Oxygen isotopic compositions of chondrules from different chondrite classes suggest that they were formed from different nebular reservoirs. It was further inferred that the oxygen isotopic composition and presumably the chemical composition also well reflect the diverse composition of the material that were assembled and melted as well as the exchange between chondrule melt and  $^{17,18}\text{O}$ -rich nebula gas (Scott 2007).

Rubin (2010) proposed that chondrite groups with large chondrules (CV, CK, CR) were typically surrounded by thick dust-rich mantles that formed in locally dusty nebula regions.

### 2.2.3.7 Timing of chondrule formation

#### ***Chondrule ages relative to CAIs***

The timing of chondrule formation has been inferred to be ~1 and ~3 Ma after the formation of the oldest CAIs (**Figure 2-12**) based on Pb-Pb absolute ages (e.g., Amelin et al. 2002, Connelly et al. 2008) and the relative chronometer using the extinct nuclide  $^{26}\text{Al}$  (e.g., Russell et al. 1996, Kita et al. 2000) (Kita and Ushikubo 2012). Alternatively, older chondrules might be erased by chondrule recycling processes (Kita et al. 2000, 2005).

Amelin et al. (2002) inferred that between the formation of CV CAIs and CR chondrules  $2.5 \pm 1.2$  Ma elapsed and that CAI- and chondrule-forming events continued for at least 1.3 Ma. Ferromagnesian chondrules in LL3.0, CO3.0 and Acfer 094 formed 1-3 Ma after CAIs based on  $^{26}\text{Al}$ - $^{26}\text{Mg}$  isochron ages (Kita et al. 2005). Al-Mg studies of relict CAIs in chondrules indicate a period of  $\geq 2$  Ma between CAI and chondrule formation (Scott 2007).

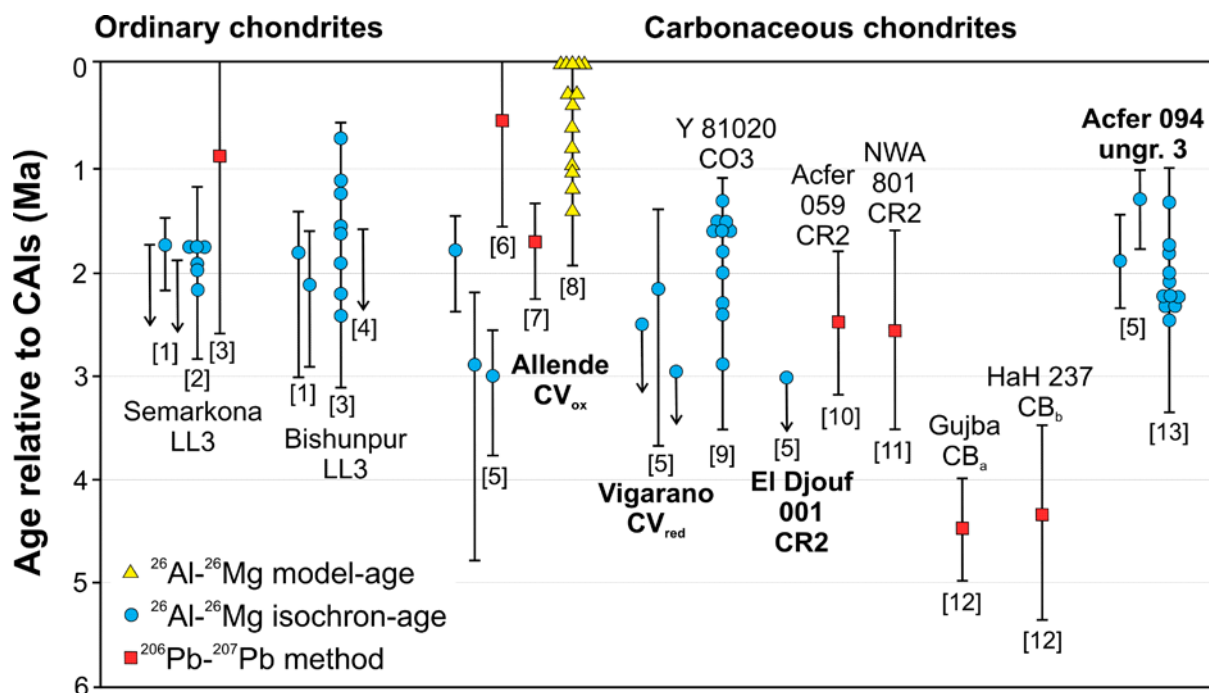


**Figure 2-10: Formation ages of chondrules from ordinary and carbonaceous chondrites relative to CAIs** (adapted after Scott 2007). Chondrule ages are inferred from the Al-Mg and U-Pb isotopic system given the Pb-Pb age of CAIs from CV Efremovka (4567.2 Ma) from Amelin et al. (2002) and an initial  $^{26}\text{Al}/^{27}\text{Al}$  ratio in CAIs of  $5 \times 10^{-5}$  (Kita et al. 2005). Meteorites indicated by bold letters were analyzed in this study (see chapter 4.1.1). Abbreviation: Y-Yamato. Sources of data: [1] McKeegan et al. (2000), [2] Kita et al. (2000), [3] unpublished data of Amelin and coworkers cited by Kita et al. (2005), [4] Kurahashi et al. (2011), [5] Hutcheon et al. (2009), [6] Amelin and Krot (2007), [7] Connelly et al. (2007), [8] Bizzarro et al. (2004), [9] Kurahashi et al. (2004), [10] Amelin et al. (2002), [11] Charles and Davis (2010), [12] Krot et al. (2005), [13] Ushikubo et al. (2010).

As some chondrules contain small inclusions of CAI material and some CAIs have been modified by a second (flash heating) event, it can be inferred that most CAIs were formed before chondrules and in some cases CAIs were reheated in a chondrule-forming event (Hewins 1997 and references therein). Russell et al. (2013) for example analyzed a compound chondrule composed of a chondrule portion and a heavily altered CAI-like portion. This is consistent with radiometric ages showing that CAIs formed before chondrules. Relict chondrules in CAIs seem to represent remelting of CAIs (Scott 2007), although other studies strongly suggest that formation of chondrules and CAIs overlapped in time and space (Bizzarro et al. 2004, Itoh and Yurimoto 2003).

The most recent results of Pb-Pb dating of individual CAIs and chondrules from CV and ungrouped carbonaceous chondrites by Connelly et al. (2012) indicates that chondrule formation started contemporaneously with CAIs and continued for at least ~3 Ma (**Figure 2-13**). These data refute the long-held view of a time gap between the formation of CAIs and chondrules, and poses problems for chondrule-forming models like nebula shock waves and colliding planetesimals, where the former is of too short duration and in the latter case at least 1 Ma is required for growth to an adequate size (Connelly et al. 2012).

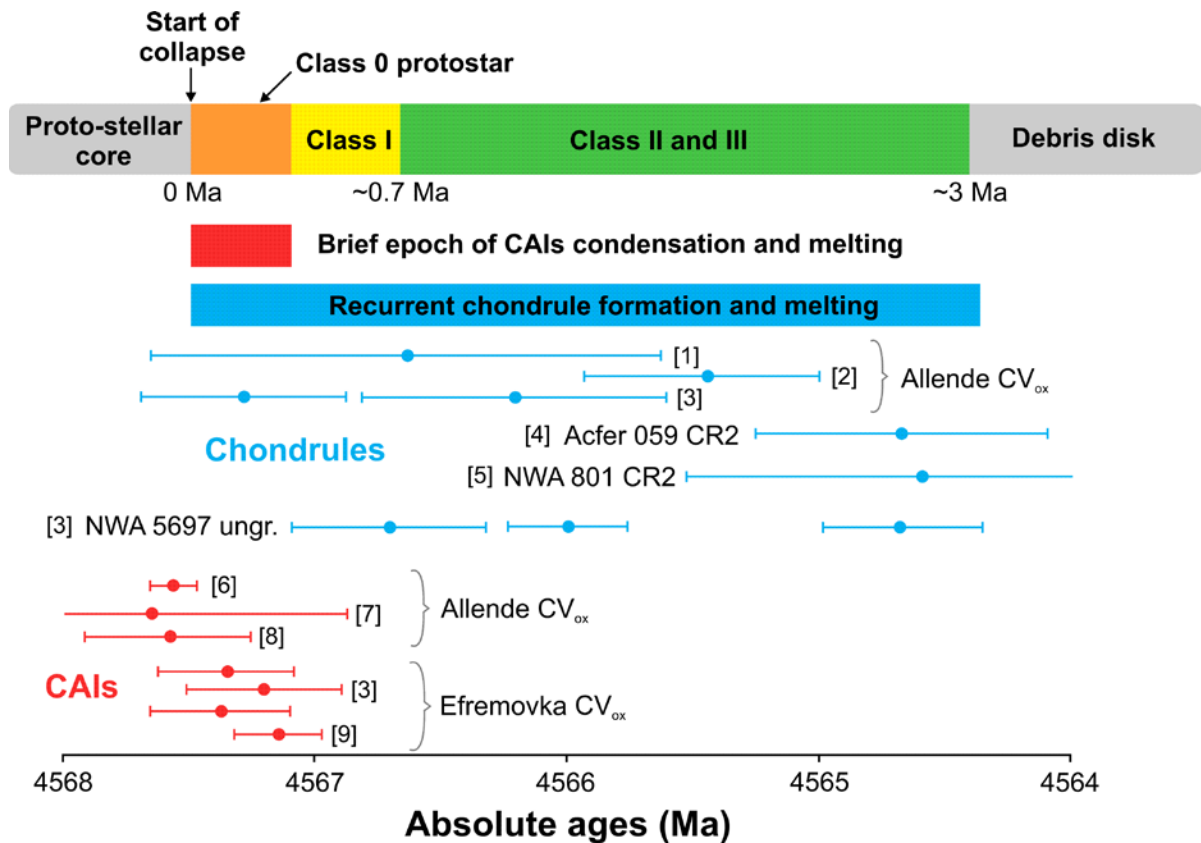


**Figure 2-11: Time scales of solid formation and disk evolution based on Pb-Pb dating of CAIs and chondrules from carbonaceous chondrites** (adapted after Connelly et al. 2012). The brief formation interval of 0.16 Ma for the CAI-forming event is consistent with the median lifetimes of class 0 protostars of ~0.1 to 0.2 Ma. The oldest chondrule age overlaps with CAI ages, indicating that the chondrule was not later heated to temperatures above BP closure temperature and a formation and thermal history indistinguishable from that of CAIs. Data for CB chondrites are omitted since they are believed to have formed from metal and silicate droplets by evaporation and/or condensation in an impact-generated vapor plume (Kita et al. 2005). Sources of data: [1] Amelia and Knot (2007), [2] Connelly et al. (2007), [3] Connelly et al. (2012), [4] Amelin et al. (2002), [5] Charles and Davis (2010), [6] Bouvier et al. (2008), [7] Connelly et al. (2008), [8] Jacobsen et al. (2008), [9] Amelin et al. (2006).

### **Duration of chondrule formation**

A short duration of chondrule formation of less than 1 Ma had been interred from  $^{26}\text{Al}$ - $^{26}\text{Mg}$  ages of Semarkona (LL 3.0) chondrules by Kita et al. (2000). However, more recently Amelin and Krot (2007) concluded from Pb-Pb ages that the entire period of chondrule formation lasted for 4-5 Ma ( $4566.6 \pm 1.0$  Ma (CV chondrite Allende) to  $4564.7 \pm 0.6$  Ma (CR chondrite Acfer 059) to  $4562.7 \pm 0.5$  Ma (CB chondrite Gujba)) and was either continuous or consisted of at least three discrete episodes. Since CB chondrites are believed to have formed from metal and silicate droplets by evaporation and/or condensation in an impact-generated vapor plume, which is not regarded to be a nebula process, the ages of CB chondrules do not provide constrains on chondrule formation of other chondrite groups and on the lifetime of the solar nebula. If the data for CB chondrites are excluded, absolute Pb-Pb ages of CV and CR chondrules and CV CAIs imply that chondrule formation continued 2-3 Ma, which is consistent with the lifetime of the nebula (Kita et al. 2005). Hutcheon et al. (2009) also concluded that a duration of ~2-3 Ma for the formation of carbonaceous chondrite chondrules most plausibly explains the observed range of initial  $^{26}\text{Al}/^{27}\text{Al}$  ratios. Additionally,  $^{26}\text{Al}$  ages among chondrules in the same chondrite vary by at least 1 Ma, indicating chondrule formation must have been repeated many times over this interval (Kita et al. 2005).

### 2.2.3.8 Processes after chondrule formation

*Mixing* of chondrule types and the prior sorting of precursor material may account for most of the variability in chondrule population and bulk chondrite composition (Scott and Taylor 1983). Connelly et al. (2012) proposed that chondrules from individual chondrite groups were formed from isotopically diverse precursor material in different regions of the protoplanetary disk and were subsequently transported to the accretion regions of their respective parent bodies.

Chondrules in carbonaceous and ordinary chondrites have related origins based for example on oxygen isotopic compositions and similar influence of metamorphism on elemental composition of chondrules and matrices (e.g., Scott and Taylor 1983). However, more recently Jones (2012) noted that mixing between different chondrule reservoirs was limited based on unique characteristics of chondrules within a given chondrite group, suggesting a rapid accretion of chondrite parent bodies following chondrule formation, before chondrule reservoirs were homogenized.

### 2.2.3.9 Primary properties of chondrules

In order to infer information about the origin of chondrules, it is important to ensure that the observed properties are characteristic of the chondrule at the time of solidification, immediately after the last high-temperature event they experienced. These primary properties of chondrules, including chemical, mineralogical and isotopic features, can be altered by *secondary processes* on the chondrite parent body, in the solar nebula or on earth (see chapter 2.1.2). Primary properties of chondrules can be determined by analyzing least altered samples (Jones et al. 2005) like ungrouped Acfer 094 and CR3 chondrites (see chapter 4.1.1).

## 2.3 Cosmogenic noble gases in meteorites

### 2.3.1 Cosmic radiation

The cosmic radiation consists of the electromagnetic background radiation ( $\lambda = 1.6$  mm) and the corpuscular radiation (Merchel 1998), which was discovered first and named “cosmic rays” by Hess in 1912 (Hörandel et al. 2002).

The basic differences between the cosmic ray source composition and the solar / local composition were described by Lingenfelter and Higdon (2007) as follows:

- i) The refractory element abundances relative to hydrogen are enriched by a roughly constant factor of  $\sim 20$  compared to the solar system abundance ratio, which is thought to result from suprathreshold injection by sputtering of ions off fast refractory grains through collisions with the ambient gas,
- ii) The volatile element abundances show a mass-dependent enrichment for the elements heavier than He ( $A > 4$ ) that reaches a factor of as much as 10 for the heaviest volatiles. This can also result from suprathreshold injection of the volatiles into the hot ambient gas scattered by fast refractory grains.
- iii) Carbon and oxygen do not fit in either scheme and are enriched by intermediate factors of 9 and 5, possibly also resulting from suprathreshold injection by sputtering of C and O ions from graphite and oxides in the fast refractory grains, with a small additional contribution from scattering of volatile C and O in the hot interstellar gas (Lingenfelter and Higdon 2007 and references therein).

It is believed that cosmic rays have three origins depending on their energy (Hörandel 2013):

- i) Particles with energies below about 100 MeV are accelerated during solar bursts in magnetic reconnections at the surface of the Sun,
- ii) Particles with energies up to several  $10^{17}$  eV are usually assumed to originate within our Milky Way; they are most likely being accelerated in supernova remnants,
- iii) Particles with the highest energies ( $>10^{18}$  eV) are usually considered to be of extragalactic origin.

The cosmic radiation is divided into two components based on their origin. **Solar cosmic ray (SCR)** and **galactic cosmic ray (GCR)** particles interact with surfaces of extraterrestrial matter, producing a large variety of stable and radioactive isotopes, so-called cosmogenic nuclides (see chapter 2.3.2). According to their different energies (**Figure 2-14**) the interactions of SCR and GCR with matter differ strongly with respect to the interaction length and types of nuclear effects involved (**Table 2-6**) (Michel et al. 1996). In addition to the energetic particles, there are the solar wind (SW) nuclei at the very low end of the energy spectrum. Due to their low energy of  $\sim 1$  keV/nucleon they simply stop (are “implanted”) on the surface of the exposed material (Eugster et al. 2006).

The time a meteoroid was exposed to cosmic rays after the ejection from the meteorite parent body is called the **cosmic ray exposure (CRE) age** (Caffee et al. 1988).

**Table 2-6: Nuclear particle effects in extraterrestrial materials** (adapted after Caffee et al. 1988).

	Solar wind (SW)	Solar cosmic rays (SCR)	Galactic cosmic rays (GCR)
Energy	1 keV	10 to 100 MeV <sup>1</sup>	mostly $\sim 1$ to 10 GeV <sup>1</sup> typically $\sim 3$ GeV
Penetration depth	$\sim 50$ nm	mm to cm	cm to m 50 cm on average <sup>2</sup>
Major observable effects	<ul style="list-style-type: none"> <li>– direct implantation</li> <li>– re-implantation of lunar atmospheric species (e.g., <math>^{40}\text{Ar}</math> excess in lunar soils)</li> <li>– radiation damage</li> </ul>	<ul style="list-style-type: none"> <li>– radionuclide production (<math>^{26}\text{Al}</math>, <math>^{53}\text{Mn}</math>)</li> <li>– track production (principally tracks produced by slowing down very heavy (<math>Z &gt; 20</math>) nuclei)</li> <li>– electronic defects (e.g., thermoluminescence)</li> </ul>	<ul style="list-style-type: none"> <li>– radionuclide production</li> <li>– stable-isotope production (e.g., <math>^{21}\text{Ne}</math>, <math>^{15}\text{N}</math>)</li> <li>– nuclear effects due to build up of nuclear cascades with depth</li> <li>– tracks</li> </ul>

<sup>1</sup> Garrison et al. (1995), <sup>2</sup> Wieler (2002b)

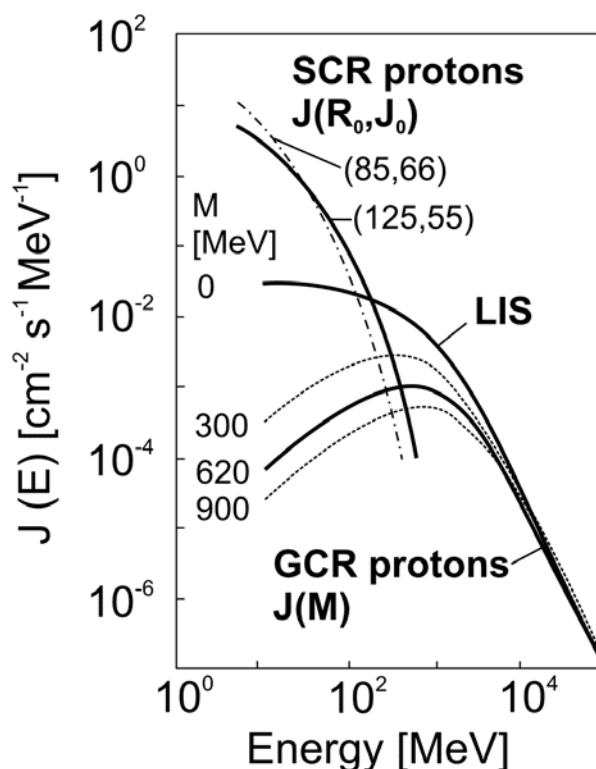
### 2.3.1.1 Solar cosmic rays (SCR)

SCR particles are emitted during solar flares, and their frequency varies with the 11-year-cycle and is well correlated with sunspot numbers. The SCR consists mainly of protons (98% on average) and  $\alpha$ -particles, whose abundance varies from flare to flare between 0.6 and 5% and accounts for 2% on average (Michel et al. 1996). The energy spectrum of SCR obeys a power law in energy, and the flux is decreasing rapidly with increasing energy (see **Figure 2-14**), for SCR the decrease is steeper than for GCR (Caffee et al. 1988).

SCR interactions are restricted to the outermost surface (depth  $< 15$  g cm<sup>-2</sup>) of the irradiated material due to their low energy (see **Table 2-6**), and the production of nuclear active secondary particles can be widely neglected (Michel et al. 1996).



**Figure 2-12: Spectra of solar and galactic cosmic ray protons at 1 AU** (Michel et al. 1996). The long-term averaged SCR spectra are derived from the analysis of lunar rocks. GCR spectra are plotted for times of an active (1969,  $M = 900$  MeV) and a quiet (1965,  $M = 300$  MeV) sun as well as the average spectrum during the last 10 Ma ( $M = 620$  MeV). Abbreviations: LIS – local interstellar spectrum ( $M = 0$ ),  $M$  – modulation of GCR at lower energies by the solar magnetic field,  $J_0$  –  $4\pi$  integral flux density of protons with energies above 10 MeV,  $R_0$  – characteristic rigidity (typical values for individual flares range from 20 to 150 MV).



Particles with energies between 0.3-3 keV (solar wind) can be detected in regoliths of meteoritic and lunar samples (e.g., Heber et al. 2012, Wieler 2000). In contrast, products of nuclear reactions induced by SCR have been predicted for a long time (Lal et al. 1967), the experimental confirmation followed later by analyzing the L chondrite Salem (e.g., Nishiizumi et al. 1990, Evans et al. 1987, Hohenberg et al. 1978). Since their penetration depth is so low, SCR influenced material is mostly lost by surface ablation during atmospheric entry (Merchel 1998) and cannot be detected in most real meteorites.

### 2.3.1.2 Galactic cosmic rays (GCR)

GCRs are the most energetic particles in the interplanetary medium, originating from outside our solar system. Their high energy links it to shock acceleration mechanisms in supernovae environments (Eugster et al. 2006). The GCR consist of 87% protons, 12%  $\alpha$ -particles and 1% heavier ions (Michel et al. 1996), and essentially all the elements the periodic table are represented in cosmic rays (Wiedenbeck 2013). Elemental abundances of GCRs are similar to solar system abundances, suggesting that GCRs and the nuclei in the sun were synthesized by similar processes (Eugster et al. 2006). While heavy nuclei (elements heavier than H and He) constitute no more than a few percent of the GCRs, they have proven to be an invaluable source of information for understanding the source material, the acceleration, and the galactic propagation of the cosmic rays (Wiedenbeck 2013). GCRs represent in general the most accessible measure of our own galaxy, although their composition has been altered by acceleration and transit in interstellar space for million of years before reaching our solar system (Caffee et al. 1988).

For energies above a few GeV/amu GCR particles have a power law spectrum, and at lower energies the GCR is modulated by the solar magnetic field (see **Figure 2-14**) and varies with the solar activity (Michel et al. 1996). Ne is the only element known to show a large difference of isotopic composition at the source compared to solar system abundances,

which may be explained by an origin of GCRs in a region with high metallicity (fraction of elements heavier than He) (Binns et al. 2005 and references therein).

Due to their higher energies (see **Table 2-6**) GCR particles penetrate into earth's atmosphere and their interactions extend several meters into the surface of planets without gas envelope, asteroids and meteoroids (Michel et al. 1996). Since their mean penetration depth in rock of about 50 cm, GCR-induced effects provide a means to study the history of meteorites as small objects in space or in the top few meters of their parent body (Wieler 2002b).

GCRs have a much broader energy spectrum than SCR and induce a large variety of low- and high-energy reactions (Caffee et al. 1988). In contrast to SCR, secondary particles (in particular neutrons) become important for GCR-induced nuclear reactions (Leya and Masarik 2009, Leya 2000, Michel et al. 1996). The secondary particle cascade produces many **spallogenic nuclides** in low-energy reactions (<100 MeV) (Caffee et al. 1988), including cosmogenic  $^{21}\text{Ne}$  from  $^{24}\text{Mg}$  by the reaction  $^{24}\text{Mg}(n,\alpha)^{21}\text{Ne}$  (Wieler 2002b) (**Figure 2-15**). This reaction dominates the production of  $^{21}\text{Ne}$  in chondritic meteorites, at average shielding, corresponding to about  $30\text{ g cm}^{-2}$ , about 70% of  $^{21}\text{Ne}$  is produced in this way (Eugster et al. 2006). Since it is low in natural abundance and easily produced by spallation reactions between energetic particles and rock-forming elements like Mg, Al, Si and Fe  $^{21}\text{Ne}$  is a good indicator of irradiation (Chaussidon and Gournelle 2006). The neutron flux within a meteoroid depends on its *size* and of the *shielding depth* of the sample within the meteoroid (Eugster et al. 2006).

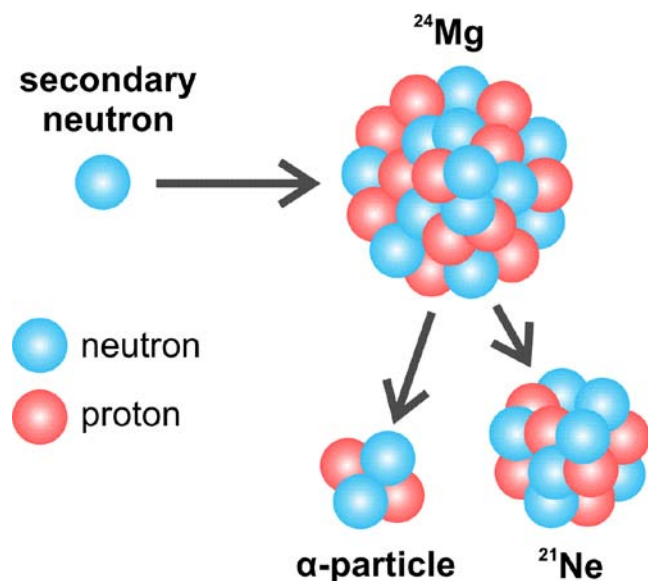


**Figure 2-13: Sketch showing a typical spallation of  $^{24}\text{Mg}$ .** The target element  $^{24}\text{Mg}$  is bombarded by a low-energy secondary neutron, which derives from a nuclear cascade build up by cosmic rays. In some cases  $^{21}\text{Ne}$  and one  $\alpha$ -particle were produced.

### 2.3.2 Cosmogenic nuclides

#### **Production of cosmogenic nuclides and their implications**

Cosmogenic nuclides are produced by nuclear interactions of both high-energy GCR protons (and associated secondary proton and, in particular neutrons) and energetic SCR protons (Garrison et al. 1995) with surfaces of extraterrestrial matter. Protons and  $\alpha$ -particles of the primary GCR produce a cascade of secondary protons and neutrons that develop within the meteoroid (Wieler 2002b). Cosmogenic nuclides can be measured by their decay (if radioactive) or as positive isotope abundance anomalies in the exposed materials. They can be interpreted with respect to the collision and exposure history of the irradiated body as well as of the history of the cosmic radiation itself, providing information which cannot be obtained by any other means (Michel et al. 1996).

Radionuclides with half-lives above 1 month and stable rare isotopes are cosmogenic nuclides of interest (**Table 2-7**). Stable products integrate over the entire history of an irradiated body, whereas abundances of radionuclides only reveal the exposure history during a time period of about 3 half-lives. Therefore, comparing abundances of both allows the analysis of possible variations of SCR and GCR intensities with time, exposure ages, terrestrial residence time and complex irradiation histories (Michel et al. 1996).

**Table 2-7: Cosmogenic radionuclides with half-lives above 1 month and stable cosmogenic nuclides frequently analyzed in meteorites** (adapted after Michel et al. 1996). *Nuclides are arranged in order of increasing  $T_{1/2}$ .*

Nuclide	$T_{1/2}$	Nuclide	$T_{1/2}$	Nuclide	$T_{1/2}$
<sup>37</sup> Ar	0.096 a	<sup>39</sup> Ar	269 a	<sup>53</sup> Mn	3.7 Ma
<sup>56</sup> Co	0.213 a	<sup>14</sup> C	5.73 ka	<sup>129</sup> I	15.7 Ma
<sup>22</sup> Na	2.6 a	<sup>59</sup> Ni	75 ka	<sup>40</sup> K	1.28 Ga
<sup>55</sup> Fe	2.7 a	<sup>41</sup> Ca	103 ka	He	stable
<sup>60</sup> Co	5.26 a	<sup>81</sup> Kr	201 ka	Ne	stable
<sup>3</sup> H	12.3 a	<sup>36</sup> Cl	300 ka	Ar	stable
<sup>44</sup> Ti	58.9 a <sup>1</sup>	<sup>26</sup> Al	716 ka	Kr	stable
<sup>32</sup> Si	133 a	<sup>10</sup> Be	1.39 Ma <sup>2</sup>	Xe	stable

<sup>1</sup> Ahmad et al. 2006, <sup>2</sup> Korschinek et al. 2010, Chmeleff et al. 2010.

### **Dependence of the production rate**

The production rate of cosmogenic nuclides in a given sample depends on the size and the shape of the pre-atmospheric object (meteoroid) and the position within this object (collectively called **shielding**) as well as (naturally) the **chemical composition** of the sample. For shielding correction the most sensitive shielding indicator for meteorites is the cosmogenic (c) ratio (<sup>22</sup>Ne/<sup>21</sup>Ne)<sub>c</sub> (e.g., Eugster et al. 2006, Wieler 2002b, Graf et al. 1990). In addition, the elemental production rate for each individual target element is also influenced to some extent by the overall chemical composition, which is called **matrix effect**. It refers to how the elemental composition influences the secondary flux of nuclear particles under fixed geometric conditions (Eugster et al. 2006). The matrix effect arises because particle fluxes and spectra are a function of the elemental production in the target (e.g., Wieler 2002b).

### **Determination of the production rates**

The methods for determining production rates of cosmogenic nuclides fall into three categories:

#### **i) Multi-meteorite studies and empirical models**

This approach includes methods based on measurements in a number of meteorites of radioactive-stable nuclide pairs, preferentially such with similar shielding dependence like <sup>26</sup>Al-<sup>21</sup>Ne, <sup>10</sup>Be-<sup>21</sup>Ne, and <sup>53</sup>Mn-<sup>21</sup>Ne. Assuming average-sized meteorites and that the radionuclide has not yet reached its saturation level, the CRE age and the production rate of the stable nuclide  $P_{stable}$  can be calculated as follows:

$$T_{exp} = \frac{1}{\lambda} \frac{A_{sat}}{A_{sat} - A_{meas}}, \text{ where } A_{sat} > A_{meas} \quad (1)$$

$$P_{stable} = \frac{C_{stable}}{T_{exp}} \quad (2)$$

with

$T_{\text{exp}}$  – CRE age

$\lambda$  – decay constant of the radionuclide

$A_{\text{sat}}$  and  $A_{\text{meas}}$  – saturation activity and measured activity of the radionuclide at the time of fall

$P_{\text{stable}}$  and  $C_{\text{stable}}$  – production rate and the measured concentration of the stable nuclide

This approach requires a simple exposure history of all meteorites, and the deduced production rates are basically mean values over the last few half-lives of the radionuclide (Wieler 2002b).

Eugster (1988) presents another multi-meteorite approach, where he calculated the production rates of cosmogenic noble gas nuclides  $P$  as a function of  $(^{22}\text{Ne}/^{21}\text{Ne})_c$  for various chondrite classes based on  $T_{81}$  CRE ages of ordinary chondrites determined by the  $^{81}\text{Kr}$ -Kr method (Wieler 2002b):

$$P(^3\text{He}) = P_3 = \frac{{}^3\text{He}_c}{T_{81}} = F_3 \left[ 2.09 - 0.43 \times \left( \frac{{}^{22}\text{Ne}}{{}^{21}\text{Ne}} \right)_c \right] \quad (3a)$$

$$P(^{21}\text{Ne}) = P_{21} = \frac{{}^{21}\text{Ne}_c}{T_{81}} = F_{21} \left[ \frac{1.61}{21.77 \times \left( \frac{{}^{22}\text{Ne}}{{}^{21}\text{Ne}} \right)_c} \right] \quad (3b)$$

$$P(^{38}\text{Ar}) = P_{38} = \frac{{}^{38}\text{Ar}_c}{T_{81}} = F_{38} \left[ 0.112 - 0.063 \times \left( \frac{{}^{22}\text{Ne}}{{}^{21}\text{Ne}} \right)_c \right] \quad (3c)$$

The production rates are given in units of  $10^{-8} \text{ cm}^3 \text{ STP/g per Ma}$ , and  $P_{21}$  was deduced using the procedure proposed by Nishiizumi et al. (1980).

As chondrite groups vary in their target elements for production of cosmogenic nuclides, the production rates  $P_j$  are normalized to L chondrites, where  $j$  represent the respective cosmogenic nuclide and for average L chondrite composition the compilation of Wasson and Kallemeyn (1988) is used:

$$F_j = \frac{F_{j,\text{sample}}}{F_{\phi L}} \quad (4)$$

This **correction factor  $F_j$**  for different chemical compositions is based on the work of Cressy and Bogard (1976) (5a), Schultz and Freundel (1985) (5b), and Freundel et al. (1986) (5c), and is defined by chemical factors  $F_j'$ :

$$F_3' = 0.0174[Ti + Cr + Mn + Fe + Ni] + 0.0266(100 - [Ti + Cr + Mn + Fe + Ni]) \quad (5a)$$

$$F_{21}' = 1.63[Mg] + 0.6[Al] + 0.32[Si] + 0.22[S] + 0.07[Ca] + 0.021[Fe + Ni] \quad (5b)$$

$$F_{38}' = 1.58[Ca] + 0.086[Fe + Ni] + 0.33[Ti + Cr + Mn] + 11[K] \quad (5c)$$

The elemental abundances are given in weight percent. Because of the matrix effect and because these equations have been derived for chondritic meteorites, the equations should not be applied to meteorites with very different composition. Furthermore, as the relation between the  $(^{22}\text{Ne}/^{21}\text{Ne})_c$  ratio and the production rate is ambiguous for relatively high shielding, for chondrites the Eugster formulas (3a) – (3b) should only be applied for  $(^{22}\text{Ne}/^{21}\text{Ne})_c$  ratios larger than about 1.08-1.10 (Wieler 2002b) and are not suitable for  $(^{22}\text{Ne}/^{21}\text{Ne})_c < 1.07$ , i.e. samples recovered from the interiors of large meteoroids (Masarik et al. 2001, Leya et al. 2001). However, the formulas by Eugster have the advantage of

yielding a unique production rate for a given value of the routinely determined shielding parameter  $(^{22}\text{Ne}/^{21}\text{Ne})_c$  (Wieler 2002b).

Using the same approach based on  $T_{81}$  CRE ages as Eugster (1988) for chondritic meteorites, Eugster and Michel (1995) derived composition- and shielding-dependent production rates for achondrites.

## ii) Single-meteorite studies and semi empirical models

This second approach includes for example the study of cosmogenic noble gases and radionuclides and nuclear tracks (e.g., Graf et al. 1990) in the Knyahinya meteorite. During fall, this large L/LL5 chondrite was split in two almost equal sized fragments (Wieler 2002b) along a near planar cross-section passing close to the centre of the main mass, which allowed sampling of the interior (Graf et al. 1990). This made it possible to determine the concentration gradients of cosmogenic nuclides as a function of preatmospheric depth, which was then used to determine the parameter of a semi empirical model (Wieler 2002b).

## iii) Physical models

With this approach all processes relevant for particle production and transport were modeled using Monte Carlo techniques with this basic equation (e.g., Leya et al. 2001, 2000):

$$P_j(R, d, M) = \sum_{i=1}^N c_i \frac{N_A}{A_i} \sum_{k=1}^3 \int_0^{\infty} \sigma_{i,j,k}(E) \times J_k(E, R, d, M) dE \quad (6)$$

with

$P_j$  – production rate of the nuclide  $j$  as a function of the meteoroid radius  $R$ , sample depth  $d$ , and the solar modulation parameter  $M$  (see chapter 2.3.1.1)

$c_i$  – abundance of the target element  $i$  (in g/g)

$N_A$  – Avogadro's number

$A_i$  – mass number (in amu)

$k$  – reaction particle type (primary or secondary proton, secondary neutron)

$\sigma_{i,j,k}(E)$  – excitation function for the production of nuclide  $j$  from element  $i$  by reactions induced by particles of type  $k$

$J_k(E, R, d, M)$  – differential flux density of particle type  $k$  as a function of energy  $E$  of the reacting particle, meteoroid radius  $R$ , sample depth  $d$ , and solar modulation parameter  $M$

The primary GCR intensity is assumed to be constant, and primary and secondary  $\alpha$ -particles are considered only approximately. The excitation functions are the most critical component of these models, because measured cross-sections of neutron-induced reactions are scarce, and secondary neutrons usually dominate the cosmogenic nuclide production. Leya and Masarik (2009) improved former models due to improved neutron cross section database and better Monte Carlo modeling of primary and secondary particle spectra. They further demonstrated that the matrix effect for carbonaceous and ordinary chondrites is negligible for all target product combinations, except for those which are dominated by thermal or very low energy neutron reactions.

For meteorite radii not larger than ~50 cm and “average” shielding values of  $(^{22}\text{Ne}/^{21}\text{Ne})_c$  of 1.08-1.14, the model predictions of physical models agree well with the calculated values by Eugster (1988). At lower shielding with  $(^{22}\text{Ne}/^{21}\text{Ne})_c > 1.13$ , modeled and

calculated production rates  $P_{21}$  as a function of the shielding parameter run parallel, with an offset of up to 30%. For this low shielding it is unclear, whether the physical model or the empirical correlation predicts  $P_{21}$  more accurately (Wieler 2002b).

### 2.3.3 Noble gases in chondrules

Noble gases in chondrules are superpositions of several different **components** like in other extraterrestrial materials. A “component” is operationally defined as an individual constituent or source of gas with a unique and well-defined isotopic composition. In general, noble gases can be divided in two components: “Trapped” components are incorporated from external sources, and “*in situ*” components are generated by nuclear processes within the sample. There are three sources dominating the inventory of noble gases in extraterrestrial materials: i) trapped components, normally gas of “solar” or “planetary” types, ii) a cosmogenic component from cosmic ray induced nuclear reactions, and iii) components from various radioactive decay processes (Hohenberg et al. 1978 and references therein). The solar pattern is due to the implantation of solar wind ions into asteroidal regolith, whereas later was recognized that the “planetary” pattern is a misnomer, since “planetary” noble gases in meteorites represent various primordial components (Porcelli et al. 2002).

It was believed that noble gases were completely lost at the time of melting during chondrule formation (e.g., Roth et al. 2011, Nakashima et al. 2009b, Vogel et al. 2004, Okazaki et al. 2001, Nakamura et al. 1999, Miura and Nagao 1997, Kim and Marty 1994). However, in chondrules from the enstatite chondrite Yamato 791790 significant amounts of trapped noble gases were discovered showing similarities with ‘subsolar’ gases. These authors suggest that the solar gases were implanted into chondrule precursor material, which incompletely lost the implanted gases by diffusion over time (Okazaki et al. 2001). Nakashima et al. (2009b) found solar wind-like noble gases in the interior of a NWA 852 chondrule, possibly acquired before or during chondrule formation and preserved in a phase with high noble-gas-retentivity like metal.

GCR and SCR can completely penetrate a chondrule assuming an average diameter of ~1 mm. In contrast, SW particles are only able to penetrate the uppermost layer (~50 nm) of extraterrestrial materials (see **Table 2-6**). Therefore, if a chondrule contains SW gases, it had been exposed to SW as free-floating object in the solar nebula or in the uppermost surface layer of a regolith on the parent body (see *chapter 2.4.2*). GCR and SCR can also be achieved from the chondrule as free-floating object or in the surface layer of a parent body regolith, however in depths of a few mm to cm.

Since noble gas components are bound in phases with different retentivity (Trieloff et al. 2005), noble gas extraction by stepwise heating is commonly used to separate different components (e.g., Trieloff et al. 2005, Ozima and Podosek 2002). For instance, trapped neon  $^{20}\text{Ne}_{\text{tr}}$  released from Allende matrix has two peaks at about 850°C and 1150°C separated by a minimum at 1000°C, whereas cosmogenic neon  $^{21}\text{Ne}_{\text{c}}$  is released at a rate that increases slowly until about 1100 or 1200°C and decreases thereafter (Smith et al. 1977). Among trapped noble gases planetary gases are being released at higher temperatures than solar wind gases (Manuel et al. 1972).

In this study temperature steps at 600°C and 1800°C were chosen. The first temperature step at 600°C is due to atmospheric contamination, which the samples may have absorbed during the freeze-thaw cycles for chondrule separation. In addition, few samples were heated up to 1900°C in order to test if the degassing at 1800°C is complete (see *chapter 4.5.1*).

## 2.4 Pre-irradiation

### 2.4.1 Definition of pre-irradiation

If a fraction of meteoritic material was irradiated by cosmic rays before the ejection from kilometer-sized parent body, this process is called pre-irradiation (Eugster et al. 2006) (**Figure 2-16**). Wieler (2002b) defines a pre-compaction exposure as the situation where certain parts of a meteorite only show an excess of cosmogenic nuclides, relative to other fractions of the meteorite, which cannot be explained by higher production rates due to higher concentrations of major target elements or favorable shielding. Roth et al. (2009) described a precompaction exposure as an irradiation of chondrules by energetic particles in the solar system prior to their compaction into meteoritic matter. Polnau et al. (2001) further excluded different outgasing characteristics of chondrules and matrix material as reason for varying production rates and hence variable concentration of cosmogenic noble gases. Studies of pre-irradiation effects can yield information about the energetic particle environment and the lifetime of chondrules as free-floating objects in the early solar system (Roth et al. 2011) and about surface processes on planetary objects (Eugster et al. 2006).

### 2.4.2 Settings of pre-irradiation

Single meteorite components like chondrules, mineral grains or fragments may have been pre-irradiated within different settings (e.g., Eugster et al. 2006, Wieler 2002b):

**i) On the parent body surfaces (regolith) (**Figure 2-16b**)** or even in other meteoroids prior to compaction into the matter that became the meteorite studied.

This setting may apply to the case of small, independent meteorite grains (< 1 mm), for example, and also chondrules. Implanted SW gases and cosmogenic nuclides produced by SCRs reside in the uppermost few mm of exposed matter. If the cosmogenic products are interpreted as being produced by GCRs, inferred CRE ages for  $2\pi$  exposure in the asteroidal regolith have in some cases found to be extremely long and incompatible with the expected lifetime of asteroidal regoliths. Thus, an exposure to an enhanced flux of early SCRs by the active initial sun was invoked (Chaussidon and Gournelle 2006).

Examples of an irradiation in the regolith include:

- Olivines in CM chondrites (Caffee et al. 1983, 1986, 1987, 1988, Hohenberg et al. 1990)
- Gas-rich meteorites composed of a mixture of compacted solar-gas-bearing dust (matrix) and solar-gas-free pebbles (inclusions) like St. Mesmin (LL6) (e.g., Schultz and Signer 1977), Fayetteville (H4) (e.g., Wieler et al. 1986, 1989, Padia and Rao 1989), and Kapoeta from the asteroid Vesta (e.g., Pedroni 1991)
- 20% of chondrules from CM chondrite Murchison, which is a meteoritic breccia (Roth et al. 2011)

**ii) In the early solar nebula** as free-floating objects (Eugster et al. 2006) (**Figure 2-16a**).

Examples of this kind of pre-irradiation are:

- Light inclusions from Weston (H4) (Schultz et al. 1972)
- Foreign chondritic clasts from Kapoeta (Pedroni et al. 1988, 1991)
- Chondrules from several ordinary chondrites (Polnau et al. 1999, 2001)
- Chondrules from Murray (CM2); Bjurböle (L/LL4) and Dhajala (H3.8) (Das and Murty 2009)

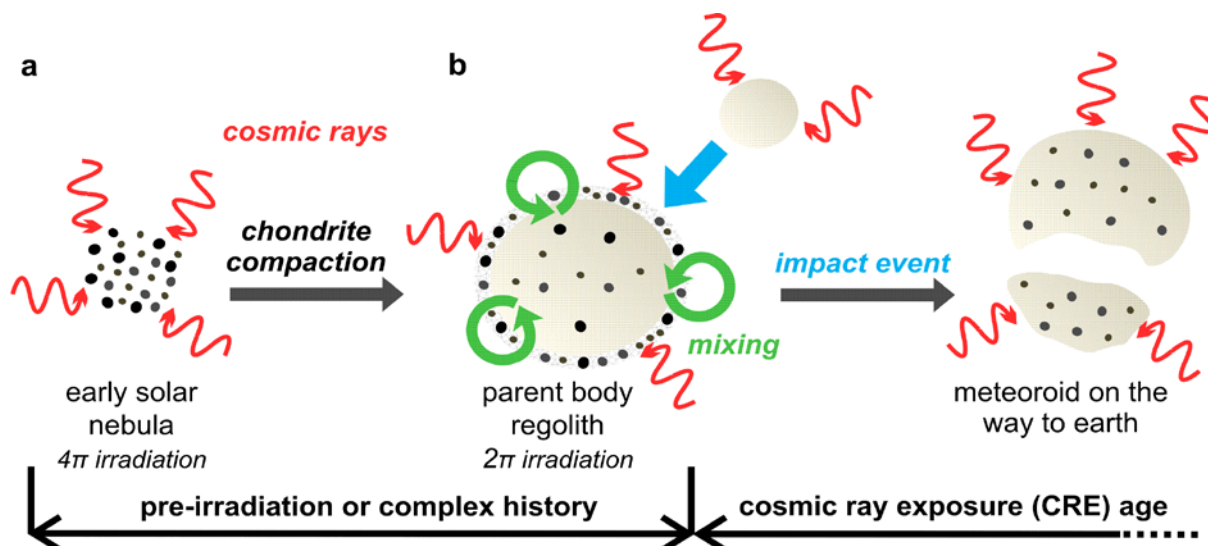


Figure 2-14: Sketch showing the pre-irradiation of single meteorite components as free-floating objects in the solar nebula (a) and in the parent body regolith (b).

The decision in which of these both settings a pre-irradiation occurs is not straightforward. There are some clues, pointing towards one setting; however these clues are not unequivocal. A high shielding parameter  $(^{22}\text{Ne}/^{21}\text{Ne})_c$  for example suggests an exposure in a near surface location like on the parent body regolith. On the other hand, small objects like chondrules irradiated by GCR will also show high  $(^{22}\text{Ne}/^{21}\text{Ne})_c$  ratios (Reedy 1989). Polnau et al. (1999) proposed that if chondrules were irradiated in a nebula environment before accretion and incorporation into parent bodies, they may show excess exposure times visible as excess concentration of cosmogenic nuclides. Chondrules would not show detectable excesses of cosmogenic gases, if they were formed and exposed to cosmic rays on the parent body since any exposure may have been too short (Polnau et al. 1999).

### 2.4.3 Pre-irradiation of chondrules

#### 2.4.3.1 Previous analyses of pre-irradiation effects in chondrules

Pre-irradiation effects in chondrules were found using noble gases in several previous studies (**Table 2-8**) in carbonaceous and ordinary chondrites.

**Polnau et al. (1999, 2001)** were the first who searched for pre-irradiation effects in chondrules from ordinary chondrites using noble gases. Polnau et al. (1999) found systematically higher concentrations of cosmogenic noble gases in one chondrule fragment relative to the matrix in the H6 chondrite ALH 76008, which is known from radioactive studies to have a two-stage exposure history (Imamura et al. 1979). The authors excluded the possibility of preferential gas loss from the fine-grained matrix and systematic errors in the corrections for variable target element chemistry, and interpreted the enhanced CRE ages of the ALH 76008 chondrule of  $0.89 \pm 0.34$  Ma as precompaction exposure. Polnau et al. (2001) found in six out of eight ordinary chondrites pre-irradiation effects of chondrules (see **Table 2-8**). In the case of H4 chondrite Sena the largest CRE age difference of 0.29 Ma between the average of all chondrules (1.39 Ma) and matrix (1.11 Ma) were measured.

Intriguing evidence for pre-irradiation of Renazzo (CR2) chondrules were provided by **Vogel et al. (2004, 2003)**, showing that cosmogenic neon  $^{21}\text{Ne}_c$  in all chondrules to be roughly one



order of magnitude more abundant relative to the matrix (average values are 3.20 and  $0.32 \times 10^{-8}$  ccSTP/g).  $^{21}\text{Ne}_c$  values for Renazzo matrix agree with previous analyses ( $0.64/0.68 \times 10^{-8}$  ccSTP/g) by Mazor et al. (1970). However, Vogel et al. (2003, 2004) did not assess their data for pre-irradiation. The authors noted that the chondrules are virtually free of any trapped gas, which is in contrast to the typical situation of a pre-irradiation that has taken place on the parent body regolith like in the case of H4 chondrite Fayetteville (Wieler et al. 1989) and howardite Kapoeta (Pedroni 1991) (see chapter 2.4.4).

In a comprehensive study **Eugster et al. (2007)** analyzed noble gases in 15 carbonaceous, ordinary and enstatite chondrites. They found equivocal results, and only data from H3.8 chondrite Dhajala may suggests some precompaction exposure of chondrules.

**Roth et al. (2011, 2009, 2008)** analyzed 26 chondrules from Allende (CV3) and 38 chondrules from Murchison (CM2) and matrix material from both meteorites, and found in seven Murchison chondrules a pre-compaction exposure record corresponding to an irradiation up to 30 Ma at present-day GCR intensity in a  $4\pi$  geometry. However, the narrow range of CRE ages of Allende and Murchison chondrules and the basic agreement of noble gas ages and radionuclide-based exposure ages of Allende and Murchison suggest that the cosmic ray record of most chondrules is plausibly explained by their recent meteoroid exposure alone. In the case of the seven pre-exposed Murchison chondrules the authors exclude the inheritance of cosmogenic noble gases from chondrule precursors. They prefer a scenario of pre-irradiation by GCR in the regolith of the Murchison parent body for up to several ten million years rather than an irradiation by an early intense flux of SCR. However, the data did not allow a firm conclusion, where the excess of cosmogenic noble gases in chondrules were acquired, and the preferred scenario does not explain the pre-irradiation of chondrules in solar gas-free meteorites.

**Table 2-8: Previous analyzed meteorites showing evidence for pre-irradiation effects in chondrules using noble gases analysis.**

Reference	Carbonaceous chondrites	Ordinary chondrites	Enstatite chondrites
Polnau et al. (1999)		ALH 76008 (H6)	
Polnau et al. (2001)		Sena (H4), Kalvesta (H6), Grassland (L4), Bowesmont (L6), Bjurböle (L/LL4), Hunter (L5)	
Vogel et al. (2003, 2004)	<b>Renazzo (CR2)</b>		
Eugster et al. (2007)		Dhajala (H3.8)	
Roth et al. (2008, 2009, 2011)	<b>Murchison (CM2)</b>		
Das and Murty (2009)	Murray (CM2)	Dhajala (H3.8), Bjurböle (L/LL4)	
Matsuda et al. (2010)		Parnallee (LL3.6)	
Das et al. (2010, 2012)	Murchison (CM2)	chondrule fragments and olivine (or olivine-rich) separates from Dhajala (H3.8), Bjurböle (L/LL4), Chainpur (LL3.4)	Parsa (EH3)
Huber et al. (2012)	Murchison (CM2)		

*Meteorite groups and types are given in brackets. Bold writing indicates intriguing evidence for pre-irradiation.*

**Das and Murty (2009)** analyzed individual chondrules from ten ordinary, carbonaceous and enstatite chondrites in order to characterize trapped noble gases and to search for precompaction cosmic-ray irradiation. Only a few chondrules from Dhajala (H3.8), Bjurböle (L/LL4) and Murray (CM2) show higher CRE ages compared to the matrix samples, suggesting that the chondrules and/or chondrule precursors have received cosmic ray irradiation before accretion into the parent body. Note that Das and Murty (2009) used the sometimes ill-constrained (e.g., Roth et al. 2011) shielding parameter  $(^{22}\text{Ne}/^{21}\text{Ne})_c$  for shielding correction, thus introducing uncertainties, although chondrule and matrix samples originated from a small meteorite fragment, and hence experienced identical shielding. Furthermore, Das and Murty (2009) did not describe in detail which correction factor (for eucrites, diogenites or howardites) they used for the determination of the production rates of cosmogenic noble gases according Eugster and Michel (1995) (see chapter 2.3.2).

**Matsuda et al. (2010)** performed laser microprobe noble gas analysis on chondrules and matrix from the LL3.6 chondrite Parnallee to analyze its formation history using the relationship between Q-gas and Ar-rich gas.  $T_3$  and  $T_{21}$  CRE ages of chondrules (6.8 to 10.0 Ma) are longer than those of the matrix sample (5.9 Ma) suggesting pre-irradiation of chondrules. However, calculated CRE ages may not be reliable because for chondrules and matrix identical elemental abundances have been assumed and hence production rates for cosmogenic He  $P_3$  and Ne  $P_{21}$  are identical.

**Das et al. (2010)** reported for chondrule fragments of Murchison (CM2), Dhajala (H3.8), Chainpur (LL4), Bjurböle (L/LL4) and Parsa (EH3) higher CRE ages relative to the respective matrix samples, indicating pre-compaction exposures in the range from 5 to 35 Ma. In olivine or olivine-rich grains separated from the same meteorites **Das et al. (2012)** determined CRE ages similar to those of the matrix with the exception of some grains from Dhajala (H3.8) and single grains from Bjurböle (L/LL4) and Chainpur (LL4) which showed exposure age excesses in the range from 2 to 20 Ma. Based on these pre-compaction exposures and different energetic particle exposures observed in fragments and grains from the same chondrule, Das et al. (2010, 2012) suggest that chondrules were exposed to enhanced SCR during or shortly after the chondrule formation, which is in agreement with previous analysis of individual olivine grains in CM chondrites (Woolum and Hohenberg 1993, Hohenberg et al. 1990, Caffee et al. 1987). However, the incorrect determination of the target element concentrations of the individual grains (the sum of all oxidized target elements accounts in some cases only for 60 wt%) may cause too low production rates of cosmogenic Ne ( $^{21}\text{Ne}_c$ ) and hence too high  $T_{21}$  CRE ages compared to the matrices. Target element concentrations of matrices were derived from previous studies possibly originating from different fragments of the respective meteorite, and thus may be not representative (Ott et al. 2013).

**Huber et al. (2012)** presented a study in combination of Roth et al. (2011) and Metzler (2004) in order to analyze the irradiation history of individual Murchison (CM2) chondrules. Metzler (2004) found track-rich olivines in clastic matrix surrounding primary rock fragments (PRFs), whereas PRFs did not contain track-rich olivines. PRFs represent aggregates from nebula components like dust-mantled chondrules which subsequently became fragmented and accreted to their final parent body (Metzler et al. 1992). Huber et al. (2012) aimed to test whether pre-irradiated chondrules are only present in clastic matrix or also in PRFs. The authors expected in the case of a pre-irradiation in the regolith (**Figure 2-17a**) that all chondrules within the same PRF should show no or identical pre-irradiation, whereas chondrules from the surrounding clastic matrix can show different pre-irradiation histories. On the other hand, in the case of a pre-irradiation prior to parent body accretion (**Figure 2-17b**) they expected different exposure ages for chondrules from the same PRF. The elemental

composition of all chondrules were assumed to be identical with the Murchison chondrules analyzed by Roth et al. (2011), and an average  $^{21}\text{Ne}$  production rate on  $0.43 \times 10^{-8}$  cc/(g Ma) was used to determine CRE ages may introducing a systematic error for CRE ages of both chondrules from PRFs and the clastic matrix. Chondrules in PFRs show no pre-irradiation effects, while 20-30% of chondrules embedded in clastic matrix experienced different degrees of pre-exposure up to 25 Ma (assuming a  $4\pi$  irradiation), which is in agreement with Roth et al. (2011). In their future work the authors will analyze more chondrules in PFRs and clastic matrix, and expand their study to another CM chondrite.

Other studies provided unequivocal results concerning pre-irradiation of chondrules. While Bland et al. (2011) concluded that fine-grained rims in Allende (CV3) chondrite were acquired in the solar nebula setting pointing towards a pre-irradiation as free-floating objects, Strashnov and Gilmour (2012) reported identical ages within uncertainties for H5 Allegan chondrules and matrix ( $5.30 \pm 0.35$  and  $7.04 \pm 1.49$  Ma) based on the  $^{81}\text{Kr}$ -Kr method.

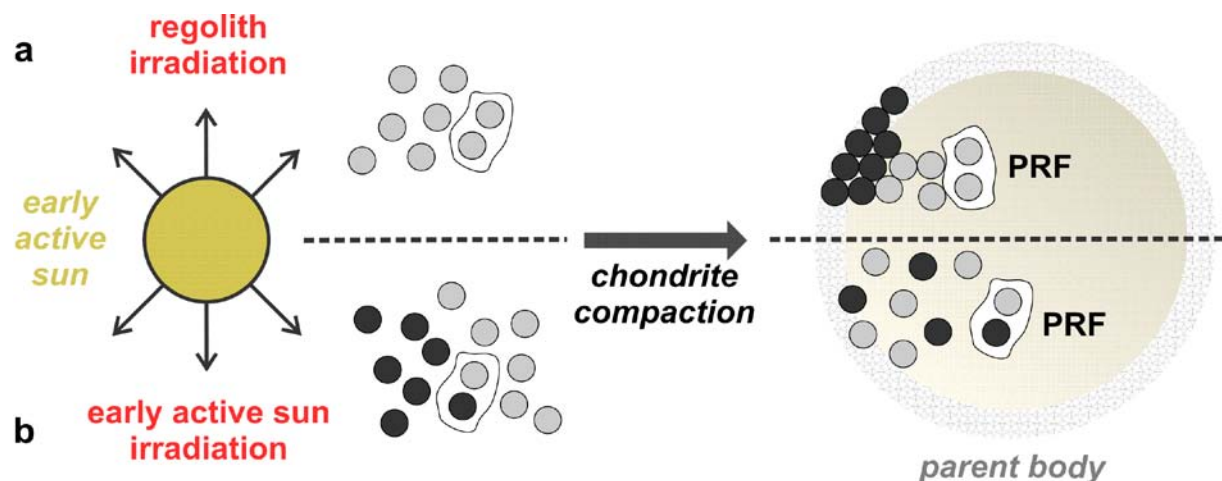


Figure 2-15: Sketch showing the pre-irradiation of primary rock fragments (PRF) in the solar nebula by the early active sun before parent body accretion (a) or in the parent body regolith (b) (adapted after Huber et al. 2012).

#### 2.4.3.2 Difficulties concerning the analysis and interpretation of pre-irradiation effects in chondrules

With respect to the analysis and interpretation of pre-irradiation effects in chondrules using noble gases the following problems are to be noted:

- i) For a reliable calculation of CRE ages it is essential to know accurately the **production rate** of cosmogenic nuclides. Since the production rate itself depends on the *shielding* and the *chemical composition* of the sample (e.g., Wieler et al. 2002b) (see chapter 2.3.2), both have to be considered carefully.

Chondrule and matrix samples analyzed in this study originate from the same meteorite fragment, therefore both experienced identical shielding. In view of this, “normal shielding” with  $(^{22}\text{Ne}/^{21}\text{Ne})_c = 1.11$  is assumed for comparison (see chapter 4.6).

The chemical composition of each chondrule and the respective matrices were analyzed using instrumental neutron activation analysis (INAA) (see chapter 4.3.1).

- ii) Preferential **recoil losses** from the matrix may cause lower CRE ages of the matrix samples.

Based on their fine-grained texture in the range between 10 nm to 5  $\mu\text{m}$  (Scott 2007, see *chapter 2.1.3*) matrix material can be affected by recoil effects. In presolar SiC grains recoil ranges of 2-3  $\mu\text{m}$  are indicated (Ott and Begemann 2000). Trappitsch and Leya (2013) reported substantial recoil losses for grain sizes below a few microns. The authors further stated decreasing production rates for  $^{21}\text{Ne}$  and  $^{22}\text{Ne}$  by SCR in grains with radii of 10  $\mu\text{m}$  and smaller (Trappitsch and Leya 2013).

- iii) Possible **gas loss** from the bulk meteorite **due to thermal metamorphism** or **lower retentivity** for cosmogenic gases.

Gas loss due to diffusion preferentially affects He, and Ne as well (e.g., Das et al. 2012), especially in high petrologic types (>4), where temperatures >600°C were reached (see **Figure 2-2**). Polnau et al. (2001) stated it might be difficult to reveal exposure age differences between chondrules and matrix, if the noble gases from a pre-exposure of the chondrules are only retained partly during metamorphism. However, Polnau et al. (1999) documented a precompaction exposure of one chondrule from H6 chondrite ALH 76008. To restrict possible gas loss due to thermal metamorphism, in this study samples with petrologic types 2 to 3 were selected (see *chapter 4.1.1*). The lower Ne and Ar retentivity of the matrix relative to the chondrules can also cause lower  $T_{21}$  and  $T_{38}$  CRE ages of the matrix (e.g., Polnau et al. 1999).

In order to elucidate whether the samples are affected by gas loss resulting from both recoil losses and thermal metamorphism, two tests were performed (“Bern line”, comparison of  $T_{21\text{-corr}}$  and  $T_{3\text{-corr}}$  CRE ages; see *chapter 5.4.3*).

- iv) Meteorites with **short exposure ages** should facilitate the detection of pre-irradiation effects (e.g., Roth et al. 2011, Polnau et al. 1999). Therefore, in this study only meteorites with CRE ages of maximum 6 Ma were selected (see *chapter 4.1.1*).

- v) Once the existence of pre-irradiation has been established, another problem is that it may not be possible to determine with certainty the **setting** where it occurred.

#### 2.4.4 Pre-irradiation of other meteorite components

Meteorite components which have been analyzed for pre-irradiation effects using noble gases include clasts, mineral grains (mostly olivine), presolar SiC grains, and CAIs separated from the matrix (**Table 2-9**).

For individual olivine grains from the matrix of CM chondrites (Murchison, Murray, Cold Bokkeveld) and H chondrites (Weston, Fayetteville), and grain size separates from the howardite Kapoeta an excess of cosmogenic Ne (relative to the CRE age) has been reported. This pre-irradiation have been acquired either i) when the grains were individually irradiated for much longer times than their CRE age, or ii) there was a higher energetic particle flux in the early solar system when they were irradiated on the parent body surfaces (Das et al. 2012). While in the case of “gas-rich” meteorites like Kapoeta with large solar gas contents reflecting an extended regolith duration both explanations may be possible (e.g., Wieler 2000b, Pun et al. 1998, Pedroni 1991, Padia and Rao 1989), for other meteorites like CM chondrites an irradiation on the parent body regolith was excluded (e.g., Woolum and Hohenberg 1993, Hohenberg et al. 1990, Caffee et al. 1988) because the required exposure

would be improper long (Das et al. 2012). Hohenberg et al. (1990) for example reported in track-rich grains from CM chondrites large excesses of cosmogenic Ne, corresponding to parent body exposure times to GCR of several  $10^7$  to several  $10^8$  years (Wieler 2002b).

**Table 2-9: Previous analyzed meteorite separates showing evidence for pre-irradiation effects using noble gases analysis.**

Reference	Sample
<i>Separated clasts</i>	
Schultz et al. (1972), Schultz and Signer (1976, 1977)	Weston (H4), St. Severin (LL6), St. Mesmin (LL6)
Lorin and Pellas (1979)	Djermaia (H)
Wieler et al. (1986, 1989)	Fayetteville (H4)
Pedroni (1991)	Howardite Kapoeta
Pun et al. (1998)	Howardite Kapoeta
Metzler et al. (2008)	Regolith breccia NWA 869 (L3-6)
<i>Separated mineral grains (mostly olivine)</i>	
Caffee et al. (1983, 1986, 1987, 1988)	Murchison and Murray (CM2), Weston (H4), Fayetteville (H4) and howardite Kapoeta, lunar soils
Padia and Rao (1989)	Fayetteville (H4) and howardite Kapoeta
Hohenberg et al. (1990), Woolum and Hohenberg (1993)	CM2 chondrites Murchison, Murray and Cold Bokkeveld
Metzler (1997)	CM chondrites Cold Bokkeveld, Mighei, Murchison and Nogoya
Wieler et al. (2000)	Howardite Kapoeta
<i>Other meteorite components: Presolar SiC grains and CAIs</i>	
Lewis et al. (1994)	Presolar SiC grains from Murchison (CM2)
Vogel et al. (2009)	CAIs from Allende (CV3)

*For chondrites meteorite groups and types are given in brackets. Abbreviation: CAIs – Calcium-aluminium-rich inclusions.*

The pre-irradiation of individual mineral grains is actively debated, because some authors (e.g., Roth et al. 2011, Jones et al. 2005, Scott and Taylor 1983) assume that the analyzed grains are relict grains representing recycled chondrules. Relict grains are believed to have been present in the solid precursor assemblage of chondrules and to have survived the melting event(s) without being completely resorbed in the melt (Jones 2012).

Wieler (1989, 2000) proposed that the correlation of solar flare tracks with cosmogenic Ne excesses observed in olivine grains from CM chondrites can be alternatively explained by the mixing of parcels of mature parent body regolith, which had been in the top meter or so of tens of millions of years, with less mature regolith. Ne excesses might be caused in this view by GCR production in the parent body regolith (Wieler 2002b).

### 3 Motivation

The analysis of pre-irradiation effects in chondrules using noble gases may provide information about the energetic particle environment and the lifetime of chondrules as free-floating objects in the solar nebula (e.g., Roth et al. 2011) as well as processes in asteroidal regoliths. This information may help in putting constraints on conditions in the early solar system, including the poorly constrained period between chondrule formation and chondrite compaction (e.g., Metzler 2012).

The motivation for this work was provided by the fact that previous work was hampered by several systematic uncertainties. Trying to avoid these, it was hoped to obtain more reliable information on the existence and size of pre-irradiation. It was also hoped to be able to establish whether any irradiation may have happened in the solar nebula. Concerning the size of pre-irradiation and the percentage of pre-irradiated chondrules, there is different information in the literature. Chondrules from meteorites without SW gases in their matrices show only minor pre-irradiation effects since the CRE ages of chondrules were found to be only slightly elevated compared to the matrix (e.g., Polnau et al. 1999, 2001). In case of Renazzo (CR2)  $T_{21-1.11}$  CRE ages of all four analyzed chondrules are elevated in the range of 1.5 to 4.5 Ma relative to the matrix according to noble gas data obtained by Vogel et al. (2003, 2004) (see chapter 5.6.1). In contrast, in meteorites that do contain SW noble gases in their matrices significant pre-irradiation effects were observed, however not in all chondrules. In the case of Murchison (CM2), for example, about 20% of chondrules were found to be pre-irradiated, by up to ~30 Ma (Roth et al. 2011). Therefore, we expected to find significant pre-irradiation effects in chondrules from meteorites containing SW gases, and only minor effects in chondrules from meteorites free of SW-implanted gases. Since pre-irradiation of chondrules in the parent body regolith as proposed for Murchison (Roth et al. 2011) does not explain pre-irradiation of chondrules from solar gas-free meteorites, and a lack of SW gases in the matrix might suggest pre-irradiation as free-floating object in the solar nebula, this study concentrates on samples free of SW gases. To ensure a reliable conclusion about the existence of pre-irradiation, the number of analyzed chondrules has to be as large as possible.

To overcome the difficulties associated with the analysis of pre-irradiation effects in chondrules using noble gases, some new methodical approaches were used. Most important, in order to obtain accurate production rates of cosmogenic nuclides, which are necessary for a reliable calculation of CRE ages, noble gas analysis and the determination of abundances of important target elements using INAA in this study were performed on the identical sample material. This eliminates problems of sample inhomogeneity. In addition, CRE ages were calculated using “normal shielding” with shielding parameter  $(^{22}\text{Ne}/^{21}\text{Ne})_c = 1.11$ . Although the “nominal” CRE ages obtained in this way are not accurate, this approach is most reliable for the *comparison* of and search for differences among the ages of different samples from the same location because uncertainties involved in the shielding correction were avoided. Furthermore, possible gas loss due to thermal metamorphism was restricted since samples with petrologic types 2 to 3 were selected only, and two different tests were performed (“Bern” line, comparison of corrected  $T_{21}$  and  $T_3$  CRE ages) to confirm the absence of gas loss. Finally, meteorites with low CRE ages (maximum of 6 Ma) were selected since here the excess spallation acquired during pre-irradiation can be better detected (Roth et al. 2011, Eugster et al. 2007, Wieler 2002b, Polnau et al. 2001).

Based on the petrologic type, CRE age and chondrule size nine carbonaceous chondrites were selected, including two CR3 chondrites and ungrouped Acfer 094, which are very pristine and hence have a high probability to have preserved evidence for pre-irradiation.

## 4 Materials and methods

### 4.1 Sample selection

#### 4.1.1 Selection criteria

To analyze pre-irradiation effects of chondrules, CV and CR chondrites were selected, because both chondrite groups contain many and on average relatively large chondrules (see **Figure 2-3**) (Weisberg et al. 2006). Additionally, CR chondrites are very primitive and are believed to record nebula processes (Abreu and Brearley 2010) (see *chapter 4.1.2.2*).

The selection criteria used to select samples within both CV and CR chondrites are as follows (cf. Das and Murty 2009, Vogel et al. 2003, Polnau et al. 2001):

- i) Only slight thermal and aqueous alteration (petrologic type 2 to 3),
  - ii) Low CRE ages (maximum of 6 Ma) and
  - iii) Chondrule size.
- i) Meteorite samples, which were only slightly thermally (e.g., Roth et al. 2011) and aqueously altered on the meteorite parent body, are unlikely to have lost gas due to heating or formation of secondary minerals. Thus, differences in CRE ages of chondrules and matrix can be identified more easily (Polnau et al. 2001). Meteorites with petrologic type 3 are only minimally influenced by aqueous or thermal alteration (see **Figure 2-2**), therefore these are preferred. Furthermore, chondrules in meteorites with low petrologic type (2-3) are clearly separated from the matrix (Weisberg et al. 2006), indicating little interaction between chondrules and matrix and facilitating chondrule separation.
- ii) Low CRE ages of a few million years imply that the meteorites acquired relatively small concentrations of cosmogenic noble gases during their meteoroid stage (e.g., Roth et al. 2011). A maximum of 6 Ma facilitate the detection of pre-irradiation effects, because the excess spallation concentration can be better observed in chondrites with short CRE ages (Roth et al. 2011, Eugster et al. 2007, Wieler 2002b, Polnau et al. 2001). This is because for a given pre-exposure the relative contribution from the pre-irradiation is larger in case of small exposure ages, which is especially important if age differences between chondrules and matrix are small. Thus, the corresponding concentration of cosmogenic neon  $^{21}\text{Ne}_c$  should not significantly exceed  $2 \cdot 10^{-8}$  ccSTP/g.
- iii) A sufficient chondrule size is important, because enough sample material has to be available for reliable noble gases measurement. If we request the amount of cosmogenic  $^{21}\text{Ne}$  to be at least 10 times the blank of our MAP 215-50 system, in case of CV3 Allende (average  $^{21}\text{Ne}_c$  concentration from 23 chondrules:  $2.34 \cdot 10^{-8}$  ccSTP/g; Roth et al. 2011), a minimum chondrule diameter of 71  $\mu\text{m}$  is required. For Murchison (average  $^{21}\text{Ne}_c$  concentration of 32 chondrules:  $0.71 \cdot 10^{-8}$  ccSTP/g; Roth et al. 2011) the corresponding value is 114  $\mu\text{m}$ .

With these criteria in mind nine meteorites were selected (**Table 4-1**) using the noble gas data compilation of Schultz and Franke (2004). However, not all of them fulfilled all criteria, while in addition we also chose meteorites for which no previous noble gas date were available, for reasons explained below. For NWA 852 a CRE age of 9 Ma had been reported (Nakashima et al. 2009a), however, with comparably low  $^{21}\text{Ne}_c$  concentration. El Djouf 001 had both higher  $^{21}\text{Ne}_c$  concentrations and CRE ages, but both selection criteria were only slightly exceeded. Since many very large chondrules could be separated (see *chapter 4.2*) and CR2 chondrites turned out especially interesting, El Djouf 001 was included in the study.

No previous noble gas measurements had been performed on MET 00426 and QUE 99177. They were included, nevertheless, because both these CR3 chondrites (as well as ungrouped Acfer 094) appeared particularly suitable to record evidence for pre-irradiation of chondrules, due to their highly primitive nature (Abreu and Brearley 2010). According to several mineralogical and petrologic indicators (see *chapter 4.1.2.2*) they must be considered two of the most primitive members of CR chondrites (Abreu and Brearley 2010, 2008), and maybe the least altered of all meteorites.

A further reason to select CV and CR chondrites was that some meteorites of these chondrite groups had already been analyzed for pre-irradiation effects of chondrules (see *chapter 2.4.3.1*) (Allende: Roth et al. 2011, Das and Murty 2009, Eugster et al. 2007) or display data of interest in this respect (Renazzo: Vogel et al. 2004, 2003). Therefore, the results of this work might confirm previous studies.

**Table 4-1: Samples selected for analysis of pre-irradiation effects of chondrules in primitive meteorites.**

Chondrite group	Sample	Source	Fall/Find <sup>a</sup>	T <sub>21</sub> CRE age (Ma)	<sup>21</sup> Ne <sub>c</sub>
<i>Carbonaceous chondrites</i>					
CR2	Renazzo	Natural History Museum, Vienna	1824	4.2/7.1 [1]	1.45/2.45 [1], 2.44[2]*
	Ei Djouf 001		1989	5.9/6.1 [3]	1.66/1.75 [3]
	NWA 852	Senckenberg Institute, Frankfurt	2001	9 [4]	1.9 [4]
CR3	MET 00426	MWG Houston,	2000	nd	nd
	QUE 99177	NASA JSC	1999	nd	nd
CV3	Allende	MPIC, Mainz	1969	5.0 [9], 5.1 [5, 7], 5.2 [6], 5.5 [1], 5.6 [8]	1.70 [6]*, 1.61 [7]*, 1.76/2.22 [8] <sup>b</sup> , 1.88 [1]
	Vigarano		1910	5.2 [1], 5.4 [10]	1.68 [9]*, 1.77 [1], 1.82/1.84 [10]
	Acfer 082	Senckenberg Institute, Frankfurt	1990	1.4 [6]	0.43/0.53 [6]*
<i>Ungrouped chondrite</i>					
ungr. 3	Acfer 094	Natural History Museum, Vienna	1990	2.5 [6], 3.3 [5]	0.78/0.79 [6]*

<sup>21</sup>Ne<sub>c</sub> in units of 10<sup>8</sup> ccSTP/g. \* <sup>21</sup>Ne<sub>c</sub> was calculated from <sup>21</sup>Ne by iteration like in this study (see *chapter 4.5*), [1] Mazor et al. (1970), [2] Reynolds and Turner (1964), [3] Bischoff et al. (1993), [4] Nakashima et al. (2009a), [5] Scherer et al. (1997a), [6] Scherer and Schultz (2000), [7] Fireman and Goebel (1970), [8] Bogard et al. (1971), [9] Hintenberger et al. (1964), [10] Pepin (1969), private communication to Mazor (1970).<sup>a</sup>Source: MetBase 7.1, <sup>b</sup>measurements of matrix fraction <200 μm mesh and a large chondrule. MET 00426 and QUE 99177 are classified as CR3s according to Abreu and Brearley (2010), Acfer 094 is classified as ungrouped 3 chondrite according to Krot et al. (2007a).

#### 4.1.2 Sample description

In order to describe the meteorite samples in more detail characteristic features of CV and CR chondrites and ungrouped Acfer 094 are mentioned before each meteorite is characterized.



#### 4.1.2.1 CV chondrites

The compositions of CI chondrites are closest to that of the solar photosphere and they are often taken to be most primitive. However, CI chondrites suffered extensive exposure to fluids (see **Figure 2-2**). CV3 and CO3 carbonaceous chondrites and unequilibrated ordinary chondrites (UOCs) have chondritic compositions and are believed to be altered very little by secondary parent body processes. Thus, they may be more useful for a better understanding of primordial materials than CI chondrites (Grady and Wright 2006). However, it has been noted that CV chondrites experienced various degrees of thermal metamorphism and aqueous alteration (see below), with some objects like Allende having experienced comparably high (for type 3 meteorite) degrees of both processes. Whether they contain petrologic evidence of nebula records in chondrules and matrix or whether this evidence is a result of asteroidal processes is one of the major questions concerning CV3 chondrites (Bonal et al. 2006).

Some characteristics of CV chondrites are (Krot et al. 2007a):

- i) Millimeter-sized chondrules (see **Figure 2-3**) with mostly porphyritic textures, most chondrules are magnesium rich and ~50 percent are surrounded by coarse-grained igneous rims,
- ii) High matrix/chondrule ratios (0.5-1.2),
- iii) High abundance of millimeter-to-centimeter-sized CAIs and AOAs.

CV chondrites are a diverse group that was originally divided into oxidized ( $CV_{ox}$ ) and reduced ( $CV_{red}$ ) subgroups on the basis of modal metal/magnetite ratio and nickel content of sulfides (McSween 1977). In chondrites of the  $CV_{ox}$  subgroup metal in chondrules has been oxidized to magnetite, and most remaining metal is Ni-rich because Fe is more readily oxidized than Ni (Jones et al. 2005). Weisberg et al. (1997) subdivided the oxidized CV chondrites into the Allende-like ( $CV_{oxA}$ ) and the Bali-like ( $CV_{oxB}$ ) subgroups. They propose that  $CV_{oxA}$  share more similarities with  $CV_{red}$  than with the  $CV_{oxB}$  (**Table 4-2**), and the former two may be more closely related, representing a continuum in degrees of oxidizing conditions of the CV parent body or in the CV nebula region. Some differing features of the  $CV_{oxB}$  chondrites may be result from parent-body alteration, but some features suggest that they initially accreted from somewhat different mix of material (Weisberg et al. 1997).

**Table 4-2: Features of the three CV subgroups** (adapted after Weisberg et al. 1997).

	$CV_{red}$	$CV_{oxA}$	$CV_{oxB}$
Matrix/chondrule ratio	0.5-0.6	0.6-0.7	0.7-1.2
Metal/magnetite ratio	2-46	e.g., Allende: 0.2	-
Fayalitic olivine in the matrix		Fa <sub>32-60</sub>	Fa <sub>10-90</sub>
Oxygen isotopes	Overlapping and slightly depleted in $^{16}O$		Mostly higher $^{17}O$ compositions

Recent studies on CV chondrites, including thermal modeling (Carpözen et al. 2011) and paleomagnetic evidence (Gattacceca et al. 2013, Elkins-Tanton et al. 2011), imply that the CV parent body was partly differentiated, with an outer chondritic shell, which was unmelted and variable metamorphosed, overlying a differentiated and incomplete melted interior.

Although, most CV chondrites are classified as petrologic type 3 (see **Figure 2-2**), there are evidence for secondary processes, which affected to various degrees most of the CV chondrites. Chondrules in CV<sub>oxA</sub> chondrites for example are replaced by magnetite, Ni-rich sulfides, fayalitic olivine (Fa<sub>30-60</sub>), nepheline, and sodalite, whereas chondrules in CV<sub>red</sub> chondrites are virtually unaltered. Phyllosilicates are abundant in matrices of CV<sub>oxB</sub>, but rare in both CV<sub>oxA</sub> and CV<sub>red</sub> chondrites (Krot et al. 2007a).

### Allende (CV<sub>oxA</sub>)

The Allende meteorite fell near the village of Pueblito de Allende, Chihuahua, Mexico on February 8, 1969 (see **Table 4-1**) over a strewing field extending 50 km and covering an area of 300 km<sup>2</sup>. At least two tons of meteoritic stones have been recovered (**Table 4-3**), with crusted individuals ranging between 1 g to one individual of 110 kg. Based on the fragmental shape of most specimens, a major disruption of the parent body had been assumed, followed by minor subsequent fragmentation (Clarke 1970).

King et al. (1969) described that hand specimen of Allende appears homogeneous from piece to piece, dark grey, with many obvious chondrules ranging from averaging approximately 2 mm to as much as 13 mm in diameter. On fractured surfaces approximately 60 percent of chondrules are broken, but the remainder has nicely preserved hemispherical surfaces. Most chondrules are well-defined to sharply defined. Petrographic analyses of thin and polished section showed less than 1 percent metal and an estimated overall average of 60 percent chondrules and 40 percent matrix. The matrix is opaque with some microcrystalline matrix in standard thick sections, whereas in sections 0.01 mm thick a greater proportion of the matrix can be seen to be microcrystalline (King et al. 1969).

Allende represents one of the most metamorphosed CV3 chondrites, it is classified as type >3.6 (Bonal et al. 2006) that was heated to 550-600°C (Huss et al. 2006), indicated from studies of the crystallinity of carbonaceous material and the abundance of presolar grains and gaseous components (Scott 2007).

Allende is of special significance, because there is far more material available than for any other carbonaceous chondrite, and CAIs and chondrules are larger in size and more frequent than in most other carbonaceous chondrites (Stracke et al. 2012).

**Table 4-3: Detailed information about the selected meteorite samples (MetBase 7.1).**

Meteorite type	Sample	Total weight	Number of pieces	Shock	Weathering	Brecciated
<i>Carbonaceous chondrites</i>						
CR2	Renazzo	1 kg	3	S1-3		yes
	El Djouf 001	1.25 kg	30	S2	W2	yes
	NWA 852	174 g	4	-	W1	no
CR3	MET 00426	31,3	1		B	no
	QUE 99177	43,6	1		Be	no
CV3	Allende	~2.000 kg	many	S1		no
	Vigarano	~15 kg	2	S1-2		yes
	Acfer 082	208 g	1	S1	W2	no
<i>Ungrouped chondrites</i>						
ungr. 3	Acfer 094	82 g	1	S1	W2	yes

*MET 00426 and QUE 99177 are classified as CR3s according to Abreu and Brearley (2010), Acfer 094 is classified as ungrouped 3 chondrite according to Krot et al. (2007a).*

### **Vigarano (CV<sub>red</sub>)**

Vigarano fell on January, 22 1910 (see **Table 4-1**) in the district Ferrara, Italy. It represents the only fall in reduced CV chondrites (Macke et al. 2011). From 2 pierces ~15 kg have been recovered (MetBase 7.1) (see **Table 4-3**).

Levi-Donati et al. (1977) described Vigarano's matrix as fine-grained, opaque, and Mg/Fe-rich. It also includes lighter transparent parts which are Ca/Al rich, and chemically resemble larger Ca/Al rich fragments scattered throughout the meteorite.

Together with Efremovka and Leoville Vigarano is one of the least metamorphosed members of this subgroup. However, Vigarano's mean porosity seems to be higher than other reduced CV chondrites (Macke et al. 2011), which may suggest that Vigarano is more altered than other reduced CV chondrites (Hurt et al. 2012). Tomeoka and Tanimura (2000) reported intense parent body hydration and subsequent aqueous alteration that was highly localized based on studies of Vigarano rims. A minor constituent of Vigarano matrix is magnetite, representing an important indicator of aqueous effects in oxidized CV chondrites, which was likely formed during asteroidal alteration rather than in the solar nebula. The authors suggest that aqueous alteration played an important role in the formation of Vigarano matrix. The fact that Vigarano is now largely anhydrous implies either relatively little water or water loss during metamorphic reheating (Hurt et al. 2012).

Scott et al. (1992) found olivines of shock stages S1 and S2. Many porphyritic chondrules have only shock stage S1 and a few chondrules contain with only S2 olivines. Therefore, the authors conclude that Vigarano may be a breccia of S1 and S2 material rather than a rock shocked to S2 levels, which is consistent with the presence of solar-wind gases (e.g., Matsuda et al. 1980). Vigarano contains some oxidized, Bali-like (CV<sub>oxB</sub>) material (Krot et al. 2000b, MacPherson and Krot 2002). Bland et al. (2006) classified Vigarano as petrologic type 3.1-3.4.

### **Acfer 082 (CV3)**

Acfer 082 is one of many meteorites, which were found in 1989 and 1990 in different areas of the Sahara Desert. One pierce with a weight of 208 g has been recovered (see **Table 4-3**) (compare Wlotzka 1991).

Acfer 082 is a typical CV3 chondrite based on petrography and mineral chemistry. Large coarse-grained CAIs, fine-grained spinel-rich and olivine-rich aggregates, chondrules and fragments are embedded in a fine-grained groundmass mainly consisting of small Fe-rich olivine laths. The average composition of matrix olivine is Fa<sub>55</sub>. Acfer 082 is quite fresh (W2) concerning weathering (see **Table 4-3**) (Geiger and Bischoff 1992). Tonui et al. (2001) reported that Acfer 082 show loss of most of the elements apart from U, Co and Au suggesting heating at very high temperatures (>700°C).

Acfer 082 has not been classified into the oxidized or reduced group of CV chondrites (Krot et al. 2007a).

#### **4.1.2.2 CR chondrites**

CR chondrites belong together with CH and CB chondrites to the CR clan (see **Figure 2-1**). Members of the CR clan are among the most pristine early solar system materials (e.g., Krot et al. 2002, Kong and Palme 1999), which largely escaped thermal processing in asteroidal settings. As many of their chondritic components preserve nebula records of their formation essentially unchanged, they provide important constraints on the solar nebula models (e.g., Schrader et al. 2011, Krot et al. 2002). Evidence for the primitive nature of CR chondrites

include i) their unequilibrated silicates, ii) metal with a solar Ni:Co ratio (see below), iii) enriched  $^{15}\text{N}$  composition, iv) high presolar grain abundance, v) abundant and diverse range of organics, and vi) the primitive nature of their insoluble organic matter (Schrader et al. 2011 and references therein).

Some characteristics of CR chondrites include (Krot et al. 2007a):

- i) Abundant large Fe,Ni-metal-rich, porphyritic magnesian (type I) chondrules, which are typically surrounded by multi-layered coarse-grained, igneous rims, containing in many cases a silica phase,
- ii) High (~0.5 wt%)  $\text{Cr}_2\text{O}_3$  content in chondrule olivines,
- iii) Abundant heavily hydrated matrix and matrix-like lithic clasts (dark inclusions),
- iv) Abundant Fe,Ni-metal with a positive nickel versus cobalt trend and a solar Ni/Co ratio,
- v) Low abundance of CAIs and AOAs; AOAs and most CAIs show a uniform  $^{16}\text{O}$  enrichment,
- vi) Whole-rock refractory lithophile elemental abundances close to solar,
- vii) Whole-rock oxygen isotopic compositions form a unique CR-mixing line.

Most of the CR chondrites are classified as petrologic type 2, containing abundant phyllosilicates, carbonates, platelet and framboidal magnetite, and sulfides (Krot et al. 2007a). However, the degree of aqueous alteration ranges from minimally altered to extensive replacement of almost all primary components (Schrader et al. 2011). Weisberg et al. (1993) stated that Al Rais is the most altered, CR chondrites from the Antarctic and Algerian ones are less altered, and Renazzo is intermediate. As GRO 95577 contains no anhydrous silicates, it was classified as type 1 (Weisberg and Prinz 2000). Additionally, three CR chondrites have been (re)classified as type 3 since they largely escaped the aqueous alteration typical of type 2 and type 1, namely SAH 00182 (Weisberg 2001), MET 00426 and QUE 99177 (Abreu and Brearley 2010).

### **Renazzo (CR2)**

Several stones fell near Ferrara, Italy, on January 15, 1824 (see **Table 4-1**) after the appearance of light and followed by three detonations. About 10 kg of the meteorite were recovered, which is now called Renazzo (Mason and Wiik 1962). The preserved mass of Renazzo is less than 1 kg (Kong and Palme 1999) (see **Table 4-3**).

Wood (1962) described that Renazzo can be seen macroscopically to consist of clearly delineated chondrules, embedded in a fine, homogeneous, dull black matrix. Chondrules are small spheres, 2 mm and less in diameter. They are frequently rimmed by metallic iron, either as a continuous shell or discrete grains. Microscopically, Renazzo chondrules can be seen to consist of an aggregation of subhedral and euhedral crystals of olivine and/or pyroxene, 0.5 mm or less in size. All chondrules have rough surfaces, some are near spherical, others appear quite shapeless. Metallic nickel-iron occurs in chondrules as irregular inclusions, 0.2 mm and less in diameter, often concentrated close to the chondrule surfaces. In thin section, the matrix of Renazzo appears to be completely opaque and homogeneous. The author concluded that Renazzo had undergone little change since its origin based on igneous characteristics of chondrules including undevitrified glass, and that it may have occupied a position close to the surface on the meteorite parent body (Wood 1962).

Later, Prinz et al. (1985) reported that chondrules make up 60 vol% of Renazzo. Formisano et al. (1993) stated that Renazzo is a well-known and very interesting meteorite, because of its anomalous isotopic composition (nitrogen, xenon) and its very bright chondrules, which

are embedded in very dark material. The size distribution of chondrules range between 0.010 mm and 1-2 mm with a peak around 0.2 mm, some chondrules reach up to 5 mm and some inclusions are of even larger size (Formisano et al. 1993). Zanda et al. (2002) reported that Renazzo chondrules are often not spherical. Least melted chondrules have fine-grained silicates and fine-grained metal dispersed throughout. With progressing melting the outline of the chondrules becomes smoother and the metal can be seen to coalesce while a metallic rim starts to develop. More extensively melted chondrules are almost spherical (Zanda et al. 2002).

Based on the abundant phyllosilicates and opaque matrix, Renazzo is classified as type 2. However, the large fraction of Fe-Ni metal, up to 12 wt% different from any other carbonaceous chondrite studied before 1990, does not fit the type 2 classification (Kong and Palme 1999). Therefore and based on the low FeO in pyroxene and olivine of Renazzo, Mason and Wiik (1962) stated that Renazzo resembles enstatite chondrites. Mason (1971) later rejected the similarity between Renazzo and enstatite chondrites. The bulk chemistry of Renazzo is also unique: It has a CI Mg-normalized refractory element concentration and a moderately volatile element pattern different from other carbonaceous chondrites (Kong and Palme 1999). Renazzo was classified as anomalous CV2 (Wasson 1974), CV2 (Takahashi et al 1978), CR2 (McSween 1979), and anomalous carbonaceous chondrite (Kallemeyn and Wasson 1982) before the designation CR (Renazzo-type) was accepted by the meteoritical community after extensive chemically and petrographically studies of Renazzo and specimen of the same type found in the Sahara and Antarctica (Kong and Palme 1999 and references therein).

Renazzo is the only representative fall of the CR group. Klerner and Palme (1999) concluded that Renazzo may have retained better evidence of planetary processes than other carbonaceous chondrites based on the i) primitive nature of Renazzo and other CR chondrites, ii) bulk composition similar to CI chondrites (except for volatiles), iii) occurrence of Cr-rich metals reflecting very reduced conditions, and iv) coexistence of phyllosilicates and reduced metal reflects the absence of significant parent body heating.

### **EI Djouf 001 (CR2)**

EI Djouf 001 was found in 1989 (see **Table 4-1**) more than 500 km southwest of the Acfer region in the Sahara desert, Algeria (Bischoff et al. 1991). A mass of 1.25 kg was recovered in 30 pierces (see **Table 4-3**). EI Djouf 001 is mineralogically and chemically very similar to and probably paired with Acfer 059, 087, 097, 114, 139, 186, 187, 209, 270, suggesting that all meteorites appear to result from one fall.

Beside large chondrules (up to 1 mm in size, mean diameter  $1.0 \pm 0.6$  mm), making up about 60 vol%, the major lithological components of the Acfer-EI Djouf meteorite are chondrule and mineral fragments, CAIs, Fe,Ni metal (about 8-10 vol%), and dark inclusions embedded in a fine-grained fragment-bearing groundmass. Most chondrules are surrounded by several mineralogically distinct layers consisting of olivines, pyroxenes, metals (or their alteration products), and sulfides. Concerning the chondrule texture POP and PO chondrules dominate, PP and BO chondrules are common, and RP chondrules (see *chapter 2.2.2*) are quite rare (Bischoff et al. 1993). Most chondrules are type I (olivine =  $Fa_{0.5-5}$ , pyroxene =  $Fs_{1-5}$ ). Chondrule cores are anhydrous and contain unaltered glassy mesostasis, in contrast to other CR chondrites, especially Renazzo and Al Rais, in which the mesostasis of many chondrules have been altered to a chlorite-rich or serpentine-rich material. Thus, it was proposed that EI Djouf 001 experienced a lesser degree of parent body alteration than other CR chondrites (Weisberg and Prinz 1991).

El Djouf 001 has terrestrial limonite- and Ca-carbonate-filled fractures throughout the sample. In thin sections El Djouf and the Acfer samples look brownish due to the presence of oxidized iron produced by weathering (W2, see **Table 4-3**), although metallic Fe,Ni is still present (Weisberg and Prinz 1991). While most metal within the matrix is coated with films of limonite, metal in chondrules and other components is quite fresh and has only a very thin rind of limonite. In the terrestrial environment approximately one third of the metal was oxidized (Bischoff et al. 1993).

### **NWA 852 (CR2)**

NWA 852 was found in 2001 (see **Table 4-1**) in the Sahara desert, Morocco. Four pieces with a mass of 174 g were recovered (see **Table 4-3**). NWA 852 contains relative large chondrules (1-2 mm in diameter), Fe,Ni metal, and dark inclusions composed of serpentine and olivine (Nakashima et al. 2009a). It has a low chondrule/matrix ratio, and olivines are Fe-rich with Fa up to 53 mol% (Russell et al. 2002). NWA 852 is paired with NWA 801 (Nakashima et al. 2009a).

Leitner et al. (2010) concluded that NWA 852 may be a link between presolar, silicate-rich, nearly unaltered CR chondrites like MET 00426 and QUE 99177 (Floss and Stadermann 2009a) and CR chondrites with lower presolar grain abundance. This conclusion is based on i) the lowest presolar silicate/oxide ratio observed so far in presolar-grain-rich material (silicate/oxide = 2.0), ii) significant amounts of intact O-anomalous grains, iii) comparable nitrogen isotopic composition to those from more pristine CR chondrites, and iv) very heterogeneously distributed molecular cloud material (Leitner et al. 2010).

### **MET 00426 & QUE 99177 (CR3s)**

Both meteorites were found 2000 and 1999 in the Antarctic regions Meteorite Hills (MET) and Queen Alexandra Range (QUE) (see **Table 4-1**). MET 00426 and QUE 99177 consist both of one piece, weighing 31.3 g and 43.6 mg, respectively (see **Table 4-3**). Mineralogical characteristics of MET 00426 and QUE 99177 are summarized in **Table 4-4**.

Abreu and Brearley (2010, 2008) reclassified both meteorites as CR3 chondrites based on the following features:

- i) Both meteorites entirely escape the effects of thermal metamorphism indicated by
  - high abundances of FeS and the extreme fine-grained characteristics of the sulfides,
  - widespread occurrence of amorphous silicate material,
  - abundant nanosulfides in their matrices and
  - fine-grained rims;
- ii) Minimal and localized parent body aqueous alteration indicated by
  - preservation of clear, unaltered chondrule glass that shows no evidence of replacement of phyllosilicates and magnetite,
  - extremely rare calcite within the matrix and
  - phyllosilicates are rare in interchondrule matrix and fine-grained rims, and occur locally within the matrix and are very fine-grained and poorly crystalline

Lin et al. (2011) described MET 00426 as extremely unequilibrated assemblage of different minerals and fragments. The meteorite is a mixture of minerals formed in very different conditions, and the borders between inclusions and matrix are well-defined. The authors reported that the glassy mesostasis is pristine and does not show any evidence for alteration, confirming the primitive nature (Lin et al. 2011).

Schrader et al. (2011) stated that QUE 99177 is the isotopically lightest whole rock CR chondrite known ( $\delta^{18}\text{O} = 2.29\text{‰}$ ,  $\delta^{17}\text{O} = -4.08\text{‰}$ ), possibly due to isotopically light unaltered matrix. Despite it experienced aqueous alteration, the authors concluded that QUE 99177 provides the best approximation of the pristine CR chondrite parent body's oxygen isotopic composition before aqueous alteration took place (Schrader et al. 2011).

MET 00426 and QUE 99177 are at least as unmetamorphosed as ALH A77307 (CO3) and unique Acfer 094 (Abreu and Brearley 2010), which have been classified as the two most pristine carbonaceous chondrites currently known (Grossman and Brearley 2005). Mineralogical and compositional characteristics are consistent with extreme low degrees of aqueous alteration. Thus, Abreu and Brearley (2010, 2008) conclude that both meteorites represent additional samples of highly primitive, but extreme rare carbonaceous chondrites of petrologic type 3.00.

The highly primitive nature of MET 00426 and QUE 99177 is also recorded in the exceptionally high abundance of O-anomalous and C-anomalous presolar grains (e.g., Nguyen et al. 2013, 2008, Abreu and Brearley 2010, 2008; Floss and Stadermann 2009a, b).

**Table 4-4: Characteristics of CR3 chondrites MET 00426 and QUE 99177 according to Mittlefehldt (2001)**

	MET 00426	QUE 99177
Dimension (cm)	4.0 x 3.0 x 2.0	4.0 x 3.0 x 2.0
Fracturing*	B/C	B
<i>Macroscopic characteristics</i>		
Exterior	<ul style="list-style-type: none"> <li>– About 40 percent is covered with a mostly weathered fusion crust resembling an overcooked brownie.</li> <li>– The rest of the surface is dark brown and looks like an amalgamation of melted brown chondrules.</li> </ul>	Completely covered with weathered brown-black fusion crust
Interior	Black and contains irregular-shaped clasts and numerous chondrules	Soft chocolate brow matrix
Chondrules	White and rust-colored, 1 to 2 mm in size	Rust and cream colored, ranging in size from 1 to 3 mm
<i>Microscopic characteristics</i>		
Chondrules	Well-defined, metal-rich chondrules up to 3 mm and metal spheres up to 1 mm	Well-defined, metal-rich chondrules up to 2 mm in diameter
Matrix	Dark matrix of FeO-rich phyllosilicate	Dark matrix of FeO-rich phyllosilicate and metal
Silicates	Unequilibrated polysynthetically twinned pyroxene is abundant	
	<ul style="list-style-type: none"> <li>– olivines range from <math>\text{Fa}_{1-32}</math>, with most <math>\text{Fa}_{0-2}</math></li> <li>– pyroxenes range from <math>\text{Fs}_{1-4}\text{Wo}_{0-1}</math></li> </ul>	<ul style="list-style-type: none"> <li>– olivines range from <math>\text{Fa}_{1-31}</math>, with most <math>\text{Fa}_{0-2}</math></li> <li>– pyroxenes range from <math>\text{Fs}_{1-7}\text{Wo}_{1-5}</math></li> </ul>

*Fracturing categories: A – Minor cracks; few or no cracks are conspicuous to the naked eye, and no cracks penetrate the entire specimen. B – Moderate cracks; several cracks extend across exterior surfaces, and the specimen can be easily broken along the cracks. C – Severe cracks; specimen readily crumbles along cracks that are both extensive and abundant.*

#### 4.1.2.3 Ungrouped Acfer 094

Acfer 094 was found in 1990 in Tamanghasset, Algeria (see **Table 4-1**). One piece with a weight of 82 g was recovered (see **Table 4-3**) (Wlotzka 1991).

In a first description Bischoff et al. (1991) reported that Acfer 094 has trace element characteristics of CM2 chondrites (Fe/Mn: 123; Se: 14.9 ppm; Zn: 205 ppm), but cannot be a CM chondrite based on the oxygen isotope composition ( $\delta^{18}\text{O}$ : 1.11;  $\delta^{17}\text{O}$ : -3.91), which is more closely related to CO3 chondrites (Geiger and Bischoff 1992). Wlotzka (1991) classified Acfer 094 as CO(CM) chondrite. Scherer et al. (1997a) classified Acfer 094 as C2-ungrouped, may be in fact unique, but share common properties with CO and CM chondrites. Finally, other authors (e.g., Greshake 1997, Newton et al. 1995) stated Acfer 094 to be an ungrouped type 3 carbonaceous chondrite breccia showing mineralogical, petrologic, nitrogen isotopic and oxygen isotopic affinities to CM and CO chondrites. While its bulk chemical composition and the abundance of non-porphyrific chondrules (see below) are similar to those of CM chondrites, oxygen isotopic composition and matrix modal abundance are similar to those of CO chondrites (Krot et al. 2007a).

Acfer 094 consists of abundant chondrules, olivine aggregates, CAIs and fragments embedded in an extreme fine-grained, sulfide-rich ground mass. The abundance of non-porphyrific chondrules (~8%) is higher than in most CO chondrites, similar to that of CM chondrites (Geiger and Bischoff 1992). The chondrule size ranges between 30 to 1200  $\mu\text{m}$ ; however, chondrules larger than 500  $\mu\text{m}$  are very rare. Some chondrules have accretionary dust matles. The meteorite shows distinct alteration features due to terrestrial weathering (W2); the bulk-rock sample is basically unshocked (S1) (see **Table 4-3**) (Newton et al. 1995).

Ushikubo et al. (2012) found that most chondrules from Acfer 094 mostly consist of minerals and glass showing isotopically homogeneous and within each chondrule indistinguishable  $\Delta^{17}\text{O}$  values. These so called host chondrules crystallized from a melt with homogeneous  $\Delta^{17}\text{O}$  values that remained unchanged during subsequent cooling of the chondrule-forming melt. Most chondrules from Acfer 094 can be assigned into a  $^{16}\text{O}$ -rich group ( $\Delta^{17}\text{O} \sim -5\text{‰}$ ) and a  $^{16}\text{O}$ -poor group ( $\Delta^{17}\text{O} \sim -2\text{‰}$ ), indicating that chondrules formed in two distinct oxygen isotope reservoirs in the solar nebula. Relict olivine grains in Acfer 094 chondrules have  $\Delta^{17}\text{O}$  values from -2 to -6‰, corresponding to the  $\Delta^{17}\text{O}$  values of  $^{16}\text{O}$ -rich and  $^{16}\text{O}$ -poor chondrule groups. This may indicate a migration of precursor solids of chondrules from Acfer 094 between the locations of two isotope reservoirs (Ushikubo et al. 2012).

Acfer 094 largely escaped thermal metamorphism and aqueous alteration (e.g., Greshake 1997, Newton et al. 1995). Grossman and Brearley (2005) reported that Acfer 094 shares many properties with the least metamorphosed CO chondrite ALH A77307, including the distribution of  $\text{Cr}_2\text{O}_3$  in olivines and uniform high S in X-ray maps.

Although weathering effects are responsible for some fractionation, Wasson and Rubin (2010) proposed that nebular effects are also resolvable in the matrix composition of Acfer 094. Differences among different areas are inherited from the solar nebula and may have been carried by porous chondrules that experienced low (about 20%) degree of melting. Additionally, Acfer 094 has been comminuted by one or more impact events may causing volatile loss. Therefore, Wasson and Rubin (2010) concluded despite preserving evidence, like an exceptionally high abundance of presolar silicate (e.g., Leitner et al. 2013 (~190 ppm), Vollmer et al. 2009 (163 ppm); Krot et al. 2007a) implying a high degree of pristinity, that Acfer 094 is far from pristine in other respects. In this context, Nguyen et al. (2013) stated the wide range of Fe contents in presolar silicates from Acfer 094, suggestive of secondary processing on the meteorite parent body.



## 4.2 Separation of chondrules

Different methods for chondrule separation are mentioned in the literature concerning noble gas analysis of chondrules, depending on the system used for noble gas analysis, chondrule size, petrologic type and friability of matrix and chondrules (Polnau et al. 1999, 2001; Vogel et al. 2003, 2004; Eugster et al. 2007, Roth et al. 2008, 2009, 2011). As in this study the MAP 215-50 system was used for noble gas analysis instead of a laser system, chondrule and matrix samples had to be completely separated from each other. Furthermore, it is essential to know the exact weight of chondrule and matrix samples to receive concentrations.

First, gently crushing of a Pseudo-Murchison sample (believed to be CM chondrite Murchison) wrapped into aluminium foil was tested. Unfortunately, no chondrules were visible and the major part of the sample was pulverized. In view of the rareness of some of our samples and the small chondrule size, a freeze-thaw technique similar to Grossman (2010a) was chosen.

One advantage of this method is that the weight of the separated chondrules and matrices can be determined exactly. Furthermore, it is possible to perform different types of analysis on a single chondrule (by dividing the chondrule into several parts). Disadvantages are the unknown position of the separated chondrules within the meteorite and the fact that it is time-consuming. While this method involves exposure to water and somewhat enhanced temperature, any possible alterations should not be of consequence for the further analyses of this study.

Then the freeze-thaw technique similar to Grossman (2010a) was tested using Allende, Vigarano (both CV3), El Djouf 001 (CR2) and Isheyevo (CH-CB) samples before applying them to the rest of our meteorites. All samples were first inspected under a binocular microscope to ensure that they contained many, and as large as possible, chondrules. The samples were immersed into distilled water and evacuated (**Figure 4-1**) using a special vacuum pump and a desiccator, so that the air of the pore spaces was sucked out and replaced by water. During dipping the vial into liquid nitrogen the water freezes and expands, causing gradual disaggregation of the sample. Finally, the sample was thawed by warming in a water bath and the complete cycle was repeated. For all treatments special teflon vials (**Figure 4-2**) were used, because of their temperature resistance.

Grossman (2010a) was able to completely disaggregate a chip of the CM chondrite Murchison after 20 freeze-thaw cycles. In our case, after 20 freeze-thaw cycles with Allende, Vigarano, El Djouf 001 and Isheyevo samples, only few dispersed particles were visible and most of the samples were intact. After personal communication with Grossman (2010b) we added additional ultrasonic treatment. Initially, this was performed using a finger-shaped sonotrode, where only one sample could be treated at the same time. To speed up the process and make it more effective, a special designed ultrasonic device was acquired, including a sonotrode with space for five teflon vials or Eppendorf tubes. With this ultrasonic device, impulse and power could be adjusted separately and very fast high temperatures of the immersed water were reached. Therefore, different tests were performed; the best results were obtained by a sonication of one hour at an impulse/break ratio of 0.25 and 100% power. Eventually we chose to use ultrasonic treatment for one hour after ten freeze-thaw cycles (see **Figure 4-1**). After this, the dark-colored supernatant containing finely dispersed particles was decanted and dried. This matrix enriched material was considered to be mostly matrix material and will be called in the following that way. The remaining solid fraction was

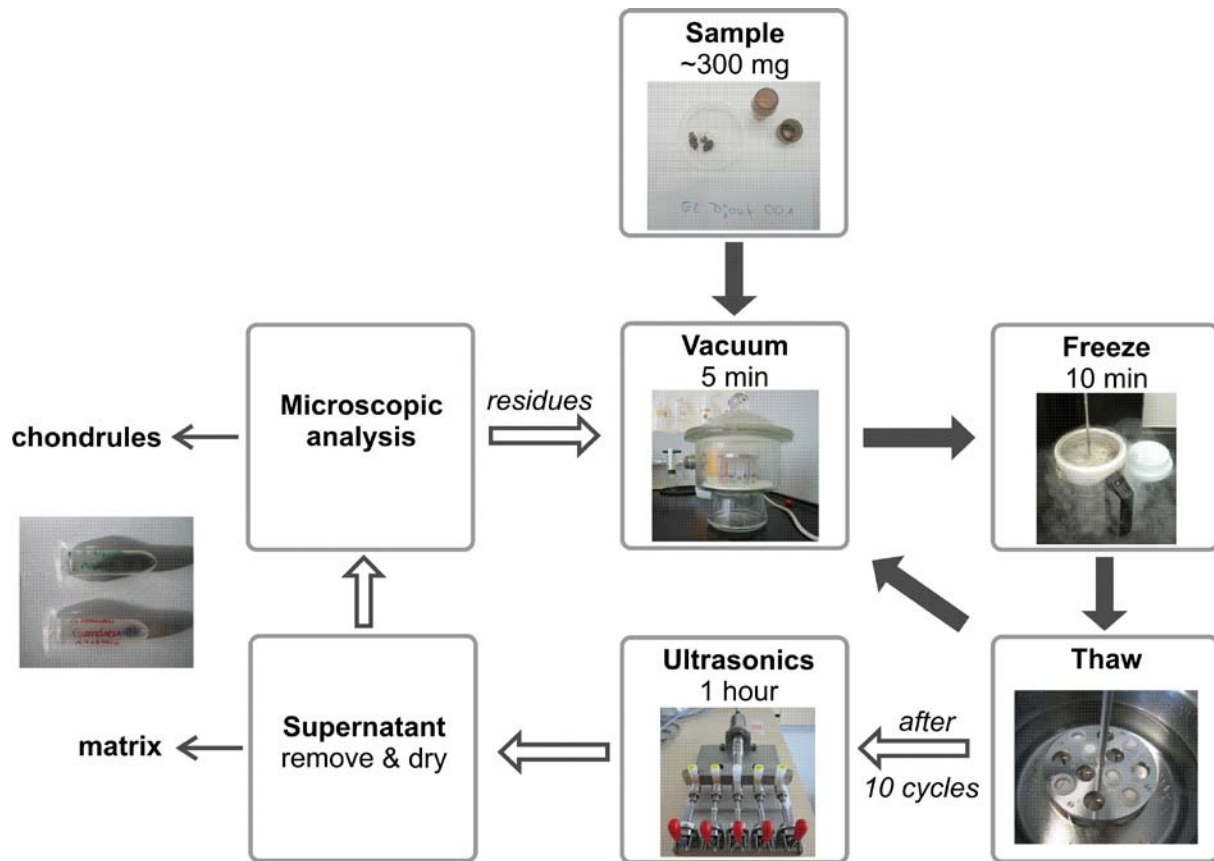


Figure 4-1: Freeze-thaw technique similar to Grossman (2010a) for chondrule separation.

analyzed under a binocular microscope and chondrules were hand-picked based on their spherical shape. They were exposed to another ultrasonic treatment for one hour to remove any possibly adhering matrix. Finally, chondrules were dried, photographed and weighted.

After testing the freeze-thaw technique as shown in **Figure 4-1** on Allende, Vigarano and El Djouf 001 samples, where many chondrules could be separated, it was decided to use this method to separate chondrules of the remaining samples. However, this freeze-thaw technique was not successful in disaggregating CH/CB<sub>b</sub>-like Isheyevo. This might be caused by high Fe,Ni metal abundances (~60 vol%). Fe,Ni metal contents in Isheyevo lithologies range between 7 and 90 vol%, whereby the metal-rich lithology (50-60 vol% Fe,Ni metal) is dominant (Ivanova et al. 2008). In Isheyevo interchondrule, fine-grained matrix material is nearly completely absent, as typical for CH and CB chondrites; fine-grained material occurs mainly as chondritic clasts (Bonal et al. 2010 and references therein). Metal grains seem

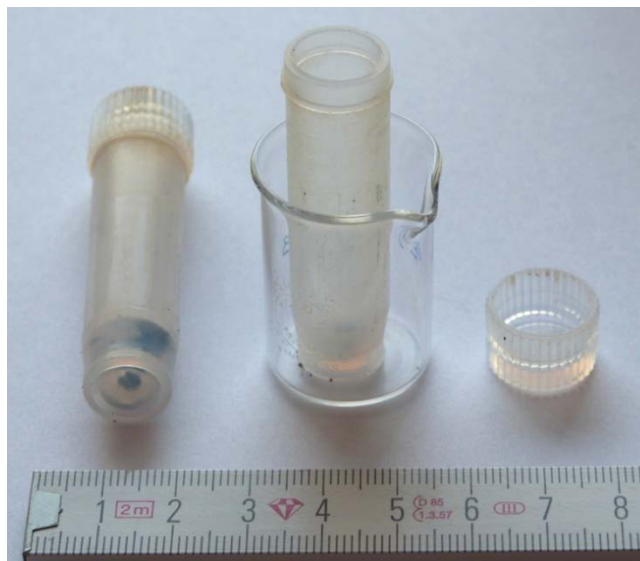


Figure 4-2: Special teflon vials used for chondrule separation.

to be interlinked with each other, which may suggest hot accretion like in the case of unequilibrated ordinary chondrites described by Metzler (2012). The presence of previously molten material between metal grains increases the cohesion of the single particles. Another reason, which might cause the failure of the freeze-thaw technique in disaggregating Isheyevu, may be the presence of thin layers of shock melts, which occasionally occur between the coarse-grained chondritic components (Ivanova et al. 2008). However, there is conflicting information concerning the shock classification (see **Table 2-1**) of Isheyevu in the literature. While some authors believe Isheyevu to be unshocked (S1) (Russell et al. 2005, Ivanova et al. 2005), other authors assume Isheyevu to be moderately shocked (S4) (Ivanova et al. 2008). Evidence for shock processing in lithic clasts seems to be rare (e.g. Ishii et al. 2009), whereas local occurrence of shock melts around some lithic clasts has been observed several times (e.g., Bonal et al. 2010, Ivanova et al. 2008).

In any case, due to the very compact structure of CH/CB<sub>b</sub>-like Isheyevu the water was hardly able to penetrate into the sample, and hence the freeze-thaw technique was not successful to disaggregate.

### 4.3 Determination of target elements

In order to determine CRE ages, it is essential to know the abundances of important target elements, which are required for the calculation of production rates of cosmogenic nuclides (see *chapter 2.3.2*).

In previous studies analyzing pre-irradiation effects in chondrules mostly electron microprobe analysis (EMPA) were used to determine target element abundances (**Table 4-5**). This technique has the advantage that the sample can be described in more detail. The main disadvantages of EMPA are that only a small volume can be analyzed and that it relies on sample homogeneity (or it requires homogenizing the sample material). However, sample homogeneity cannot be guaranteed, as shown by Ebel et al. (2008), who analyzed Renazzo chondrules using 3D X-ray microtomography.

As the focus of this work is the determination of CRE ages of chondrules and matrix samples, and hence it is essential to know representative target element abundances from entire chondrule and matrix material, we decided to investigate the majority of chondrules using instrumental neutron activation analysis (INAA). Only some selected chondrules were analyzed using SEM.

**Table 4-5: Methods used for the determination of target elements in studies analyzing pre-irradiation effects of chondrules**

Reference	Method
Polnau et al. (1999, 2001)	ICP-MS
Eugster et al. (2007)	ICP-OES/ICP-MS
Roth et al. (2008, 2009, 2011)	EMPA; SEM-EDS (Allende), SEM-BSE (Murchison)
Das and Murty (2009)	EMPA
Matsuda et al. (2010)	SEM-EDS
Das et al. (2010, 2012)	SEM-EDS
Huber et al. (2012)	nd

*The given references only include studies in which CRE ages have been determined.*

### 4.3.1 INAA analysis

Instrumental neutron activation analyses (INAA) were performed at the Australian Nuclear Science and Technology Organisation (ANSTO) in Kirrawee DC using the  $k_0$ -method. For more details see Bennett (2008) and Murrie et al. (2013). For our samples a short term irradiation was sufficient, and after waiting for about four weeks the irradiated samples were available for noble gas analysis.

To test if the detection limits of INAA were sufficient for analyzing the elements of interest in a few mg of meteoritic sample material, we first analyzed small samples of the L chondrite ALH 81032 (Wasson und Kallemeyn 1988) before turning to the chondrule samples. Subsequently, it was possible to adapt the neutron flux on the sample weight.

Samples were irradiated with thermal neutron fluxes ranging between  $1.4$  and  $2 \times 10^{13} \text{ cm}^{-2} \text{ s}^{-1}$  for 30 s to 45 min (usually not more than 15 min), depending on their weight. The energy spectrum is highly thermalized, with a ratio of thermal to epithermal neutrons of 1200 (Bennett 2008).

Based on nuclear cross sections it can be shown that no detectable Ne will be produced during irradiation with thermal neutrons (see *chapter 5.1.1*). Additionally, we analyzed a terrestrial sample to demonstrate this in practice.

Using INAA for the analysis of target element abundances has several advantages. First, it is possible to measure the abundances of a broad suite of elements, including trace elements with low abundances (Jones et al. 2005), of the order ppm to ppb and less (Greenberg et al. 2011), and it has a high reproducibility. Second, and of special importance of this study, because this method is non-destructive (e.g., Greenberg et al. 2011), further analyses can be performed on the same sample used for INAA analyses. For noble gas measurements in particular, it is also advantageous that the samples (unlike in case of EMPA) are not embedded in epoxy. A disadvantage is that with INAA silicon could not be measured (Jones et al. 2005) in our samples.

### 4.3.2 SEM analysis

For some selected chondrules SEM analyses were performed at the University of Heidelberg using a LEO 440 scanning electron microscope (SEM), equipped with an energy dispersive X-ray (EDX) analysis system (INCA, Oxford Instruments). A spectra database was used as standard, which contains typical spectra for minerals usually present in meteoritic samples. Samples were measured at an acceleration voltage of 20 kV. In order to get an overview of the samples, the chondrule samples were embedded in epoxy, polished and examined using the SEM. Mineralogical features including major minerals, texture, occurrence and grain sizes of chondrule rims, and weathering characteristics, could be identified.

After obtaining an overview of the embedded chondrules using the SEM, all investigated chondrules were divided into 16 equal-sized quadrants covering the greatest possible area of the embedded chondrule to provide a representative picture. In each of the quadrants, the elemental composition was determined using the SEM. Subsequently, results from all quadrants were combined to obtain the elemental composition for the bulk chondrules (see *chapter 5.1.2*). The given uncertainties refer to all quadrants and are therefore larger than uncertainties for few quadrants or a single quadrant. The elemental composition of chondrules determined by SEM analyses is given in wt% to enable a comparison with the values obtained by INAA analyses.

SEM analyses, like EMPA analyses, have the disadvantage that only a composition of a random section through each chondrule is measured, which might not be representative.

Furthermore, only elements present in abundances greater than ~0.05 wt% can be measured (Jones et al. 2005).

Please note that chondrules analyzed using the SEM were generally not analyzed using INAA or for noble gases. One exception is chondrule EI-ch11 from EI Djouf 001, which was splitted into two halves: Both were analyzed using INAA; in addition EI-ch11a was used for noble gas analyses and EI-ch11b was analyzed using the SEM. Since only EI Djouf chondrule EI-ch11b was analyzed using the SEM and INAA a comparison of both methods is restricted. Hence, most results from SEM analyses cannot be applied to chondrules used for INAA and noble gas analyses based on the different histories of chondrules.

#### 4.4 Mineralogical analysis

For some chondrules, for which the elemental composition had been determined using SEM, additional detailed mineralogical analyses were performed. For this, different sections with typical and/or interesting mineralogical features containing different phases were selected and the elemental composition was determined using point measurements and in some cases profile and area measurements (*see chapter 5.2*); concentrations are given as oxides (wt%) as usual for mineralogical considerations.

Chondrules, which were analyzed in more detail, were selected concerning how representative they were of the respective meteorite and how clear an assignment to a chondrule type could be made.

#### 4.5 Noble gas measurements

Noble gases He, Ne and Ar were analyzed using an MAP 215-50 noble gas electron source mass spectrometer at the Max Planck Institute for Chemistry Mainz. Details concerning the mass spectrometer, measuring procedures, and data reduction are given in Scherer et al. (1998), Schwenger et al. (2007) and Cartwright et al. (2013).

##### Measurement method

Chondrule and matrix samples were weighted and wrapped into Ni foil (<38 mg) and stored in the glass sample holder. To remove atmospheric gases, samples were baked in vacuum for one day at 120°C before noble gas extraction.

The samples were dropped into the cold Mo-crucible of a resistance-heated double vacuum Ta oven and stepwise heated. Since the samples were complete degassed at 1900°C, which was tested by several trials, two temperature steps at 600°C and 1800°C were chosen. The data for the release at 1900°C is omitted in the final results because it was practically equal to blank (Cartwright et al. 2013). Samples were degassed at ~600°C and ~1800°C for 40 min and 30 min, respectively and measured successively. For the blanks empty Ni foils were degassed. Due to the generally low gas amounts in chondrules, a precise blank correction was important (e.g., Vogel et al. 2004). Upper limits on blanks (in cc STP) were:  $^3\text{He}$   $5.7 \times 10^{-12}$ ,  $^4\text{He}$   $1.5 \times 10^{-10}$ ,  $^{20}\text{Ne}$   $3.4 \times 10^{-12}$ ,  $^{21}\text{Ne}$   $5.0 \times 10^{-14}$ ,  $^{22}\text{Ne}$   $8.5 \times 10^{-13}$ ,  $^{36}\text{Ar}$   $4.7 \times 10^{-12}$ ,  $^{38}\text{Ar}$   $9.6 \times 10^{-13}$ .

A Ti getter as well as Zr-Al getters were used to clean the noble gases from other gases released from the heated sample, where the latter react with the getter's surface. Noble gases were separated from each other using activated charcoal cooled by liquid nitrogen. Ar,

Kr and Xe were absorbed on the activated charcoal at  $\sim -196^\circ\text{C}$ , while He and Ne remain in the gaseous phase in the system. Hence, He and Ne were measured first. Thereafter, He and Ne were pumped off. Then the heavy noble gases Ar, Kr and Xe were released by heating the charcoal to  $\sim 150^\circ\text{C}$ .

In the mass spectrometer noble gases were ionized by electron impact, accelerated by an electric field and deflected by a magnetic field. Depending on the charge/mass ratio ions move on circular paths. Due to the variations of the magnetic field isotopes can be focused and measured on the detector (faraday) or multiplier in counting mode (Scherer et al. 1998).

### Data reduction

For the data reduction, the data of our samples were corrected for the extraction blank as well as for interference masses, including  $\text{H}_3$  and HD at mass 3 for He,  $\text{H}_2^{18}\text{O}$ , doubly charged  $^{40}\text{Ar}$  and  $\text{CO}_2$  at masses 20 and 22 for Ne, and hydrocarbons (like  $\text{C}_3$ ,  $\text{C}_3\text{H}_2$ ) as well as  $\text{H}^{35,37}\text{Cl}$  at masses 36 and 38 for Ar. The sensitivities for He, Ne and Ar were determined by regular analysis of a “calibration” gas mixture, which has a standard atmospheric isotopic composition except for He ( $^3\text{He}/^4\text{He} \sim 1$ ). The calibration enables us also to correct the effects of mass discrimination during analysis. Our data include the uncertainties in the above described corrections except a possible systematic error in the amount of calibration gas delivered by the gas pipette (Cartwright et al. 2013).

### Calculation of the cosmogenic component

Noble gases in a meteorite sample are composed of a trapped and a cosmogenic component with variable compositions, plus in case of He radiogenic  $^4\text{He}$ . There are different trapped components (e.g., solar, HL gas, Q gas) with distinct compositions, and the composition of the cosmogenic component depends on shielding and the target chemistry.

To deduce the cosmic-ray-produced fraction of a noble gas nuclide in a meteorite, it is necessary to correct for other noble gas components. To this end, the isotopic composition or at least some crucial isotopic ratios of the various components should be well constrained (see below) (Wieler 2002a). An unequivocal determination of the cosmogenic neon component is not possible, because more than two variable components influence the noble gas composition of a sample. However, a rather precise determination of the cosmogenic component is possible, if the cosmogenic component dominates, which is often the case for chondrules.

Cosmogenic components (abundance of  $^{21}\text{Ne}_c$  and cosmogenic  $^{21}\text{Ne}/^{22}\text{Ne}$  ratio) were determined using an iteration process assuming values for trapped ( $^{21}\text{Ne}/^{22}\text{Ne} = 0.032 \pm 0.004$ , Heber et al. 2009;  $^{20}\text{Ne}/^{22}\text{Ne}$  estimated by formula 7) and cosmogenic components ( $^{20}\text{Ne}/^{22}\text{Ne} = 0.83 \pm 0.03$ , Wieler 2002b).

$$\left(\frac{^{20}\text{Ne}}{^{22}\text{Ne}}\right)_{\text{estimated}} = \left(\frac{^{20}\text{Ne}}{^{22}\text{Ne}}\right)_{\text{measured}} + \left[10 + \left(\frac{^{21}\text{Ne}}{^{22}\text{Ne}}\right)_{\text{measured}} - 0.3\right] \quad (7)$$

Alternatively, using the same assumptions, trapped  $^{20}\text{Ne}/^{22}\text{Ne}$  and cosmogenic  $^{21}\text{Ne}/^{22}\text{Ne}$  can be derived by a fit to the measured data. However, this requires that the components have identical composition in the samples / temperature steps included in the fit, which cannot be taken for granted.

## 4.6 Production rate of cosmogenic noble gases

Reliable production rates for cosmogenic noble gas nuclides are essential for the calculation of reliable CRE ages. In previous studies analyzing pre-irradiation effects in chondrules different equations for the production of cosmogenic noble gases were used (see chapter 2.3.2) (**Table 4-6**). Most authors used empirical models, which required the knowledge of the chemical composition of the sample only. Only Roth et al. (2008, 2009, 2011) used physical models requiring the chemical composition as well as an assumption concerning meteorite size and shielding depth.

In this study production rates were calculated using the equations of Eugster (1988) (formulas 3a-3c in chapter 2.3.2), within the production rate for  $^{38}\text{Ar}$  is reduced by 13% following Schultz et al. (1991). For the correction factor  $F_j$  average L chondrite composition from the compilation of Wasson and Kallemeyn (1988) and the formulas by Cressy and Bogard (1976) ( $F_3'$  for  $^3\text{He}$ ), Schultz and Freundel (1985) ( $F_{21}'$  for  $^{21}\text{Ne}$ ), and Freundel et al. (1986) ( $F_{38}'$  for  $^{38}\text{Ar}$ ) (formulas 5a-c) were used. For  $F_{21}'$  Si was calculated by converting the major elements into oxides, and assuming the remainder to be  $\text{SiO}_2$  (see chapter 5.1.1); for sulfur an abundance of 2 wt% was assumed. Where the concentration of the target elements were below the detection limit, half of the detection limit was used.

As the chemical composition between matrix and chondrules and between chondrules can vary considerably (e.g. Roth et al. 2011, Ebel et al. 2008), abundances of important target elements were determined for each chondrule and matrix sample. For all chondrules and for most matrix samples the same material was used for noble gas measurements, avoiding the use of aliquots.

**Table 4-6: Equations used for calculating production rates of cosmogenic noble gases in studies analyzing pre-irradiation-effects in chondrules.**

Reference	Formula for the calculation of production rates
Polnau et al. (1999)	<i>Eugster (1988)</i> using the correction factors for $^3\text{He}$ , $^{21}\text{Ne}$ and $^{38}\text{Ar}$ by <i>Cressy and Bogard (1976)</i> , <i>Schultz and Freundel (1985)</i> , and <i>Freundel et al. (1986)</i> for different chemical compositions
Polnau et al. (2001)	<i>Eugster and Michel (1995)</i> , normalized to chemical compositions and shielding
Eugster et al. (2007)	<i>Eugster and Michel (1995)</i> for chemical defined samples (mostly equation for diogenites, eucrite formula for Acfer 059); otherwise <i>Eugster 1988</i> (L or H chondrites, as applicable)
Roth et al. (2008, 2009)	<i>Leya et al. (2000)</i> with assumptions about meteorite size and shielding depth
Das and Murty (2009)	<i>Eugster and Michel (1995)</i> for chondrules, <i>Eugster (1988)</i> for the bulk meteorites
Matsuda et al. (2010)	<i>Eugster (1988)</i> with average shielding (i.e. $(^{22}\text{Ne}/^{21}\text{Ne})_c = 1.11$ ) using the correction factors for $^3\text{He}$ , $^{21}\text{Ne}$ and $^{38}\text{Ar}$ by <i>Cressy and Bogard (1976)</i> , <i>Schultz and Freundel (1985)</i> , and <i>Freundel et al. (1986)</i> for different chemical compositions
Das et al. (2010, 2012)	<i>Eugster and Michel (1995)</i> for diogenites
Roth et al. (2011)	<i>Leya and Masarik (2009)</i> with assumptions about meteorite size and shielding depth
Huber et al. (2012)	an average $^{21}\text{Ne}_c$ production rate of $0.43 \times 10^{-8}$ STP/(gMa) was used based on the elemental compositions of Murchison chondrules and assuming uniform production rates (Roth et al. 2011)

*The given references only include studies in which CRE ages have been determined.*

Cosmogenic noble gas nuclides were calculated with and without shielding correction. For the shielding-corrected production rates  $P_{\text{corr}}$  the shielding parameter  $(^{22}\text{Ne}/^{21}\text{Ne})_c$  was used as determined from the noble gas measurements. If the ratio of trapped to cosmogenic component is high, this does not allow the determination of the  $(^{22}\text{Ne}/^{21}\text{Ne})_c$  ratio (e.g., Eugster 1988) and shielding-uncorrected production rates  $P_{1.11}$  with (i.e.  $(^{22}\text{Ne}/^{21}\text{Ne})_c = 1.11$ ) are given only.

The given uncertainties for the production rates include uncertainties from the abundances of target elements determined using INAA and uncertainties from noble gas measurements (i.e. shielding parameter). Uncertainties from the average composition of L chondrites (Wasson and Kallemeyn 1988) necessary for calculating the correction factor  $F_j$  (see *chapter 2.3.2*) and systematic uncertainties from the formula of Eugster (1988) are not considered.

#### 4.7 Calculation of cosmic ray exposure ages

Based on equation (2) (see *chapter 2.3.2*) cosmic ray exposure (CRE) ages for He, Ne, and Ar were calculated as follows:

$$T_j = \frac{c_j}{P_j} \quad (8)$$

with

$T_j$  – CRE age of the cosmogenic noble gas nuclide  $j$  (in Ma)

$c_j$  – abundance of the cosmogenic noble gas nuclide  $j$  (in cc/g)

$P_j$  – production rate of the cosmogenic noble gas nuclide  $j$  (in cc/(g Ma))

There are two limiting factors concerning the accuracy of production rates required for the calculation of CRE ages using cosmogenic nuclides: Single-stage exposure is assumed as well as a constant mean GCR flux over the timescales of interest (Wieler 2002b).

The given uncertainties for the CRE ages only include uncertainties from the determination of target elements (necessary for calculation of the production rates) and the uncertainties from noble gas measurements ( $^{21}\text{Ne}_c$ , shielding parameter).

#### 4.8 Calculation of $^{40}\text{K}$ - $^{40}\text{Ar}$ ages

The  $^{40}\text{K}$ - $^{40}\text{Ar}$  system is based on the decay of  $^{40}\text{K}$  to  $^{40}\text{Ar}$  with  $T_{1/2} = 1.28$  Ga (see **Table 2-7**). This is a dual decay, with 11% decaying to  $^{40}\text{Ar}$  by electron capture (e.g., McSween and Huss 2010, Renne et al. 2010, Farley et al. 2013). Since Ar is a gas and is effectively absent from solids when they crystallize from melts or condense from a gas phase, the addition of radiogenic Ar is easy to recognize. Hence, the  $^{40}\text{K}$ - $^{40}\text{Ar}$  system is an important system used for age dating. In contrast,  $\beta^-$  decay (89%) of  $^{40}\text{K}$  leads to  $^{40}\text{Ca}$ , which is the major isotope of Ca, which in turn is also more abundant than K in most minerals. Hence, the addition of radiogenic  $^{40}\text{Ca}$  is typically hard to detect, and the K-Ca system is only useful in systems with very high K/Ca ratios (McSween and Huss 2010).

However, only few  $^{40}\text{K}$ - $^{40}\text{Ar}$  ages of meteorites correspond to their formation times as solid objects or the formation times of their parent bodies. This is because the K-Ar chronometer is easily reset by moderate heating and most meteorites experienced thermal events, produced by internal metamorphism or impacts on the parent body. On the upside,  $^{40}\text{K}$ - $^{40}\text{Ar}$  ages are therefore useful for determining the times of secondary meteorite heating (Bogard 2011).



For the calculation of  $^{40}\text{K}$ - $^{40}\text{Ar}$  ages, K abundances were available from the INAA analyses (see chapter 4.3.1) and the abundance and isotopic composition of Ar was determined by the noble gas measurements (see chapter 4.5).  $^{40}\text{K}$  was calculated from the K abundance (0.01167%), while all of  $^{40}\text{Ar}$  was treated as radiogenic (note the almost complete absence of the  $^{40}\text{Ar}$  in trapped Ar in meteorites). The  $^{40}\text{K}$ - $^{40}\text{Ar}$  ages were calculated as follows (McSween and Huss 2010):

$$t = \frac{1}{\lambda_{\text{total}}} \ln \left( \frac{\lambda_{\text{total}}}{\lambda_{\text{EC}}} \frac{{}^{40}\text{Ar}^*}{{}^{40}\text{K}} + 1 \right) \quad (9)$$

with

$t$  –  $^{40}\text{K}$ - $^{40}\text{Ar}$  age (Ma)

$\lambda_{\text{total}}$  – combined decay constant for the decay of  $^{40}\text{K}$  to  $^{40}\text{Ar}$  and  $^{40}\text{Ca}$  ( $5.543 \times 10^{-10} \text{ a}^{-1}$ )

$\lambda_{\beta}$  – decay constant for the  $\beta^-$  decay of  $^{40}\text{K}$  to  $^{40}\text{Ca}$  ( $4.962 \times 10^{-10} \text{ a}^{-1}$ )

$\lambda_{\text{EC}}$  – decay constant for the electron capture of  $^{40}\text{K}$  to  $^{40}\text{Ar}$  ( $0.581 \times 10^{-10} \text{ a}^{-1}$ )

$^{40}\text{Ar}^*$  – radiogenic Ar

## 5 Results and discussion

### 5.1 Target elements

#### 5.1.1 INAA analysis

Elemental abundances including target elements for cosmogenic noble gases were determined by INAA.

#### *Influence of the sample weight and size on INAA analysis*

In order to work out optimal irradiation conditions for our small samples and to test sample homogeneity, some INAA analyses with aliquots of the typical L chondrite ALH 81032 were performed. Different aliquots of finely and coarsely powdered ALH 81032 were irradiated for 1 to 15 minutes with a neutron flux of  $(1.556 \pm 0.018) \times 10^{13} \text{ cm}^{-2} \text{ s}^{-1}$  (**Table 5-1**, **Figure 5-1**).

There is generally no significant difference between finely and coarsely powdered ALH 81032 aliquots (23 and 24 mg), which were irradiated for two minutes each. Thus, these measurements essentially provide an indication of the reproducibility of our measurements. Furthermore, it can be seen that the sample weight has no appreciable effect on our results. Both observations led us to proceed to measure also small meteorite samples with INAA. Naturally, in this case some elements like Ca, K and Ti have higher uncertainties, and Ni abundances are close to the detection limit. Interestingly, abundances of Al (see **Figure 5-1c**) and Ca in all ALH 81032 aliquots are somewhat lower than the average composition of L chondrites (Wasson and Kallemeyn 1988).

**Table 5-1: Elemental abundances of fine- and coarse-grained aliquots from L chondrite ALH 81032 determined using INAA.**

	L chondrite	sample weight (mg)				
		1.5	fine-grained		coarse-grained	
			10	24	23	57
Mg (%)	14.9	14.6(1.2)	14.3(1.2)	15.2(1.2)	14.8(1.2)	14.3(1.0)
Fe (%)	21.5	20.3(1.6)	27(6)	18.4(1.4)	24(14)	20.8(1.4)
Ni (%)	1.2	<0.8	1.5(4)	<0.7	1.4(8)	1.09(36)
S (%)	2.2	<6	<8	<7	<4	<6
Ca (%)	1.31	1.00(40)	1.01(14)	1.19(12)	0.99(16)	1.07(22)
Al (%)	1.22	1.09(8)	1.09(8)	1.13(8)	1.08(8)	1.02(8)
Na (%)	0.7	0.76(6)	0.66(6)	0.69(6)	0.72(6)	0.666(52)
Cr (%)	0.388	0.42(4)	0.41(6)	0.38(4)	0.39(6)	0.380(26)
Mn (%)	0.257	0.253(18)	0.248(2)	0.244(18)	0.250(18)	0.257(18)
K (mg/kg)	825	700(400)	610(180)	700(140)	960(180)	510(180)
Ti (mg/kg)	630	900(600)	500(400)	800(400)	700(400)	480(180)

*Uncertainties (1 s. d.) are given in parenthesis. Values for the L chondrite derive from Wasson and Kallemeyn (1988).*

#### **Influence of INAA analysis on the abundance of cosmogenic noble gas nuclides**

##### **i) Why has the experiment with the diorite been performed?**

To test if the irradiation of samples during INAA analyses produces interfering amounts of cosmogenic noble gas nuclides, in particular nuclear  $^{21}\text{Ne}_n$ , we irradiated a terrestrial sample and performed noble gas measurements on the irradiated and an analog

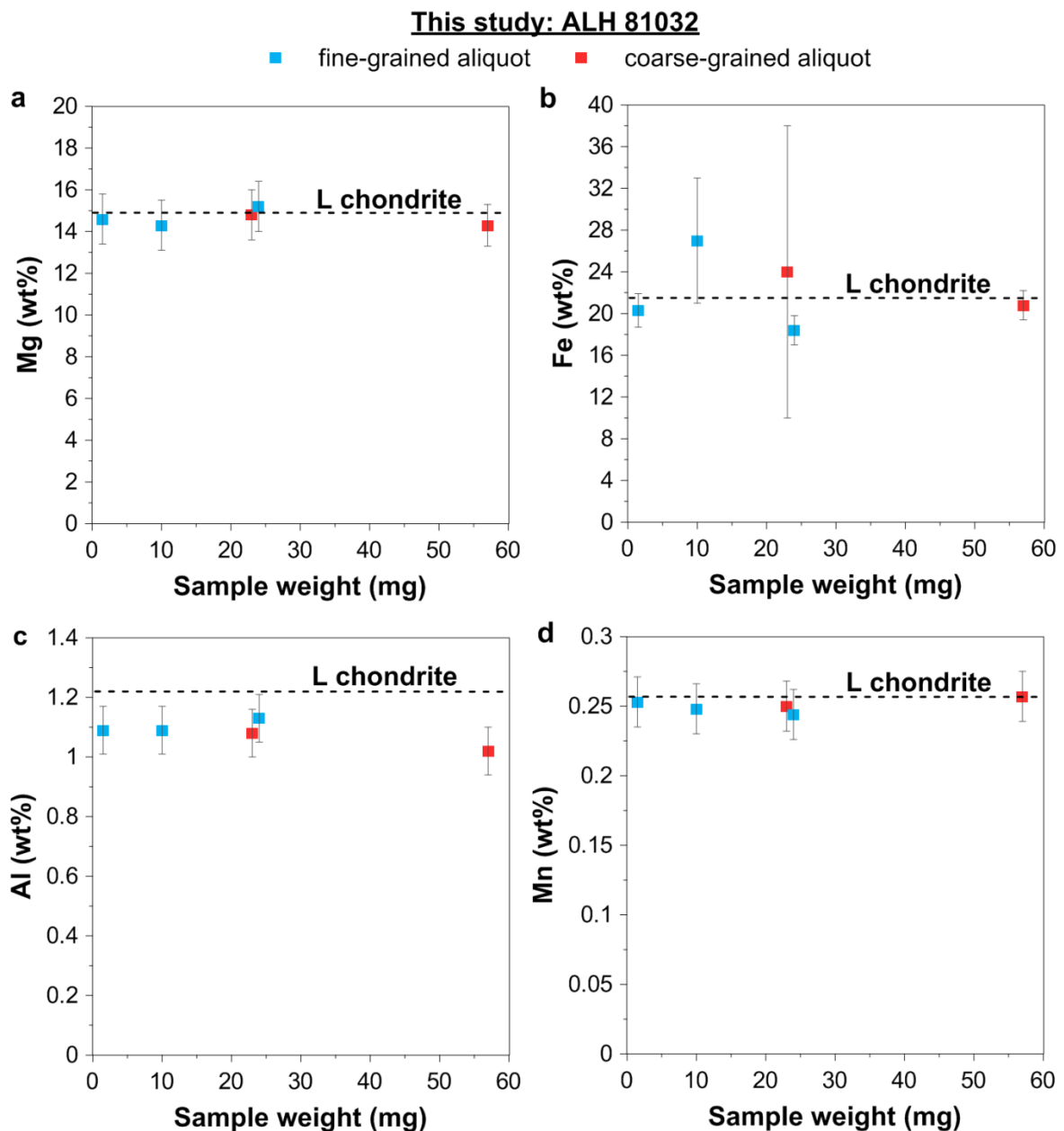


**Figure 5-1: Selected target element abundances from ALH 81032 aliquots determined with INAA. Values for the L chondrite derive from Wasson and Kallemeyn (1988).**

unirradiated sample. For this, we chose a large diorite sample and a longer irradiation time than typically used for our samples, in order to be more sensitive for “cosmogenic” noble gas nuclides (**Table 5-2**). The sample was another piece of the material from the Odenwald (Germany) region used by Michel et al. (1986) for simulating the cosmic ray irradiation of stone meteorites.

### **ii) Diorite and nucleogenic noble gases**

In addition it has to be considered that even the unirradiated diorite sample contains some “nucleogenic” contributions from reactions in the terrestrial environment, mostly caused as byproducts of U and Th  $\alpha$ -decay.

The nucleogenic production rate of Ne, He and Ar depends on several factors, including the elemental and isotopic composition of the target elements within the source rock, the neutron and  $\alpha$ -particle energy spectrum, the neutron/ $\alpha$ -particle production ratio, and the isotopic yield from the nuclear reactions. The  $\alpha$ -particles derive from U and Th decay, while the neutrons are produced from particle collisions with other elements (Graham 2002). The most important pathways for the natural production of nucleogenic Ne, He and Ar are given in **Table 5-3** (Wetherill 1954, Ballentine and Burnard 2002).

**Table 5-2: Noble gas data for unirradiated and irradiated diorite samples.**

	unirradiated diorite	irradiated diorite
$^3\text{He}$ [ $10^{-11}$ cc/g]	4.17(1.81)	257(10)
$^4\text{He}$ [ $10^{-8}$ cc/g]	2600(115)	2669(111)
( $^3\text{He}/^4\text{He}$ ) [ $10^{-4}$ ]	0.017(24)	0.958(18)
$^{20}\text{Ne}_n$ [ $10^{-8}$ cc/g]	0.40(11)	0.44(5)
$^{21}\text{Ne}_n$ [ $10^{-11}$ cc/g]	<b>0.26(12)</b>	<b>0.68(13)</b>
$^{40}\text{Ar}$ [ $10^{-8}$ cc/g]	859(19)	743(30)
$^{38}\text{Ar}_n$ [ $10^{-10}$ cc/g]	-0.11(36)	2.25(42)
$^{36}\text{Ar}_{tr}$ [ $10^{-8}$ cc/g]	0.78(2)	0.86(2)
$^{40}\text{Ar}/^{36}\text{Ar}_{tr}$	1107(12)	862(25)

Uncertainties (1 s. d.) are given in parenthesis.  
Abbreviation: n – nuclear

**Table 5-3: Reactions describing the production of nucleogenic Ne, He and Ar (Wetherill 1954).**

Reaction	Half life (a)	
<i>Neon Ne</i>		
$^{17,18}\text{O}(\alpha, n)^{20,21}\text{Ne}$		
$^{23}\text{Na}(n, \alpha)^{20}\text{Ne}$		
$^{24,25}\text{Mg}(n, \alpha)^{21,22}\text{Ne}$		
$^{19}\text{F}(\alpha, n)^{22}\text{Na}(\beta^+)^{22}\text{Ne}$	$^{22}\text{Na}$	2.602
<i>Helium He</i>		
$^6\text{Li}(n, \alpha)^3\text{H}(\beta^-) \rightarrow ^3\text{He}$	$^3\text{H}$	12.32
<i>Argon Ar</i>		
$^{35}\text{Cl}(n, \gamma)^{36}\text{Cl}(\beta^-)^{36}\text{Ar}$	$^{36}\text{Cl}$	301 000
$^{35}\text{Cl}(\alpha, p)^{38}\text{Ar}$		
$^{37}\text{Cl}(n, \gamma)^{38}\text{Cl}(\beta^-)^{38}\text{Ar}^a$		
$^{41}\text{K}(n, \alpha)^{38}\text{Ar}$		

<sup>a</sup>Ballentine and Burnard (2002).  
Bold marked reactions are likely (see text).

### iii) Additional contributions from the INAA analyses

Turning to the irradiated sample, based on the long half lives of  $^{22}\text{Na}$ ,  $^3\text{H}$  and  $^{36}\text{Cl}$  (see **Table 5-3**) we expect only minor additional production of  $^{22}\text{Ne}$ ,  $^3\text{He}$  and  $^{36}\text{Ar}$  produced via these precursors in the irradiated diorite compared to the unirradiated diorite. Also, because of the high reaction energy thresholds of the reactions  $^{41}\text{K}(n, \alpha)^{38}\text{Ar}$  (~9 MeV, Wetherill 1954, Eikenberg et al. 1993) and  $^{24,25}\text{Mg}(n, \alpha)^{21,22}\text{Ne}$  (2-4 MeV, Ballentine and Burnard 2002), **which were not reached during INAA analyses**, the production of  $^{38}\text{Ar}$  and  $^{21,22}\text{Ne}$  by these reaction seems unlikely.

### iv) Estimation of the influence of INAA analyses on the samples

When comparing the results of the irradiated diorite with our chondrule and matrix samples, we have to consider following:

- **Different chemical compositions.** The diorite contains lower Mg abundances (2.05 wt%, Michel et al. 1986), which is the most important target element for spallation production  $^{21}\text{Ne}_c$  (e.g., Wieler 2002b, Leya et al. 2001, Eugster 1988). Additionally, the diorite is also low in Fe (4.83 wt%, Michel et al. 1986) and enriched in Ca (4.50 wt%) and Al (7.89 wt%) (Michel et al. 1986). Diorites are also generally enriched in U (e.g., 2.33 ppm in diorites from East China, Gao et al. 1998).

To consider the lower Mg abundances in the diorite, we introduced a **factor a**, describing the ratio of Mg abundances in the samples relative to the diorite. As examples samples with the low and high abundances of Mg are given (see **Table 5-4**).

- The *enhanced irradiation dose of the diorite sample* compared to the majority of our meteorite samples will lead to higher production of cosmogenic nuclides. Therefore, we introduced a **factor b**, which describes the ratio of doses of the samples to that of the irradiated diorite. We chose chondrules with a low dose and matrix samples with a high dose (see **Table 5-4**) to cover the entire range of applied doses.

Both factors influence the concentration of apparent  $^{21}\text{Ne}_n$  in the samples. Taking both factors and the measured difference of the unirradiated and irradiated diorite into account,  $^{21}\text{Ne}_n$  in the matrix and chondrule samples ranges between  **$0.101 \times 10^{-11}$  cc/g and  $16.99 \times 10^{-11}$  cc/g for Vi-ch3 and Al-mat** (see **Table 5-4**); this corresponds to 0.005% and 0.732% of the measured  $^{21}\text{Ne}_c$  in the respective sample.

**Table 5-4: Influence of Mg abundance (factor a) and dosis (factor b) on the  $^{21}\text{Ne}_n$  concentration in the irradiated diorite.**

	<b>Factor a: Mg</b>	<b>Factor b: Dosis</b>	<b><math>\Delta^{21}\text{Ne}_n</math> diorite</b>
Chondrule	3.339 (Vi-ch3)	12.11 (Vi-ch3)	16.99
Matrix	0.037 (Al-mat)	6.488 (Al-mat)	0.101

*$\Delta^{21}\text{Ne}_n$  is given in  $10^{-11}$  cc/g.  $\Delta^{21}\text{Ne}_c$  is only minimally influenced by both factors in Al-mat, whereas Vi-ch3 shows the maximum influence of both factors.  
Abbreviations: ch-chondrule, mat-matrix, Vi-Vigarano, Al-Allende.*

#### *Comparison of $^{21}\text{Ne}_n$ in diorites based on $^4\text{He}/^{21}\text{Ne}_c$ ratios in crustal rocks*

The apparent  $^{21}\text{Ne}_n$  concentration in the unirradiated diorite can be explained by a comparison with the  $^4\text{He}/^{21}\text{Ne}_c$  ratio in crustal rocks, which typically accounts for  $\sim 1.71 \pm 0.09 \times 10^7$  (Ballentine and Burnard 2002). Using this ratio and the measured  $^4\text{He}$  values (see **Table 5-2**),  $^{21}\text{Ne}_n$  concentrations of  $0.26 \times 10^{-11}$  cc/g and  $0.27 \times 10^{-11}$  cc/g were calculated for the unirradiated and irradiated diorite. While this calculated  $^{21}\text{Ne}_n$  concentration of the unirradiated diorite fits with the measured value, the  $^{21}\text{Ne}_n$  concentration of the irradiated diorite exceeds the calculated value, suggesting that INAA can slightly produce  $^{21}\text{Ne}_n$ .

#### *Influence of INAA on He and Ar*

In the case of He we assume that the nucleogenic He is produced by non-thermal neutrons, because  $^3\text{H}$  from the reaction  $^6\text{Li}(n, \alpha)^3\text{H}$  had not decayed to  $^3\text{He}$  significantly at the time of He measurement (see) and the target chemistry plays a minor role only. For Ar the situation is more complicated.  $^{38}\text{Ar}$  will be efficiently produced by the reaction  $^{37}\text{Cl}(n, \gamma)^{38}\text{Cl}(\beta^-)^{38}\text{Ar}$  during INAA. Based on the measured Cl abundances of the samples, the irradiation parameter (irradiation time and neutron flux) as well as the cross section for this reaction of 0.42 barn the contribution of reactor produced on  $^{38}\text{Ar}_c$  was calculated: The values are in most cases significant, but generally <20%. In addition, abundant trapped gases in some chondrule and matrix samples make the determination of the cosmogenic and nucleogenic component for Ar difficult.

These considerations demonstrate that INAA has no significant effect on  $^{21}\text{Ne}_c$  in which we are interested in. This conclusion is based on the **high reaction threshold of reactions producing  $^{21}\text{Ne}_c$**  and that **thermal neutrons** are used for the INAA analysis. Additional, possibly contributing reactions have **low cross sections** and the **abundances of target elements** for (n,  $\gamma$ )-reactions (e.g.,  $^{20}\text{Ne}$  and  $^{21}\text{Ne}$  for production of  $^{21}\text{Ne}$  and  $^{22}\text{Ne}$ , respectively, by this reaction) are low. In contrast,  $^3\text{He}$  is slightly and  $^{38}\text{Ar}_c$  is significantly influenced by INAA. That is a further reason (see chapter 5.3.1) to focus on the noble gas results from neon in the following.

### Elemental abundances

Results of the INAA analyses are given in **Appendix 1 & 2**. Included in **Appendix 1** is silicon (Si), which was not measured; but calculated by converting the other major elements into oxides and assuming the rest to be  $\text{SiO}_2$ . For that, it had to be assumed, in which oxidation state iron (Fe) occurs in the chondrules and matrix samples. Fe can be present as metal ( $\text{Fe}^0$ ), as  $\text{Fe}^{+2}$  in silicate minerals and in sulfide, and/or (minor in our case) as  $\text{Fe}^{3+}$  (along with  $\text{Fe}^{+2}$ ) in magnetite ( $\text{Fe}_3\text{O}_4$ ). The oxidation state of chondrules can vary within an individual chondrite, ranging from being reduced to relatively oxidized (Jones et al. 2005). To determine Si contents, we considered three possibilities:

- 1) Estimate the form of Fe from our SEM analysis.
- 2) Take the form of Fe from the literature. Ebel et al. (2008) analyzed chondrules from CR2 Renazzo and found that Fe is present to about 75% reduced in metal and the remaining 25% is present as FeO in silicates.
- 3) Assume Fe to be totally oxidized (providing a lower limit to the Si content) or occurring totally as metal and sulfide (providing an upper limit to the Si content). These minimum and maximum values are listed in **Appendix 1**.

Possibility 2) was not used, because it is questionable if the results from CR2 Renazzo analyzed by Ebel et al. (2008) are generally applicable for CR3 and CV chondrites or even other CR2 chondrites. Possibility 1) was also not chosen, because not all samples were analyzed using SEM. As Si enters into the calculation of the production rate of cosmogenic neon (see chapter 4.6), in the following neon results are given for both minimal and maximal Si abundances, i.e. possibility 3) was preferred. Since cosmogenic Ne production on Si is mostly small compared to that produced on Mg, *differences are mostly minor and of no consequence for the conclusions* obtained in this work (see chapter 5.3.3). All figures displaying  $T_{21}$  CRE ages show results calculated with **Si<sub>50</sub>**, i.e. for the calculation of the production rate of cosmogenic neon  $P_{21}$  the mean value of minimum and maximum Si abundances was used.

However, it is suggested that the production rates of cosmogenic neon  $P_{21}$  and  $T_{21}$  CRE ages of most chondrules calculated with *maximal Si abundances correspond more closely to the real conditions* based on these two arguments:

- Most chondrules are type I (FeO-poor) chondrules (Zanda 2004).
- Prior (1916, 1920) proposed that “the less the amount of nickel-iron in chondritic stones, the richer it is in nickel and the richer in iron are the magnesium silicates”. The Ni/Fe ratios of chondrules from Renazzo, El Djouf 001, Vigarano and Acfer 094 are lower compared to those of the matrix samples (**Table 5-5**). According to Prior’s rule, Fe may thus occur mainly as metal and sulfide in these chondrules in accordance with Ebel et al. (2008).

**Table 5-5: Ni/Fe ratios of all matrix (mat) and chondrules (ch) samples.**

Sample	Ni/Fe	Sample	Ni/Fe	Sample	Ni/Fe
<i>CR2 chondrites</i>		<i>CR3 chondrites</i>		<i>CV3 chondrites</i>	
Re-mat	0.0570(7)	MET-mat	<0.0514	Al-mat	0.0552(5)
Re-ch1	0.0444(11)	MET-ch1	0.0570(3)	Al-ch3	0.0869(7)
Re-ch2	0.0563(8)	MET-ch2	0.0781(9)	Al-ch6	0.0700(15)
El-mat	0.0652(6)	MET-ch3	0.0680(4)	Vi-mat	0.0584(12)
El-ch2	<0.0167	MET-ch4	0.0567(7)	Vi-ch1	<0.0797
El-ch3	<0.2188	MET-ch5	0.0652(9)	Vi-ch2	<0.0381
El-ch4	0.0587(13)	MET-ch6	0.0562(8)	Vi-ch3	0.0353(6)
El-ch5	<0.0260	QUE-mat	0.0477(4)	A82-mat	0.0533(12)
El-ch6	<0.0880	QUE-ch1	0.0592(5)	A82-ch1	0.0937(28)
El-ch7	0.0617(9)	QUE-ch2	<0.2076	A82-ch2	0.0529(6)
El-ch8	<0.0447	QUE-ch3	0.0668(8)	A82-ch3	0.0501(8)
El-ch9	0.0576(8)	QUE-ch4	0.0674(13)		
El-ch10	0.0565(9)	QUE-ch5	0.0785(3)		
El-ch11a	<0.0597	QUE-ch6	0.0675(7)		
NWA-mat	0.0557(7)	<i>Ungrouped 3 chondrite</i>			
NWA-ch1	0.0879(8)	A94-mat	<0.0485		
NWA-ch2	0.0743(6)	A94-ch1	<0.0469		

Uncertainties (1 s. d.) are given in parenthesis. Where values are marked in gray, Ni concentrations were below the detection limit; the listed values were calculated with the detection limit.

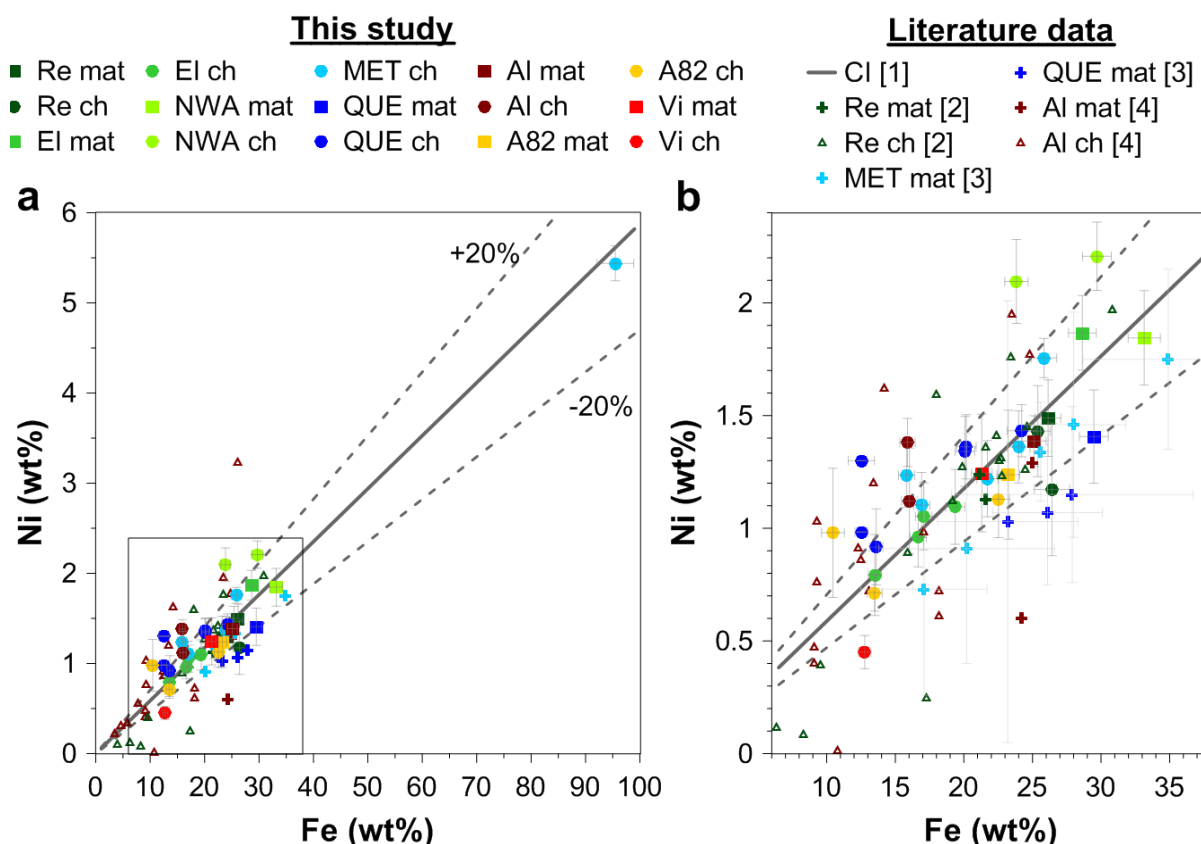


**Figure 5-2: Relative abundances of Ni versus Fe of all chondrule (ch) and matrix (mat) samples (a) and an inset of the left corner (b). Samples where the Ni concentrations were below the detection limit are omitted. Typical values for Ni/Fe of CI chondrites are indicated by a solid line and derive from [1]. Sources of data: 1-Wasson and Kallemeyn (1988), 2-Kong and Palme (1999), 3-Abreu and Brearley (2010), 4-Rubin and Wasson (1987).**

Ni/Fe ratios of most samples plot within a 20% interval around typical values for CI chondrites (see **Figure 5-2**). Values for our Renazzo chondrules agree with Renazzo chondrules analyzed by Kong and Palme (1999), whereas our matrices from Renazzo and QUE 99177 have higher Ni and Fe abundances than those measured previously (Kong and Palme 1999, Abreu and Brearley 2010); this might be caused by sample inhomogeneity. Fe abundances of Allende matrix from our measurements agree well with those from Rubin and Wasson (1987), while our Allende matrix has a higher Ni abundance. Our Allende chondrules plot in the interval of Allende chondrules from Rubin and Wasson (1987).

Ni/Fe ratios of three CV chondrites matrix samples are comparable with the value typical for CV chondrites (0.057) (Wasson and Kallemeyn 1988) (see **Table 5-5**). Our two Allende chondrules have higher Ni/Fe ratios (Ni/Fe: 0.0700 and 0.0869) compared to most Allende chondrules analyzed by Roth et al. (2011) (Ni/Fe: 0.047 to 0.111; mean: 0.071, only three chondrules have Ni/Fe ratios  $\geq 0.090$ ).

Major elemental compositions of chondrules show a great diversity both within and among chondrite groups (Jones et al. 2005). Relative abundances of Fe, Si and magnesium (Mg) of chondrules and matrix samples are shown in **Figure 5-3**. Most chondrules and matrix samples plot between the olivine and pyroxene tie-lines, indicating that Fe, Mg, Si and oxygen (O) account for >85% of their mass (Jones et al. 2005). In general, chondrules show higher Mg abundances and lower Fe and Si abundances compared to matrix samples (except Vi-ch1, Vi-ch2, El-ch), which may be caused by evaporation of major lithophiles and loss of Fe by reaction to gas phase and physical loss (e.g. Scott 2007, Jones et al. 2005,

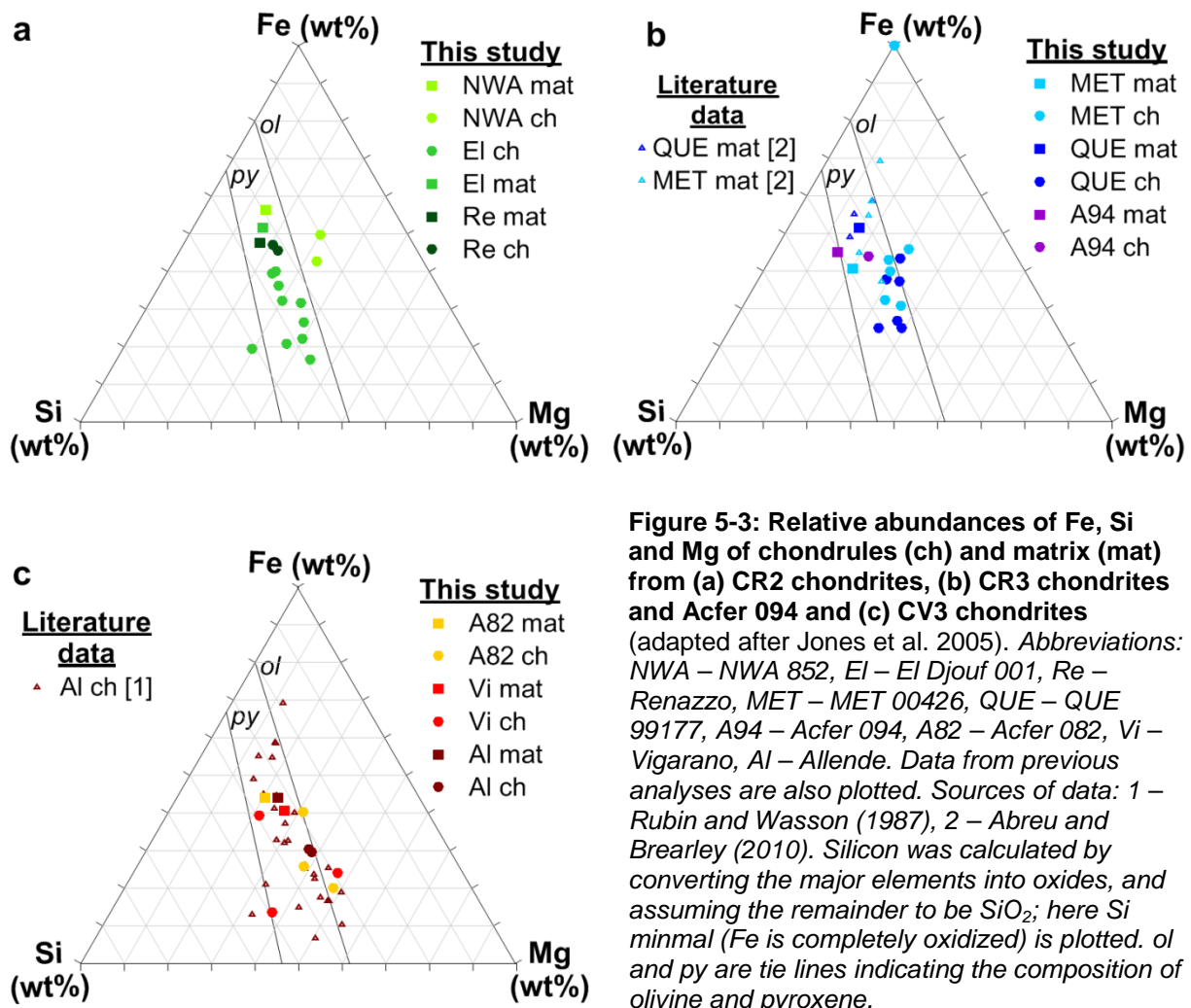


**Figure 5-3: Relative abundances of Fe, Si and Mg of chondrules (ch) and matrix (mat) from (a) CR2 chondrites, (b) CR3 chondrites and Acfer 094 and (c) CV3 chondrites** (adapted after Jones et al. 2005). *Abbreviations: NWA – NWA 852, El – El Djouf 001, Re – Renazzo, MET – MET 00426, QUE – QUE 99177, A94 – Acfer 094, A82 – Acfer 082, Vi – Vigarano, Al – Allende. Data from previous analyses are also plotted. Sources of data: 1 – Rubin and Wasson (1987), 2 – Abreu and Brearley (2010). Silicon was calculated by converting the major elements into oxides, and assuming the remainder to be SiO<sub>2</sub>; here Si minimal (Fe is completely oxidized) is plotted. ol and py are tie lines indicating the composition of olivine and pyroxene.*



Hewins 1997) (see *chapter 2.2.3.2*). Chondrules of CR3 chondrites (**Figure 5-3b**) show only a slight spread of Si and Mg contents compared to El Djouf 001 or Vigarano chondrules (**Figure 5-3a, c**). MET-ch1 seems to be a metal chondrule consisting mainly of Fe and Ni and similar to metal spheres with diameters up to 1 mm described by Mittlefehldt (2001) (see *chapter 4.1.2.2*). Our MET 00426 and QUE 99177 matrices and Allende chondrules are comparable with previous measurements (see **Figure 5-3b, c**).

The representation in **Figure 5-3** is affected by the uncertainty from the Si calculation. This uncertainty is avoided in **Figure 5-4**, where elemental abundances of Fe and Mg are shown relative to CI composition. In general, matrix samples show higher Fe and lower Mg abundances compared to most chondrules, which may indicate different compositions of precursor materials, open-system behavior during chondrule formation (see *chapter 2.2.3.2*) and/or secondary alteration. Our results for Allende chondrules plot in the interval of Allende chondrules analyzed by Rubin and Wasson (1987) (**Figure 5-3c, Figure 5-4**).

In **Figure 5-5** elemental abundances for chondrules and matrix of all samples relative to Mg and CI chondrite abundance are shown; the elements are arranged according their geochemical properties (lithophile, siderophile) and within each group in the order of increasing volatility (e.g., Kong and Palme 1999). In most chondrules, refractory elements (Al, Ca, Ti) are not fractionated relative to one another, i.e. their abundance pattern is flat (Jones et al. 2005). In contrast, matrices of El Djouf 001 and Vigarano are enriched in titanium (Ti) and vanadium (V) (see **Figure 5-5b, h**). At the first view, high Ti and V abundances of El Djouf 001 matrix do not agree with the findings by Bischoff et al. (1993), who reported that the composition of the nonvolatile fraction of the Acfer-El Djouf meteorite is surprisingly similar to CI chondrites instead of CV and H chondrites, which show either enrichment or depletion of refractory elements.

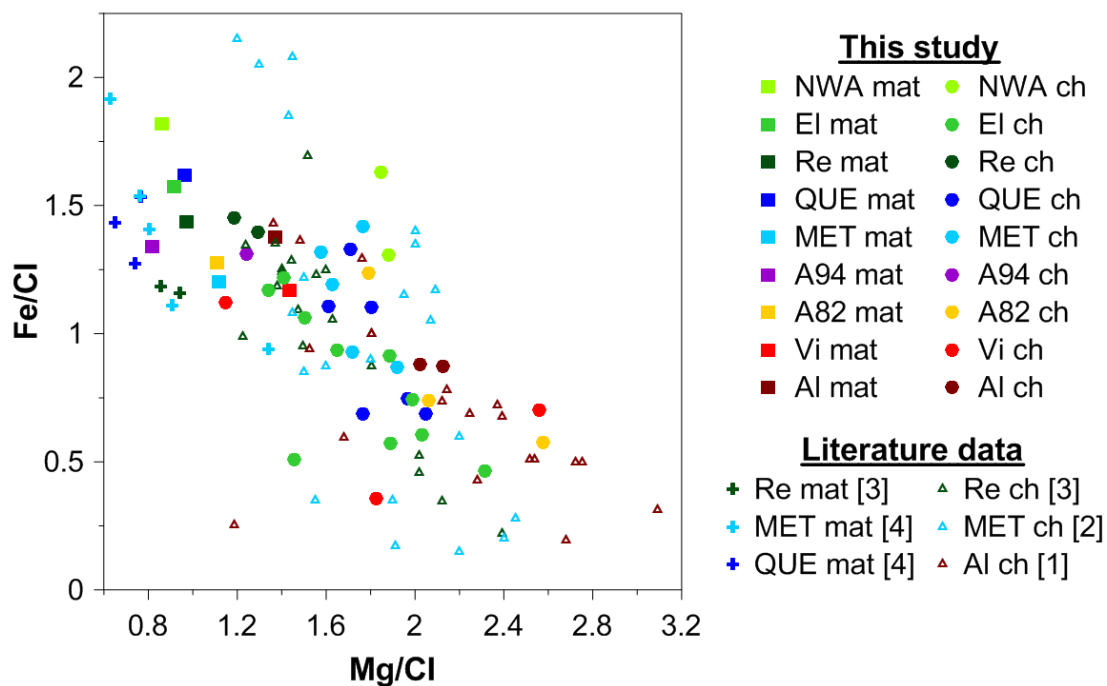


**Figure 5-4: Relative abundances of Fe vs. Mg for all chondrules (ch) and matrix (mat) samples relative to CI** (adapted after Jones et al. 2005). Values for CI elemental abundances are from Lodders (2003). Abbreviations: NWA – NWA 852, El – El Djouf 001, Re – Renazzo, QUE – QUE 99177, MET – MET 00426, A94 – Acfer 094, A82 – Acfer 082, Vi – Vigarano, Al – Allende. Data from previous analyses are also plotted. Sources of data: 1 – Rubin and Wasson (1987), 2 – Berlin (2009), 3 – Kong and Palme (1999), 4- Abreu and Brearley (2010). MET ch1 is not shown.

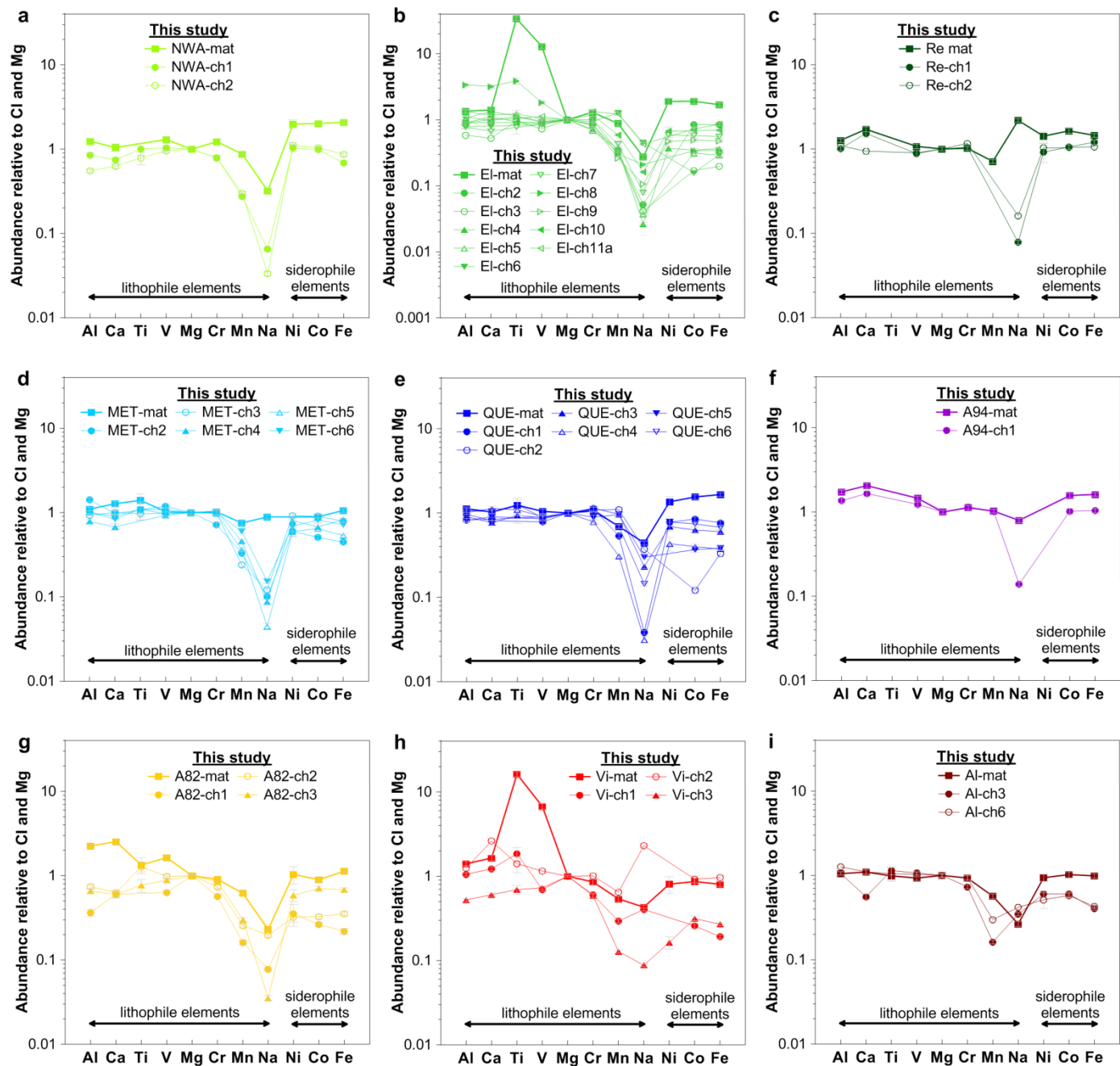


**Figure 5-5: Elemental abundances for chondrules (ch) and matrix (mat) of all samples relative to Cl and Mg** (adapted after Abreu and Brearley 2010, Jones et al. 2005, Wasson et al. 2000). Elements are arranged in groups according the geochemical properties and within these groups in order of increasing volatility. Values for Cl elemental abundances are from Lodders 2003. Where the concentrations were below detection limits, values are not shown. Abbreviations: NWA – NWA 852 (a), EI – El Djouf 001 (b), Re – Renazzo (c), MET – MET 00426 (d), QUE – QUE 99177 (e), A94 – Acfer 094 (f), A82 – Acfer 082 (g), Vi – Vigarano (h), Al – Allende (i).

However, after closer examination, different Ti and V abundances from El Djouf 001 matrix and chondrules seem reasonable, because chondrules account for at least 60 wt% of the bulk meteorite. A comparably high abundance of chondrules was determined after finishing freeze-thaw cycles, pointing in the same direction. Relatively high concentration of refractory elements in matrices of CV chondrites Acfer 082 and Vigarano may reflect the relatively high fraction of CAIs (see *chapter 4.1.2.1*) (Bischoff et al. 1993).

Chondrules show generally a depletion of elements more volatile than Fe, which are typically more abundant in the matrix (Scott 2007). Sodium (Na) abundances are very low in chondrules, as this element may have been lost during chondrule formation (e.g., Jones et al. 2005). In general, Na can also be removed by weathering from meteorites, even if their terrestrial age is only very short (Kallemeyn and Wasson 1982). However, it is not clear, if the variations in Na contents in carbonaceous chondrites are due to weathering effects in all cases (Bischoff et al. 1993). Based on the huge variations of Na in components of carbonaceous chondrites Bischoff et al. (1993) suggested that there are good reasons to expect primary fractionation resulting in Na depletion. Kong and Palme (1999) reported that in Renazzo chondrules refractory and common elements are not fractionated, whereas volatile elements are depleted and fractionated; these findings are in agreement with the results of our analyzed Renazzo chondrules (see **Figure 5-5c**).

Most chondrules of CR2 chondrites, CR3 chondrites and ungrouped Acfer 094 have abundance ratio patterns similar to low FeO chondrules in the ungrouped carbonaceous chondrite LEW 85332 (Wasson et al. 2000), in particular flat abundance ratio of lithophiles and siderophiles and low volatiles (especially Na). Low FeO chondrules in LEW 85332 are believed to have formed earlier than FeO-rich chondrules, i.e. when most metal was unoxidized and refractory lithophiles were largely present in an unfractionated refractory component (Wasson et al. 2000) (see *chapter 2.2.3.5*).

Furthermore, elemental abundance patterns for matrices of MET 00426, QUE 99177 and Renazzo are mostly consistent with the results of Abreu and Brearley (2010).

We tested the homogeneous distribution of elemental abundances within a chondrule using two halves of one El Djouf 001 chondrule. A subsequent SEM analysis of one half enables us to compare both results and to conclude which technique is most suitable for the analysis of elemental abundances in chondrules.

Most target elements in both El Djouf 001 halves are identical within uncertainties (**Figure 5-6, Appendix 1 & 2**). However, there are some target elements and other elements, which differ in both halves like Al and Ca (**Figure 5-6b**). These differences might be caused by the irregular distribution of minerals like Ca pyroxenes in the chondrule of type IAB/B (AB: pyroxene-olivine (intermediate); B: pyroxene-rich) El Djouf 11 (see below).

### **Possible chondrule types**

In order to classify our chondrules according to the schemes by Scott and Taylor (1983), Jones and Scott (1989) and Jones (1990, 1992a, b; 1994, 1996) (see *chapter 2.2.2*), we compared the elemental composition of our chondrules with the bulk composition for major chondrule types (Lauretta et al. 2006 and references therein), assuming that Fe is present to about 75% reduced in metal and the remaining 25% is present as FeO in silicates according to Ebel et al. (2008). This assumption is derived from Ebel et al. (2008) based on the mean value of five analyzed Renazzo chondrules, with Fe in metal ranging between 25 and 95 of total Fe. It is questionable if these results are generally applicable for CR3 and CV chondrites or even other CR2 chondrites.

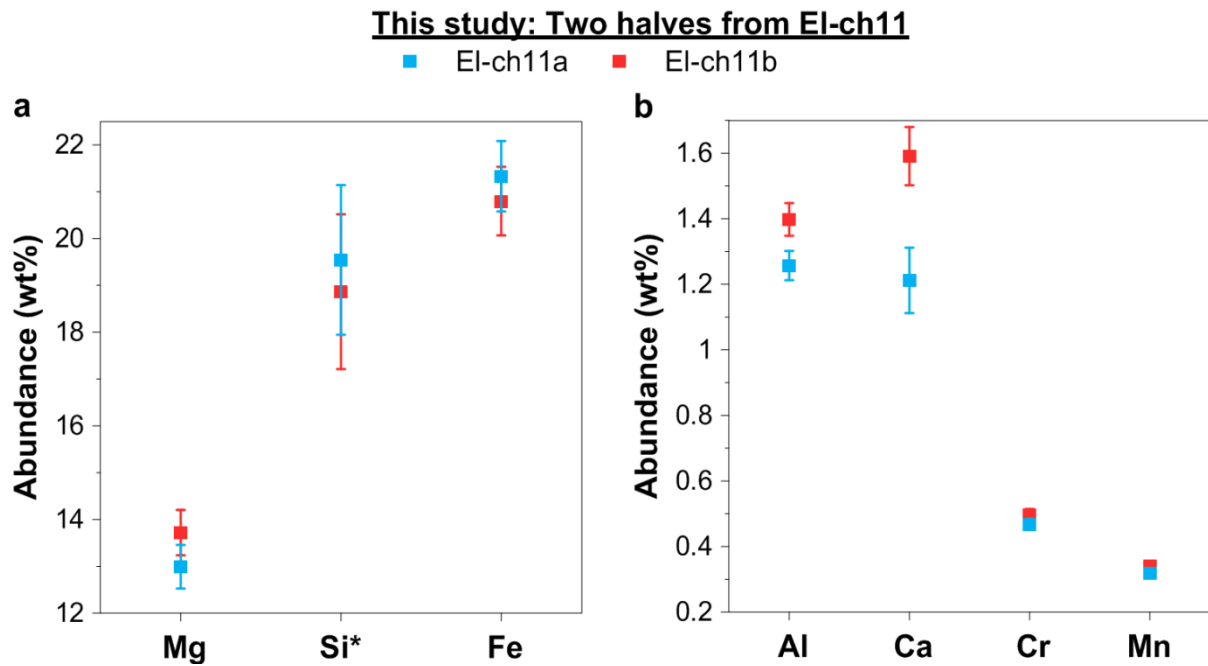


**Figure 5-6: Selected abundances of target elements in two halves of one EI Djouf 001 chondrule (EI-ch11) determined with INAA.** \*Si was calculated by converting the major elements into oxides, and assuming the remainder to be  $\text{SiO}_2$ . Iron is a special case, since it also occurs as metal and sulfide. For “Si minimal” Fe is assumed as being completely oxidized in silicates as FeO, for “Si maximal” Fe is assumed to be present exclusively as metal and sulfide. Here,  $\text{Si}_{50}$  (i.e. the mean value of minimum and maximum Si abundances) is shown.

Please note further that the abundance of  $\text{SiO}_2$  depends on the form of Fe, which was assumed for the following considerations. Additionally a clear distinction between type IAB and type IB as well as type IIAB and type IIB based on elemental abundances only is not straightforward. For a clear distinction optical microscopy showing textural properties (see **Figure 2-7 and 2-8**) is required. Therefore, the given chondrule types are tentative.

From 36 chondrules the majority of chondrules (31) can be classified as type I (FeO-poor) with FeO abundances <7.80 wt% and four chondrules (Re-ch1, Re-ch2, NWA-ch2, MET-ch3) as type II (FeO-rich); chondrule MET-ch1 is a metal chondrule (**Figure 5-7a, Table 5-6**). This result agrees with the finding by Zanda (2004) and Tenner et al. (2011), who stated that most chondrules in carbonaceous chondrites and CR3 chondrite MET 00426 are type I.

For a distinction between types A ( $\text{SiO}_2$ -poor, olivine >80%), AB (intermediate) and B ( $\text{SiO}_2$ -rich, pyroxenes >80%) (see *chapter 2.2.2*) we used the **(Mg+Fe)/Si ratio** (atom/atom) in the silicates, which for pyroxenes is ~1 and for olivines ~2 (intermediate (Mg+Fe)/Si between 1.4 and 1.6). Chondrules in CV chondrites are dominated by type IA (**Figure 5-7b**). For CR chondrites and Acfer 094 we additionally used available **Mg#** (i.e. Mol%  $\text{MgO}/\{\text{MgO} + \text{FeO}\}$ ) in the silicates for the calculation of (Mg + Fe)/Si ratios. Chondrules in CR chondrites and Acfer 094 vary greatly in the Mg# of their olivines/pyroxenes (35-100) (Tenner et al. 2012), and in olivines/pyroxenes of MET 00426 and QUE 99177 chondrules Mg# is mostly >95 (Tenner et al. 2011, 2012). The Mg# of our chondrules is in all cases >50. In contrast to CV chondrites, chondrules in CR chondrites and Acfer 094 are mostly pyroxene-rich (type IB) (**Figure 5-7c**). Only chondrules NWA-ch1 from NWA 852 and EI-ch3-5 from EI Djouf 001 were classified as types IA and IAB, respectively. The presence of type I and II chondrules in

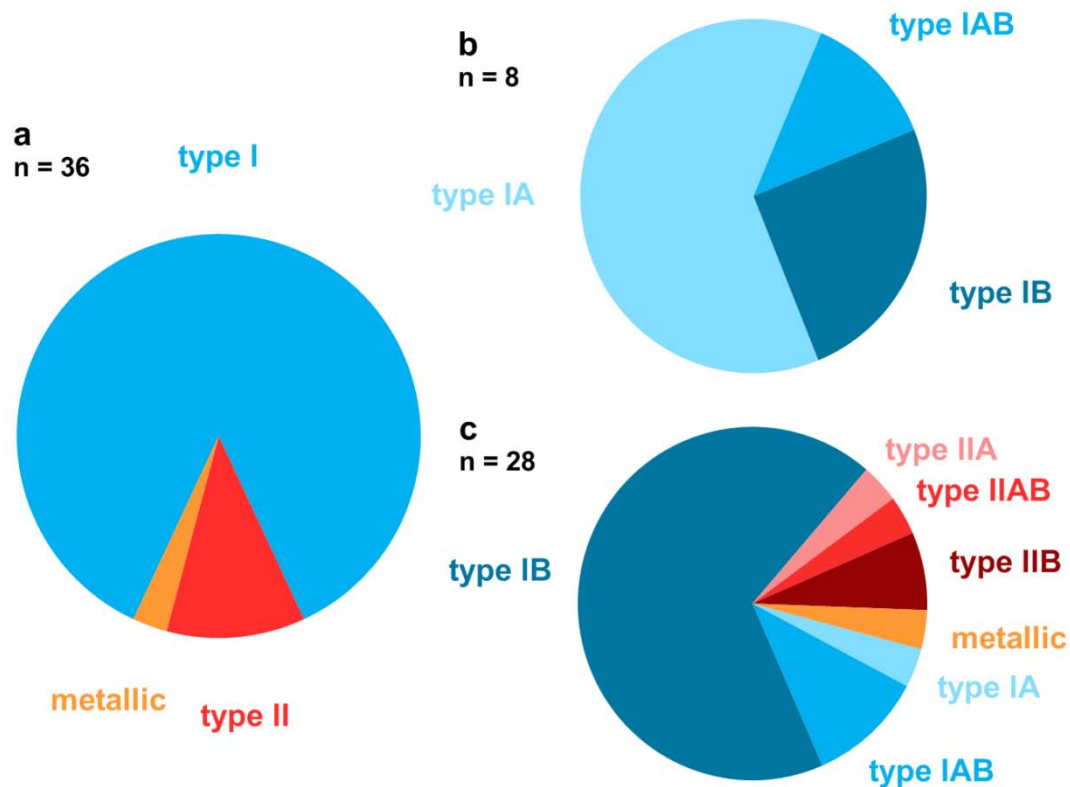


Figure 5-7: Classification of all analyzed chondrules (a), CV chondrite chondrules (b), and chondrules from CR chondrites and Acfer 094 (c) according to Wood (1962) and McSween et al. (1977, 1983) and Scott and Taylor (1983), Jones and Scott (1989) and Jones (1990, 1994, 1996). The numbers indicate the number of chondrules.

Table 5-6: Tentative chondrule types according the schemes by Scott and Taylor (1983), Jones and Scott (1989) and Jones (1990, 1992a, b; 1994, 1996).

Sample	Chondrule type	Sample	Chondrule type	Sample	Chondrule type
<i>CR2 chondrites</i>		<i>CR3 chondrites</i>		<i>CV3 chondrites</i>	
Re-ch1	IIB	MET-ch1	metallic	Al-ch3	IA
Re-ch2	IIB	MET-ch2	IB	Al-ch6	IA
EI-ch2	I(II)B*	MET-ch3	IIAB	Vi-ch1	IB
EI-ch3	IAB	MET-ch4	I(II)B*	Vi-ch2	IB
EI-ch4	IAB	MET-ch5	IB	Vi-ch3	IA
EI-ch5	IAB	MET-ch6	IB	A82-ch1	IA
EI-ch6	IB	QUE-ch1	I(II)B*	A82-ch2	IAB
EI-ch7	IB	QUE-ch2	IB	A82-ch3	IA
EI-ch8	IB	QUE-ch3	IB		
EI-ch9	IB	QUE-ch4	IB		
EI-ch10	IB	QUE-ch5	IB		
EI-ch11a	IB	QUE-ch6	IB		
NWA-ch1	I(II)A*	<i>Ungrouped 3 chondrite</i>			
NWA-ch2	IIA	A94-ch1	I(II)B*		

Chondrules were classified is based on the bulk composition for major chondrule types (Lauretta et al. 2006 and references therein), assuming that Fe is present to about 75% reduced in metal according to Ebel et al. (2008). For a distinction between the types A, AB and B (Mg+Fe)/Si ratios in silicates only in case of CV chondrite chondrules, and in case of chondrules from CR chondrites and Acfer 094 (Mg+Fe)/Si ratios and Mg# (see text) in silicates were used. \*Chondrules were classified as type I(II), because the FeO abundances ranges between 7.0 and 7.8 wt%, which is close to typical values for type II chondrules >7.8 wt% (Lauretta et al. 2006 and references therein). Abbreviations: ch-chondrule, Re-Renazzo, EI-EI Djouf 001, NWA-NWA 852, MET-MET 00426, QUE-QUE 99177, A94-Acfer 094, Al-Allende, Vi-Vigarano, A82-Acfer 082.

CR chondrites may point towards different oxidation-reduction conditions in case of different chondrule precursors (chondrule formation as repetitive process) (e.g., Hewins and Zanda 2012, Scott and Taylor 1983) or towards changing conditions in case of one chondrule precursor (e.g., Schrader et al. 2013, Jones et al. 2005, Kunihiro et al. 2004) (see *chapter 2.2.3.5*). However, the abundance of chondrules from CV chondrites might be too low to sample one rare type II chondrule. In our later discussion of possible pre-irradiation effects we will also consider if there is a relationship between pre-irradiation and chondrule type (see *chapter 5.6.1*).

### 5.1.2 SEM analysis

Elemental abundances of chondrule bulk are given in **Table 5-7**.

One half of El Djouf 001 chondrule was analyzed using INAA and SEM analyses for elemental abundances. The abundance of important target elements determined by both methods is identical within uncertainties (**Figure 5-8**). The uncertainties for the elemental abundances inferred from SEM analyses are larger, as we ascribed significant errors due to variation of modal phase abundances (see *chapter 4.3.2*).

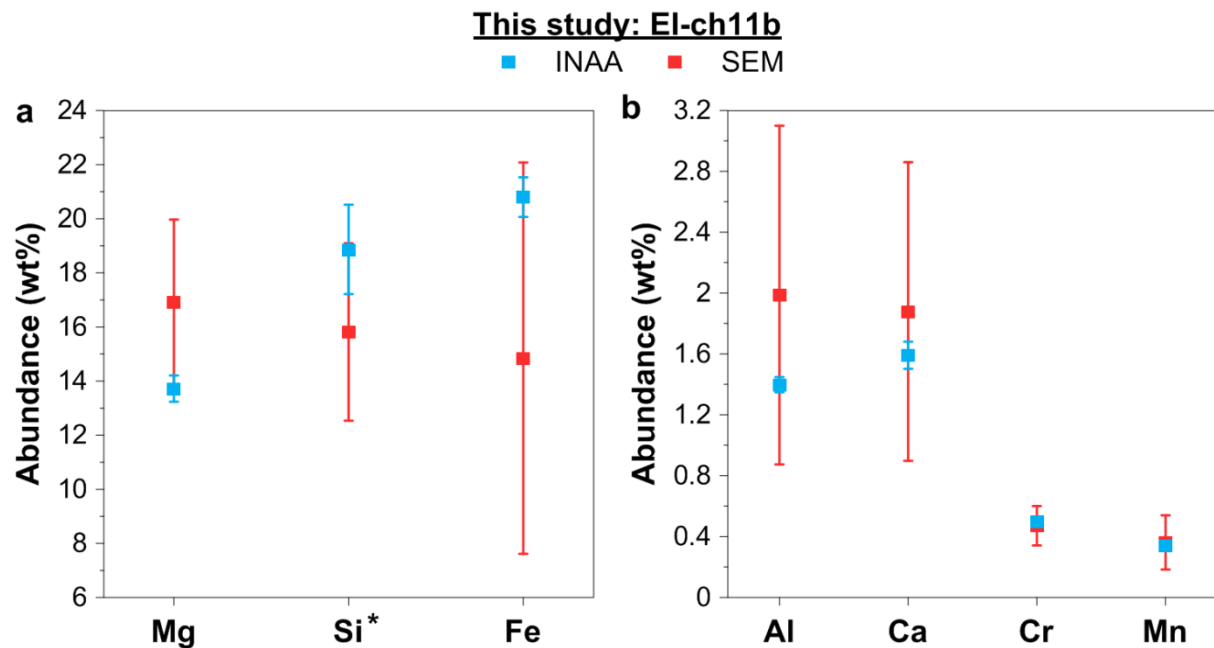
**Table 5-7: Elemental abundances for selected chondrules determined with SEM.**

	Mg	Si	Fe	Al	Ca	Na	Ni
Al-ch1	18.64(5)	19.03(5)	8.158(41)	3.025(24)	2.972(19)	0.599(12)	
Al-ch2	5.245(20)	20.24(5)	1.565(40)	12.11(4)	10.07(6)	1.698(86)	0.076(33)
Al-ch4	17.60(5)	19.82(4)	4.392(53)	3.730(63)	4.048(57)	1.612(36)	
A082-ch4	28.41(2)	18.64(2)	3.964(49)	0.644(21)	0.683(12)		0.045(6)
A082-ch5	15.53(17)	15.92(5)	20.19(21)	0.852(9)	1.084(15)		0.542(18)
A082-ch6	15.74(8)	14.49(5)	20.91(10)	1.454(30)	1.301(23)	0.049(26)	0.818(20)
MET-ch7	13.08(10)	14.57(4)	32.63(11)	0.814(7)	0.946(14)	0.038(11)	1.710(19)
QUE-ch7	24.24(7)	19.52(6)	4.263(79)	1.955(17)	1.789(33)		0.163(48)
El-ch11b	17.00(9)	15.86(6)	14.83(5)	1.966(34)	1.871(14)	0.326(9)	0.659(22)

	Cr	Mn	K	Ti	P	S	Cl
Al-ch1	0.323(13)	0.057(36)	0.029(11)	0.137(26)			0.023(6)
Al-ch2	0.191(24)		0.036(17)	0.176(10)		0.149(14)	0.387(36)
Al-ch4	0.277(14)		0.113(24)	0.198(14)		0.032(5)	0.353(11)
A082-ch4	0.254(4)			0.021(3)		0.036(15)	0.022(5)
A082-ch5	0.531(7)	0.087(43)		0.028(12)	0.080(34)	1.535(10)	
A082-ch6	0.385(10)				0.048(25)	1.246(22)	
MET-ch7	0.376(16)	0.240(17)			0.046(25)	0.727(10)	
QUE-ch7	0.449(16)	0.097(42)				0.033(6)	
El-ch11b	0.467(17)	0.356(18)		0.036(8)	0.032(5)	0.169(10)	

Abundances are given in wt%. Uncertainties (1 s. d.) are given in parenthesis. Where fields are marked in gray, concentrations were below the detection limit.



**Figure 5-8: Selected abundances of target elements in one half of the El Djouf 001 chondrule El-ch11b determined by INAA and by SEM.** \*In case of INAA Si was calculated by converting the major elements into oxides, and assuming the remainder to be  $\text{SiO}_2$ . Iron is a special case, since it also occurs as metal and sulfide. For “Si minimal” Fe is assumed as being completely oxidized in silicates as FeO, for “Si maximal” Fe is assumed to be present exclusively as metal and sulfide. Here,  $\text{Si}_{50}$  (i.e. the mean value of minimum and maximum Si abundances) is shown.

## 5.2 Mineralogy

SEM pictures showing the bulk chondrules and selected sections including point, area and profile measurements are given in **Figures 5-9 to 5-13**.

### CR2 chondrite El Djouf 001

The El Djouf 001 chondrule (**Figure 5-9a**) has a maximum length of ~1.5 mm and a height of ~1 mm, which agrees with the mean diameter ( $1.0 \pm 0.6$  mm) given by Bischoff et al. (1993). Chondrule margins are mostly relatively smooth, except the lower part of the chondrule having two semicircular recesses, which suggests that there small compound chondrules have been attached. On the chondrule margins no rim is visible, which is unusual because chondrules from CR2 chondrites are typically surrounded by multi-layered coarse-grained, igneous rims (Krot et al. 2007a).

The whole El Djouf 001 chondrule is crossed by veins composed of oxidized Fe,Ni metal (**Figure 5-9b**), suggesting together with oxide rims around Fe,Ni metal (kamacite) moderate to severe weathering effects (W2, see **Table 4.3**).

Olivine ( $\text{Fa}_{2-5}$ ) is the most abundant mineral, which may indicate that this chondrule is a typical type I chondrule described by Weisberg and Prinz (1991). Oxidized Fe,Ni metal occurs as veins and pocket-shaped inclusions (**Figure 5-9c**). In addition to olivines and oxidized Fe,Ni metal, pyroxenes (mostly enstatite), Fe,Ni metal (kamacite, points 8 & 16 in intersects 3 & 5), Ca-carbonates, and some feldspar (andesine) are present in the El Djouf 001 chondrule.

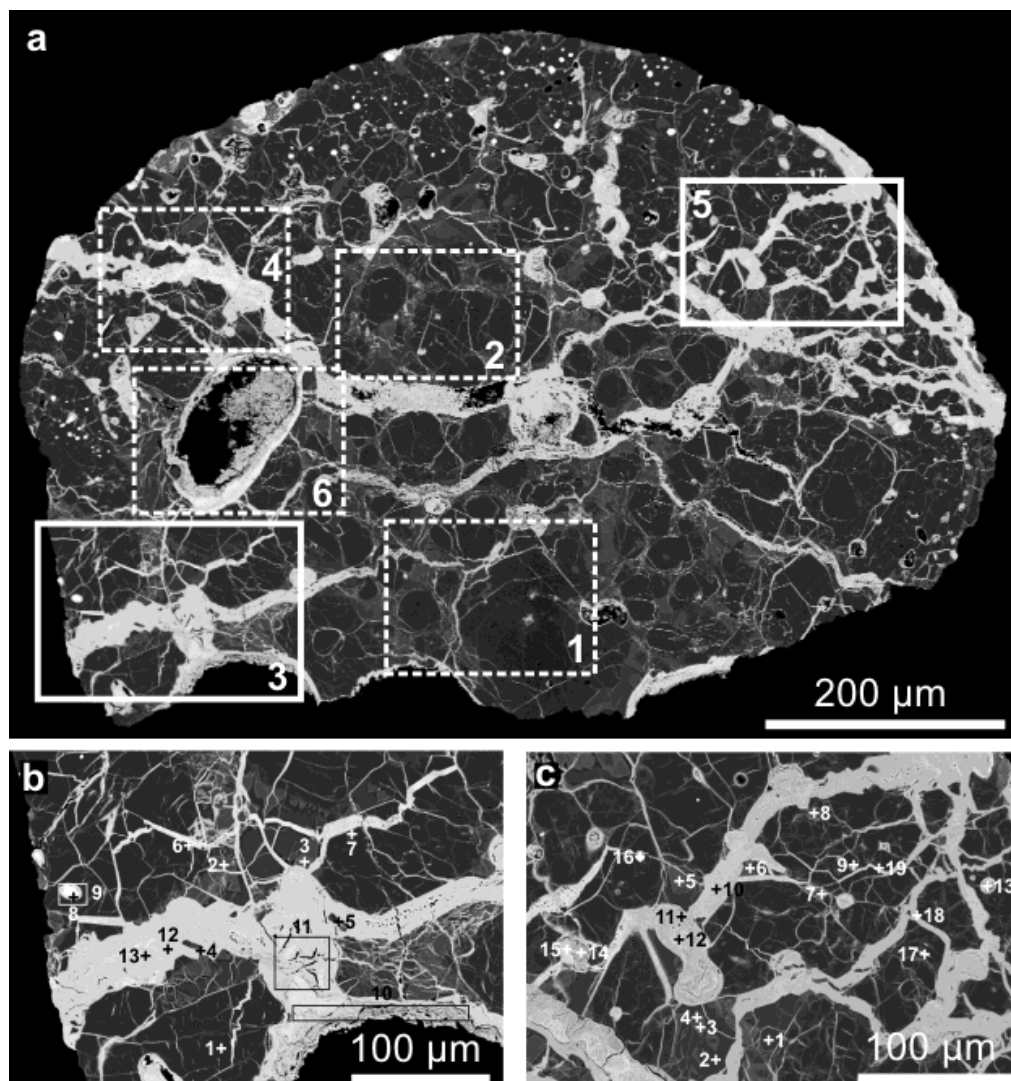


**Figure 5-9:** Back scattered electron images of El Djouf chondrule El-ch11b (a) and intersects 3 (b) and 5 (c). The intersects with solid frames are shown in detail.

### **CR3 chondrites**

The chondrule from **MET 00426** (**Figure 5-10a**) has a maximum length of ~1.8 mm and a maximum height of ~1.2 mm, which is consistent with the chondrules analyzed by Abreu and Brearley (2010) and Mittlefehldt (2001).

This chondrule consist mainly of Fe,Ni metal and pyroxenes (enstatite). Abundant Fe,Ni metal is typical for CR chondrites (e.g., Abreu and Brearley 2010); in the centre of the chondrule it is present as large irregular shaped inclusions, whereas at the chondrule margins it mostly occurs as small droplets. Veins of oxidized Fe,Ni metal and oxide rims around metal grains (**Figure 5-10b**) suggest incipient weathering (see **Table 4-3**). The chondrule is enclosed by a fine-grained rim, which was lost on the upper chondrule part, containing fine sulfides and phosphorus (**Figure 5-10c**). Additionally, the fine-grained matrix may contain carbon (C) in area measurements of intersects 1 and 4. However, the C abundance cannot be quantified with certainty using SEM because the sample has to be coated with C for EDX analyses. In the middle right part a dark phase is present, which might resemble exsolution lamellae of pyroxenes as described by Weinbruch et al. (2003). Furthermore, there is some diopside (e.g., point 4 in intersect 2, **Figure 5-10b**), mostly associated with Fe,Ni metal or oxide rims.



The **QUE 99177** chondrule (**Figure 5-11a**) has an average diameter of ~1 mm, which agrees with the chondrules described by Abreu and Brearley (2010) and Mittlefehldt (2001). This chondrule has no igneous rim, except on the right lower part. The missing chondrule rim and the uneven margin may suggest that some material has been lost during freeze-thaw cycles and sample preparation. In this context, Mittlefehldt (2001) reported that QUE 99177 chondrules are in general well-defined, and Abreu and Brearley (2010) have identified igneous rims only on some chondrules.

The texture of this QUE 99177 chondrule seems to be porphyritic: Large rounded olivine minerals ( $Fa_{1-4}$ ) are set in a clear glassy mesostasis and resemble those present in the QUE 99177 sample described by Abreu and Brearley (2010). Olivines have clear grain boundaries and are zoned. Furthermore, some pyroxenes (enstatite) and crystalline mesostasis occur in the chondrule, showing in some cases a stripe-like structure (profile 1 in the left part of **Figure 5-11b**). In addition, the chondrule contains lots of bright inclusions (see **Figure 5-11b**) composed of Fe,Ni metal (up to ~80  $\mu\text{m}$  as in **Figure 5-11c**) as well as some pocket-shaped, intersect-filling or round inclusion composed of pyroxenes (ferrosilite). Some grain fragments (diopside-like) (e.g., points 20-22 in **Figure 5-11b**) has been also identified. In contrast to the MET 00426 chondrule, this QUE 99177 has no veins.

### **CV3 chondrites**

The chondrule from **Acfer 082** (**Figure 5-12a**) has a diameter of ~750  $\mu\text{m}$ . Although some parts of the chondrule have been lost during sample preparation, it is almost spherical, and it has only on the middle right part a thick fine-grained rim attached (**Figure 5-12b**).

Olivine (mostly  $Fa_{1-8}$ ) is most abundant. Minor abundant pyroxenes (mostly enstatite) are mostly present near chondrule margins. In contrast to pyroxenes, olivines are zoned. Additionally, there are few Fe,Ni inclusions and kamacite reaching in some cases up to ~50  $\mu\text{m}$  (**Figure 5-12c**), which are mostly near the chondrule margins and show in most cases oxide rims. The Acfer 082 chondrule has lots of fine veins, which are enriched in Fe. The oxidation rims around Fe, Ni inclusions and the occurrence of abundant veins implies moderate weathering (W2, see **Table 4.3**). Additionally, there are some spaces between large olivine minerals, which are filled with Ca-clinopyroxenes (augite-like) and Fe sulfides.

The **Allende** chondrule (**Figure 5-13a**) has a maximum diameter of ~800  $\mu\text{m}$  and is therefore slightly smaller than chondrules in CV chondrites on average (1 mm, Scott 2007). This well-defined chondrule is nearly completely surrounded by an igneous rim, except on the lower left part, which might suggest that this is a fracture where a part of the chondrule has been broken. At the round inlet at the lower right the Allende chondrule might be associated with another smaller chondrule, which has also been broken. Few small droplet-like inclusions are arranged in the transition between chondrule and chondrule rim (**Figure 5-13b**).

The texture of this Allende chondrule seems to be porphyritic. Olivine (mostly  $Fa_{15-22}$ ) and clinopyroxene (mostly augite or pigeonite) dominate. Olivine and pyroxenes are equally distributed. In contrast to pyroxene, olivine minerals are zoned: In the inner parts Mg abundance is high and Fe abundance is low, whereas in the outer parts the situation is vice versa. Based on this zoning of olivine (**Figure 5-13c**) and the higher crystallization temperature of olivine (Bowen reaction series, Bowen 1928), it might be concluded that olivine crystallized first and pyroxene minerals formed later between them. Furthermore, there is a schlieren feature around an olivine grain towards pyroxene (see **Figure 5-13c**), and the fine-grained rim may contain carbon (C) in some cases (intersects 3 and 11). Additionally to olivines and pyroxenes, there is some feldspar (mostly albite-like) and few inclusions, which might represent Fe, Ni sulfides or oxides.

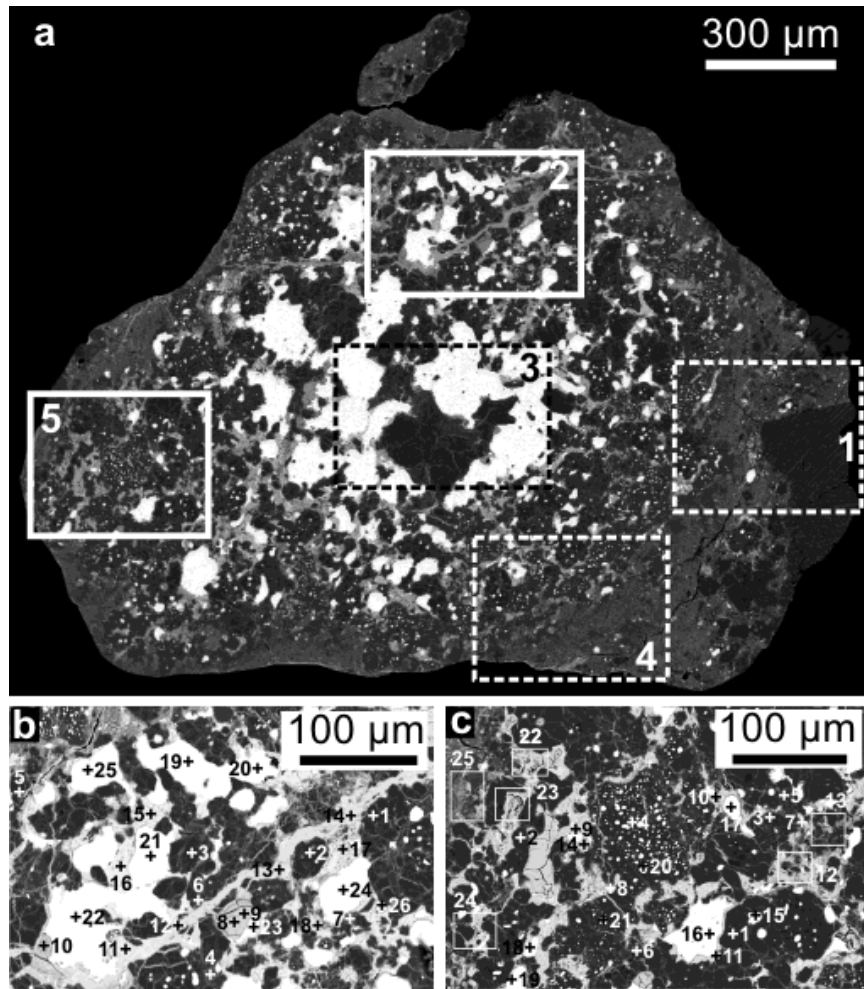


Figure 5-10: Back scattered electron image of one MET 00426 chondrule (a) and intersects 2 (b) and 5 (c). The intersects with solid frames are shown in detail.

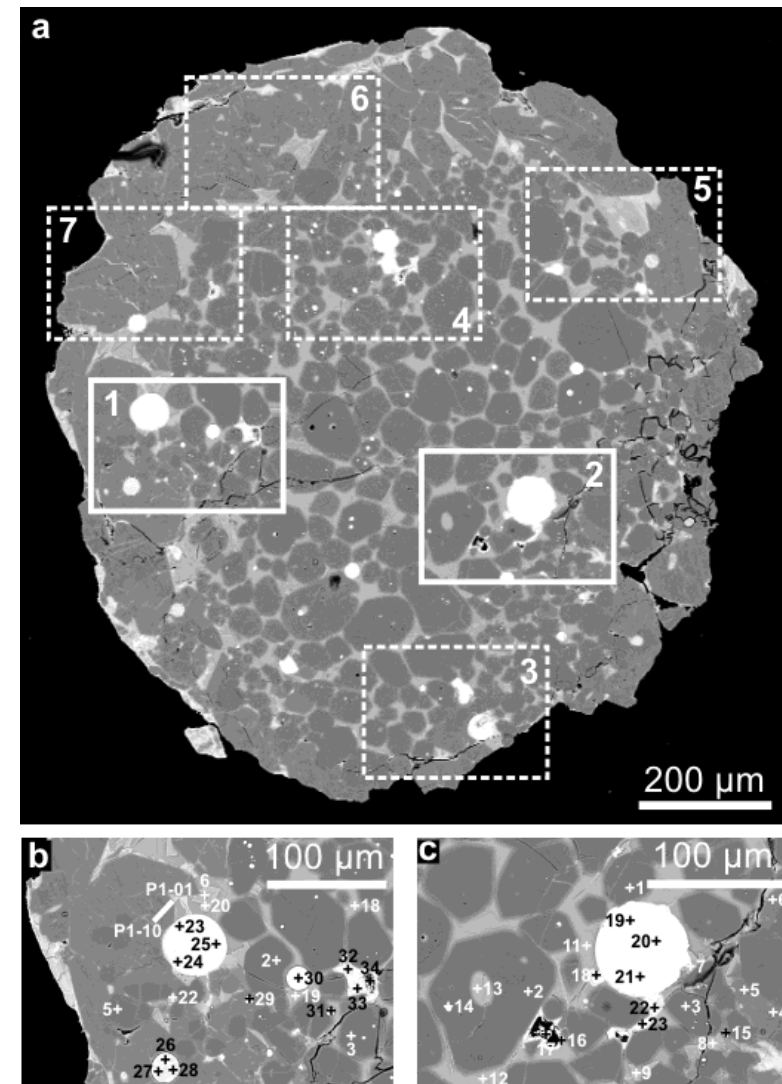


Figure 5-11: Back scattered electron image of one QUE 99177 chondrule (a) and intersects 1 (b) and 2 (c). The intersects with solid frames are shown in detail.

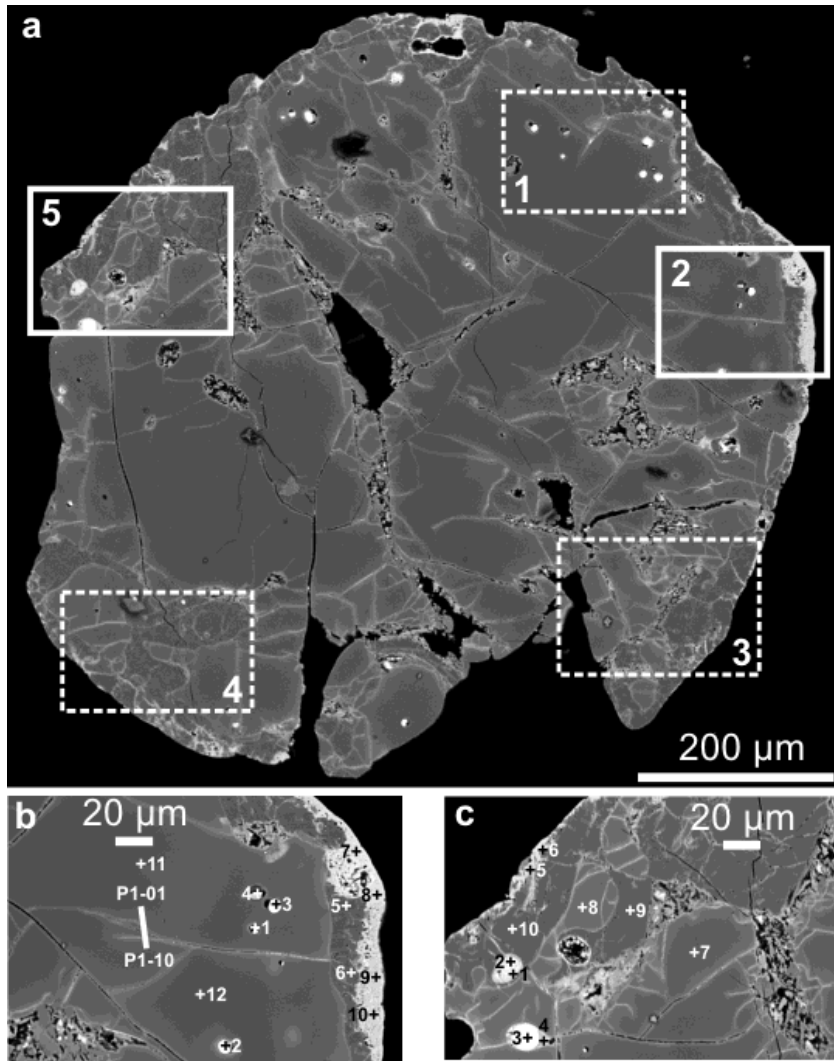


Figure 5-12: Back scattered electron image of one Acfer 082 chondrule (a) and intersects 2 (b) and 5 (c). The intersects with solid frames are shown in detail.

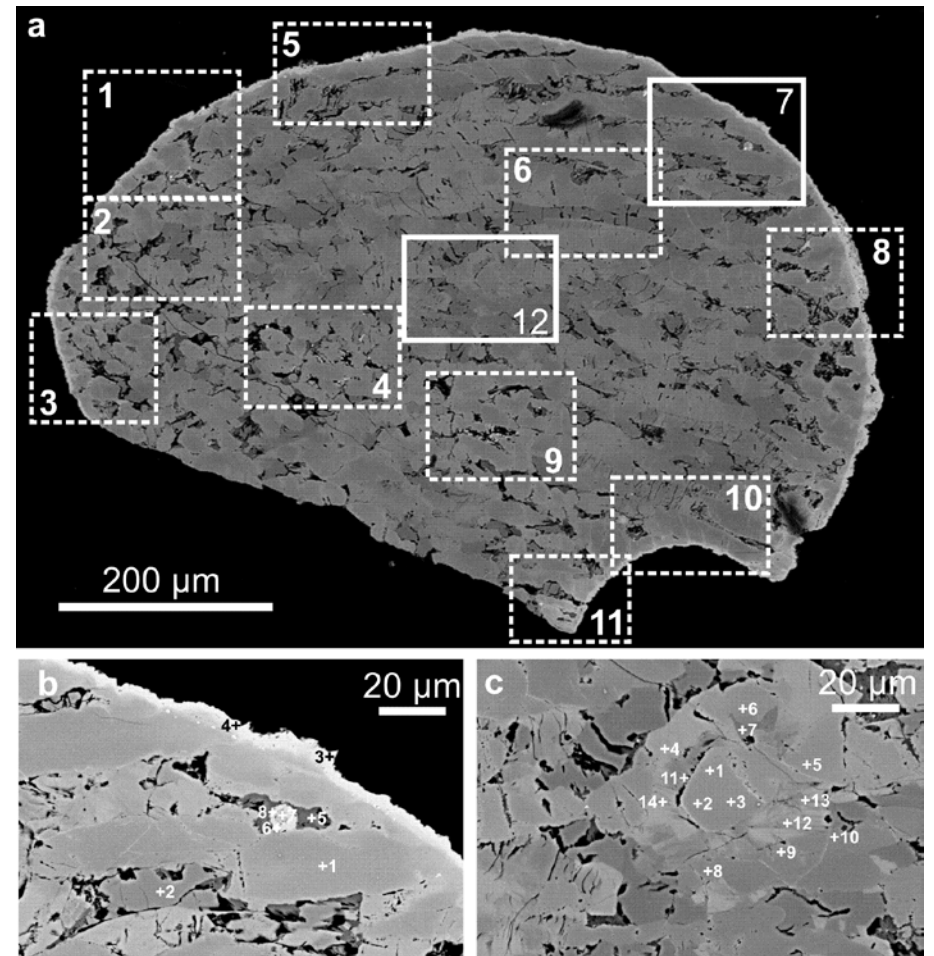


Figure 5-13: Back scattered electron image of one Allende chondrule (a) and intersects 7 (b) and 12 (c). The intersects with solid frames are shown in detail.

## 5.3 Noble gases in chondrules and matrix

### 5.3.1 Concentrations

Data for Ne, He, and Ar summarized in **Tables 5-8 to 5-10** and the complete data is given in **Appendix 3 to 5**. Neon results for Vigarano matrix samples 1 and 2 are equal within errors, confirming sample homogeneity and measurement reproducibility.

The focus of this study is on Ne, because He can be easily affected by gas loss due to diffusion (e.g., Das et al. 2012) and recoil losses (e.g., Trappitsch and Leya 2013), and Ar is mostly dominated by trapped components in primitive meteorites. Hence, Ne provides most reliable data concerning concentration and CRE ages (e.g., Roth et al. 2011, Huber et al. 2012).

#### Neon Ne

Concentrations of  $^{21}\text{Ne}_c$  in most chondrules are enhanced compared to the matrix (**Table 5-8, Appendix 3**). One reason for the higher  $^{21}\text{Ne}_c$  abundance in chondrules is the mostly higher abundance of Mg, which represents the most important target element for  $^{21}\text{Ne}_c$  (e.g., Schultz and Freundel 1985).

Interestingly, only half of MET 00426 chondrules have enhanced  $^{21}\text{Ne}_c$  concentrations. Remarkable are in particular the low  $^{21}\text{Ne}_c$  concentrations of Re-ch1, MET-ch1, and A82-ch3 (see *chapter 5.3.2*). The relative high shielding parameter ( $^{22}\text{Ne}/^{21}\text{Ne}$ )<sub>c</sub> for our CR chondrite samples indicate generally low shielding, i.e. samples resided close to the surface of the parent body object. Shielding parameters of matrix and chondrule samples are in most cases relatively similar, confirming our measurement accuracy and the assumption of identical shielding conditions for the calculation of CRE ages (see *chapter 4.7*). In contrast, our CV chondrites show low values for ( $^{22}\text{Ne}/^{21}\text{Ne}$ )<sub>c</sub>, indicating substantial shielding (e.g., Polnau et al. 1999) typical for greater depth in a large body or for the interior in a smaller body. Shielding parameters of matrix and chondrule samples of CV chondrites are also identical within errors.  $^{21}\text{Ne}_c$  concentration in Allende matrix ( $1.89 \pm 0.03 \cdot 10^{-8}$  cc/g, **Table 5-8**) agree with 26 bulk or matrix samples in Schultz and Franke (2004) (average  $^{21}\text{Ne}_c = 1.84 \cdot 10^{-8}$  cc/g) (Eugster et al. 2007). Furthermore, Allende chondrules show higher  $^{21}\text{Ne}_c$  concentrations compared to the matrix (39% and 30%), which is comparable with on average 30% higher  $^{21}\text{Ne}_c$  concentrations of Allende chondrules relative to the matrix in Schultz and Franke (2004). Concentration of  $^{21}\text{Ne}_c$  in Allende chondrules agree with previous analyses by Roth et al. (2011) ( $2.3 \pm 0.3 \cdot 10^{-8}$  cc/g). Chondrule MET-ch1 contains only a small amount of  $^{21}\text{Ne}_c$  because it is mostly Fe. The measured concentration together with production rates from the literature (e.g., Eugster (1988) formula 3a-c, see *chapter 2.3.2*) yields an exposure age in agreement with that for the matrix (see **Table 5-15** in *chapter 5.4.2*).

#### Helium He

Concentrations of  $^3\text{He}$  in matrix samples of CR chondrites include in most cases significant amounts of trapped SW  $^3\text{He}$  (**Table 5-9, Appendix 4**), and are hence higher than those in chondrules (except Renazzo and QUE 99177). In such cases  $^3\text{He}$  cannot be used for calculating a CRE age. Chondrules in CV chondrites usually contain higher  $^3\text{He}$  concentrations compared to the matrix; exceptions are chondrules Vi-ch2 and A82-ch3.

$^{21}\text{Ne}_c$  and  $^3\text{He}$  concentration give (within error) concordant exposure ages (neglecting the samples with extreme high trapped solar  $^3\text{He}$ ). As the production of  $^3\text{He}$  is hardly influenced by the chemical composition (e.g., Wieler 2000, Eugster 1988), this implies that the chemical composition is not the reason for the observed excess of  $^{21}\text{Ne}_c$  and  $^3\text{He}$  in the chondrules (Matsuda et al. 2009).

**Table 5-8: Concentrations of  $^{21}\text{Ne}_c$ , shielding parameters ( $^{22}\text{Ne}/^{21}\text{Ne}_c$ ), production rates ( $P_{21\text{-corr}}$ ,  $P_{21\text{-}1.11}$ ), and CRE ages ( $T_{21\text{-corr}}$ ,  $T_{21\text{-}1.11}$ ) of all matrix (mat) and chondrule (ch) samples.  $P_{21\text{-corr}}$  and  $T_{21\text{-corr}}$  were calculated with shielding correction,  $P_{21\text{-}1.11}$  and  $T_{21\text{-}1.11}$  were calculated without shielding correction, i.e.  $(^{22}\text{Ne}/^{21}\text{Ne})_c = 1.11$  (“average shielding”). For the Si abundance we calculated both “Si minimal” (Fe is assumed to be completely oxidized in silicates as FeO) and “Si maximal” (Si is assumed to occur as metal and sulfide only). See chapter 5.1.1 and Appendix 1.**

	$^{21}\text{Ne}_c$	$(^{22}\text{Ne}/^{21}\text{Ne})_c$	$P_{21\text{-corr}}$ Si minimal	$T_{21\text{-corr}}$	$P_{21\text{-corr}}$ Si maximal	$T_{21\text{-corr}}$	$P_{1\text{-}1.11}$ Si minimal	$T_{21\text{-}1.11}$	$P_{1\text{-}1.11}$ Si maximal	$T_{21\text{-}1.11}$
<i>CR2 chondrites</i>										
Re-mat	0.838(59)	1.286(126)	0.132(42)	6.368(2.066)	0.139(24)	6.040(1.126)	0.236(7)	3.556(272)	0.248(7)	3.383(256)
Re-ch1	0.205(164)	<sup>b</sup>	<sup>b</sup>	<sup>b</sup>	<sup>b</sup>	<sup>b</sup>	0.267(8)	0.768(617)	0.279(8)	0.734(590)
Re-ch2	1.207(90)	1.250(115)	0.174(56)	6.919(2.267)	0.182(37)	6.614(1.417)	0.284(9)	4.248(343)	0.296(9)	4.077(323)
El-mat	0.834(46)	<sup>a</sup>	<sup>a</sup>	<sup>a</sup>	<sup>a</sup>	<sup>a</sup>	0.222(9)	3.761(236)	0.238(7)	3.544(219)
El-ch2	1.268(73)	1.171(66)	0.242(57)	5.237(1.268)	0.250(59)	5.073(1.228)	0.308(9)	4.112(266)	0.318(9)	3.984(256)
El-ch3	2.319(128)	1.115(26)	0.447(53)	5.187(676)	0.451(53)	5.142(670)	0.458(14)	5.062(320)	0.462(14)	5.019(317)
El-ch4	2.131(87)	1.135(55)	0.363(81)	5.867(1.327)	0.369(82)	5.777(1.306)	0.404(12)	5.279(268)	0.410(12)	5.197(262)
El-ch5	2.199(129)	1.178(23)	0.319(27)	6.888(714)	0.323(28)	6.807(705)	0.417(13)	5.272(347)	0.422(13)	5.210(342)
El-ch6	1.902(127)	1.161(30)	0.321(32)	5.929(708)	0.325(32)	5.857(699)	0.394(12)	4.827(354)	0.399(12)	4.768(352)
El-ch7	1.937(112)	1.081(66)	0.401(137)	4.833(1.677)	0.410(140)	4.724(1.639)	0.349(10)	5.550(362)	0.357(10)	5.425(352)
El-ch8	1.611(95)	1.179(68)	0.270(63)	5.978(1.436)	0.273(64)	5.907(1.419)	0.353(9)	4.559(295)	0.359(9)	4.505(290)
El-ch9	2.017(118)	1.113(63)	0.378(106)	5.342(1.537)	0.385(108)	5.235(1.505)	0.383(12)	5.259(347)	0.391(12)	5.154(338)
El-ch10	1.549(94)	1.185(29)	0.242(23)	6.390(730)	0.249(24)	6.216(709)	0.324(4)	4.777(296)	0.333(4)	4.647(287)
El-ch11a	1.395(110)	1.187(30)	0.221(23)	6.302(827)	0.229(24)	6.102(799)	0.298(9)	4.679(397)	0.308(9)	4.531(382)
NWA-mat	0.240(27)	<sup>a</sup>	<sup>a</sup>	<sup>a</sup>	<sup>a</sup>	<sup>a</sup>	0.209(12)	1.137(132)	0.225(7)	1.058(122)
NWA-ch1	10.53(83)	1.111(28)	0.366(71)	28.76(5.99)	0.377(73)	27.89(5.80)	0.368(12)	28.59(2.42)	0.380(12)	27.73(2.34)
NWA-ch2	12.34(97)	1.125(35)	0.327(65)	37.73(8.08)	0.349(71)	35.39(7.72)	0.349(12)	35.39(3.03)	0.363(12)	34.01(2.89)
<i>CR3 chondrites</i>										
MET-mat	2.033(252)	<sup>a</sup>	<sup>a</sup>	<sup>a</sup>	<sup>a</sup>	<sup>a</sup>	0.266(8)	7.609(976)	0.276(8)	7.333(939)
MET-ch1	0.178(11)	<sup>a</sup>	<sup>a</sup>	<sup>a</sup>	<sup>a</sup>	<sup>a</sup>	0.029(2)	6.243(650)	0.029(2)	6.243(650)
MET-ch2	2.308(144)	1.045(151)	<sup>a</sup>	<sup>a</sup>	<sup>a</sup>	<sup>a</sup>	0.392(12)	5.894(409)	0.399(12)	5.782(400)
MET-ch3	1.315(73)	<sup>a</sup>	<sup>a</sup>	<sup>a</sup>	<sup>a</sup>	<sup>a</sup>	0.349(11)	3.769(242)	0.361(11)	3.641(233)
MET-ch4	2.157(268)	<sup>a</sup>	<sup>a</sup>	<sup>a</sup>	<sup>a</sup>	<sup>a</sup>	0.326(10)	6.617(847)	0.337(10)	6.396(817)
MET-ch5	1.305(111)	<sup>a</sup>	<sup>a</sup>	<sup>a</sup>	<sup>a</sup>	<sup>a</sup>	0.359(11)	3.632(328)	0.367(11)	3.553(320)
MET-ch6	4.595(530)	<sup>a</sup>	<sup>a</sup>	<sup>a</sup>	<sup>a</sup>	<sup>a</sup>	0.345(11)	13.60(1.62)	0.348(10)	13.20(1.57)
QUE-mat	0.609(72)	<sup>a</sup>	<sup>a</sup>	<sup>a</sup>	<sup>a</sup>	<sup>a</sup>	0.230(7)	2.659(323)	0.244(7)	2.508(303)

QUE-ch1	0.994(68)	1.241(148)	0.217(91)	4.568(1.945)	0.225(94)	4.423(1.883)	0.345(11)	2.878(218)	0.357(11)	2.786(210)
QUE-ch2	1.228(86)	1.285(42)	0.231(25)	5.324(692)	0.234(26)	5.246(681)	0.412(13)	2.984(229)	0.418(13)	2.940(225)
QUE-ch3	1.421(97)	1.266(54)	0.214(31)	6.643(1.075)	0.220(32)	6.474(1.047)	0.364(11)	3.902(292)	0.374(11)	3.803(283)
QUE-ch4	0.470(39)	1.275(52)	0.230(32)	2.048(331)	0.233(32)	2.016(325)	0.400(12)	1.175(105)	0.407(12)	1.156(103)
QUE-ch5	2.649(217)	1.116(135)	<sup>a</sup>	<sup>a</sup>	<sup>a</sup>	<sup>a</sup>	0.372(11)	7.19(621)	0.378(11)	7.006(610)
QUE-ch6	1.311(153)	1.267(57)	0.198(30)	6.616(1.270)	0.204(31)	6.434(1.234)	0.338(10)	3.882(467)	0.347(9)	3.775(453)
<i>CV3 chondrites</i>										
Al-mat	1.893(27)	1.084(27)	0.334(50)	5.616(823)	0.357(50)	5.297(768)	0.296(12)	6.401(303)	0.316(9)	5.989(276)
Al-ch3	2.635(65)	1.058(24)	0.546(77)	4.824(707)	0.567(80)	4.644(680)	0.419(9)	6.282(317)	0.436(13)	6.048(301)
Al-ch6	2.457(109)	1.066(17)	0.505(50)	4.865(528)	0.525(52)	4.678(506)	0.404(13)	6.076(328)	0.421(12)	5.843(312)
Vi-mat1	1.498(80)	1.118(88)	0.299(114)	5.003(1.926)	0.309(118)	4.846(1.846)	0.310(9)	4.832(298)	0.320(9)	4.681(287)
Vi-mat2	1.674(117)	1.118(67)	0.299(87)	5.594(1.671)	0.309(90)	5.419(1.618)	0.310(9)	5.400(413)	0.320(9)	5.231(398)
Vi-ch1	2.406(247)	1.050(25)	0.541(83)	4.447(822)	0.545(84)	4.412(817)	0.394(7)	6.100(650)	0.397(11)	6.054(645)
Vi-ch2	1.576(105)	1.124(111)	<sup>a</sup>	<sup>a</sup>	<sup>a</sup>	<sup>a</sup>	0.271(11)	5.819(423)	0.280(8)	5.628(407)
Vi-ch3	2.321(116)	1.013(59)	0.748(310)	3.102(1.295)	0.757(314)	3.064(1.279)	0.484(15)	4.796(284)	0.490(15)	4.737(280)
A82-mat	0.300(21)	1.095(73)	0.283(99)	1.057(378)	0.295(104)	1.015(363)	0.264(8)	1.134(86)	0.275(8)	1.089(82)
A82-ch1	1.043(75)	1.074(33)	0.584(105)	1.784(345)	0.590(106)	1.766(342)	0.489(15)	2.133(157)	0.490(15)	2.111(155)
A82-ch2	0.771(53)	1.107(24)	0.419(48)	1.839(244)	0.426(48)	1.812(241)	0.414(13)	1.864(141)	0.420(13)	1.836(138)
A82-ch3	0.046(5)	1.065(72)	0.497(224)	0.092(43)	0.464(189)	0.099(42)	0.359(11)	0.128(14)	0.369(11)	0.124(14)
<i>Ungrouped 3 chondrite</i>										
A94-mat	0.460(37)	<sup>a</sup>	<sup>a</sup>	<sup>a</sup>	<sup>a</sup>	<sup>a</sup>	0.220(6)	2.126(180)	0.231(6)	2.024(171)
A94-ch1	0.609(58)	<sup>a</sup>	<sup>a</sup>	<sup>a</sup>	<sup>a</sup>	<sup>a</sup>	0.281(9)	2.169(216)	0.292(9)	2.088(207)

Uncertainties (1 s. d.) are given in parenthesis. Abundances of  $^{20}\text{Ne}_r$  and  $^{21}\text{Ne}_c$  in units of  $10^{-8}$  cc/g.  $P_{21}$  and  $T_{21}$  are given in  $10^{-8}$  cc/(g Ma) and Ma, respectively. <sup>a</sup>Large uncertainties because of large dominant trapped component. <sup>b</sup>Large uncertainties because of Ne-E contribution.

**Table 5-9: Concentrations of  $^3\text{He}$ , production rates ( $P_{3\text{-corr}}$ ,  $P_{3\text{-}1.11}$ ), and CRE ages ( $T_{3\text{-corr}}$ ,  $T_{3\text{-}1.11}$ ) of all matrix (mat) and chondrule (ch) samples.  $P_{3\text{-corr}}$  and  $T_{3\text{-corr}}$  were calculated with shielding correction,  $P_{3\text{-}1.11}$  and  $T_{3\text{-}1.11}$  were calculated without shielding correction, i.e.  $(^{22}\text{Ne}/^{21}\text{Ne})_c = 1.11$  ("average shielding").**

	$^3\text{He}$	$P_{3\text{-corr}}$	$T_{3\text{-corr}}$	$P_{3\text{-}1.11}$	$T_{3\text{-}1.11}$
<b>CR2 chondrites</b>					
Re-mat	3.942(159)	1.510(23)	2.610(112)	1.585(22)	2.488(106)
Re-ch1	1.251(625)	<sup>b</sup>	<sup>b</sup>	1.584(33)	<sup>b</sup>
Re-ch2	6.333(162)	1.529(24)	4.142(124)	1.588(23)	3.988(118)
El-mat	18.94(32) <sup>a</sup>	<sup>a</sup>	<sup>a</sup>	1.558(26)	12.15(37)
El-ch2	6.498(121)	1.590(17)	4.088(87)	1.616(17)	4.022(86)
El-ch3	10.85(19)	1.694(7)	6.408(118)	1.696(7)	6.399(117)
El-ch4	9.854(193)	1.653(14)	5.960(210)	1.664(14)	5.921(208)
El-ch5	9.779(187)	1.653(9)	5.917(182)	1.683(9)	5.809(178)
El-ch6	8.978(202)	1.660(9)	5.409(126)	1.683(9)	5.336(124)
El-ch7	9.609(236)	1.654(17)	5.811(154)	1.641(16)	5.856(155)
El-ch8	7.837(153)	1.662(8)	4.716(143)	1.693(8)	4.629(140)
El-ch9	8.317(144)	1.643(16)	5.064(148)	1.644(16)	5.059(148)
El-ch10	7.754(149)	1.594(18)	4.865(109)	1.626(19)	4.768(107)
El-ch11a	7.029(654)	1.583(16)	4.440(416)	1.616(16)	4.349(407)
NWA-mat	322.8(18.0) <sup>c</sup>	<sup>a</sup>	<sup>a</sup>	1.540(29)	209.7(12.3)
NWA-ch1	42.13(2.50)	1.593(12) <sup>a</sup>	26.44(54)	1.594(22)	26.43(54)
NWA-ch2	49.32(2.94)	1.552(25) <sup>a</sup>	31.79(53)	1.558(25)	31.66(53)
<b>CR3 chondrites</b>					
MET-mat	66.49(2.51) <sup>a</sup>	<sup>a</sup>	<sup>a</sup>	1.615(17)	<sup>a</sup>
MET-ch1	11.48(67)	<sup>a</sup>	<sup>a</sup>	1.141(74)	10.06(88)
MET-ch2	40.91(3.30)	<sup>a</sup>	<sup>a</sup>	1.648(16)	<sup>a</sup>
MET-ch3	13.84(35)	<sup>a</sup>	<sup>a</sup>	1.584(22)	8.738(254)
MET-ch4	103.3(6.6) <sup>a</sup>	<sup>a</sup>	<sup>a</sup>	1.597(21)	<sup>a</sup>
MET-ch5	26.86(1.47) <sup>a</sup>	<sup>a</sup>	<sup>a</sup>	1.641(16)	<sup>a</sup>
MET-ch6	62.90(3.09)	<sup>a</sup>	<sup>a</sup>	1.611(20)	<sup>a</sup>
QUE-mat	4.545(177) <sup>a</sup>	<sup>a</sup>	<sup>a</sup>	1.565(26)	2.905(123)
QUE-ch1	7.403(366)	1.539(26)	4.810(251)	1.595(25)	4.642(241)
QUE-ch2	9.456(963)	1.587(20)	5.959(611)	1.664(20)	5.682(583)
QUE-ch3	10.27(34)	1.551(18)	6.622(232)	1.619(19)	6.346(222)
QUE-ch4	3.879(234)	1.590(14)	2.441(149)	1.663(14)	2.333(142)
QUE-ch5	16.29(92)	<sup>a</sup>	<sup>a</sup>	1.668(10)	9.765(554)
QUE-ch6	9.914(403)	1.552(18)	6.389(270)	1.619(18)	6.122(259)
<b>CV3 chondrites</b>					
Al-mat	8.574(158)	1.602(21)	5.351(163)	1.591(21)	5.338(164)
Al-ch3	9.440(295)	1.669(15)	5.656(252)	1.646(14)	5.734(256)
Al-ch6	9.170(404)	1.666(17)	5.505(298)	1.646(2)	5.570(301)
Vi-mat2	5.968(264)	1.605(22)	3.718(172)	1.609(2)	3.710(172)
Vi-ch1	7.979(555)	1.739(7)	4.589(320)	1.711(7)	4.663(324)
Vi-ch2	5.604(210)	<sup>a</sup>	<sup>a</sup>	1.626(19)	3.445(169)
Vi-ch3	7.564(358)	1.704(12)	4.440(213)	1.669(11)	4.533(217)
A82-mat	0.986(40)	1.604(24)	0.615(27)	1.603(24)	0.615(27)
A82-ch1	1.551(233)	1.699(24)	0.913(138)	1.682(24)	0.922(139)
A82-ch2	1.425(50)	1.666(14)	0.855(31)	1.665(14)	0.856(31)
A82-ch3	0.117(14)	1.634(21)	0.072(9)	1.608(21)	0.073(9)
<b>Ungrouped 3 chondrite</b>					
A94-mat	2.365(98)	<sup>a</sup>	<sup>a</sup>	1.601(18)	1.477(63)
A94-ch1	3.499(680)	<sup>a</sup>	<sup>a</sup>	1.602(21)	2.184(425)

Uncertainties (1 s. d.) are given in parentheses. Abundances of  $^3\text{He}$  in units of  $10^8$  cc/g.  $P_3$  and  $T_3$  are given in  $10^8$  cc/(g Ma) and Ma, respectively. In most cases  $^3\text{He}$  is given as measured; only in a few cases  $^3\text{He}$  was calculated from  $^4\text{He}$  and  $^3\text{He}/^4\text{He}$  because of the smaller error. <sup>a</sup>Large uncertainties because of large dominant trapped component; NWA-ch1, NWA-ch2, MET-ch2 and MET-ch6 are also influenced by solar wind, making the determination of the cosmogenic  $^3\text{He}$  abundance unreliable. <sup>b</sup>Large uncertainties because of Ne-E contribution.

**Table 5-10: Concentrations of  $^{38}\text{Ar}_c$ , production rates ( $P_{38\text{-corr}}$ ,  $P_{38-1.11}$ ), and CRE ages ( $T_{38\text{-corr}}$ ,  $T_{38-1.11}$ ) of all matrix (mat) and chondrule (ch) samples.  $P_{38\text{-corr}}$  and  $T_{38\text{-corr}}$  were calculated with shielding correction,  $P_{38-1.11}$  and  $T_{38-1.11}$  were calculated without shielding correction, i.e.  $(^{22}\text{Ne}^{21}\text{Ne})_c = 1.11$  ("average shielding").**

	$^{38}\text{Ar}_c$	$P_{38\text{-corr}}$	$T_{38\text{-corr}}$	$P_{38-1.11}$	$T_{38-1.11}$
<b>CR2 chondrites</b>					
Re-mat	<sup>a</sup>	<sup>a</sup>	<sup>a</sup>	0.055(3)	<sup>a</sup>
Re-ch1	<sup>a</sup>	<sup>a</sup>	<sup>a</sup>	0.053(4)	<sup>a</sup>
Re-ch2	0.173(84)	0.045(11)	3.832(2.078)	0.058(3)	2.989(1.466)
El-mat	<sup>a</sup>	<sup>a</sup>	<sup>a</sup>	0.054(3)	<sup>a</sup>
El-ch2	<sup>a</sup>	0.030(4)	4.607(3.605)	0.033(2)	4.166(3.225)
El-ch3	0.117(60)	0.025(2)	4.677(2.434)	0.025(1)	4.637(2.406)
El-ch4	<i>not determined</i>				
El-ch5	0.171(32)	0.045(2)	3.811(736)	0.050(1)	3.403(642)
El-ch6	0.135(56)	0.035(2)	3.886(1.380)	0.038(2)	3.575(1.260)
El-ch7	<sup>a</sup>	0.043(5)	<sup>a</sup>	0.041(2)	<sup>a</sup>
El-ch8	0.352(101)	0.067(8)	5.222(1.630)	0.076(2)	4.654(1.343)
El-ch9	<sup>a</sup>	0.039(4)	4.042(2.562)	0.039(2)	4.020(2.516)
El-ch10	0.117(50)	0.034(3)	3.465(1.499)	0.038(2)	3.056(1.312)
El-ch11a	0.136(61)	0.058(4)	2.336(1.052)	0.066(2)	2.056(1.312)
NWA-mat	<sup>a</sup>	<sup>a</sup>	<sup>a</sup>	0.060(3)	8.890(7.920)
NWA-ch1	0.833(71)	0.059(4)	14.04(1.84)	0.059(3)	14.01(1.35)
NWA-ch2	0.828(161)	0.059(4)	14.07(2.92)	0.060(2)	13.74(2.75)
<b>CR3 chondrites</b>					
MET-mat	<sup>a</sup>	<sup>a</sup>	<sup>a</sup>	0.078(2)	<sup>a</sup>
MET-ch1	0.588(31)	<sup>a</sup>	6.111(1.378)	0.074(9)	7.920(1.014)
MET-ch2	<sup>a</sup>	<sup>a</sup>	<sup>a</sup>	0.053(2)	<sup>a</sup>
MET-ch3	<sup>a</sup>	<sup>a</sup>	<sup>a</sup>	0.043(3)	<sup>a</sup>
MET-ch4	<sup>a</sup>	<sup>a</sup>	<sup>a</sup>	0.060(3)	<sup>a</sup>
MET-ch5	<sup>a</sup>	<sup>a</sup>	<sup>a</sup>	0.055(2)	<sup>a</sup>
MET-ch6	<sup>a</sup>	<sup>a</sup>	<sup>a</sup>	0.067(3)	<sup>a</sup>
QUE-mat	<sup>a</sup>	<sup>a</sup>	<sup>a</sup>	0.068(3)	<sup>a</sup>
QUE-ch1	<sup>a</sup>	0.030(9)	<sup>a</sup>	0.038(3)	<sup>a</sup>
QUE-ch2	0.130(49)	0.030(3)	4.365(1.729)	0.041(3)	3.168(1.221)
QUE-ch3	<sup>a</sup>	0.050(6)	<sup>a</sup>	0.066(2)	<sup>a</sup>
QUE-ch4	<sup>a</sup>	0.046(6)	<sup>a</sup>	0.063(2)	<sup>a</sup>
QUE-ch5	<sup>a</sup>	<sup>a</sup>	<sup>a</sup>	0.087(2)	<sup>a</sup>
QUE-ch6	0.217(199)	0.050(6)	<sup>a</sup>	0.066(2)	<sup>a</sup>
<b>CV3 chondrites</b>					
Al-mat	0.384(56)	0.042(3)	9.167(1.710)	0.040(2)	9.538(1.736)
Al-ch3	0.220(11)	0.034(2)	6.502(508)	0.031(2)	7.030(493)
Al-ch6	0.274(17)	0.047(3)	5.821(325)	0.044(2)	6.226(312)
Vi-mat1	<sup>a</sup>	0.051(6)	<sup>a</sup>	0.051(3)	<sup>a</sup>
Vi-mat2	<sup>a</sup>	0.051(6)	<sup>a</sup>	0.051(2)	<sup>a</sup>
Vi-ch1	0.163(77)	0.040(2)	4.124(1.970)	0.036(1)	4.515(2.151)
Vi-ch2	<sup>a</sup>	<sup>a</sup>	<sup>a</sup>	0.060(2)	9.087(34.416)
Vi-ch3	0.151(103)	0.034(3)	<sup>a</sup>	0.030(1)	<sup>a</sup>
A82-mat	0.061(30)	0.070(8)	<sup>a</sup>	0.069(3)	0.885(432)
A82-ch1	0.085(13)	0.032(4)	2.684(505)	0.030(3)	2.837(515)
A82-ch2	0.078(4)	0.030(2)	2.589(226)	0.030(2)	2.601(205)
A82-ch3	0.048(21)	0.051(2)	<sup>a</sup>	0.051(2)	0.936(418)
<b>Ungrouped 3 chondrite</b>					
A94-mat	<sup>a</sup>	<sup>a</sup>	<sup>a</sup>	0.079(2)	<sup>a</sup>
A94-ch1	<sup>a</sup>	<sup>a</sup>	<sup>a</sup>	0.084(3)	<sup>a</sup>

Uncertainties (1 s. d.) are given in parenthesis. Abundances of  $^{38}\text{Ar}_c$  in units of  $10^{-8}$  cc/g.  $P_{38}$  and  $T_{38}$  are given in  $10^{-8}$  cc/(g Ma) and Ma, respectively. <sup>a</sup>Large uncertainties because of large dominant trapped component.



### Argon Ar

In most samples Ar is dominated by trapped components (**Table 5-10, Appendix 5**).  $^{36}\text{Ar}/^{38}\text{Ar}$  ratios are mostly lower than the values for Q gas ( $5.34 \pm 0.02$ , Busemann et al. 2000) due to the presence of cosmogenic  $^{38}\text{Ar}$  augmented by some  $^{38}\text{Ar}$  produced during the neutron activation. Abundances of  $^{38}\text{Ar}$  have, however, too large uncertainties for useful application in this work and will not be further considered.

### 5.3.2 Neon isotopes

Neon isotopic composition for all samples are shown in three-isotope plots (**Figures 5-14 to 5-16**), together with results of previous noble gas analysis.

#### CR2 chondrites

All chondrules from CR2 chondrites except Re-ch1 are dominated by cosmogenic noble gases (**Figure 5-14**). In contrast, matrix samples show the clear signature of trapped

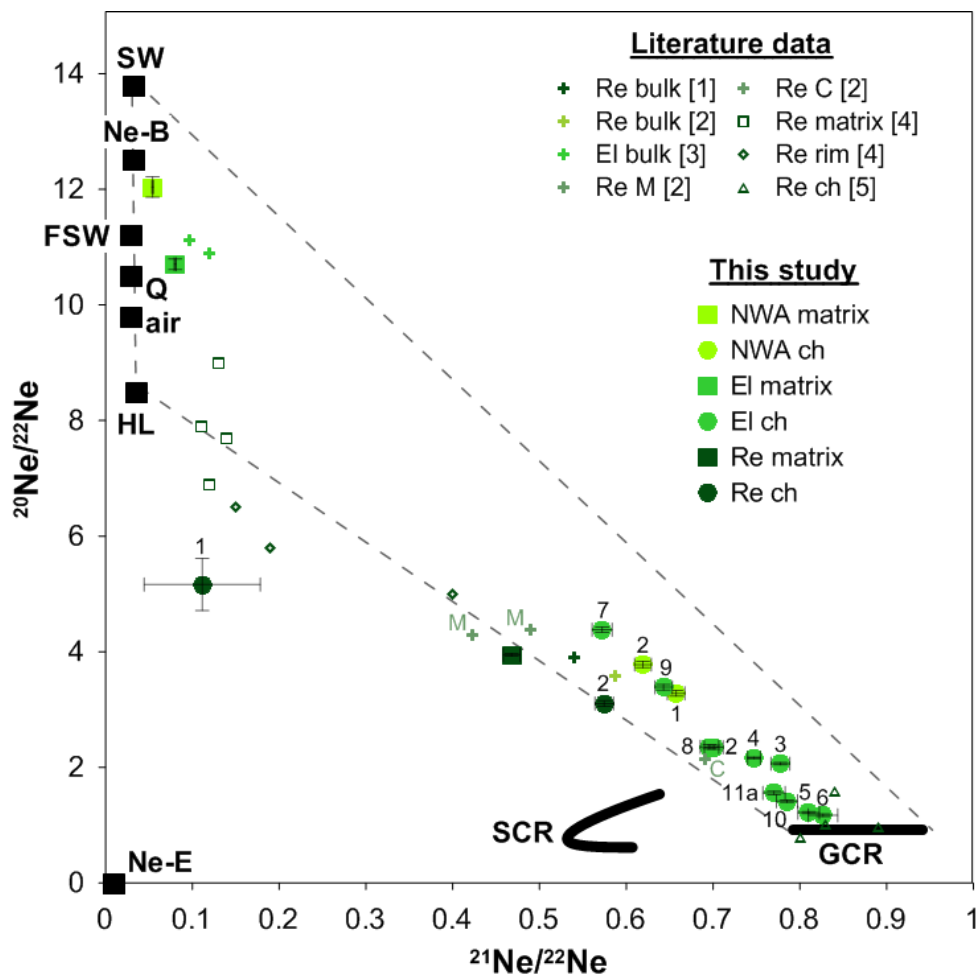


**Figure 5-14: Three isotope plot of neon for CR2 chondrites NWA 852 (NWA), EI Djouf 001 (EI) and Renazzo (Re).** Data from previous analyses of bulk (crosses), matrix (squares), rims (diamonds) and chondrules (triangles) are also plotted. Sources of data: 1-Reynolds and Turner (1964), 2-Mazor et al. (1970), 3-Bischoff et al. (1993), 4-Vogel et al. (2003), 5-Vogel et al. (2004). Values for solar wind (SW) [Heber et al. 2009], Ne-B gas [Black 1972], fractionated SW (FSW) [Wieler 2002a], Q gas [Ott 2002], air [Eberhardt et al. 1965], HL gas [Huss and Lewis 1994], Ne-E [Ott 2002], neon produced by solar galactic rays (SCR) [Reedy 1992] and galactic cosmic radiation (GCR) [Wieler 2002b] are also shown. Abbreviations: ch-chondrule, C-non-magnetic fraction, enriched in chondrules; M-magnetic fraction,  $\rho < 2.5 \text{ g/cm}^3$ . Chondrules are labelled with numbers.

components. El Djouf 001 and NWA samples form an approximate mixing line between a cosmogenic component and Q gas or a mixture of Q gas and SW. Renazzo matrix is less influenced by trapped neon components, and Renazzo samples may fall on a mixing line with HL gas instead. High concentrations of  $^{20}\text{Ne}$  and  $^4\text{He}$  (see **Appendix 3 & 4**), and the high ( $^{20}\text{Ne}/^{22}\text{Ne}$ ) ratios indicate dominant solar components in NWA 852 and El Djouf 001 matrices. In the Renazzo matrix the concentration of solar gases is much smaller, indicating that NWA 852 and El Djouf 001 are more mature regolith breccias than Renazzo (Bischoff et al. 1993).

The results for NWA 852 agree with noble gas analyses for paired NWA 801 (Nakashima et al. 2009a), showing a dominant solar component for NWA 801 matrix and a dominant cosmogenic component for chondrules.

Our El Djouf 001 matrix measurements agree well with those of El Djouf 001 bulk by Bischoff et al. (1993). The dominance of trapped components in El Djouf 001 matrix can be explained by the fact that it represents a regolith breccia, where the surface material is exposed to low energy solar wind and SCR particles and surface gardening is an important process.

Results for Renazzo chondrules from this study are somewhat different from those previously obtained (Vogel et al. 2004). However, Re-ch2 show a similar neon composition as Renazzo bulk samples (Reynolds and Turner 1964, Mazor et al. 1970) and Renazzo matrix is similar to a magnetic fraction of Renazzo bulk analyzed by Mazor et al. (1970). Interestingly, Re-ch1 shows a low  $^{21}\text{Ne}/^{22}\text{Ne}$  ratios similar to matrix and rim material from Renazzo (Vogel et al. 2003), questioning whether Re-ch1 is a chondrule. The low  $^{20}\text{Ne}/^{22}\text{Ne}$  ratios of Re-ch1 (as well as low ( $^{21}\text{Ne}/^{22}\text{Ne}$ )<sub>c</sub>) can be caused by Ne-E, found in graphite and is thought to originate primarily from the decay of  $^{22}\text{Na}$  produced in novae (Amari et al. 1995).

### **CR3 chondrites and ungrouped Acfer 094**

Chondrules from MET 00426 contain surprisingly abundant trapped noble gases (**Figure 5-15**), which may represent SW gas similar to noble gases present in regolith samples after fractionation and gas loss (Ne-B), having a ( $^{20}\text{Ne}/^{22}\text{Ne}$ )<sub>c</sub> ratio of  $12.3 \pm 0.3$  (Polnau et al. 1999). Chondrules from QUE 99177, on the other hand, contain abundant cosmogenic noble gases, and the matrix clearly contains HL gas. All samples from QUE 99177 fall on a mixing line between a cosmogenic component and HL gas. Chondrule and matrix sample from Acfer 094 plot near HL gas and are comparable with the previous measurements by Scherer and Schultz (2000).

### **CV3 chondrites**

Nearly all chondrules from CV3 chondrites are stronger influenced by cosmogenic noble gases compared with their matrix samples (**Figure 5-16**). Most chondrules plot near the cosmogenic end point like chondrules previously measured (Roth et al. 2011, Vogel et al. 2004). All samples from our CV chondrites seem to be influenced by SW gas, HL gas, and possibly by some Q gas.

Neon isotopic ratios of chondrule A82-ch3 are similar to those of a bulk sample of Acfer 082, in spite of very different gas concentrations (Scherer and Schultz 2000). Chondrule Vi-ch2 is similarly influenced by trapped components as Vigarano matrix and plots near Vigarano bulk analyses (Mazor et al. 1970, Matsuda et al. 1980). Therefore, both may be not chondrules but rather rounded matrix fragments. Low Mg abundances and high Fe abundances in both samples point into the same direction (see **Appendix 1**).

Data for Allende matrix are similar to previous Allende bulk (Bogard et al. 1971, Schultz and Signer 1973, Levsky 1972, Smith et al. 1977, Scherer and Schultz 2000) and matrix

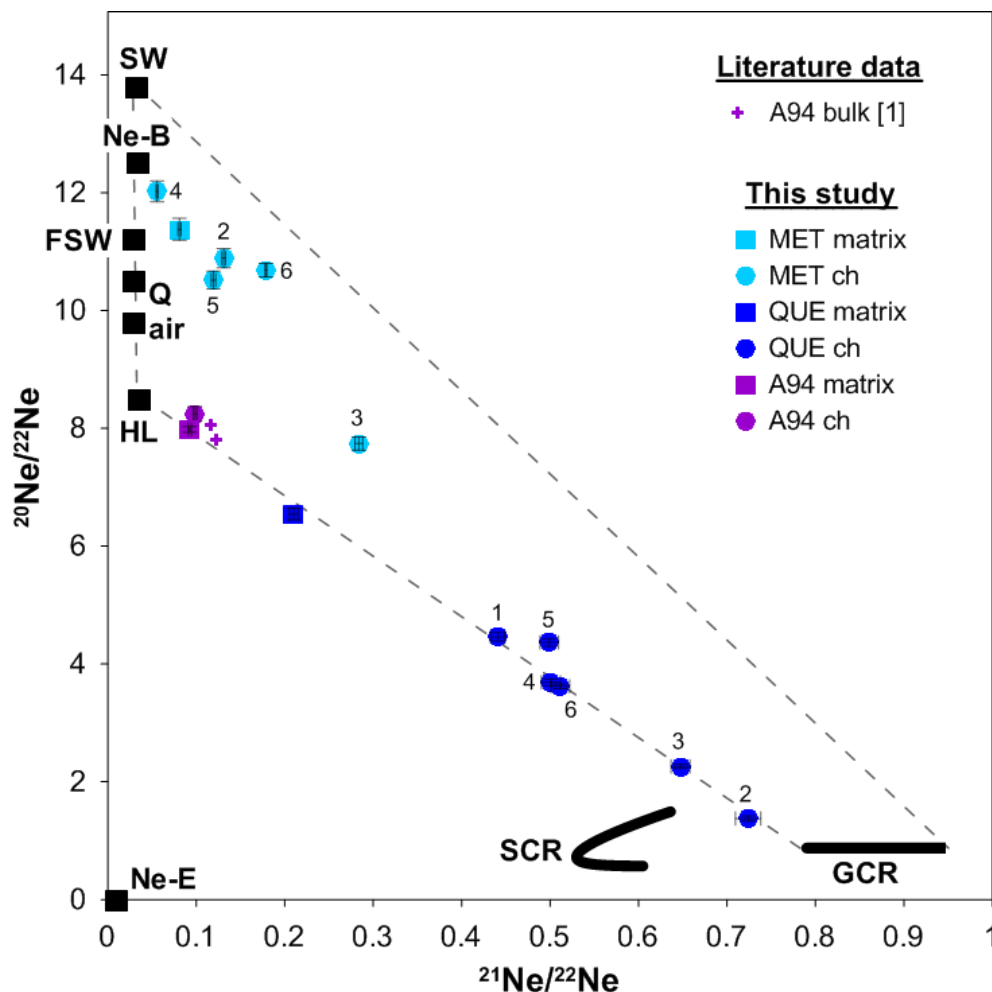


**Figure 5-15: Three isotope plot of neon for ungrouped Acfer 094 (A94) and CR3 chondrites QUE 99177 (QUE) and MET 00426 (MET).** Data from previous analyses of bulk (crosses) are also plotted. Sources of data: 1-Scherer et al. (2000). Values for solar wind (SW) [Heber et al. 2009], Ne-B gas [Black 1972], fractionated SW (FSW) [Wieler 2002a], Q gas [Ott 2002], air [Eberhardt et al. 1965], HL gas [Huss and Lewis 1994], Ne-E [Ott 2002], neon produced by solar galactic rays (SCR) [Reedy 1992] and galactic cosmic radiation (GCR) [Wieler 2002b] are also shown. Abbreviation: ch-chondrule. Chondrules are labelled with numbers. MET-ch1 is not shown.

measurements (Eugster et al. 2007). Allende matrix analyses by Vogel et al. 2003 and Roth et al. (2011) are generally stronger influenced by trapped components compared to the Allende matrix material analyzed in this study.

Allende chondrules of this study plot in a narrow field near the cosmogenic end point, whereas Allende chondrules analyzed by Roth et al. (2011) cover a wider field (e.g., A1-Ch1 has a  $^{21}\text{Ne}/^{22}\text{Ne}$  ratio of 0.242 and a  $^{20}\text{Ne}/^{22}\text{Ne}$  ratio of 7.73).

### **Neon components released at 600°C and 1800°C**

Stepwise heating is commonly used to separate different noble gas components (e.g., Trieloff et al. 2005, Ozima and Podosek 2002). In a three-isotope plot for Ne a shift towards the cosmogenic endpoint with increasing temperature is visible (**Figure 5-17**). This is in agreement with Manuel et al. (1972) and Smith et al. (1977) (see chapter 2.3.3) In most cases, this shift is much larger for chondrules than for matrix samples.

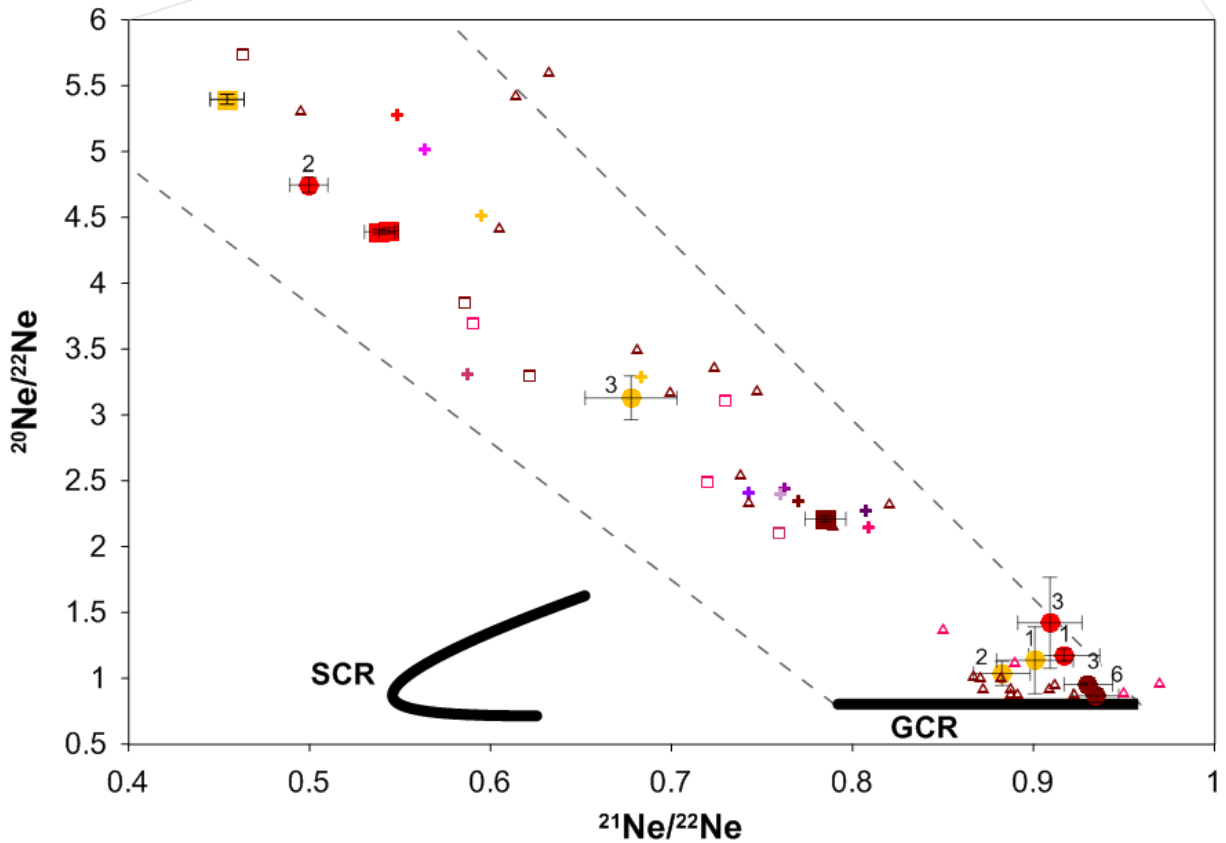
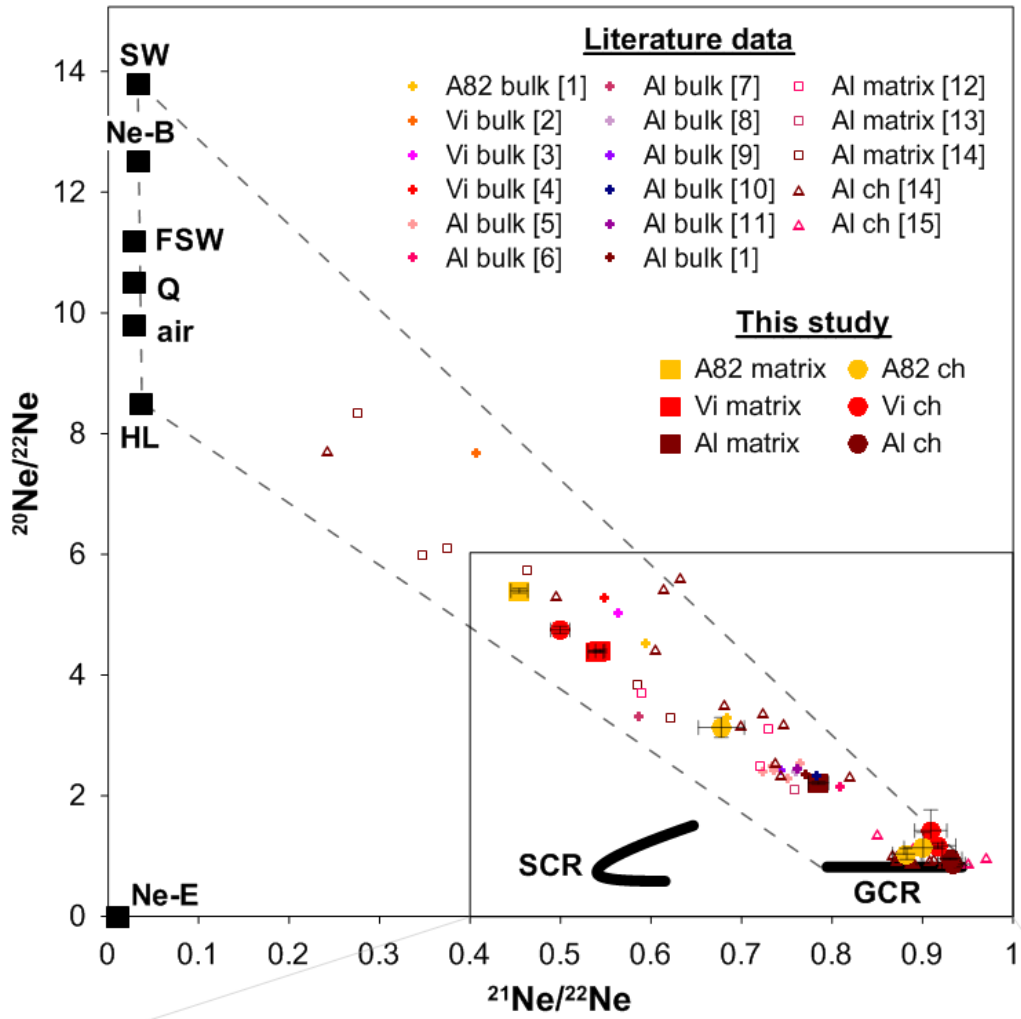


**Figure 5-16: Three isotope plot of neon for CV3 chondrites Acfer 082 (A82), Vigarano (Vi) and Allende (Al).** Data from previous analyses of bulk (crosses), matrix (squares) and chondrules (triangles) are also plotted. Sources of data: 1-Scherer and Schultz (2000), 2-Hintenberger et al. (1964), 3-Mazor et al. (1970), 4-Matsuda et al. (1980), 5-Fireman and Goebel (1970), 6-Bogard et al. (1971), 7-Manuel et al. (1972), 8-Levsky (1972), 9-Schultz and Signer (1973) personal communication, cited in Schultz and Franke (2004), 10-Lewis et al. (1975), 11-Smith et al. (1977), 12-Vogel et al. (2003), 13-Eugster et al. (2007), 14-Roth et al. (2011), 15-Vogel et al. (2004). Values for solar wind (SW) [Heber et al. 2009], Ne-B gas [Black 1972], fractionated SW (FSW) [Wieler 2002a], Q gas [Ott 2002], air [Eberhardt et al. 1965], HL gas [Huss and Lewis 1994], Ne-E [Ott 2002], neon produced by solar galactic rays (SCR) [Reedy 1992] and galactic cosmic radiation (GCR) [Wieler 2002b] are also shown. An inset is shown for the lower right corner. Abbreviation: ch-chondrule. Chondrules are labelled with numbers.

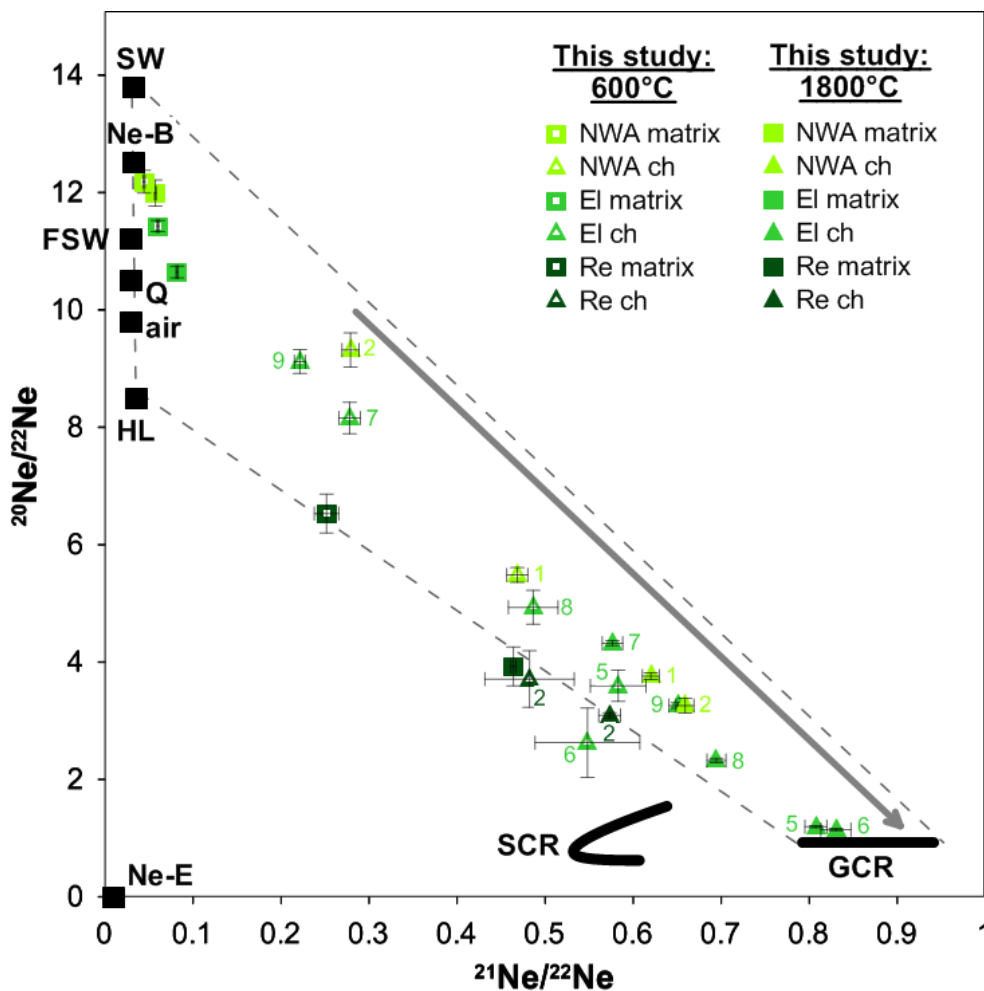


**Figure 5-17: Three isotope plot of neon for CR2 chondrites NWA 852 (NWA), EI Djouf 001 (EI) and Renazzo (Re) released at 600°C and 1800°C.** Values for solar wind (SW) [Heber et al. 2009], Ne-B gas [Black 1972], fractionated SW (FSW) [Wieler 2002a], Q gas [Ott 2002], air [Eberhardt et al. 1965], HL gas [Huss and Lewis 1994], Ne-E [Ott 2002], neon produced by solar galactic rays (SCR) [Reedy (1992)] and galactic cosmic radiation (GCR) [Wieler 2002b] are also shown. The arrow labels a shift towards the cosmogenic component. Samples with minor gas release at 600°C causing large uncertainties (Re-ch1, NWA-ch1) are not shown. For EI Djouf 001 only selected chondrules are shown because of clarity. Abbreviation: ch-chondrule. Chondrules are labelled with numbers.

### 5.3.3 Production rates

#### **Production rates of samples from this study**

Since dominant solar wind component causes large uncertainties of the parameter  $(^{22}\text{Ne}/^{21}\text{Ne})_c$  required for the calculation of the shielding-corrected production rates of cosmogenic nuclides (see **Tables 5-8 to 5-10**), here only uncorrected production rates with  $(^{22}\text{Ne}/^{21}\text{Ne})_c = 1.11$  are considered.

Production rates of  $^{21}\text{Ne}_c$  (**Table 5-8, Figure 5-18a**) are generally higher in chondrules compared to the respective matrix samples. Chondrules MET-ch1 and Vi-ch2 are exceptions. Metal chondrule MET-ch1 has very low  $P_{21-1.11}$  values ( $0.029 \pm 2 \times 10^{-8}$  cc/(g\*Ma)) due to high Fe / low Mg, Al, Si abundances, and Vi-ch2 has slightly lower  $P_{21-1.11}$  values compared with Vigarano matrix ( $0.271 \pm 0.011 \times 10^{-8}$  cc/(g\*Ma) vs.  $0.310 \pm 0.009 \times 10^{-8}$  cc/(g\*Ma)).

The uncertainties of  $P_{21-1.11}$  due to calculated Si abundances ( $\text{Si}_{\min}$  and  $\text{Si}_{\max}$ ) are usually in the range of 0.4 and 1.5% relative to  $P_{21-1.11}$  calculated with  $\text{Si}_{50}$  for chondrules (see **Table 5-11**); matrices with lower Mg abundances have higher differences up to 3.6% in case of NWA 852 matrix.

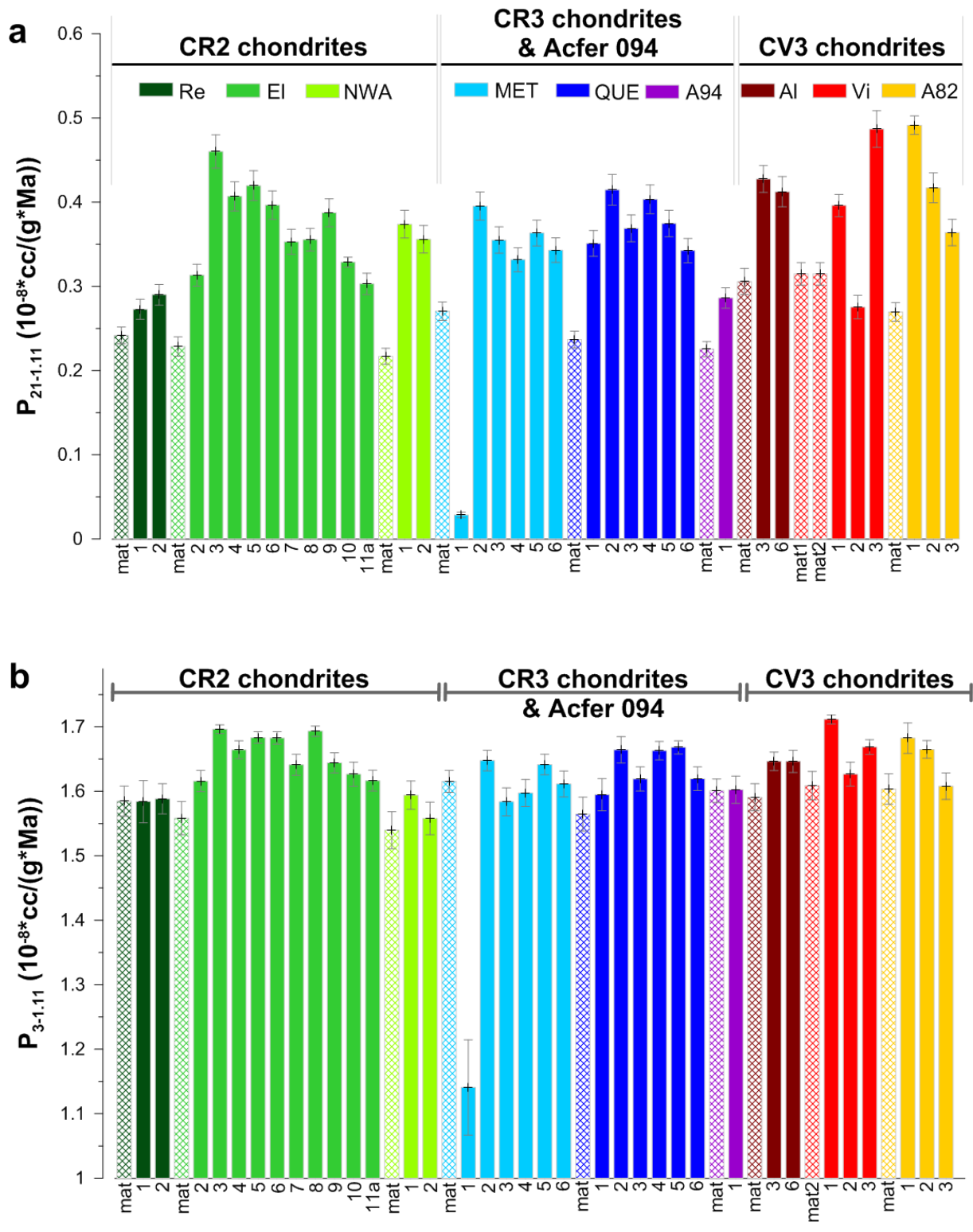
**Table 5-11: Uncertainty of  $P_{21-1.11}$  due to minimal and maximal Si abundances relative to  $P_{21-1.11}$  calculated with  $\text{Si}_{50}$ .**

Sample	Uncertainty (%)	Sample	Uncertainty (%)	Sample	Uncertainty (%)
<i>CR2 chondrites</i>		<i>CR3 chondrites</i>		<i>CV3 chondrites</i>	
Re-mat	2.536	MET-mat	1.845	Al-mat	3.326
Re-ch1	2.246	MET-ch1	0.000	Al-ch3	1.899
Re-ch2	2.054	MET-ch2	0.957	Al-ch6	1.962
El-mat	2.962	MET-ch3	1.724	Vi-mat1	1.590
El-ch2	1.590	MET-ch4	1.697	Vi-mat2	1.590
El-ch3	0.428	MET-ch5	1.101	Vi-ch1	0.372
El-ch4	0.780	MET-ch6	1.485	Vi-ch2	1.666
El-ch5	0.592	QUE-mat	2.896	Vi-ch3	0.623
El-ch6	0.609	QUE-ch1	1.622	A82-mat	2.016
El-ch7	1.140	QUE-ch2	0.739	A82-ch1	0.516
El-ch8	0.594	QUE-ch3	1.288	A82-ch2	0.756
El-ch9	1.010	QUE-ch4	0.799	A82-ch3	1.443
El-ch10	1.382	QUE-ch5	0.800		
El-ch11a	1.611	QUE-ch6	1.395		
NWA-mat	3.581	<i>Ungrouped 3 chondrite</i>			
NWA-ch1	1.537	A94-mat	2.462		
NWA-ch2	1.989	A94-ch1	1.899		

Abbreviations: mat-matrix, ch-chondrule, Re-Renazzo, El-El Djouf 001, NWA-NWA 852, MET-MET 00426, QUE-QUE 99177, A94-Acfer 094, Al-Allende; Vi-Vigarano, A82-Acfer 082,  $\text{Si}_{50}$  - mean value of minimum and maximum Si abundances.

Production rates of  $^3\text{He}$  (**Table 5-9, Figure 5-18b**) of matrix and chondrule samples are identical within uncertainties for Renazzo, NWA 852, MET 00426 and Acfer 094. In contrast, most QUE 99177 chondrules and all chondrules from El Djouf 001 and Allende have slightly elevated  $P_{3-1.11}$  relative to the respective matrix. The fact that the production of  $^3\text{He}$  is hardly influenced by the chemical composition (e.g., Wieler 2000, Eugster 1988) and the correlation between  $P_{21-1.11}$  and  $P_{3-1.11}$  may suggest the reliability of the formula by Eugster (1988) for the calculation of production rates (see *chapter 2.3.2*).

Production rates of  $^{38}\text{Ar}_c$  (**Table 5-10, Figure 5-18c**) have no clear tendency. While  $P_{38-1.11}$  values for some chondrules and matrix are identical within uncertainties (Renazzo, NWA 852, Acfer 094),  $P_{38-1.11}$  values for some matrix samples are higher than the values for chondrules (MET 00426, Acfer 082) or lie in the range of  $P_{38-1.11}$  values of chondrules (El Djouf 001, QUE 99177, Vigarano).



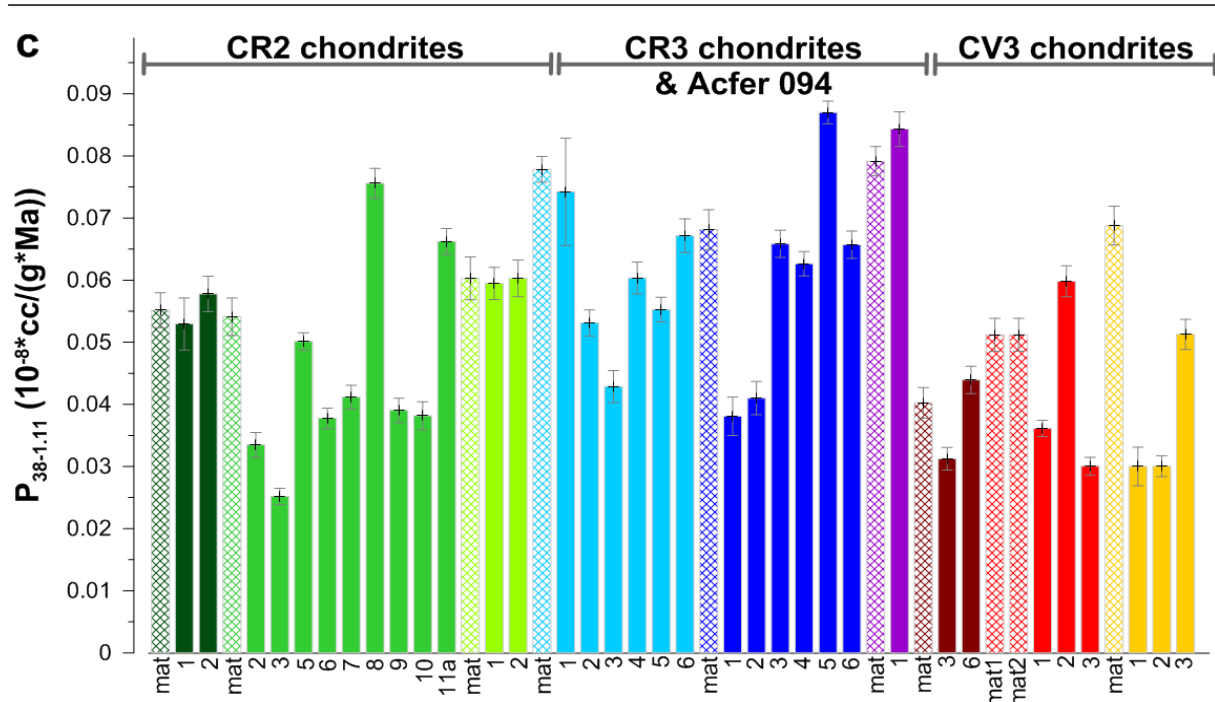


**Figure 5-18: Uncorrected production rates for Ne (a), He (b) and Ar (c) of all chondrule (ch) and matrix (mat) samples.** Production rates were calculated using the formula by Eugster (1988) (see chapter 2.3.2) and without shielding correction, i.e., for a shielding parameter ( $^{22}\text{Ne}/^{21}\text{Ne}$ ) = 1.11.  $P_{21-1.11}$  was calculated with  $Si_{50}$ . Matrix samples are indicated by diagonal crossed bars.

#### Reliability of the formula by Eugster (1988)

In order to test the reliability of the formula by Eugster (1988) used in this study for the calculation of production rates, we examined two different approaches:

- i) Comparison of production rates from the literature calculated using a formula other than that of Eugster (1988) with production rates of the same samples calculated with the formula by Eugster (1988). This approach requires the knowledge of abundances of target elements and noble gas data. The focus is here on meteorites with short CRE ages up to 10 Ma. Polnau et al. (2001) used the formula by Eugster and Michel (1995) and Eugster et al. (2007) used the same formula (mostly equation for diogenites, eucrite formula for Acfer 059) (see **Table 4.6**).

The differences of  $P_{3\text{-corr}}$  due to the used formula lie on average below <0.5% for samples from ordinary chondrites analyzed by Polnau et al. (2001) and CM chondrite Murray and CV chondrite Allende analyzed by Eugster et al. (2007) (**Table 5-12**).

The formula by Eugster (1988) used in this study provides in most cases slightly higher production rates, resulting in lower CRE ages (see formula (8) in chapter 4.7). The differences in  $P_{21\text{-corr}}$  amount on average to 3.1% and 7.5% in both studies. Samples with CRE ages <6 Ma (L6 Bowesmont, LL5 Hunter, H6 Kalvesta, Allende chondrules) generally have differences in  $P_{21\text{-corr}}$  in the range of 1 and 3.4% (see **Table 5-12**). This comparably small systematical bias affects both the production rates of matrix and chondrule samples, so the effect on differences in exposures is even smaller.



**Table 5-12: Differences of production rates and CRE ages calculated with the formula by Eugster (1988) and Eugster and Michel (1995).**

Reference	Sample	Helium		Neon	
		$\Delta P_{3\text{-corr}}$	$\Delta T_3$ CRE age	$\Delta P_{21\text{-corr}}$	$\Delta T_{21}$ CRE age
Polnau et al. (2001)	Bjurböle mat	-0.305	0.032	1.246	-0.096
	Bjurböle ch	-0.141	0.037	-2.992	0.340
	Bowesmont mat	-0.111	0.023	2.932	-0.183
	Bowesmont ch	-0.375	0.021	3.430	-0.203
	Grassland mat	-0.641	0.029	-4.216	0.393
	Grassland ch	-0.534	0.033	-4.610	0.444
	Hunter mat	-0.364	0.000	1.081	-0.006
	Hunter ch	-0.782	0.111	1.930	-0.013
	Kalvesta mat	-0.734	0.001	-2.360	0.019
	Kalvesta ch	-0.751	0.008	-5.943	0.064
	<i>Average</i>	<i>-0.474</i>	<i>0.030</i>	<i>3.074</i>	<i>0.176</i>
Eugster et al. (2007)	Acfer 059 mat	-0.339	0.047	-8.308	0.771
	Acfer 059 ch	-0.435	0.032	34.35	-2.713
	Allende mat	-0.743	0.030	-7.340	0.546
	Allende ch A1	-0.703	0.083	-1.116	0.109
	Allende ch A38	-0.377	0.057	-1.312	0.069
	Allende ch B1	-0.423	-0.014	-5.413	0.220
	Allende ch K100	-0.599	0.008	-1.284	0.110
	Allende ch SHE	-0.365	-0.015	-1.237	0.059
<i>Average</i>	<i>-0.498</i>	<i>0.036</i>	<i>7.545</i>	<i>0.575</i>	

$\Delta P_{3\text{-corr}}$  and  $\Delta T_3$  CRE age were calculated according to Eugster and Michel (1995) and are given in % and Ma relative to the values calculated with the formula by Eugster (1988), where  $Si_{50}$  was used. Abbreviations: mat - matrix, ch - chondrules

- ii) Comparison of production rates of our samples calculated using the formula by Eugster (1988) with production rates from the same samples obtained using the model by Leya and Masarik (2009), which requires the assumption of a meteoroid radius and sample depth. Here, Allende was chosen as an example with a meteoroid radius of 65 cm (Nishiizumi et al. 1991) and a shielding depth of 20 cm based on the shielding parameters for Allende matrix and chondrules; this is also in accordance with Roth et al. (2011). Allende matrix and chondrule samples have identical production rates  $P_3$  and  $P_{21}$  obtained using the model of Leya and Masarik (2009) due to identical shielding and only minor differences in the elemental composition of target elements. Both production rates for He  $P_{3\text{-corr}}$  and  $P_{3-1.11}$  calculated using the formula by Eugster (1988) are significantly lower compared to  $P_3$  obtained using the model of Leya and Masarik (2009) (see **Table 5-13**). In contrast,  $P_{21-1.11}$  calculated with the Eugster (1988) formula agrees well with  $P_{21}$  obtained using the physical model by Leya and Masarik (2009). As Ne provides the most reliable CRE ages (see *chapter 5.3.1*) and “nominal” CRE ages without shielding correction (e.g., shielding parameter  $(^{22}\text{Ne}/^{21}\text{Ne})_c = 1.11$ ) are the most reliable approach for the comparison of samples that experienced identical shielding (see *chapter 5.4.2*),  $P_{21-1.11}$  calculated using the formula by Eugster (1988) seems to be suitable for the comparison of CRE ages between our chondrule and matrix samples.

Based on the small differences between the production rates calculated by Eugster (1988) and Eugster and Michel (1995) and the good agreement of  $P_{21-1.11}$  calculated by Eugster (1988) and  $P_{21}$  obtained using the model by Leya and Masarik (2009), we decided to use the equation by Eugster (1988) for the calculation of production rates in this work.

**Table 5-13: Production rates obtained using the formula by Eugster (1988) and the model by Leya and Masarik (2009).**

Sample	Shielding parameter ( $^{22}\text{Ne}/^{21}\text{Ne}$ ) <sub>c</sub>	Eugster (1988)				Leya and Masarik (2009)	
		P <sub>3-corr</sub>	P <sub>21-corr</sub>	P <sub>3-1.11</sub>	P <sub>21-1.11</sub>	P <sub>3</sub>	P <sub>21</sub>
Al-mat	1.08(3)	1.602(21)	0.346(71)	1.591(21)	0.346(71)	1.865	0.420
Al-ch3	1.06(3)	1.669(15)	0.557(111)	1.646(14)	0.428(16)	1.899	0.436
Al-ch6	1.07(2)	1.666(17)	0.515(72)	1.646(17)	0.412(18)	1.869	0.421

Production rates are given in  $10^{-8}\text{cc}/(\text{g}\cdot\text{Ma})$ .  $P_{21\text{-corr}}$  and  $P_{21-1.11}$  were obtained using the formula by Eugster (1988) with  $\text{Si}_{50}$ . For the calculations using the model of Leya and Masarik (2009) carbon (C) abundances of 0.3 wt% in chondrules and 0.5 wt% in matrix were assumed.

Uncertainties (1 s. d.) are given in parenthesis.

### Abundance of target elements and matrix effect

Another aspect influencing the production rate is the **abundance of target elements**. Since the Mg abundance of chondrules and the respective matrix differ considerably (see chapter 5.1.1, **Appendix 1**) and Mg represents the most important target element for  $^{21}\text{Ne}_c$  (e.g., Schultz and Freundel 1985), one may expect significant different production rates of  $^{21}\text{Ne}_c$ . The differences are highlighted in **Figure 5-19**. Most chondrules have higher  $P_{21-1.11}$  values compared to the matrix, with  $P_{21-1.11}$  (chondrule/matrix) mostly ranging between 1.13 (Renazzo chondrule Re-ch1) and 1.53 (QUE 99177 chondrule QUE-ch5) (see **Figure 5-19**). Some chondrules have especially high  $P_{21-1.11}$  values, El Djouf 001 chondrule El-ch3 reaches a  $P_{21-1.11}$  (chondrule/matrix) ratio of 2.01. The metal chondrule from MET 00426 MET-ch1 naturally has the lowest value.

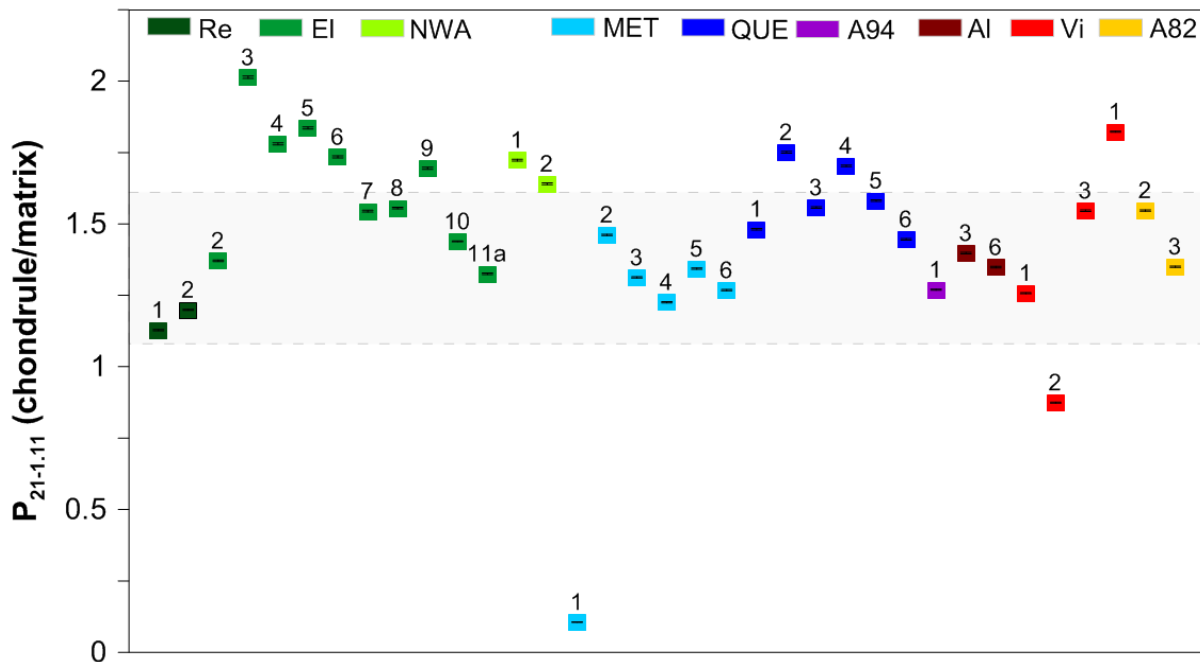


**Figure 5-19:  $P_{21-1.11}$  production rates of chondrules relative to those of the corresponding matrix samples.**  $P_{21-1.11}$  were calculated using the formula by Eugster (1988) (see chapter 4.6) with  $\text{Si}_{50}$ . The gray marked field labels the range, where most chondrules plot. Chondrules are labeled with numbers. Abbreviations: Re – Renazzo, EI – El Djouf 001, NWA – NWA 852, MET – MET 00426, QUE – QUE 99177, A94 – Acfer 094, AI – Allende, Vi – Vigarano, A82 – Acfer 082.

In addition to the direct dependency on the abundance of the important target elements, the production rates also depend on the general composition of the meteorite, which influences the development of the cascade of secondary nuclear-active particles, which is the so-called matrix effect (Wieler 2002b, Eugster et al. 2006, see *chapter 2.3.2*). Generally it is expected to be <10% for stony meteorites (Wieler 2002b), and naturally to be of little importance for the comparison of samples that experienced the same shielding.

## 5.4 Cosmic ray exposure ages of chondrules and matrix

### 5.4.1 Shielding-corrected ages

#### 5.4.1.1 This study

A shielding correction using the parameter  $(^{22}\text{Ne}/^{21}\text{Ne})_c$  allows the comparison of CRE ages from this study with those from other studies of the same meteorite, but possibly originating from different pieces with different shielding conditions (see *chapter 4.7*). Shielding corrected  $T_{21\text{-corr}}$  CRE ages are summarized in **Table 5-14** and **Figures 5-20 to 5-22**.

#### CR2 chondrites

$T_{21\text{-corr}}$  CRE ages of chondrules and matrix samples from CR2 chondrites are mostly identical within errors (see **Table 5-14**). While  $T_{21\text{-corr}}$  CRE ages of Renazzo and El Djouf 001 samples are below 7 Ma (**Figure 5-20b, c**),  $T_{21\text{-corr}}$  of NWA 852 chondrules are surprisingly high with values >28 Ma (**Figure 5-20a**).

#### CR3 chondrites and ungrouped Acfer 094

QUE 99177 matrix, chondrule QUE-ch5 and all samples from MET 00426 and Acfer 094 show large uncertainties, because with a large dominant SW component the shielding

**Table 5-14: Shielding-corrected  $T_{21\text{-corr}}$  CRE ages of all matrix (mat) and chondrules (ch) samples calculated with  $\text{Si}_{50}$ .**

Sample	$T_{21\text{-corr}}$ (Ma)	Sample	$T_{21\text{-corr}}$ (Ma)	Sample	$T_{21\text{-corr}}$ (Ma)
<b>CR2 chondrites</b>					
Re-mat	6.20(2.32) <sub>b</sub>	MET-mat	<sup>a</sup>	Al-mat	5.48(1.12)
Re-ch1		MET-ch1	<sup>a</sup>	Al-ch3	4.73(98)
Re-ch2	6.77(2.65) <sub>a</sub>	MET-ch2	<sup>a</sup>	Al-ch6	4.77(73)
El-mat		MET-ch3	<sup>a</sup>	Vi-mat1	4.92(2.68)
El-ch2	5.16(1.77)	MET-ch4	<sup>a</sup>	Vi-mat2	5.51(2.33)
El-ch3	5.16(95)	MET-ch5	<sup>a</sup>	Vi-ch1	4.43(1.16)
El-ch4	5.82(1.86)	MET-ch6	<sup>a</sup>	Vi-ch2	<sup>a</sup>
El-ch5	6.85(1.00)	QUE-mat	<sup>a</sup>	Vi-ch3	3.08(1.82)
El-ch6	5.89(1.00)	QUE-ch1	4.50(2.71)	A82-mat	1.04(52)
El-ch7	4.78(2.34)	QUE-ch2	5.29(97)	A82-ch1	1.78(49)
El-ch8	5.94(2.02)	QUE-ch3	6.56(1.50)	A82-ch2	1.83(34)
El-ch9	5.29(2.15)	QUE-ch4	2.03(46)	A82-ch3	0.10(6)
El-ch10	6.30(1.02)	QUE-ch5	<sup>a</sup>		
El-ch11a	6.20(1.15) <sub>a</sub>	QUE-ch6	6.53(1.77)		
NWA-mat		<b>Ungrouped 3 chondrite</b>			
NWA-ch1	28.3(8.3)	A94-mat	<sup>a</sup>		
NWA-ch2	36.6(11.2)	A94-ch1	<sup>a</sup>		

Uncertainties (1 s. d.) are given in parenthesis. <sup>a</sup>Too uncertain, because shielding parameter could not be determined because of large dominant solar wind component. <sup>b</sup>Large uncertainties because of Ne-E contribution. Abbreviations: Re-Renazzo, El-El Djouf 001, NWA-NWA 852, MET-MET 00426, QUE-QUE 99177, A94-Acfer 094, Al-Allende; Vi-Vigarano, A82-Acfer 082.

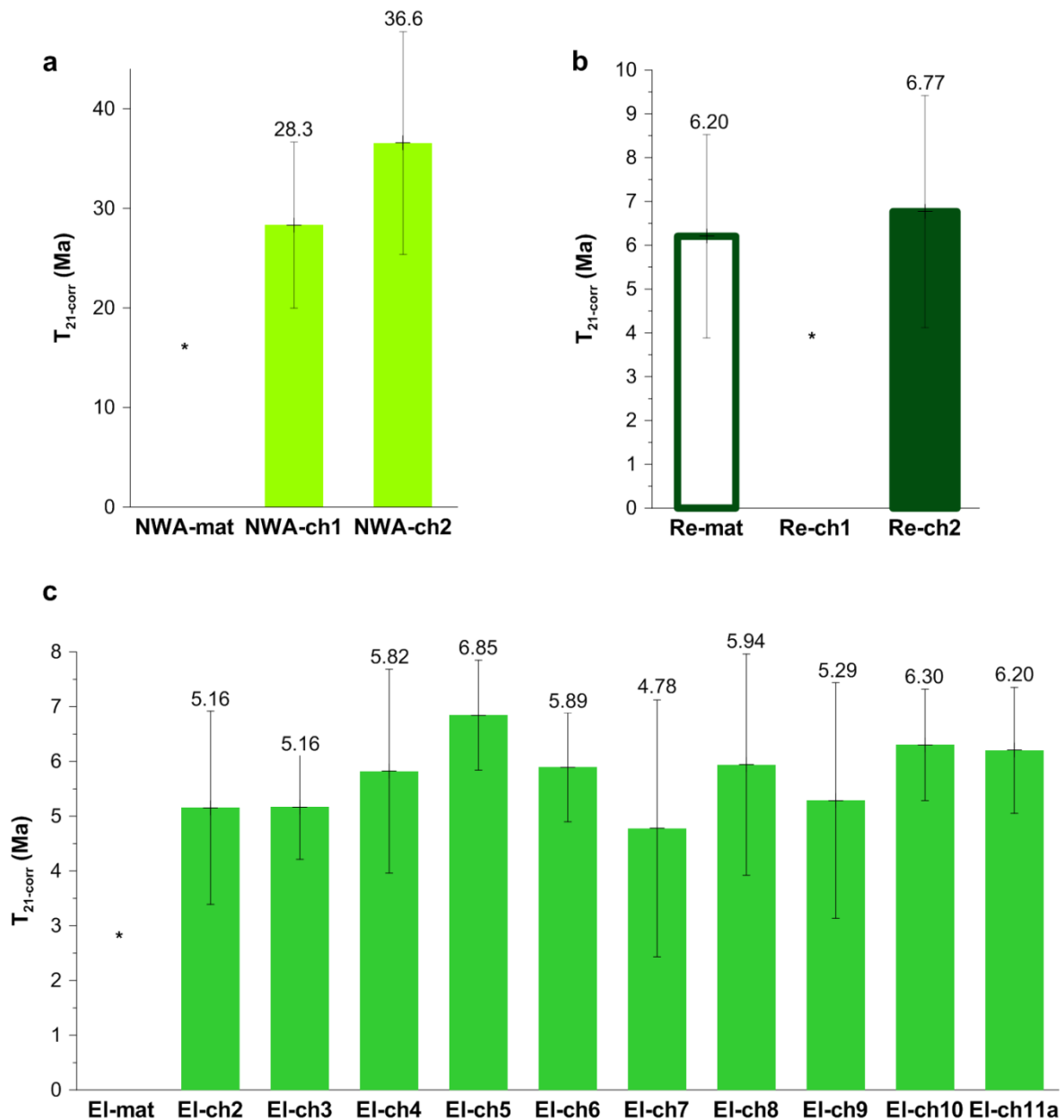


**Figure 5-20:**  $T_{21-corr}$  CRE ages of chondrules (ch) and matrix (mat) from CR2 chondrites NWA 852 (NWA) (a), Renazzo (Re) (b) and EI Djouf 001 (EI) (c) calculated with  $Si_{50}$ . \*Values are not shown due to large shielding uncertainties because of dominant solar wind component or because of Ne-E contribution (Re-ch1).

parameter necessary for calculation of the production rates are highly uncertain.  $T_{21-corr}$  CRE ages of most QUE 99177 chondrules range between 4.5 and 6.6 Ma (see **Table 5-14**, **Figure 5-21**).

### CV3 chondrites

The shielding-corrected  $T_{21-corr}$  CRE age of Allende matrix is about 0.7 Ma longer compared to the chondrules, but the ages are indistinguishable within their respective uncertainties (see **Table 5-14**, **Figure 5-22b**). Acfer 082 samples have  $T_{21-corr}$  CRE ages around 1.0, 1.8, and 0.10 Ma, respectively (**Figure 5-22a**), and Vigarano samples range between 3.1 and 5.5 Ma (**Figure 5-22c**).

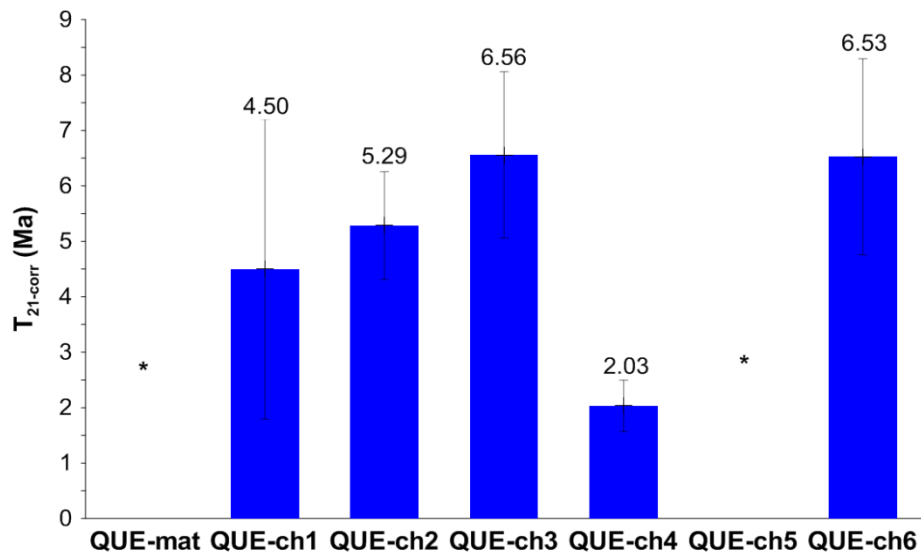


**Figure 5-21:**  $T_{21-corr}$  CRE ages of chondrules (ch) and matrix (mat) from CR3 chondrite QUE 99177 (QUE) calculated with  $Si_{50}$ . \* Values are not shown due to large shielding uncertainties because of dominant solar wind component.

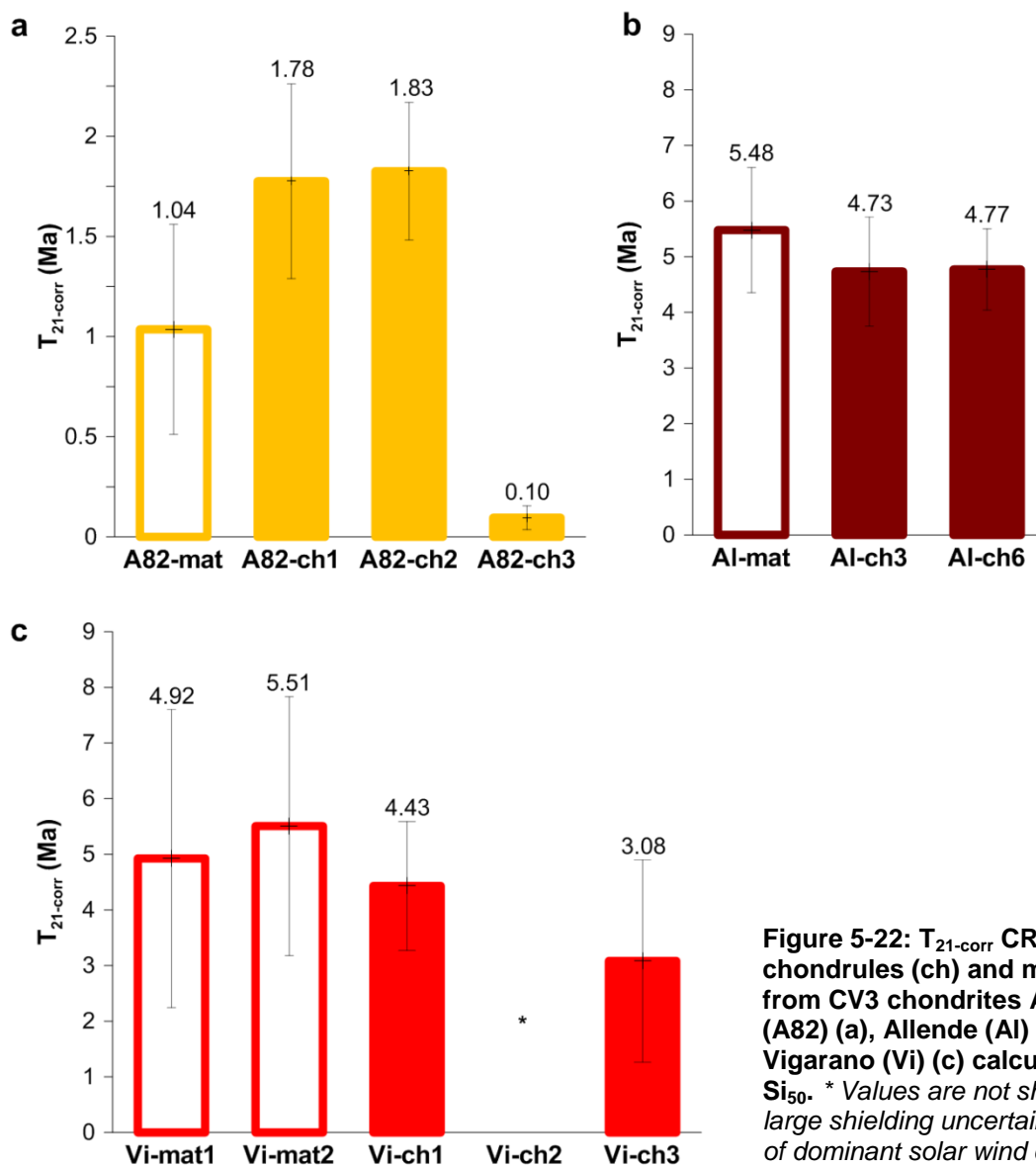


**Figure 5-22:**  $T_{21-corr}$  CRE ages of chondrules (ch) and matrix (mat) from CV3 chondrites Acfer 082 (A82) (a), Allende (Al) (b) and Vigarano (Vi) (c) calculated with  $Si_{50}$ . \* Values are not shown due to large shielding uncertainties because of dominant solar wind component.

### 5.4.1.2 Comparison with literature data

A summary of  $T_{21\text{-corr}}$  CRE ages of CR2 and CV3 chondrites analyzed in this study and in previous studies is shown in **Figure 5-23**. For CR3 chondrites MET 00426 and QUE 99177 as well as ungrouped Acfer 094 no CRE ages from previous studies are available.

$T_{21\text{-corr}}$  CRE ages of Renazzo matrix and chondrules lie in the range of previous bulk (Mazor et al. 1970) and chondrule measurements (Vogel et al. 2003) (**Figure 5-23a**). CRE ages of El Djouf 001 bulk (Bischoff et al. 1993) are identical to those of our El Djouf 001 chondrules within errors. A complete different situation is true for NWA 852: While previously analyzed bulk material has a CRE age of  $\sim 9$  Ma (Nakashima et al. 2009a), our chondrules have CRE ages of  $\sim 30$  Ma. Solar-rich grains in NWA 852 chondrules analyzed by Nakashima (2009a) show an excess of  $^{21}\text{Ne}_c$ , suggesting additional  $^{21}\text{Ne}_c$  production during cosmic-ray exposure

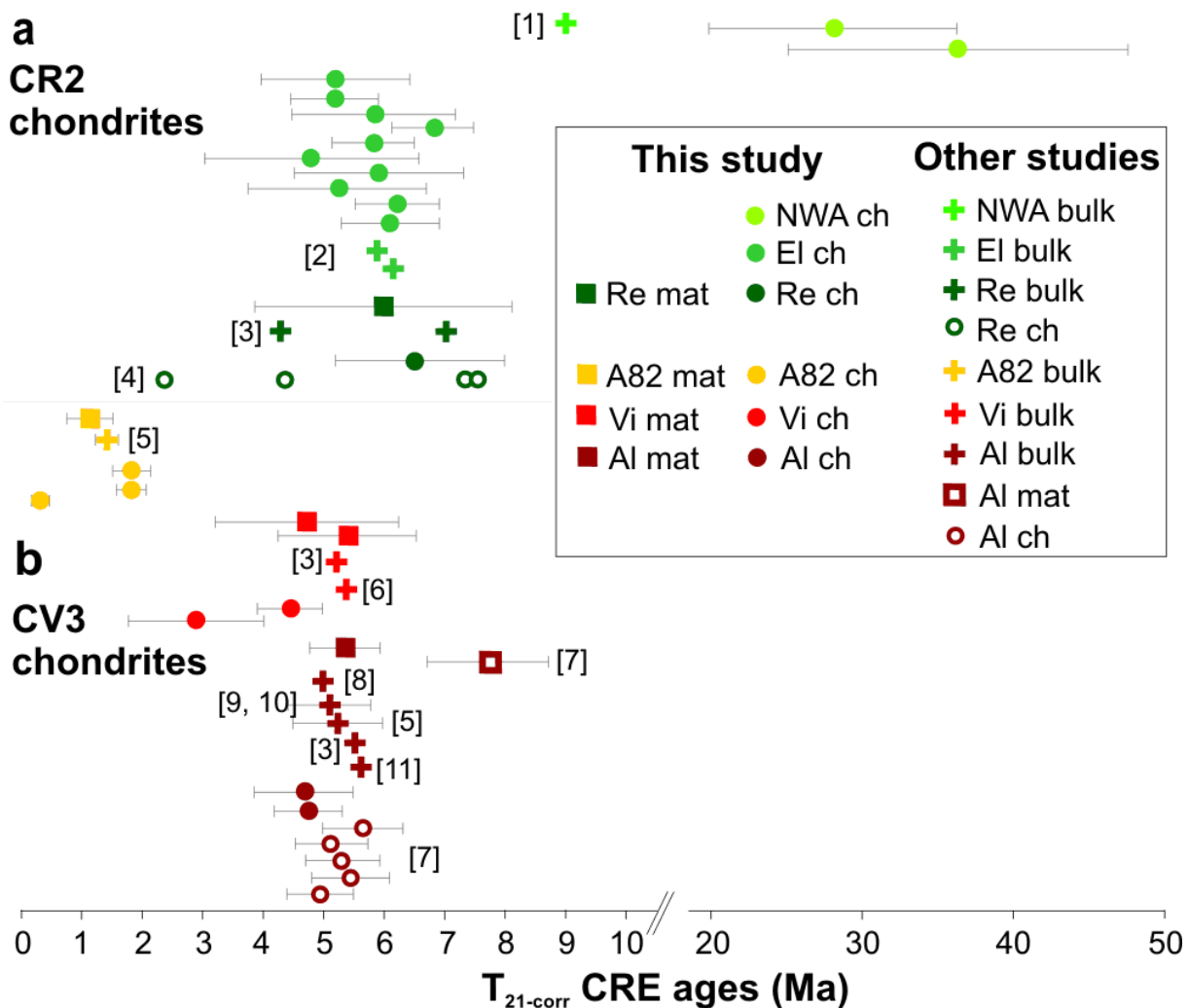


**Figure 5-23:  $T_{21\text{-corr}}$  CRE ages of CR2 chondrites (a) and CV3 chondrites (b) analyzed in this study and previous studies.**  $T_{21\text{-corr}}$  CRE ages of this study were calculated with  $Si_{50}$ . Samples with large shielding uncertainties because of dominant SW contribution or Ne-E contribution are omitted. Abbreviations: ch-chondrule, NWA-NWA 852; EI-El Djouf 001, Re-Renazzo, A82-Acfer 082; Vi-Vigarano, Al-Allende. Sources of data: 1-Nakashima et al. (2009a), 2-Bischoff et al. (1993), 3-Vogel et al. (2004), 4-Mazor et al. (1970), 5-Scherer and Schultz (2000), 6-Pepin (1969), private communication to Mazor, cited in Mazor (1970), 7-Eugster et al. (2007), 8-Hintenberger et al. (1964), 9-Scherer et al. (1997a), 10-Fireman and Goebel (1970), 11-Bogard et al. (1971).  $T_{21\text{-corr}}$  CRE ages from [3] were calculated using the formula by Eugster (1988) according to this study and the elemental composition from Ebel et al. (2008).

on the meteorite parent body. Please note that Nakashima et al. (2009a) calculated the CRE age of NWA 852 matrix using average chemical composition of CR chondrites (Weisberg et al. 1993), a production rate assuming average shielding (Weisberg et al. 1993), and interferred the amount of  $^{21}\text{Ne}_c$  produced during transit to earth as corresponding to the ordinate intercept of a plot showing  $^{21}\text{Ne}_c$  and  $^{20}\text{Ne}_{\text{solar}}$ .

CRE ages of Allende matrix agrees well with previous bulk measurements (**Figure 5-23b**). However, the CRE  $^{21}\text{Ne}$  ages of Allende matrix of Eugster et al. (2007) ( $7.7 \pm 1.0$  Ma) is somewhat higher than that of Allende matrix determined in this study ( $5.48 \pm 1.12$  Ma). CRE ages of Allende chondrules from this and previous analysis (Eugster et al. 2007) agree within errors. CRE ages of Vigarano matrix are comparable to former bulk analyses (Scherer and Schultz 2000, Mazor et al. 1970, Pepin 1969); the same is true for Acfer 082.

#### 5.4.1.3 Reliability of shielding-corrected CRE ages

Besides the comparison of CRE ages from samples analyzed in this study with CRE ages from previously analyzed samples there is an additional possibility to test the reliability of the shielding-corrected CRE ages for our samples: The **comparison of  $T_{3\text{-corr}}$  and  $T_{21\text{-corr}}$  ages**.

Most samples have  $T_{3\text{-corr}}$  and  $T_{21\text{-corr}}$  CRE ages that are identical within errors (**Figure 5-24**), which suggests there was no gas loss (see *chapter 5.4.3*).  $T_{3\text{-corr}}$  and  $T_{21\text{-corr}}$  CRE ages of samples without dominant solar wind component or Ne-E contribution (see **Table 5-14**)

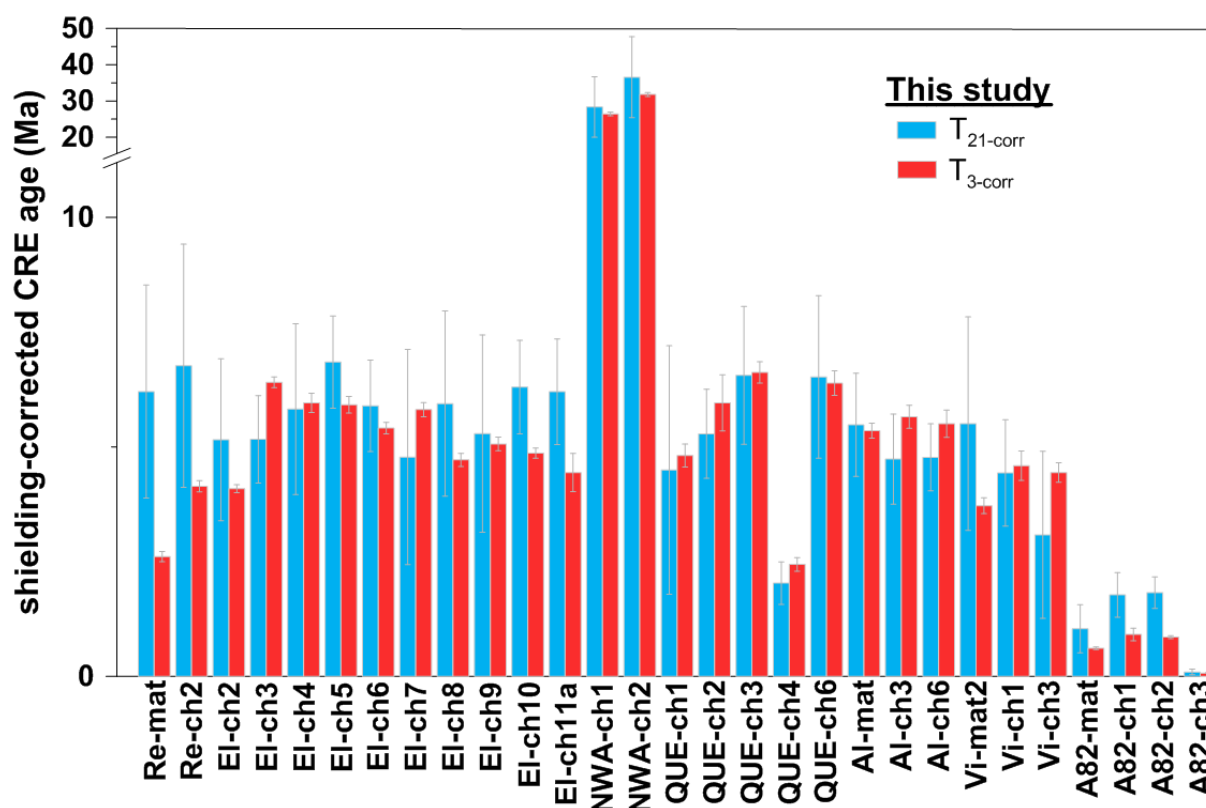


**Figure 5-24: Shielding-corrected  $T_3$  and  $T_{21}$  CRE ages of all chondrule and matrix samples.**  $P_{21\text{-corr}}$  necessary for  $T_{21\text{-corr}}$  was calculated with  $\text{Si}_{50}$ . Re-ch1 is not given due to the large uncertainties because of Ne-E contribution. EI-mat, NWA-mat, all MET samples, QUE-ch5, A94-mat, A94-ch1 and Vi-ch2 are not shown, because shielding parameter could not be determined due to a large dominant solar wind component (Ne) (see Tables 5-8 & 5-14) making the determination of the cosmogenic  $^3\text{He}$  abundance unreliable (see Table 5-9). Abbreviations: mat-matrix, ch-chondrule, Re-Renazzo, EI-EI Djouf 001, NWA-NWA 852, QUE-QUE 99177, Al-Allende, Vi-Vigarano, A82-Acfer 082.

correlate well ( $R = 0.96$ ). Higher  $T_{21\text{-corr}}$  ages of Renazzo matrix, El Djouf chondrules El-ch10 and El-ch11a, and Acfer 082 chondrules A82-ch1 and A82-ch2 may be caused by diffusive loss of cosmogenic He (see *chapter 5.4.3*), which is more easily lost than cosmogenic Ne or Ar (Polnau et al. 1999).

Based on the good agreement of  $T_{21\text{-corr}}$  with  $T_{3\text{-corr}}$  CRE ages and  $T_{21\text{-corr}}$  CRE ages of our samples with previously analyzed samples,  $T_{21\text{-corr}}$  and  $T_{3\text{-corr}}$  CRE ages of our samples seem to be reliable.

#### 5.4.2 Shielding-uncorrected (“nominal”) ages

Our chondrule and matrix samples originate from the same meteorite fragment. Therefore, both experienced identical shielding. Considering this, we use for comparison the assumption of “normal shielding” with the shielding parameter  $(^{22}\text{Ne}/^{21}\text{Ne})_c = 1.11$ . These so-called “nominal” CRE ages are not accurate, but since there are also uncertainties involved in the shielding correction, the approach is the most reliable for the *comparison* of the ages of different samples from the same location.

“Nominal”  $T_{21\text{-}1.11}$  CRE ages of chondrule and matrix samples of this study are given in **Table 5-15** and **Figures 5-25 to 5-27**.

**Table 5-15: Shielding-uncorrected  $T_{21\text{-}1.11}$  CRE ages of all matrix (mat) and chondrule (ch) samples calculated with  $\text{Si}_{50}$  abundances.**

Sample	$T_{21\text{-}1.11}$ (Ma)	Sample	$T_{21\text{-}1.11}$ (Ma)	Sample	$T_{21\text{-}1.11}$ (Ma)
<i>CR2 chondrites</i>		<i>CR3 chondrites</i>		<i>CV3 chondrites</i>	
Re-mat	3.47(37)	MET-mat	7.47(1.35)	Al-mat	6.19(41)
Re-ch1	0.751(854) <sup>a</sup>	MET-ch1	6.24(92)	Al-ch3	6.17(44)
Re-ch2	4.16(47)	MET-ch2	5.84(57)	Al-ch6	5.96(45)
El-mat	3.65(32)	MET-ch3	3.70(33)	Vi-mat1	4.76(41)
El-ch2	4.05(37)	MET-ch4	6.51(1.18)	Vi-mat2	5.32(57)
El-ch3	5.04(45)	MET-ch5	3.59(46)	Vi-ch1	6.08(92)
El-ch4	5.24(37)	MET-ch6	13.4(2.3)	Vi-ch2	5.72(59)
El-ch5	5.24(49)	QUE-mat	2.58(44)	Vi-ch3	4.77(40)
El-ch6	4.80(50)	QUE-ch1	2.83(30)	A82-mat	1.11(12)
El-ch7	5.49(50)	QUE-ch2	2.96(32)	A82-ch1	2.12(22)
El-ch8	4.53(41)	QUE-ch3	3.85(41)	A82-ch2	1.85(20)
El-ch9	5.21(48)	QUE-ch4	1.17(15)	A82-ch3	0.13(2)
El-ch10	4.71(41)	QUE-ch5	7.06(87)		
El-ch11a	4.61(55)	QUE-ch6	3.83(65)		
NWA-mat	1.10(18)	<i>Ungrouped 3 chondrite</i>			
NWA-ch1	28.2(3.4)	A94-mat	2.08(25)		
NWA-ch2	34.7(4.2)	A94-ch1	2.13(30)		

Uncertainties (1 s. d.) are given in parenthesis. <sup>a</sup>Large uncertainties because of Ne-E contribution. Abbreviations: Re-Renazzo, El-El Djouf 001, NWA-NWA 852, MET-MET 00426, QUE-QUE 99177, A94-Acfer 094, Al-Allende; Vi-Vigarano, A82-Acfer 082.

#### CR2 chondrites

All chondrules from CR2 chondrites El Djouf 001 and NWA have enhanced  $T_{21\text{-}11}$  CRE ages compared to the matrix (**Figure 5-25c**). While the age difference of El Djouf 001 chondrules relative to matrix range from 0.4 to 1.9 Ma, NWA 852 chondrules have  $T_{21\text{-}11}$  CRE ages that are 27.1 and 32.9 Ma longer than the respective matrix age (**Figure 5-25a**) strongly pointing towards a pre-irradiation.



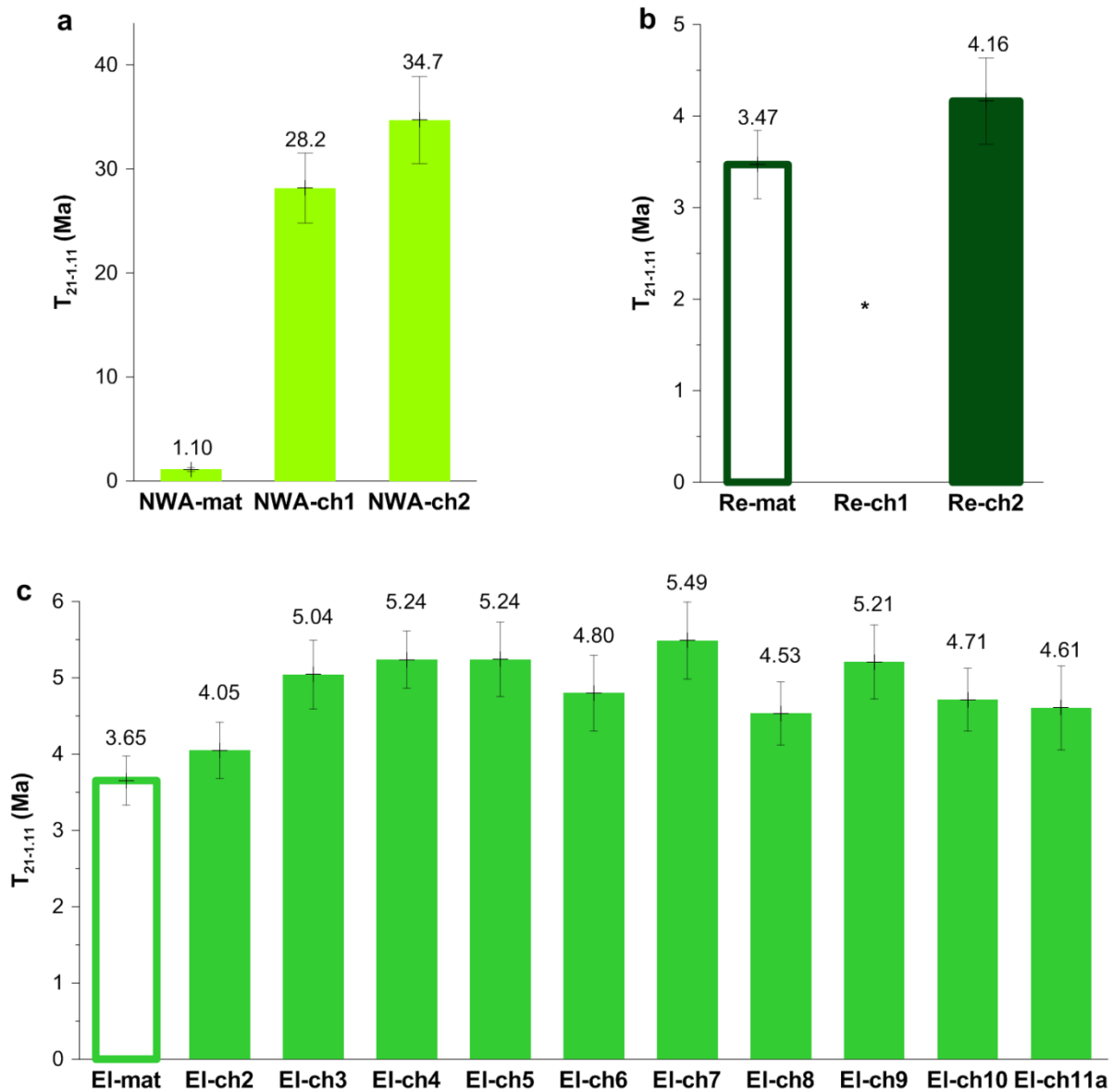
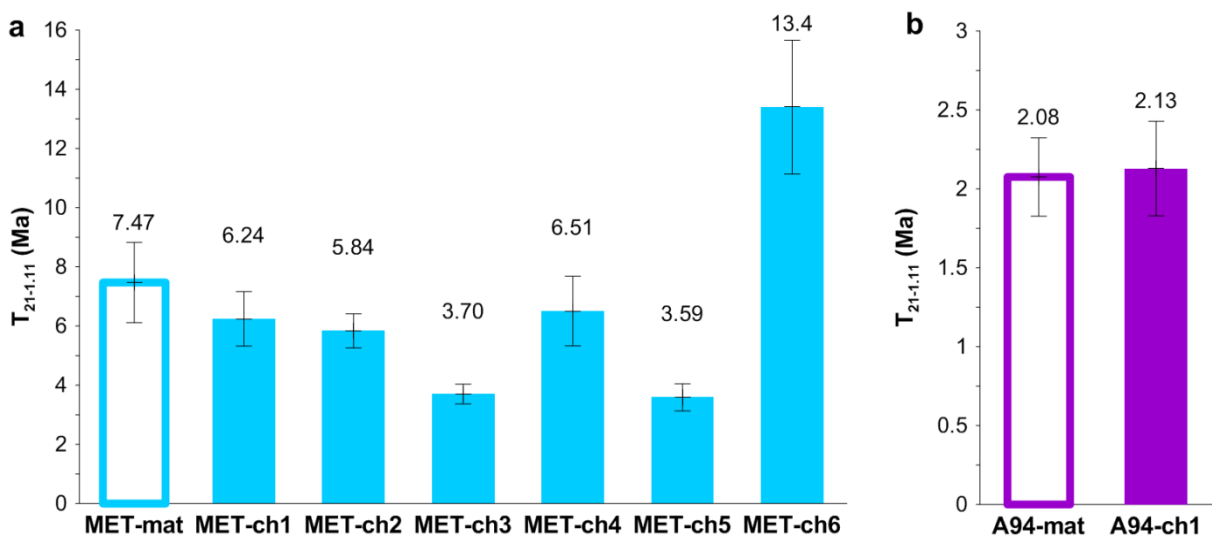
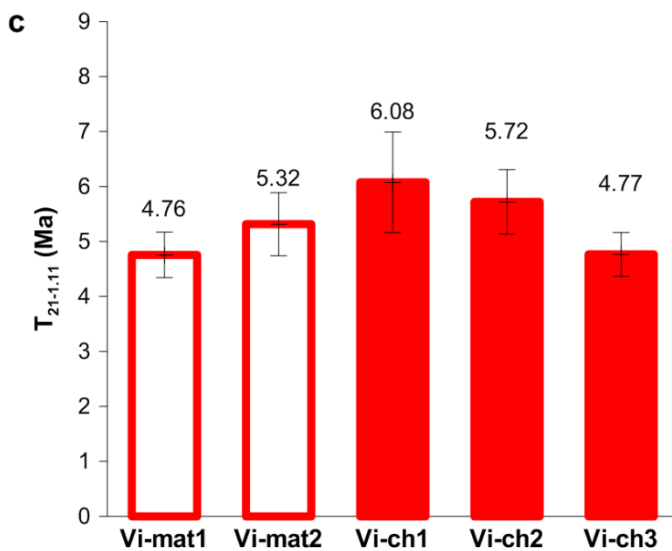
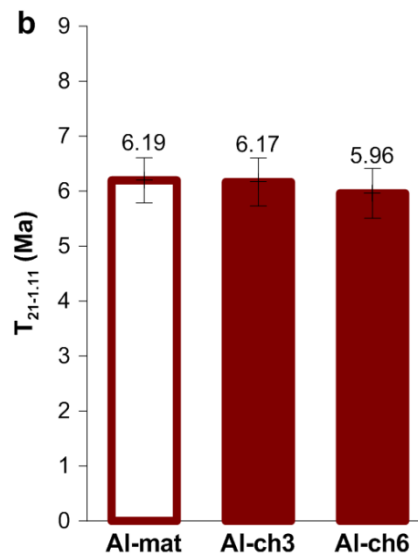
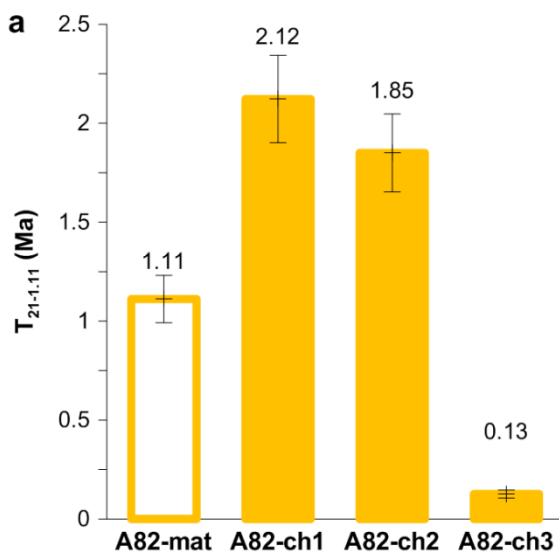
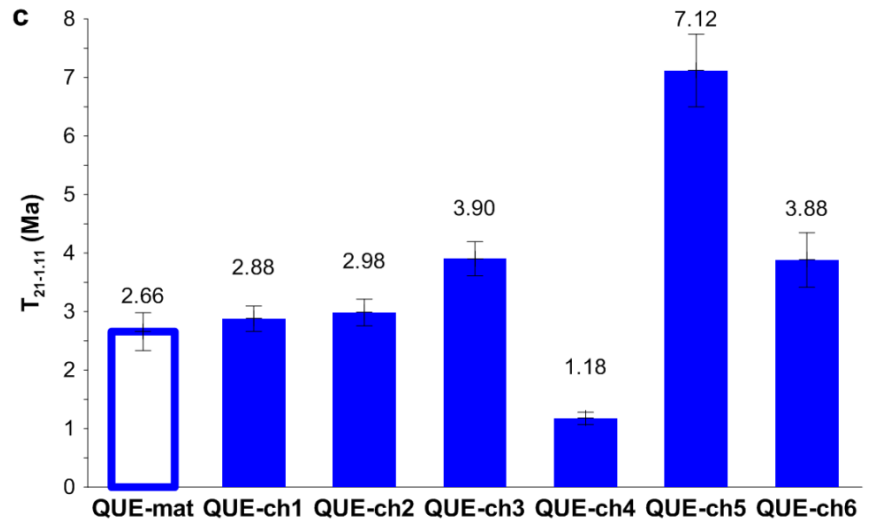


Figure 5-25:  $T_{21-1,11}$  CRE ages of chondrules (ch) and matrix (mat) from CR2 chondrites NWA 852 (NWA) (a), Renazzo (Re) (b) and El Djouf 001 (EI) (c) calculated with  $Si_{50}$ . \* Values are not shown because of Ne-E contribution.



**Figure 5-26:**  $T_{21-1.11}$  CRE ages of chondrules (ch) and matrix (mat) from CR3 chondrite MET 00426 (MET) (a), QUE 99177 (QUE) (b) and ungrouped Acfer 094 (A94) (c) calculated with  $Si_{50}$ .



**Figure 5-27:**  $T_{21-1.11}$  CRE ages of chondrules (ch) and matrix (mat) from CV3 chondrites Acfer 082 (A82) (a), Allende (Al) (b) and Vigarano (Vi) (c) calculated with  $Si_{50}$ .

$T_{21-1.11}$  CRE ages of Renazzo matrix and chondrule Re-ch2 agree within errors (**Figure 5-25b**); this is contrary to the results of Vogel et al. (2004, 2003) (see *chapter 2.4.3.1*) who found one order of magnitude higher  $^{21}\text{Ne}_c$  concentrations in Renazzo chondrules relative to the matrix, pointing strongly towards pre-irradiation effects.

### **CR3 chondrites and ungrouped Acfer 094**

For the remaining samples the situation is more complicated than in the case of El Djouf 001 and NWA 852. While three chondrules from CR3 chondrite QUE 99177 have higher  $T_{21-11}$  CRE ages compared to the matrix, the remaining three chondrules have indistinguishable or even lower ages (**Figure 5-26c**). The same is true for MET 00426; here chondrules MET-ch3 and MET-ch5 have significantly lower  $T_{21-1.11}$  CRE ages than the matrix (**Figure 5-26a**). Acfer 094 matrix and chondrule A94-ch1 are identical within errors (**Figure 5-26b**).

### **CV3 chondrites**

$T_{21-1.11}$  CRE ages of Allende (**Figure 5-27b**) and Vigarano chondrules (**Figure 5-27c**) are indistinguishable from those of the respective matrix samples. Therefore, here is no hint for pre-irradiation effect. In the case of Allende chondrules this is in agreement with previous studies by Roth et al. (2011, 2009, 2008), Eugster et al. (2007) and Vogel et al. (2004, 2003). In contrast, Acfer 082 chondrules A82-ch1 and A82-ch1 have elevated  $T_{21-1.11}$  CRE ages relative to the matrix up to 1.0 and 0.7 Ma (**Figure 5-27a**). Please note that chondrules Vi-ch2 and A82-ch3 are doubtful chondrules (see *chapter 5.3.2*).

## **5.4.3 Noble gas loss**

Gas losses from the matrix material or chondrules would lower the respective CRE ages. In general, He is more mobile and hence more sensitive to gas loss than Ne and Ar (Das et al. 2012). Furthermore, matrices are more sensitive to gas loss because of their fine-grained texture compared to the chondrules.

In order to test if sample material has suffered gas loss, there are different methods:

### **i) “Bern line”**

Meteorites that suffered  $^3\text{He}$  loss, fall in a plot showing  $(^3\text{He}/^{21}\text{Ne})_c$  versus  $(^{22}\text{Ne}/^{21}\text{Ne})_c$ , below the correlation line, the so-called “Bern line” (e.g., Das et al. 2012, Polnau et al. 2001, Nishiizumi et al. 1980, Eberhardt et al. 1965), which is defined by the equation (Nishiizumi et al. 1980)

$$\left(\frac{^3\text{He}}{^{21}\text{Ne}}\right) = 21.77 * \left(\frac{^{22}\text{Ne}}{^{21}\text{Ne}}\right) - 19.32 \quad (7)$$

As most samples plot within  $\pm 15\%$  of the “Bern line” (**Figure 5-28**), no evidence for a loss of noble gases due to diffusion (Polnau et al. 2001) is obvious. Exceptions are matrices from Renazzo and Acfer 094 and one Acfer 082 chondrule, which lie slightly below the “Bern line” indicating the possibility of some diffusive loss. Note, however, that the “Bern line” may shift somewhat depending on the chemical composition (Leya and Masarik 2009). Samples with significant concentrations of trapped He plot above the “Bern line”, and the most extreme cases (matrices from NWA 852 and El Djouf 001 and most MET 00426 chondrules) are omitted in **Figure 5-28**. Eugster (1988) proposed that low values

for  $(^3\text{He}/^{21}\text{Ne})_c$  may also be due to a complex exposure history with extremely strong shielding in a large pre-atmospheric mass, perhaps at  $2\pi$  exposure geometry.

## ii) Comparison of CRE ages derived from different noble gas isotopes

As in most primitive meteorites Ar is dominated by trapped components providing unreliable  $T_{38}$  CRE ages, the focus is here on  $T_3$  and  $T_{21}$ .

Similar CRE ages derived from  $^3\text{He}$  and  $^{21}\text{Ne}$  further suggest no or only little loss of noble gases due to diffusion. Most samples have similar  $T_{3\text{-corr}}$  and  $T_{21\text{-corr}}$  CRE ages (see **Figure 5-24**). Note that samples with high trapped solar  $^3\text{He}$  have higher apparent  $T_{3-1.11}$  CRE ages than  $T_{21-1.11}$  CRE ages.

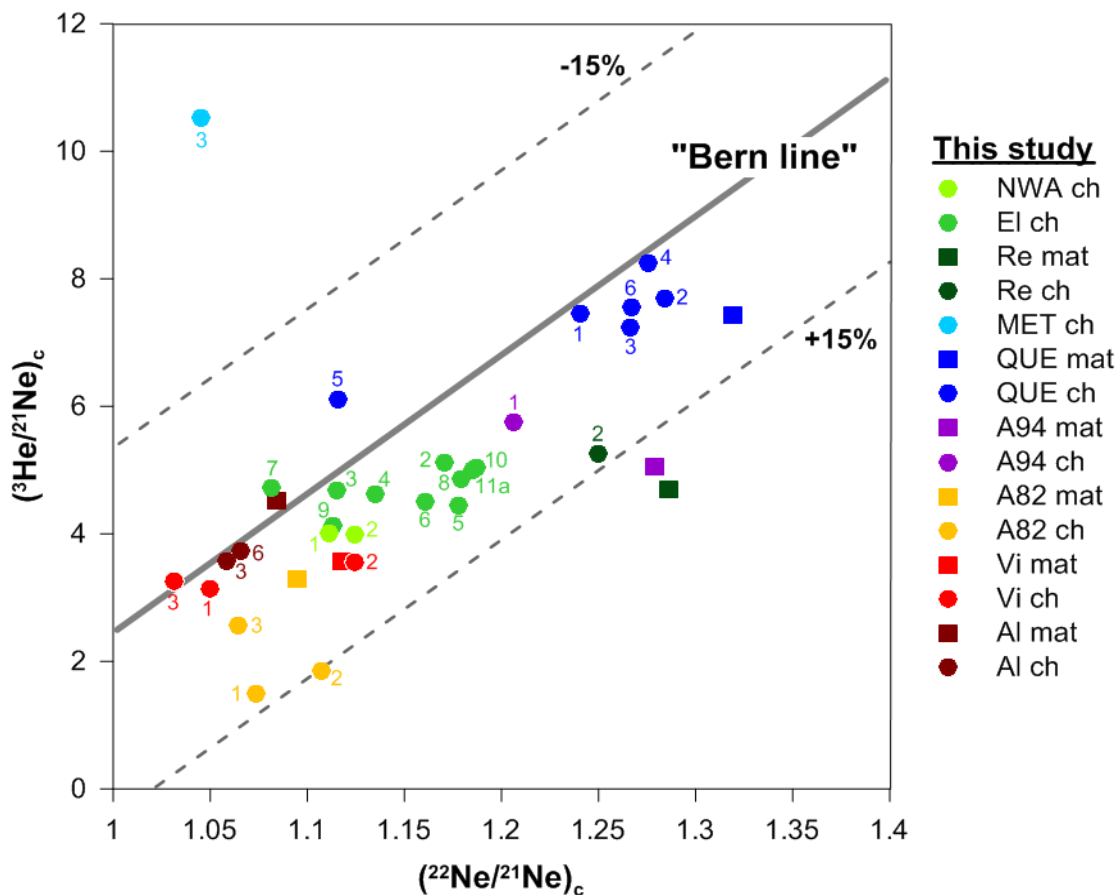


**Figure 5-28: Plot showing  $(^3\text{He}/^{21}\text{Ne})_c$  versus  $(^{22}\text{Ne}/^{21}\text{Ne})_c$  for all chondrule (ch) and matrix (mat) samples. The "Bern line" is defined as follows:  $(^3\text{He}/^{21}\text{Ne})_c = 21.77 \times (^{22}\text{Ne}/^{21}\text{Ne})_c - 19.32$  (Nishiizumi et al. 1980, Eberhardt et al. 1965). Samples with squares more than 15% are suspect because of gas loss and uncertainties in the Ne measurement and did not provide reliable CRE ages. Samples with extreme high trapped solar  $^3\text{He}$  (NWA-mat, El-mat, MET-mat, most MET 00426 chondrules) are not shown. Abbreviations: NWA-NWA 852, El-El Djouf 001, Re-Renazzo, MET-MET 00426, QUE-QUE 99177, A94-Acfer 094, A82-Acfer 082, Vi-Vigarano, Al-Allende.**

## 5.5 $^{40}\text{K}$ - $^{40}\text{Ar}$ ages of chondrules and matrix

$^{40}\text{Ar}$ - $^{40}\text{K}$  ages of chondrules and matrix samples are given in **Table 5-16**. Many samples have K abundances below the detection limit of INAA, and the listed ages were calculated using  $1/2$  of the detection limit. These  $^{40}\text{Ar}$ - $^{40}\text{K}$  ages are not reliable and are thus not considered in the following.

Only Allende matrix and chondrule Al-ch6 have  $^{40}\text{K}$ - $^{40}\text{Ar}$  ages  $\sim 4.6$  Ga, which may represent the formation of the meteorite parent body (e.g., Bogard 2011). For the other samples, ages are lower, which indicates that they were affected by thermal events, which caused loss of  $^{40}\text{Ar}$  from the crystal structure of minerals (McSween and Huss 2010) having a low retentivity like feldspars (e.g., Hopp et al. 2014). In contrast, in Allende samples Ar is contained in more retentive phases like pyroxene or plagioclase (e.g., Ivanova et al. 2008). A fine-grained K carrier phase like micrometer-sized phyllosilicates facilitates disturbances by  $^{40}\text{Ar}$  loss due to later reheating processes (Ivanova et al. 2008).

A possible loss of  $^{40}\text{Ar}$  may indicate that  $^{21}\text{Ne}_c$  was lost as well. However, significant loss of  $^{21}\text{Ne}_c$  can be excluded based on the following considerations:

- i) Higher retentivity of  $^{21}\text{Ne}_c$  due to higher retention temperatures of  $^{21}\text{Ne}_c$  carrier phases (olivine, pyroxene) relative to  $^{40}\text{Ar}$  carrier phases (feldspar) (Hopp et al. 2014),
- ii) All chondrules show no evidence for a loss of He (see chapter 5.4.3), which is more easily lost than cosmogenic  $^{21}\text{Ne}$  (Polnau et al. 1999).

Different  $^{40}\text{Ar}$ - $^{40}\text{K}$  ages in a single meteorite as in the case of El Djouf 001 may suggest that the samples were affected to different degrees by metamorphism or impact events due to mixing processes on the meteorite parent body regolith.

Furthermore, lower  $^{40}\text{Ar}$ - $^{40}\text{K}$  ages of El Djouf 001 and QUE 99177 matrices may suggest that chondritic matrix experienced higher temperatures compared to the chondrules even at low shock pressures (S1) as suggested by Bland et al. (2012).

**Table 5-16:  $^{40}\text{K}$ - $^{40}\text{Ar}$  ages of all matrix (mat) and chondrule (ch) samples.**

Sample	$T_{40}$ (Ma)	Sample	$T_{40}$ (Ma)	Sample	$T_{40}$ (Ma)
<i>CR2 chondrites</i>		<i>CR3 chondrites</i>		<i>CV3 chondrites</i>	
Re-mat	721.0(119.3)	MET-mat	927.4(150.9)	Al-mat	4864(279)
Re-ch1	109.3(1078)	MET-ch1	<sup>a</sup>	Al-ch3	1025(89)
Re-ch2	662.9(121.8)	MET-ch2	350.5(64.3)	Al-ch6	4755(198)
El-mat	559.2(34.1)	MET-ch3	3372(314)	Vi-mat1	1175(178)
El-ch2	1692(293)	MET-ch4	334.6(63.7)	Vi-mat2	249.6(53.0)
El-ch3	1300(88)	MET-ch5	191.1(39.2)	Vi-ch1	1813(365)
El-ch4	nd	MET-ch6	516.6(93.3)	Vi-ch2	1966(208)
El-ch5	275.9(54.5)	QUE-mat	298.0(56.6)	Vi-ch3	4954(338)
El-ch6	3345(129)	QUE-ch1	1740(271)	A82-mat	123.1(23.9)
El-ch7	282.9(58.6)	QUE-ch2	3382(108)	A82-ch1	2691(339)
El-ch8	339.7(66.8)	QUE-ch3	1283(185)	A82-ch2	1821(139)
El-ch9	3318(186)	QUE-ch4	961.0(155.9)	A82-ch3	256.7(48.4)
El-ch10	1009(123)	QUE-ch5	84.37(18.33)		
El-ch11a	1247(183)	QUE-ch6	577.8(102.7)		
NWA-mat	575.8(101.6)	<i>Ungrouped 3 chondrite</i>			
NWA-ch1	159.7(45.0)	A94-mat	208.0(39.5)		
NWA-ch2	2301(262)	A94-ch1	246.8(52.4)		

Uncertainties (1 s. d.) are given in parenthesis. <sup>a</sup>Large uncertainties because no K has been determined in this metal chondrule mainly composed of Fe and Ni. Where values are marked in gray, K concentrations were below the detection limit; the listed values were calculated using 1/2 the detection limit. Abbreviations: Re-Renazzo, El-El Djouf 001, NWA-NWA 852, MET-MET 00426, QUE-QUE 99177, A94-Acfer 094, Al-Allende; Vi-Vigarano, A82-Acfer 082.

## 5.6 Pre-irradiation of chondrules

### 5.6.1 Samples with potentially pre-irradiated chondrules

Chondrules analyzed in this study tracing potentially pre-irradiation effects are shown in **Figure 5-29** (see **Table 5-15**). Since for Renazzo and Acfer 094 only a small number of chondrules were analyzed which show  $T_{21-1.11}$  CRE ages indistinguishable from the corresponding matrix, no reliable conclusion concerning pre-irradiation effects can be reached. Therefore, these meteorites are not discussed further.

Allende and Vigarano chondrules have  $T_{21-1.11}$  CRE ages indistinguishable from the matrix (**Figure 5-29c**). Therefore, **no pre-irradiation effects** could be found. In the case of Allende this is in accordance with Roth et al. (2011, 2009, 2008), Eugster et al. (2007) and Vogel et al. (2004, 2003).

In contrast, NWA 852 and El Djouf 001 chondrules show **strong evidence** for pre-irradiation because all chondrules have elevated  $T_{21-1.11}$  CRE ages relative to the matrix (**Figure 5-29a**). Some chondrules from QUE 99177, MET 00426 (**Figure 5-29b**) and Acfer 082 show **apparent pre-irradiation** effects. However, since the MET 00426 matrix has an elevated  $T_{21-1.11}$  CRE age compared to two chondrules (MET-ch3 & MET-ch5), both MET 00426 matrix

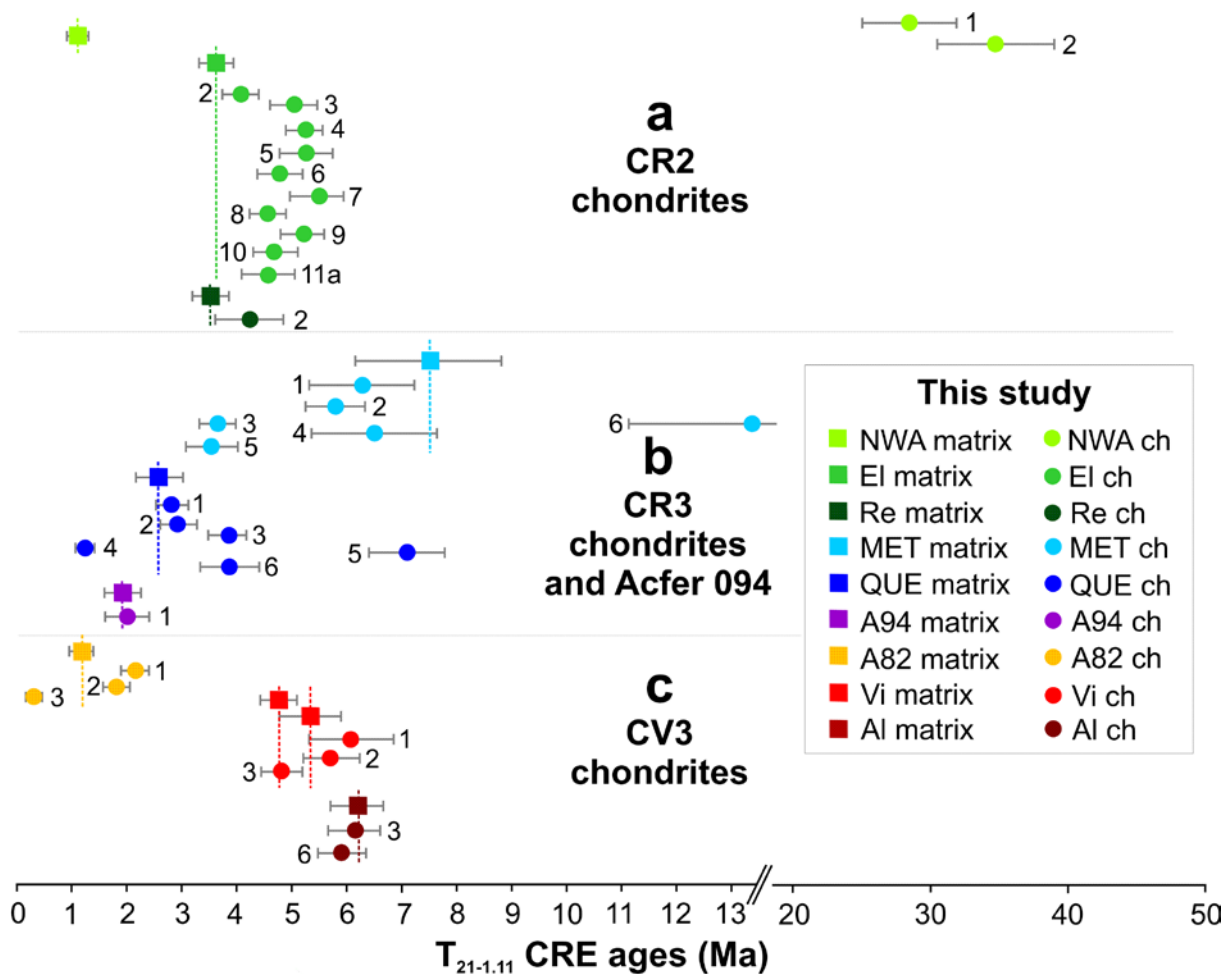


**Figure 5-29:**  $T_{21-1.11}$  CRE ages of chondrules from CR2 chondrites (a), CR3 chondrites (b), and CV3 chondrites (c).  $T_{21-1.11}$  CRE ages of this study were calculated with  $Si_{50}$ . Re-ch1 is omitted due to the large uncertainty because of Ne-E contribution. Abbreviations: ch-chondrule, NWA-NWA 852, El-El Djouf 001, Re-Renazzo, MET-MET 00426 QUE-QUE 99177, A94-Acfer 094, A82-Acfer 082, Vi-Vigarano, Al-Allende.

and chondrule MET-ch6 appear to have been pre-irradiated. The same is true for QUE 99177 matrix, which has an elevated  $T_{21-1.11}$  CRE age compared to chondrule QUE 99177 QUE-ch4. Alternative explanations are the loss of evidence for pre-irradiation from MET 00426 chondrules having lower  $T_{21-1.11}$  CRE ages or that these chondrules resided in other regions of the early solar nebula or the regolith, where they were shielded from cosmic radiation. The **indication for pre-irradiation of matrix material** is an important new finding of this work in terms of analyzing pre-irradiation effects in primitive meteorites.

### ***Duration of pre-irradiation***

The chondrules showing pre-irradiation effects from this study were not analyzed in previous studies concerning pre-irradiation effects. Hence, a comparison is not feasible. However, in the following results of this study and previous studies were compared in terms of the duration of pre-irradiation and the percentage of pre-irradiated chondrules, which may help in deducing the setting of pre-irradiation, especially differences in regolith processes.

NWA 852 chondrules were pre-irradiated over ~27 and ~33 Ma (**Figure 5-30a**), which is comparable with the values of Murchison (CM2) chondrules (~30 Ma by Roth et al. 2011, ~25 Ma by Huber et al. 2012). However, only 20% of Murchison chondrules showed pre-irradiation effects (Roth et al. 2011). In the contrary, both of our analyzed NWA 852 chondrules are pre-irradiated.

The pre-exposure of El Djouf chondrules El-ch2 (0.4 Ma) and El-ch8 (0.9 Ma) and Acfer 082 chondrule A82-ch2 (0.7 Ma) (see **Figure 5-30a, b**) is comparable to the Murray (CM2) chondrule, which may have experienced a pre-exposure of ~0.6 Ma (Das and Murty 2009). Since all El Djouf chondrules show pre-exposure effects of a similar time span, the assumption of a pre-irradiation of chondrules seems to be reasonable.

Vogel et al. (2003, 2004) analyzed among other carbonaceous chondrites five chondrule and matrix samples from Renazzo and found one order of magnitude higher  $^{21}\text{Ne}_c$  abundances in the chondrules (see *chapter 2.4.3.1*). Based on the noble gas data from Vogel et al. (2003, 2004) and using the abundances of target elements for the chondrules from Ebel et al. (2008) (average of five chondrules) and for the matrix from this study, the  $T_{21}$  CRE ages for their samples were calculated using the formula by Eugster (1988) with “normal” shielding (i.e.  $(^{22}\text{Ne}/^{21}\text{Ne})_c = 1.11$ ). This method may not yield exact CRE ages rather than a close estimation. Huber et al. (2012) took a similar approach as they used the elemental composition of analyzed Murchison chondrules derived by Roth et al. (2011). All five Renazzo chondrules analyzed by Vogel et al. (2004) have elevated  $T_{21-1.11}$  CRE ages relative to the matrix (Vogel et al. 2003) in the range of 1.5 to 4.5 Ma ( $T_{21-1.11}$  CRE ages of Renazzo chondrules analyzed by Vogel et al. (2004): 5.6, 2.5, 4.6 and 4.4 Ma). That all Renazzo chondrules show pre-irradiation effects agrees with the findings for CR2 chondrites from this study.

The pre-exposure of CR3 chondrules lies in the range of El Djouf 001 (CR2) chondrules or between El Djouf 001 and NWA 852 chondrules (see **Figure 5-30a**). Concerning the percentage of pre-irradiated chondrules CV3 chondrite Acfer 082 and CR3 chondrites MET 00426 and QUE 99177 have considerable lower values (67, 17, and 50%, see **Figure 5-30c**) than chondrules from CR2 chondrites. However, a pre-irradiation of these chondrules seems to be possible because the percentage of pre-irradiated chondrules is relative to the respective matrix, which seems also to be pre-irradiated.

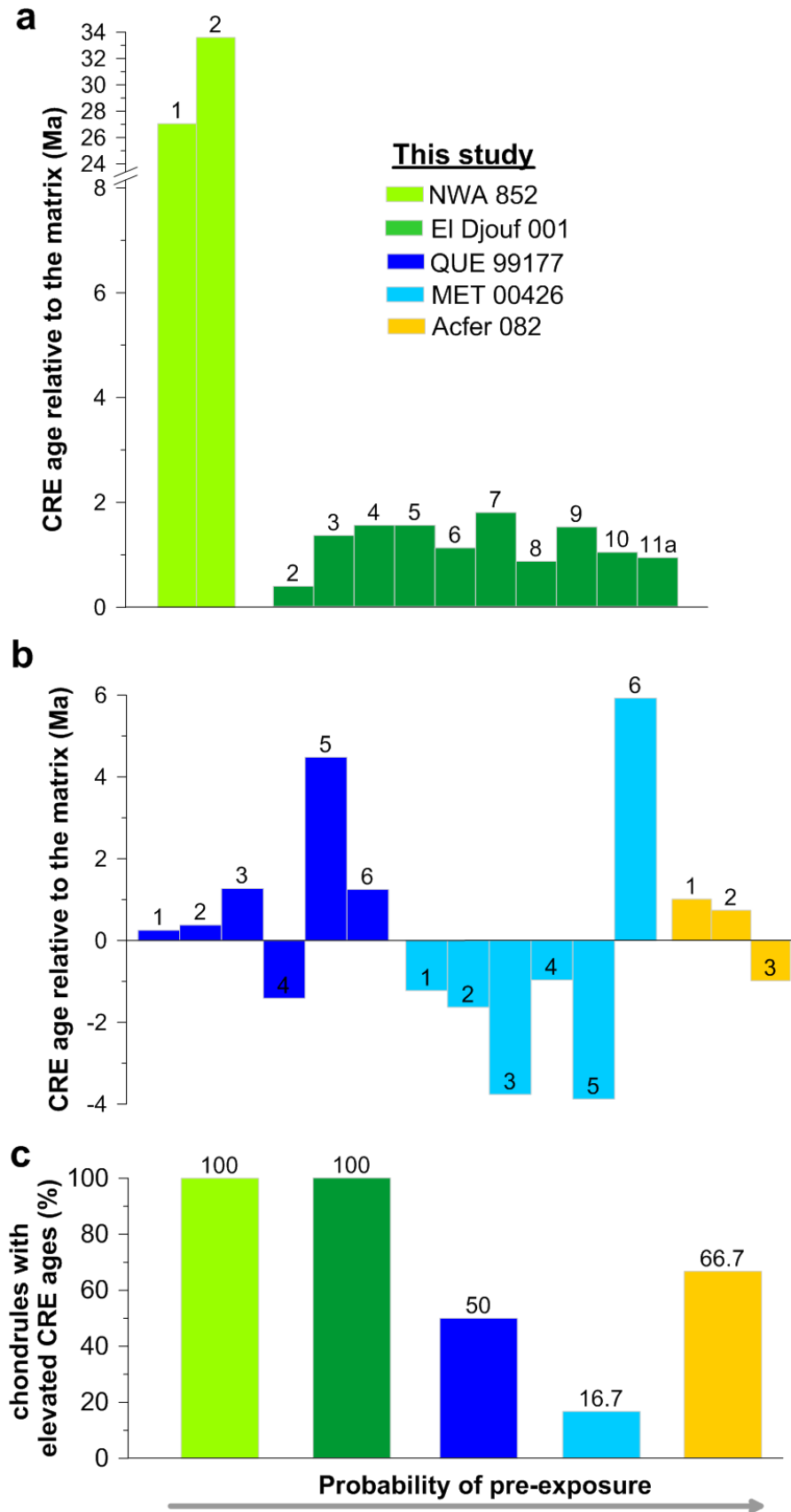


Figure 5-30: CRE ages of chondrules relative the respective matrix (a, b) and percentage (c) of pre-irradiated chondrules from this study based on  $T_{21-1.11}$  CRE ages calculated with  $Si_{50}$  abundances.  $T_{21-1.11}$  CRE ages were calculated using the formula by Eugster (1988) and “normal shielding” with shielding parameter  $(^{22}Ne/^{21}Ne)_c = 1.11$ . Chondrules are labeled with numbers. The probability of pre-exposure of chondrules is underestimated because the matrix also seems to be pre-irradiated, especially in the case of CR3 chondrites (see text).



### Is there a relationship between pre-irradiation of chondrules and chondrule type?

An analysis of possible relationships between pre-irradiation and chondrule types is challenging because of the limited number of pre-irradiated chondrules and because the classification of chondrules is only tentative (see chapter 5.1.1: Possible chondrule types).

In **Table 5-17** and **Figure 5-31** the pre-exposure and type of all chondrules analyzed in this study tracing pre-irradiation effects are given. Only the NWA 852 chondrules and El Djouf 001 chondrule El-ch2 are classified as type I(II)A, IIA or I(II)B, having considerable higher (in case of NWA 852 chondrules) or lower (in case of El-ch2) pre-exposure compared to the remaining chondrules. For the other El Djouf 001 chondrules there may be three peaks: For type IB ~1 Ma (El-ch6, 8, 10 & 11a) and ~1.7 Ma (El-ch7 & 9) and for type IAB ~1.6 Ma. Chondrules from CR3 chondrites belong to type IB, but their pre-exposure scatters between 1.2 and 6.9 Ma. In contrast, the pre-exposure of the two Acfer 082 (CV3) chondrules is similar although they belong to different chondrule types.

If the pre-irradiation happened in the solar nebula, the different pre-exposure of type I vs. type II chondrules may point toward a spatially limited (repetitive?) chondrule formation processes under diverse conditions (see chapter 2.2.3.5). In this scenario a later mixture of both chondrule types and different exposure histories of chondrules in a nebula setting seems reasonable.

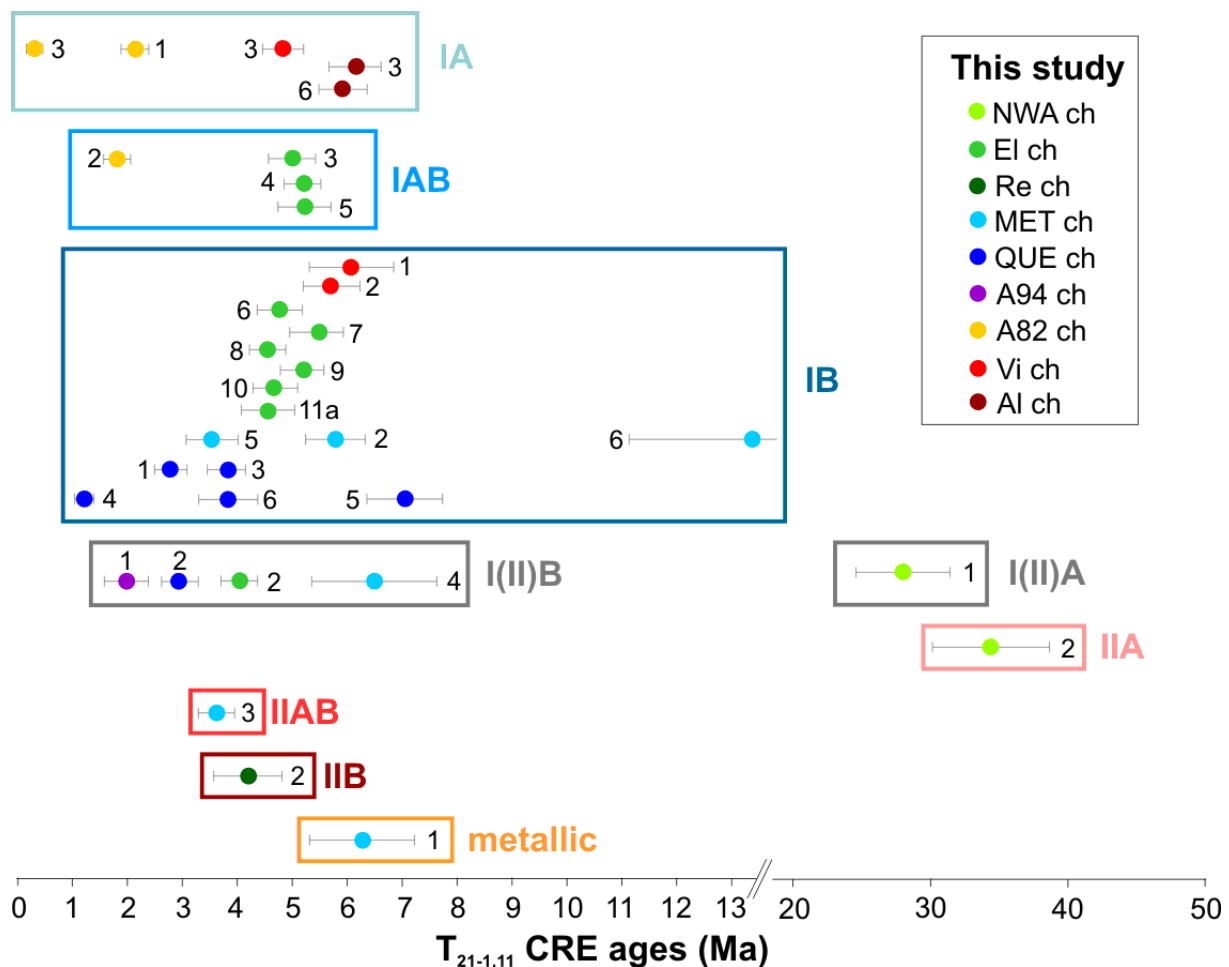


**Figure 5-31:**  $T_{21-1.11}$  CRE ages of all analyzed chondrules arranged according to their chondrule type.  $T_{21-1.11}$  CRE ages of this study were calculated with  $Si_{50}$ . Abbreviations: ch-chondrule, NWA-NWA 852, El-El Djouf 001, Re-Renazzo, MET-MET 00426, QUE-QUE 99177, A94-Acfer 094, A82-Acfer 082, Vi-Vigarano, Al-Allende.

**Table 5-17: Pre-exposure and type of chondrules analyzed in this study and tracing pre-irradiation effects.**

Sample	Pre-exposure (Ma)	Chondrule type	Sample	Pre-exposure (Ma)	Chondrule type
<b>CR2 chondrites</b>			<b>CR3 chondrites</b>		
NWA-ch1	26.6	I(II)A	MET-ch6	6.9	
NWA-ch2	32.9	IIA	QUE-ch3	1.2	IB
El-ch2	0.4	I(II)B	QUE-ch5	4.5	
El-ch3	1.4		QUE-ch6	1.2	
El-ch4	1.6	IAB	<b>CV3 chondrites</b>		
El-ch5	1.6		A82-ch1	1.0	IA
El-ch6	1.1		A82-ch2	0.7	IAB
El-ch7	1.8				
El-ch8	0.9	IB			
El-ch9	1.6				
El-ch10	1.1				
El-ch11a	1.0				

*Pre-exposure is defined as the difference of  $T_{21-1.11}$  CRE ages between chondrule and the respective matrix.  $T_{21-1.11}$  CRE ages were calculated using the formula by Eugster (1988), “normal shielding” with shielding parameter  $(^{22}\text{Ne}/^{21}\text{Ne})_c = 1.11$  and  $\text{Si}_{50}$  abundances. Given chondrule types are tentative (see chapter 5.1.1: Possible chondrule types).*

## 5.6.2 Difficulties concerning the interpretation of pre-irradiation effects, arguments for a pre-irradiation of chondrules and this study’s limitation

### 5.6.2.1 Difficulties concerning the interpretation of pre-irradiation effects in chondrules

The difficulties why a pre-irradiation of chondrules (as a whole) might be difficult to discern are mostly connected with the assignment of pre-irradiation effects as previously described (see chapter 2.4.3.2):

#### i) In the case of meteorites with long CRE ages possible pre-irradiation effects cannot be discerned (e.g., Roth et al. 2011, Polnau et al. 1999).

For this reason meteorites with CRE ages of maximum 6 Ma were selected only (see chapter 4.1.1). For CR3 chondrites MET 00426 and QUE 99177 as well as ungrouped Acfer 094 no previous noble gas data were available.  $T_{21\text{-corr}}$  CRE ages of QUE 99177 chondrules (see **Table 5-14**) show a maximum of 6.6 Ma for QUE-ch3. In the case of all other samples from CR3 chondrites and Acfer 094  $T_{21\text{-corr}}$  CRE ages are too uncertain, since the shielding parameter could not be determined because of large dominant trapped component.

#### ii) Production rates depend on chemistry and shielding.

The production rate depends on the chemical composition and shielding of the sample (see chapter 2.3.2). Noble gas measurements and INAA analysis for the determination of target element abundances were generally performed on the same sample material (see chapter 4.6). Therefore, an aliquot problem is avoided and the elemental abundances of target elements of each chondrule and matrix sample are known, necessary for the calculation of production rate.

There is also an influence of overall chemical composition on the production rate of Ne (see **Figure 5-19**, chapter 5.3.3). However, for stony meteorites this matrix effect is assumed to be <10% (Wieler 2002b).

To test the reliability of the formula by Eugster (1988), which was used in this study for the calculation of the production rates, the results of this formula were compared to the results obtained using the equation of Eugster and Michel (1995) as well as the approach of Leya and Masarik (2009) (see chapter 5.3.3). Production rates for neon calculated with the formula by Eugster (1988) are in good agreement with both the formula by Eugster and Michel (1995) and the model by Leya and Masarik (2009) (see **Table 5-12 & 5-13**). Therefore, the use of the formula by Eugster (1988) is justified for the comparison.

Since our chondrule and matrix samples originate from the same meteorite fragment, both experienced identical shielding (see chapter 5.4.2). For the comparison of CRE ages in this study “nominal” CRE ages were used with shielding parameter  $(^{22}\text{Ne}/^{21}\text{Ne})_c = 1.11$ . This approach using “nominal” CRE ages is most reliable for the comparison of CRE ages of different samples originating from a small sample volume (Roth et al. 2011).

### iii) Preferential recoil losses from the matrix may cause lower CRE ages of the matrix samples.

The fine-grained texture of matrix material (between 10 nm and 5  $\mu\text{m}$ , Scott 2007) causes a susceptibility for recoil losses, which are indicated to be in the range of 2-3  $\mu\text{m}$  in presolar SiC grains for Ne (Ott and Begemann 2000) and ~50  $\mu\text{m}$  for He (Ott et al. 2009, Ziegler 2004). Hence, grains smaller than a few microns can suffer substantial recoil losses (Trappitsch and Leya 2013).

On the other hand, if a matrix grain in a granular medium (like on the meteorite parent body regolith) would be affected by recoil loss, the lost cosmogenic noble gas nuclide will be reimplanted into neighboring grains (e.g., Ott and Begemann 2000). A recoil loss of our samples can be excluded because  $T_{3\text{-corr}}$  and  $T_{21\text{-corr}}$  CRE ages agree well (see chapter 5.4.3).

### iv) Possible gas loss from the bulk meteorite/matrix due to thermal metamorphism

Possible gas loss from the bulk meteorite/matrix due to thermal metamorphism was restricted by the selection of meteorites with petrological type 2 to 3 (see chapter 4.1.1). Furthermore, a possible gas loss due to diffusion was tested using the Bern line and the comparison of  $T_{3\text{-corr}}$  and  $T_{21\text{-corr}}$  CRE ages of all chondrule samples (see chapter 5.4.3). It was demonstrated that the matrices from pre-exposed chondrules were not affected by gas loss, because they either plot far above the “Bern line” in case of high trapped  $^3\text{He}$  (matrices from El Djouf 001, NWA 852 and MET 00426) or within  $\pm 15\%$  of the “Bern line” (matrices from QUE 99177 and Acfer 082) (see **Figure 5-28**). This conclusion is confirmed by the comparison of  $T_{3-1.11}$  and  $T_{21-1.11}$  CRE ages (see **Figure 5-24**).

Concerning the retentivity of the matrix for cosmogenic noble gases, Polnau et al. (1999) concluded that only minor differences between chondrule and matrix CRE ages can be assigned to lower Ne and Ar retentivity of the matrix. This conclusion is based on the comparison of  $T_3$ ,  $T_{21}$ ,  $T_{38}$  and  $T_{81}$  CRE ages in chondrites with losses of radiogenic (r) gases. Data from Laochenzen (H5), Nantong (H6), and Lishui (L5) (Eugster et al. 1993) show that cosmogenic  $^{21}\text{Ne}$  and  $^{38}\text{Ar}$  are not or only slightly depleted in meteorites with significant  $^3\text{He}_c$ ,  $^4\text{He}_r$ , and  $^{40}\text{Ar}_r$  loss. Furthermore, the systematic observed in a large

number of chondrites show that  $T_{21}$  and  $T_{38}$  give reliable CRE ages (Marti and Graf 1992, Polnau et al. 1999).

Furthermore, when shocked, chondritic matrix experienced much higher temperatures compared to the chondrules, even when the shock pressure was low (shock stage S1) (Bland et al. 2012).

The difficulties why a pre-irradiation of chondrules might not be expected are as follows (see *chapter 2.4.3.2*):

**i) A pre-irradiation of chondrules in the early solar system has been considered as not possible due to high dust densities.**

A pre-irradiation of chondrules in the early solar system requires low dust densities, because at high dust/gas ratios (present especially in the midplane) the chondrules would have shielded from cosmic rays. In this case, chondrules could be exposed to cosmic rays only at the surface of the protoplanetary disk. This scenario is consistent with the formation of chondrules from individual chondrite groups in different regions of the protoplanetary disk and subsequent transport to the accretion regions (e.g., Connelly et al. 2012), or the formation of chondrules close to the sun and redistribution throughout the solar system (X-wind model by Shu et al. 2001, 1997, 1996, solar nebula jet flows by Liffman 2005). In the outer edges of the protoplanetary disk an irradiation of chondrules might be possible due to lower dust/gas ratios. A redistribution of chondrules possibly above the solar accretion disk allows the irradiation of chondrules even if they were formed in regions with high dust densities in the midplane of the protoplanetary disk (e.g., Cuzzi and Alexander 2006, Wasson 1993) (*see chapter 2.2.3.6*).

This scenario of a possible irradiation of chondrules at lower dust densities at the outer edges of the protoplanetary disk is supported by studies concluding that chondrules spent some time free-floating in the protoplanetary nebula (e.g., Cuzzi 2011) and that chondrite formation cannot have immediately followed chondrule formation (e.g., Alexander et al. 2008).

**ii) The lifetime of small objects in the inner solar system is limited due to drift into the sun.**

In the absence of turbulence mm-sized chondrules and cm-sized CAIs take  $10^5$  and  $10^4$  years to migrate 1 AU (Weidenschilling 1977). However, Scott (2007) reported that chondrules and CAIs can be transported from the inner edges to the periphery of the protoplanetary disk by disk winds (Liffman 2005, Shu et al. 2001, 1997, 1996) or outward radial diffusion in a weakly turbulent nebula may counteract inward drift owing to gas drag (Scott 2007 and references therein).

Additionally, after sinking to the midplane of the protoplanetary disk, probably as dense, km-sized concentrations acting as aerodynamically units (Hewins 1997 and references therein, *see chapter 2.2.3.6*), chondrules might be incorporated into planetesimals and be preserved (Weidenschilling 1977). The formation of km-sized to embryo-sized objects only takes  $\sim 10^5$  to  $10^6$  years in the asteroid belt (Alexander et al. 2001), which is of the same order as the lifetime of objects with diameters between  $\sim 0.1$  and  $\sim 1$  mm (Weidenschilling 1977), i.e. typical chondrule sizes.

Furthermore, Scott (2007) concluded based on the median lifetime of 3 Ma for protostellar disks and despite the uncertain degree of turbulence in disks that other disks beside the solar nebula were sufficiently turbulent to have preserved small particles for several million years (Natta et al. 2006, Haisch et al. 2001).

**iii) A pre-irradiation of chondrules on parent body surfaces (regolith) is not possible.**

A regolith is defined as layer or mantle of loose, incoherent, rocky material of whatever origin that nearly everywhere forms the surface of the land and the rest on coherent bedrock (Housen and Wilkening 1982 and references therein). It is composed of granular materials that can range in size from a few microns (dust) or a few hundreds of microns (sand) to a few centimeters or meters (gravels, pebbles, boulders) (Murdoch et al. 2013).

Based on calculations, which depend on target strength and ejecta velocities, it has been assumed that due to their low gravity asteroids were not able to retain the regolith, especially for asteroids with 10 km size and smaller (e.g., Housen et al. 1979). In contrast, Langevin and Maurette (1980) estimated regolith thickness theoretically and proposed that weak asteroid-sized bodies were capable of retaining only little ejecta (<100 m), while strong bodies larger than 50 km would have regoliths of 100-900 m depending on asteroid size. Later, Housen et al. (1992) and Asphough and Nolan (1992) concluded, using semi-theoretical models, that even asteroids in the 10 km size range and low target strength are capable of retaining substantial regoliths.

That the *surfaces of small bodies like asteroids or comets in our solar system are covered by granular materials* has been shown by spacecraft images and also by in situ observations of the asteroids Eros and Itokawa. Additionally, there is strong evidence that this *regolith is very complex and active* (Murdoch et al. 2013 and references therein). The main question is the determination of the thickness of the regolith and how it varies with topography (Sears 2004).

Although there are significant *differences between regolith processes on asteroids and such on the Moon* (e.g., Miyamoto et al. 2007, McKay et al. 1989), only speculations and extrapolations using ideas from the Moon have been possible until very recently, when a *sample from an asteroid regolith has been brought back*. In 2005 the spacecraft Hayabusa landed at the asteroid Itokawa and collected the first asteroid sample, which was returned in 2010. Based on surface properties, which include the presence of few large boulders larger than several meters across, a gradual decrease of the average size of regolith particles and the spatial density of large rocks from the transition zone to the center of the sample terrain Muses Sea, and the concentration of smooth terrains in local lows of gravity-centrifugal potential, it was suggested that possibly comminution and transportation processes of regolith materials between the surrounding rough terrain and the smooth Muses Sea terrain may still be occurring. In this case, the thickness of the regolith is likely to be more than several meters (Yano et al. 2006 and references therein).

The differences between the Moon and asteroids include the lower gravitational fields, lower impact velocities and more volatile target compositions for the asteroids. On the Moon the production rate of regolith decreased from a few millimeters per year ~3 Ga ago to <1 mm/a at present, because the thickness of the regolith built up and it became more difficult for impacts to penetrate the bedrock (Sears 2004). On asteroids with a size of 100 km ejecta from km-sized craters spread over large regions. Since the scale of regolith mixing processes is linked with the median range of ejecta, *regolith mixing is more intense on asteroids than on the Moon* (Langevin 1982). It has been proposed that on a 100 km asteroid, regolith mixing and deposition would occur 2 times faster than on the Moon, at a 40 times larger scale. This author modeled that a ~1 m thick ejecta blanket develops a ~20 cm thick “skin” in 12.5 Ma (Langevin 1982), which is remarkably similar to the results for Djermaia H chondrite (Lorin and Pellas 1979). Hörtz and Schaal

(1981) suggested that the accelerated total growth of asteroidal surface deposits leads to *relatively short surface residence times* of individual meteorite components, which is another significant difference between asteroidal and lunar surface materials.

**Seismic “shaking”** of the whole regolith was described by Langevin (1982) as a process, which on the Moon plays a minor role only. It occurs on a strong body whenever a crater larger than  $\sim 1/20$ th of its size is formed (Schultz and Gault 1975, Langevin and Maurette 1980, Hörz and Schaal 1981). Seismic “shaking” could occur 100 to 1000 times until the asteroid fragments. The main effects of this process include:

- i) Global vertical mixing of the regolith every few million years (Langevin 1982);
- ii) Redistribution of surface grains from a  $\sim 5$  cm thick “skin” (Langevin and Maurette 1980), which could bury selectively the smallest grains (Hörz and Schaal 1981). Hörz and Schaal (1981) suggested that much of the energy that would lead to spallation or elastic deformation on dense, unfractured bodies may actually lead to mechanical agitation of surface deposits, especially in a low-gravity environment. Asteroids “shake” therefore more frequently than massive planets and their ejecta deposits may be agitated more frequently. An interesting and speculative consequence is the resulting *efficient grain size separation mechanism*: “Coarse” grain sizes form a relatively fixed matrix bed, through which “fine” grain sizes may percolate to the bottom. The authors concluded that this **segregation (Figure 5-32)** is commonly observed in industrial processes (e.g., Shinbrot and Muzzio 1998, Rosato et al. 2002), and leads to relatively coarse-grained lag surfaces (Hörz and Schaal 1981).
- iii) A “vibrating table” lateral transport process (Langevin 1982).

However, Langevin (1982) noted that caution is required when comparing the models of present day asteroidal regolith formation with the characteristics of materials that have very old compaction ages like carbonaceous chondrites, because meteoroid and particle environment of the first few hundred million years of the history of the solar system was certainly very different from the present environment.

A number of studies (e.g., Rosato et al. 1987, 2002, Möbius et al. 2001, Huerta and Ruiz-Suárez 2004, Shinbrot 2004) investigated the processes in a vibrating granular medium. It was proposed that a local geometrical void-filling mechanism can lead to size segregation with larger particles (intruders) on top, the so-called **Brazil-nut effect** (Kudrolli 2004). The Brazil-nut effect has been attributed to several processes (Tancredi et al. 2012 and references therein):

- i) The *percolation effect*, causing that smaller particles pass through the holes created by larger particles;
- ii) *Geometrical recognition*, causing that small particles readily fill small openings below the larger particles;
- iii) *Global convection*, causing an uplift of the large particles, but not allowing re-entry in the down-stream;
- iv) The large particle still follows a *ballistic upraise* due to its larger kinetic energy, penetrating into the bed due to its inertia.

For the Brazil-nut effect the size ratio between small and large particles is the dominant factor and particle-specific properties like density, inelasticity and friction also play

important roles (Tancredi et al. 2012). The shaking on asteroids that may cause the Brazil-nut effect is activated by large enough but non-disruptive collisions (Murdoch et al. 2013) and explosions such as the release of energy by the liberation of internal stresses or the re-accommodation of material (Tancredi et al. 2012). To make things more complicated, however, also the so called *reverse Brazil-nut effect* (Hong et al. 2001, Möbius et al. 2001, Shinbrot 2004, Kudrolli 2004) may occur. Although large heavy intruder particles can raise in vibrating beds of finer grains, equally large light intruders can sink (termed the reverse). Additionally, Metzger et al. (2011) stated that the presence of other species of intermediate size besides the smallest and largest sizes causes dramatic reductions in the final degree of segregation compared to a simple binary mixture.

Since vacuum and low-gravity environments are difficult to reproduce, *numerical simulations* are the most promising technique for the study of granular media under these conditions (Tancredi et al. 2012). Using the discrete element method Tancredi et al. (2012) were able to show that shaking-induced size segregation, i.e. the Brazil-nut effect, does occur even in low-gravity environments as on the surface of small bodies like km-sized asteroids in the solar system. Shaking-induced density segregation is also observed in low-gravity environments, although it is not complete (Tancredi et al. 2012). This is in agreement with Murdoch et al. (2013) who concluded that it is likely that particle segregation does occur in the reduced-gravity environment found on asteroids' surfaces.

Furthermore, Miyamoto et al. (2007) found strong indication for the relocation of gravels on the surface of Itokawa after their accumulation/deposition, which implies that the surface has been subjected to global vibrations possibly due to impact-induced shaking. The presence of all smooth terrains in areas with low gravitational and rotation potential (see above) on the surface of Itokawa and the filling of small local lows by smooth materials suggest global processes that segregate and migrate the finest gravels to low points and to the interior, where they can clog the gaps between larger blocks (Miyamoto et al. 2007).

Caffee et al. (1986) stated that in a *fast-growing regolith*, excess  $^{21}\text{Ne}$  in grains should not occur since the grains would be buried fast and quickly shielded from cosmic rays.

Another idea is that the evaporation of water and other volatiles from the regolith can produce a **temporary atmosphere** that would “fluidize” the dust and create conditions suitable for aerodynamic and gravity sorting of chondrules. The flux and the velocities of

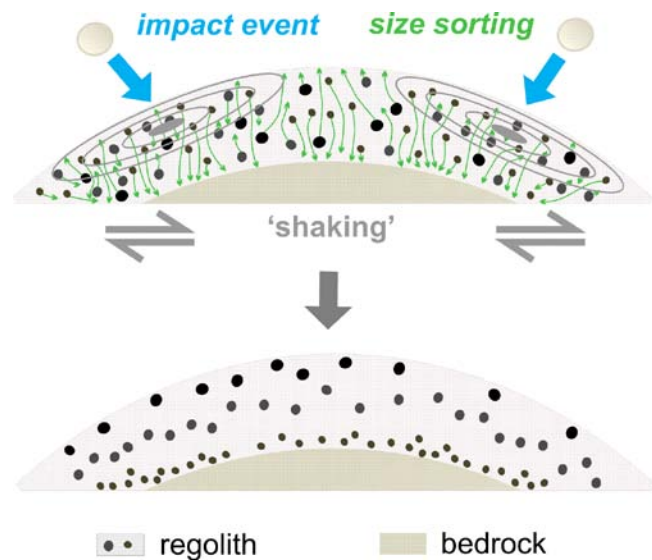


**Figure 5-32: Sketch showing the apparent size sorting (Brazil-nut effect) on the meteorite parent body regolith** (after Hörz and Schaal 1981). “Shaking” or vibrating of the granular medium is induced by impacts or explosions (Tancredi et al. 2012).

the fluid required to create these conditions on asteroids are surprisingly small because of the small size of the parent body (Sears 2004).

Overall, a preferential exposure of chondrules in a meteorite parent body regolith seems well possible assuming size sorting by segregation (Brazil-nut effect). Implanted SW gases found in olivine grains from Itokawa regolith material (Nagao et al. 2011) and in MET 00426 matrix and chondrules (Ne-B, see **Figure 5-15**) indicate that the samples resided at the surface of the regolith.

**v) Pre-irradiation effects in chondrules vs. matrix or bulk meteorite have to be distinguished from pre-irradiation effects in single grains and clasts** found in solar gas-rich meteorites (Wieler 2002b).

Single grains or clasts in gas-rich meteorites appear in some cases to have been pre-irradiated in the parent body regolith (e.g., Wieler 2000, Hohenberg et al. 1990, Caffee et al. 1988) (see *chapter 2.4.4*). Since chondrules formed early in solar system history and were already present as entities in the regolith, they cannot contain single grains or clasts, which were individually, i.e. without being part of the chondrule, pre-irradiated in the regolith. For meteorites without SW gases in the matrices it is also unlikely that they contain components which were pre-irradiated in the regolith. On the other hand, SW-rich matrices may very well contain pre-irradiated grains or clasts; thus the calculated nominal CRE ages of these matrices enriched with pre-irradiated grains or clasts are elevated compared to pure matrix material. As a consequence, elevated nominal CRE ages of chondrules relative to such enriched matrix may in fact underestimate the pre-irradiation of chondrules. The same is true if fragments of pre-irradiated chondrules produced during freeze-thaw cycles were part of the analyzed matrix material (see *chapter 4.2*).









### 5.6.2.2 General arguments for a pre-irradiation of chondrules

Besides neutralizing arguments why a pre-irradiation of chondrules (as a whole) should not be expected or difficult to discern (**Table 5-18**), there are observations which clearly show that chondrules were pre-irradiated. These observations include:

- i)** Some chondrules show **elevated nominal CRE ages relative to the matrix**, which cannot be explained by different abundances of target elements or shielding. This pre-irradiation of chondrules is recorded by an excess of  $^{21}\text{Ne}_c$ . Pre-irradiated chondrules are from
- ALH 76008 (H6) (Polnau et al. 1999),
  - Sena (H4), Kalvesta (H6), Grassland (L4), Hunter (L5), Bowesmont (LL6) (Polnau et al. 2001),
  - Dhajala (H3.8) (Eugster et al. 2007, Das and Murty 2009),
  - Bjurböle (L/LL4) (Polnau et al. 2001, Das and Murty 2009),
  - Parnallee (LL3.6) (Matsuda et al. 2010),
  - Murchison (CM2) (Roth et al. 2011, Huber et al. 2012),
  - NWA 852, El Djouf 001 (both CR2), QUE 99177, MET 00426 (both CR3) and Acfer 082 (CV3) (this study).



Table 5-18: Difficulties concerning the analysis of pre-irradiation effects in chondrules.

Difficulties	Neutralizing argument
<b>Reasons why a pre-irradiation of chondrules might be difficult to discern</b>	
In meteorites with long CRE ages pre-irradiation effects cannot be discerned.	 <ul style="list-style-type: none"> <li>• Selection of meteorites with short CRE ages (&lt;6 Ma)</li> <li>• First trial for meteorites without previous noble gas analysis (CR3 chondrites and Acfer 094)</li> </ul>
P <sub>21</sub> depends on chemistry and shielding.	 <ul style="list-style-type: none"> <li>• Matrix effect in stony meteorites &lt;10% (Wieler 2002b)</li> <li>• Use of T<sub>21-1.11</sub> “nominal” CRE ages without shielding correction</li> </ul>
Recoil losses from the matrix can cause lower CRE ages.	 <ul style="list-style-type: none"> <li>• T<sub>3-corr</sub> and T<sub>21-corr</sub> CRE ages agree well despite of different ranges of recoil loss (~2-3 μm for Ne (Ott and Begemann 2002, ~50 μm for He, Ott et al. 2009, Ziegler 2004). Differences between chondrule and matrix CRE ages are only minor for Ne and Ar (Polnau et al. 2001).</li> <li>• T<sub>21</sub> and T<sub>38</sub> are reliable CRE ages (Marti and Graf 1992, Polnau et al. 1999).</li> </ul>
Possible gas loss from the bulk meteorite/matrix due to thermal metamorphism and the lower retentivity for cosmogenic gases in the matrix.	 <ul style="list-style-type: none"> <li>• Selection of samples limited thermal metamorphism (petrologic types 2 to 3)</li> <li>• No evidence for gas loss in matrices of pre-irradiated chondrules</li> </ul>
Pre-irradiation records in single grains or clasts can obscure pre-irradiation records in matrices or chondrules.	 <ul style="list-style-type: none"> <li>• Unlikely for chondrules, in particular in case of meteorites without SW gases in their matrices</li> <li>• Likely for matrices containing SW gases. However, elevated nominal CRE ages of chondrules relative to these enriched matrices may underestimate the pre-irradiation record of chondrules.</li> </ul>
<b>Reasons why a pre-irradiation of chondrules might not be expected</b>	
A pre-irradiation of chondrules in the early solar system is not possible due to high dust densities.	 <ul style="list-style-type: none"> <li>• Redistribution of chondrules (X-wind model, jet flows, outward radial diffusion) to the outer edges of the protoplanetary disk with lower dust densities, where an irradiation was possible.</li> </ul>
The lifetime of small objects in the inner solar system is limited.	 <ul style="list-style-type: none"> <li>• Transport of chondrules to the outer edges of the protoplanetary disk.</li> <li>• After sinking in the midplane chondrules might be preserved by the incorporation into planetesimals.</li> <li>• Other disks were sufficient turbulent to have preserved small particles for millions of years (Natta et al. 2006, Haida et al. 2001).</li> </ul>
A pre-irradiation of chondrules on parent body surfaces (regolith) is not possible.	 <ul style="list-style-type: none"> <li>• Size sorting in a granular medium is possible (so-called Brazil-nut effect, e.g., Shinbrot 2004, Rosato et al. 1987) even in low-gravity environments (Tancredi et al. 2012, Murdoch et al. 2013).</li> <li>• A temporary atmosphere due to the evaporation of volatiles may produce conditions suitable for size sorting (Sears 2004).</li> </ul>

- ii) **Different CRE ages of chondrules within a single meteorite** (Hohenberg et al. 1990, Eugster et al. 2007, Roth et al. 2011, Huber et al. 2012) suggest either different irradiation environments or identical irradiation and subsequent gas loss affecting some chondrules.
- iii) **A missing pre-irradiation of chondrules from some chondrites does not necessary exclude the pre-irradiation of chondrules from other chondrites** since chondrules might have been formed and irradiated in locally different regions of the early solar nebula (depending on the dust density). This scenario is supported by numerous arguments including for example:
- Chondrite groups with large chondrules (CV, CK and CR) have typically thick dust-rich mantles that formed in dusty nebular environments. Additionally, these chondrite groups have low proportions of RP and C chondrules (see *chapter 2.2.2*), high proportions of enveloping compound chondrules, high proportions of chondrules with igneous rims, and relative low proportions of type-I chondrules containing sulfide. In the contrary, chondrite groups with smaller chondrules (CM, CO, OC, R, EH, EL) have the opposite properties (Rubin 2010).
  - CAI modal abundances and  $\Delta^{17}\text{O}$  abundances vary among chondrite groups depending on the distance from Sun (Rubin 2010).

Considering these observations and the arguments why a pre-irradiation of chondrules is difficult to discern or should not be expected (see **Table 5-18**), pre-irradiation of chondrules from NWA 852, El Djouf 001, QUE 99177 (QUE-ch1-4, QUE-ch5&6), MET 00426 (MET-ch6) and Acfer 082 (A82-ch1&2) is indicated. In addition, the matrices of MET 00426 and QUE 99177 show also evidence for pre-irradiation.

### 5.6.2.3 Limitation of this study

The limitation of this study refers to the setting of pre-irradiation of chondrules, which cannot be determined with certainty. The analysis of the setting of pre-irradiation of chondrules (in the regolith on the meteorite parent body vs. solar nebula setting, see *chapter 2.4.2*) is challenging, because helpful parameters like the shielding parameter  $(^{22}\text{Ne}/^{21}\text{Ne})_c$  are not unequivocal (see *chapter 5.6.3*).

### 5.6.3 Settings of pre-irradiation of chondrules

#### **Comparison with Murchison (CM2) and Renazzo (CR2)**

In the study of Roth et al. 2011 only 20% of analyzed Murchison chondrules showed enhanced nominal  $T_{21}$  CRE ages relative to the matrix, ranging up to 32.9 Ma of pre-exposure. In contrast, all chondrules from NWA 852 and El Djouf 001 analyzed in this study have enhanced nominal  $T_{21}$  CRE ages relative to the matrix (see *chapter 5.6.1*). These differences concerning the percentage of pre-irradiated chondrules and the duration of pre-irradiation may suggest different processes in the respective parent body regoliths. However, while El Djouf 001 is clearly different, the situation for NWA 852 may be similar to Murchison based on the large  $T_{21}$  CRE differences. Also, in this case, although pre-irradiation was observed in all chondrules, no reliable conclusion can be drawn concerning the percentage of pre-irradiated chondrules because only a small number (2) of chondrules was analyzed.

All five Renazzo chondrules analyzed by Vogel et al. (2004) show pre-irradiation effects relative to the matrix (Vogel et al. 2004), which agrees with the results for NWA 852 and El Djouf 001 concerning the percentage of pre-irradiated chondrules. The duration of pre-irradiation in case of Renazzo is similar to that of El Djouf 001 chondrules.

### **Pre-irradiation caused by SCR or GCR?**

Cosmogenic noble gases can be produced by both SCR and GCR particles. However, secondary neutron formation is important for spallation (see chapter 2.3.1.2) due to SCR can be widely neglected (Michel et al. 1996). SCR-produced  $^{21}\text{Ne}$  in meteorites has only rarely been positively identified (Leya et al. 2001).

Garrison et al. (1995) suggested that the  $^{21}\text{Ne}/^{22}\text{Ne}$  ratio can be generally used to distinguish between SCR and GCR components in many meteorites. As SCR and GCR components were produced by different suites of energetic particles, production mechanisms of  $(^{21}\text{Ne}/^{22}\text{Ne})_c$  are not the same and hence the ratio shows characteristic differences between SCR and GCR (Garrison et al. 1995). While values of around 0.90 for  $^{21}\text{Ne}/^{22}\text{Ne}$  are typical for GCR Ne (Wieler 2002b), irradiation of chondritic matter with a (present-day) SCR energy spectrum would lead to lower  $^{21}\text{Ne}/^{22}\text{Ne}$  ratios on the order of 0.6 only (Garrison et al. 1995).

In **Figure 5-33** Mg/(Al+Si) ratios are plotted against  $(^{21}\text{Ne}/^{22}\text{Ne})_c$ . According to this plot, chondrules from QUE 99177 may require a SCR contribution, while Ne in chondrules from El Djouf 001, NWA 852 and Acfer 082 is fully compatible with production by GCR. Closer inspection using the model of Leya and Masarik (2009) shows that the situation is more complex than envisioned by Garrison et al. (1995). This is because these authors did not include Na as important target element. Doing so causes a shift towards lower  $(^{21}\text{Ne}/^{22}\text{Ne})_c$  values as shown in **Figure 5-34**. Low  $(^{21}\text{Ne}/^{22}\text{Ne})_c$  observed for our QUE 99177 chondrules can thus well be realized by GCR irradiation only, if irradiated in a near-surface position. Additionally, for our pre-exposed chondrules a pre-irradiation solely or mainly by SCR can be excluded because in this case significant lower  $^3\text{He}/^{21}\text{Ne}$  ratios are typical (Trappitsch and Leya 2013).

Concerning where the irradiation occurred, the shielding parameter  $(^{22}\text{Ne}/^{21}\text{Ne})_c$  is not unambiguous. For example, a sample in a small object (like chondrules) has a high  $(^{22}\text{Ne}/^{21}\text{Ne})_c$ , but this is also the case for a sample irradiated in a large object in a near-surface position.

On the other hand, the different penetration depths of GCR (~50 cm on average, Wieler et al. 2002b), SCR (mm to cm) and SW (~50 nm, Caffee et al. 1988) (see chapter 2.3.1) in stony meteorites can be used to put constraints on the position of the sample during exposure to radiation. The considerably longer pre-irradiation and in most cases higher concentration of trapped (solar) gases of NWA 852 chondrules compared to El Djouf 001 chondrules may imply in the case of a pre-irradiation on the meteorite parent body that NWA 852 chondrules resided in a near-surface position (up to 1 or 2 m depth) on the CR meteorite parent body, whereas El Djouf 001 chondrules were shielded from cosmic radiation in much deeper regions and spent less time in a near-surface position. On the other hand, the highly varying  $T_{21-1.11}$  CRE ages of QUE 99177 and MET 00426 chondrules (see **Figure 5-29**) may imply a pre-irradiation as free-floating objects in the solar nebula. This might be caused by more intense mixing processes of chondrules with potentially different irradiation history in the solar nebula compared to those in the meteorite parent body. Especially for QUE chondrules, a pre-irradiation in the solar nebula is reasonable because of the lack of SW gases (see **Figure 5-15**).

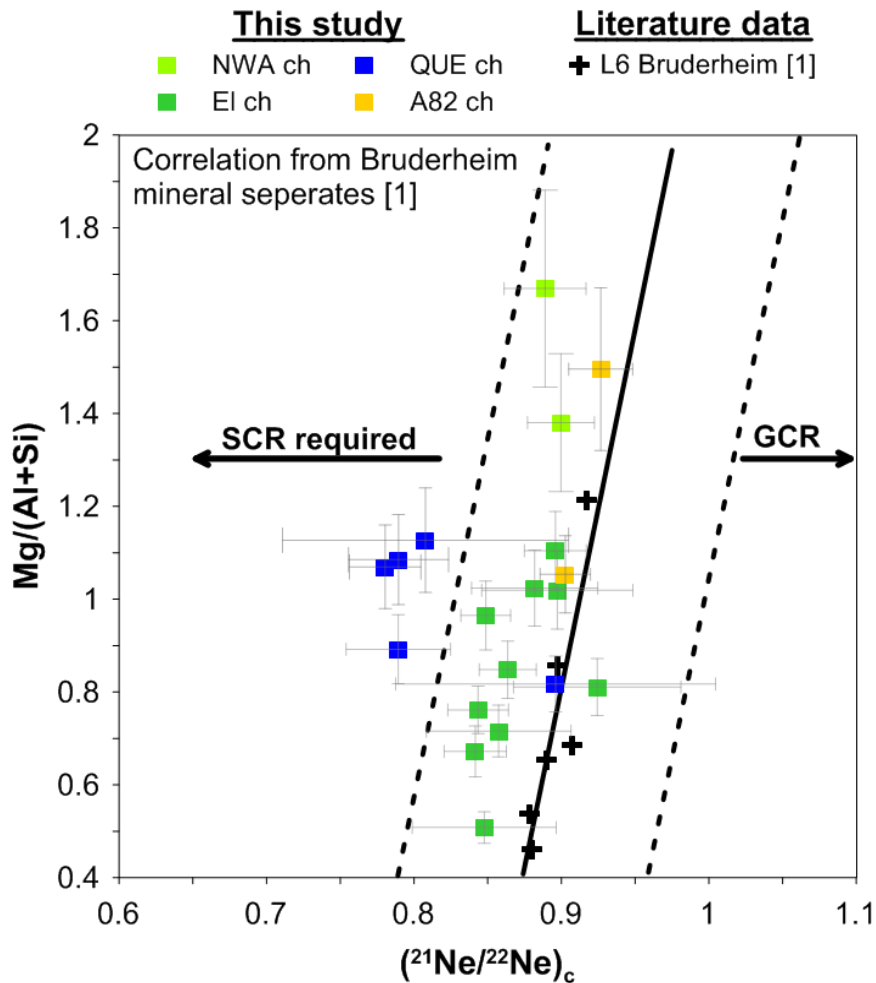


**Figure 5-33: Mg/(Al+Si) vs.  $(^{21}\text{Ne}/^{22}\text{Ne})_c$  for selected chondrules and matrix samples from CR2 chondrites NWA 852 (NWA) and EI Djouf 001 (EI), CR3 chondrite QUE 99177 (QUE) and CV3 chondrites Acfer 082 (A82), Vigarano (Vi) and Allende (Al) relying on mineral separates from the Bruderheim meteorite (adapted after Das and Murty 2009). The solid bold line indicates a regression of values from L6 Bruderheim, the dashed lines indicates deviations of 10%. Literature data are also shown (1- Bogard and Cressy 1973). Values for  $(^{21}\text{Ne}/^{22}\text{Ne})_c$  are plotted as measured. NWA – NWA 852, EI – EI Djouf 001, A82 – Acfer 082, Vi- Vigarano, Al – Allende. SCR – solar cosmic radiation, GCR – galactic cosmic radiation.**

The pre-irradiation of chondrules in the solar nebula did not necessarily exclude a subsequent pre-irradiation in the regolith of the meteorite parent body. Chondrule QUE-ch5 for example has a much higher  $T_{21-1.11}$  CRE age compared to all other chondrules from the respective meteorite (see **Figure 5-29**), and contains abundant trapped noble gases (HL) but apparently no SW gases (see **Figure 5-15**). This may imply that most QUE 99177 chondrules were pre-irradiated in the solar nebular (and thus having higher  $T_{21-1.11}$  CRE ages relative to the matrix) and that QUE-ch5 was resided subsequently longer in a near-surface location than other QUE 99177 chondrules.

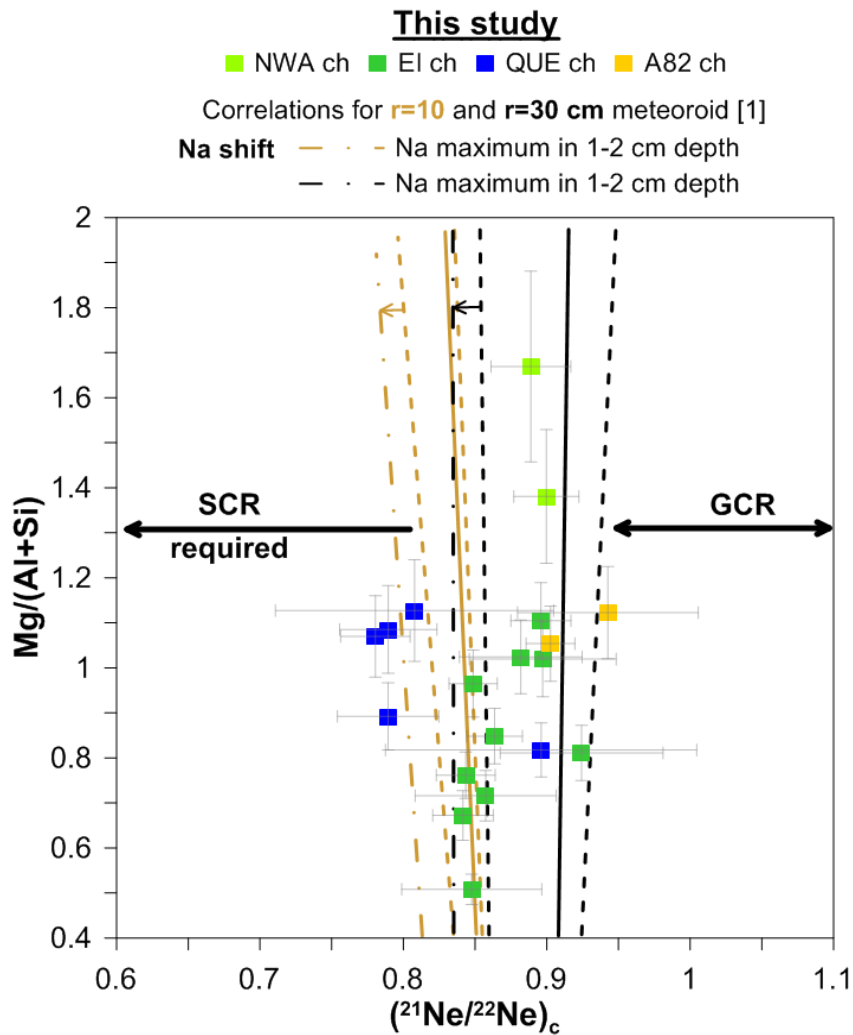


**Figure 5-34:**  $\text{Mg}/(\text{Al}+\text{Si})$  vs.  $(^{21}\text{Ne}/^{22}\text{Ne})_c$  for chondrules (ch) from QUE 99177 for meteoroids with 10 and 30 cm radius. Values for  $(^{21}\text{Ne}/^{22}\text{Ne})_c$  of the regression lines are calculated using the model of Leya and Masarik (2009) [1] for different depths (left dashed line: surface position, middle solid bold line: middle position, right dashed line: center position) and the elements Mg, Si and Al only. A shift towards lower  $(^{21}\text{Ne}/^{22}\text{Ne})_c$  values caused by high sodium (Na) abundances (= maximum of QUE chondrules is 0.388 wt%) is indicated by dash dot lines marked with arrows. Values for  $(^{21}\text{Ne}/^{22}\text{Ne})_c$  are plotted as measured. NWA – NWA 852, EI – EI Djouf 001, A82 – Acfer 082, Vi- Vigarano, AI – Allende. SCR – solar cosmic radiation, GCR – galactic cosmic radiation.

## 6 Summary and future work

Noble gases can provide insights into the origin and history of meteorites and their parent bodies (e.g., Crabb and Anders 1981) as well as processes in the early solar system. In more detail, analyzing noble gases in chondrules may provide information about the energetic particle environment and the lifetime of chondrules as free-floating objects (Roth et al. 2011) in the early solar system and/or about processes in asteroidal regoliths. Therefore, the aim of this study was the search for pre-irradiation effects in chondrules from primitive meteorites using improved methods eliminating systematic uncertainties present in previous work.

Among the nine analyzed carbonaceous chondrites, CR2 chondrites NWA 852 and El Djouf 001 show strong evidence for pre-irradiation effects in all chondrules, because they have elevated  $T_{21-1.11}$  CRE ages relative to the matrix. The large excesses of  $^{21}\text{Ne}_c$  and  $^3\text{He}$  relative to the matrix cannot be explained by different abundances of target elements (different shielding was also excluded due to the common use of “normal” shielding with  $(^{22}\text{Ne}/^{21}\text{Ne})_c = 1.11$ ). While the age differences of the ten analyzed El Djouf 001 chondrules relative to the matrix range from 0.4 to 1.9 Ma, the NWA 852 chondrules have much higher apparent CRE ages that are 27.1 and 32.9 Ma longer than that of the respective matrix. This situation is comparable with that for Murchison (CM2), where about 20% of Murchison chondrules show pre-exposure of up to ~30 Ma (Roth et al. 2011, Huber et al. 2012). The differences concerning the percentage of pre-irradiated chondrules and the duration of pre-irradiation (in case of El Djouf 001) may suggest different processes in the respective parent body regoliths. For El Djouf 001 the situation is clearly different compared to Murchison, whereas the situation for NWA 852 may be similar to Murchison based on the large  $T_{21-1.11}$  CRE differences. In this case, although pre-irradiation was observed in all analyzed chondrules, no reliable conclusion can be drawn concerning the percentage of pre-irradiated chondrules because only a small number (2) was analyzed.

Apparent pre-irradiation effects were found in several chondrules from MET 00426, QUE 99177, and Acfer 082 which have elevated  $T_{21-1.11}$  CRE ages relative to the matrix. Intriguingly, though, since the MET 00426 and QUE 99177 matrices have elevated  $T_{21-1.11}$  CRE ages compared to at least one of their chondrules, not only chondrules but also matrix from MET 00426 and QUE 99177 appears to have been pre-irradiated. This is an important new finding of this work in terms of analyzing pre-irradiation effects in primitive meteorites.

No evidence for pre-irradiation were found in chondrules from Allende, which is in accordance with the results from previous studies (Roth et al. 2011, Das et al. 2010, Eugster et al. 2007, Vogel et al. 2004, 2003). No evidence was also found in case of the other CV3 meteorite studied, Vigarano.

For Renazzo and Acfer 094 no reliable conclusion concerning pre-irradiation can be reached, because only a small number of chondrules were analyzed, which show  $T_{21-1.11}$  CRE ages indistinguishable from the corresponding matrix.

General difficulties with / for pre-irradiation of chondrules, which include for example the dependency of the production rate of cosmogenic noble gas nuclides on chemistry and shielding, recoil losses from the matrix grains, preferential noble gas loss due to thermal metamorphism from the matrix, and the impossibility of pre-irradiation of chondrules in the early solar system and in the parent body surfaces (regolith), could be neutralized by methodical approaches and/or theoretical considerations. On the other hand, there are clear indications for the pre-irradiation of chondrules, which include i) elevated CRE ages of some chondrules relative to the matrix from previous studies and this study, which cannot be explained by different abundances of target elements or shielding; this pre-irradiation of

chondrules corresponds to an excess of  $^{21}\text{Ne}_c$ ; ii) different CRE ages of chondrules within a single meteorite, which suggests either different irradiation environments or identical irradiation and subsequent gas loss affecting some chondrules, and iii) the possibility of locally different regions of chondrule formation and of different irradiation histories. Considering these observations and the general difficulties, a pre-irradiation of all chondrules from NWA 852 and El Djouf 001 as well as some chondrules from QUE 99177, MET 00426 and Acfer 082 is indicated. In addition, the matrices of MET 00426 and QUE 99177 show also evidence for pre-irradiation.

The setting of pre-irradiation of chondrules cannot be determined with certainty in this study as well as in other studies analyzing pre-irradiation effects, because parameters like the shielding parameter ( $^{22}\text{Ne}/^{21}\text{Ne}_c$ ), which may help in deciding where the chondrules were pre-irradiated (in the regolith on the meteorite parent body vs. solar nebula setting), are not unequivocal. While for NWA 852 and El Djouf 001 the dominant solar components in the matrices suggest a pre-irradiation of chondrules in the parent body regolith, the highly varying  $T_{21-1.11}$  CRE ages of QUE 99177 and MET 00426 chondrules may imply a pre-irradiation as free-floating objects in the solar nebula. Based on the lack of SW gases, especially for QUE 99177 chondrules, a pre-irradiation in the solar nebula appears highly likely.

In future work the analysis of pre-irradiation effects in more chondrules from chondrites analyzed in this study showing pre-irradiation effects, especially NWA 852, can help in obtaining a more representative data set, in particular concerning the percentage of pre-irradiated chondrules. In addition, the analysis of chondrules and matrix from enstatite and CB chondrites seems to be promising. Jones (2012) proposed that enstatite chondrite chondrules are samples from completely different reservoirs than those sampled by ordinary or carbonaceous chondrites, i.e. chondrule precursors dominated by pyroxene, specifically enstatite. In the enstatite chondrite Y-791790 Okazaki et al. (2001) found significant amounts of trapped noble gases in chondrules with elemental ratios ( $^{36}\text{Ar}/^{132}\text{Xe}$ ,  $^{84}\text{Kr}/^{132}\text{Kr}$ ) similar to those of subsolar gas, which is in contrast to the normal situation where chondrules are poor in trapped gases (e.g., Vogel et al. 2004). Similarly, Okazaki et al. (2010) analyzed a set of 18 enstatite chondrites and found trapped noble gases, which they interpreted to be of subsolar origin, which could be fractionated solar wind having been implanted into chondrule precursor material in the solar nebula. Clearly, if a radiation by solar wind happened in the solar nebula of which the signature was preserved, it is to be expected that also records from cosmic radiation, which produces cosmogenic noble gases much more tightly bound than solar wind, are preserved. However, among the chondrules analyzed by Eugster et al. (2007) were also such from the EH4 chondrite Indarch where no evidence for pre-irradiation was found. Among the enstatite chondrites, based on their low  $T_{21}$  CRE ages (Patzert and Schultz 2001) PCA 91238 (EH3), EET 87746 (EH4), MAC 88136, LEW 87226 (both EL3), and TIL 91714 (EL5) seem to be promising candidates for further work. While TIL 91714 shows an increased degree of thermal metamorphism, nevertheless possible pre-irradiation records might also be preserved in this case, given the fact that Polnau et al. (1999) appears to have found a precompaction exposure for a chondrule of the H6 chondrite ALH 76008. The small chondrule size of EH chondrites (PCA 91238: 0.045-0.9 mm, average 0.26 mm, Schneider et al. 2002; EET 87746: 0.05-0.15 mm, Lofgren and DeHart 1995) may be a problem, because handling during freeze-thaw cycles for chondrule separation may be difficult and the small sample weight might cause large uncertainties of INAA analysis and noble gas measurements. CB chondrites can be interesting in terms of analyzing pre-irradiation effects in chondrules, since CB chondrules are believed to have formed from a vapor-melt plume

produced by a giant impact between planetary embryos after the dissipation of the solar nebula (e.g., Krot et al. 2007b, Kita et al. 2005), where an unshielded exposure of chondrules was possible.

The small chondrule size of EH chondrites and the compact structure of CB chondrites complicating the separation of chondrules using the freeze-thaw technique like in the case of CH/CB Isheyevo (see chapter 4.2), suggest the use of a high sensitivity laser extraction noble gas mass spectrometer system like the Noblesse noble gas spectrometer (Ott et al. 2010), which has been used to analyze micro-meteorites (e.g., Baecker 2014, Baecker et al. 2012).

In addition, in order to put an upper limit in the actual “recent” cosmic ray exposure age, analyses of some chondrules from the CR3 chondrites MET 00426 and QUE 99177 for the cosmogenic radionuclides  $^{10}\text{Be}$ ,  $^{26}\text{Al}$ , and  $^{36}\text{Cl}$  are in progress (Merchel et al. 2014). Since these meteorites are found from the Antarctica, the determination of CRE ages is not straightforward based on a single radionuclide, but the combination of several radionuclides with different half lives ( $^{10}\text{Be}$ : 1.4 Ma,  $^{26}\text{Al}$ : 0.7 Ma,  $^{36}\text{Cl}$ : 0.3 Ma) should allow to correct for the effect of decay during terrestrial residence, in particular in combination with the also planned analysis of  $^{41}\text{Ca}$  (half life: 0.1 Ma) (Ott et al. 2014).



## 7 References

- Abreu N. M. and Vreearley A. J. (2008) Petrologic and chemical effects of the onset of aqueous alteration on the matrices of CR chondrites: GRA 95229. *39<sup>th</sup> Lunar and Planetary Science Conference*, abstract# 2013.
- Abreu N. M. and Brearley A. J. (2010) Early solar system processes recorded in the matrices of two highly pristine CR3 carbonaceous chondrites, MET 00426 and QUE 99177. *Geochimica et Cosmochimica Acta*, *74*(3), 1146-1171.
- Ahmad I., Greene J. P., Moore E. F., Ghelberg S., Ofan A., Paul M. and Kutschera W. (2006) Improved measurement of the <sup>44</sup>Ti half-life from a 14-year long study. *Physical Review, C* *74*, 065803.
- Alexander C. M. O'D., Boss A. P. and Carlson R. W. (2001) The early evolution of the inner solar system: A meteoritic perspective. *Science*, *293*, 64-68.
- Alexander C. M. O'D., Grossman J. N., Ebel D. S. and Ciesla F. J. (2008) The formation conditions of chondrules and chondrites. *Science*, *320*, 1617-1619.
- Allen J. S., Nozette S. and Wilkening L. L. (1980) A study of chondrule rims and chondrule irradiation records in unequilibrated ordinary chondrites. *Geochimica et Cosmochimica Acta*, *44*(8), 1161-1175.
- Amari S., Lewis R. S. and Anders E. (1995) Interstellar grains in meteorites: III. Graphite and its noble gases. *Geochimica et Cosmochimica Acta*, *59*(7), 1411-1426.
- Amelin Y., Krot A. N., Hutcheon I. D. and Ulyanov A. A. (2002) Lead isotopic ages of chondrules and calcium-aluminum-rich inclusions. *Science*, *297*(5587), 1678-1683.
- Amelin Y., Wadhwa M. and Lugmair G. (2006) Pb-isotopic dating of meteorites using <sup>202</sup>Pb-<sup>205</sup>Pb double-spike: comparison with other high-resolution chronometers. *37<sup>th</sup> Lunar and Planetary Science Conference*, abstract#1970.
- Amelin Y. and Krot A. (2007) Pb isotopic age of the Allende chondrules. *Meteoritics & Planetary Science*, *42*(7-8), 1321-1335.
- Asphaug E. and Nolan M. C. (1992) Analytical and numerical predictions for regolith production on asteroids. *Lunar and Planetary Science Conference*, *XXII*, 43-44.
- Baecker B., Cordier C., Folco F., Trieloff M., Cartwright J. A. and Ott U. (2012) Noble gas inventory of micrometeorites from the Transantarctic Mountains. *43<sup>rd</sup> Lunar and Planetary Institute Science Conference*, #abstract1824.
- Baecker B. (2014) Primordial and other noble gases in micrometeorites. Ph.D thesis, Heidelberg University, Heidelberg, Germany, 363 pp.
- Ballentine C. J. and Burnard P. G. (2002) Production, release and transport of noble gases in the continental crust. In: Noble Gases in Geochemistry and Cosmochemistry, (ed. D. Porcelli, C. J. Ballentine. and R. Wieler), Geochemical Society & Mineralogical Society of America, *Reviews in Mineralogy and Geochemistry*, *47*, 481-538.
- Bennett J. W. (2008) Commissioning of NAA at the new OPAL reactor in Australia. *Journal of Radioanalytical and Nuclear Chemistry*, *278*(3), 671-673.
- Berlin J. (2009) Mineralogy and bulk chemistry of chondrules and matrix in petrologic type 3 chondrites: Implications for early solar system processes. PhD thesis, University of New Mexico, Albuquerque, New Mexico, USA.
- Bigolski J. N., Weisberg M. K., Connolly H. C. Jr. and Ebel D. S. (2013) Microchondrules in unequilibrated ordinary chondrites: Insights into chondrule formation. *44<sup>th</sup> Lunar and Planetary Science Conference*, abstract #2239.
- Bigolski J. N., Weisberg M. K., Ebel D. S. and Connolly H. C. Jr. (2014) Microchondrules: Records of multiple heating events in the solar nebula and implications for type II chondrule formation. *45<sup>th</sup> Lunar and Planetary Science Conference*, abstract #1879.
- Binns W. R., Wiedenbeck M. E., Arnould M., Cummings A. C., George J. S., Goriely S., Israel M. H., Leske R. A., Mewaldt R. A., Meynet G., Scott L. M., Stone, E. C. and von Rosewing T. T. (2005) Cosmic-ray neon, Wolf-Rayet stars, and the superbubble origin of galactic cosmic rays. *The Astrophysical Journal* *634*(1), 351-364.

- Bischoff A., Palme H., Clayton R. N., Mayeda T. K., Grund T., Spettel B., Geiger T., Endress M., Beckerling W. and Metzler K. (1991) New carbonaceous and type 3 ordinary chondrites from the Sahara desert. *Meteoritics*, 26, 318-319.
- Bischoff A., Palme H., Ash R. D., Clayton R. N., Schultz L., Herpers U., Stöffler D., Grady M. M., Pillinger C. T., Spettel B., Weber, H., Grund T., Endreß M. and Weber D. (1993) Paired Renazzo-type (CR) carbonaceous chondrites from the Sahara. *Geochimica et Cosmochimica Acta*, 57(7), 1587-1603.
- Bischoff A. (2001) Meteorite classification and the definition of new chondrite classes as a result of successful meteorite search in hot and cold deserts. *Planetary and Space Science*, 49(8), 769-776.
- Bizzarro M., Baker J. A. and Haack H. (2004) Mg isotope evidence for contemporaneous formation of chondrules and refractory inclusions. *Nature*, 431(7006), 275-278.
- Black D. C. (1972) On the origins of trapped helium, neon and argon isotopic variations in meteorites—I. Gas-rich meteorites, lunar soil and breccia. *Geochimica et Cosmochimica Acta*, 36(3), 347-375.
- Bland P. A., Alard O., Benedix G. K., Kearsley A. T., Menzies O. N., Watt L. E. and Rogers N. W. (2005) Volatile fractionation in the early solar system and chondrule/matrix complementarity. *Proceedings of the National Academy of Sciences*, 102(39), 13755-13760.
- Bland P. A., Zolensky M. E., Benedix G. K. and Sephton M. A. (2006) Weathering of chondritic meteorites. In *Meteorites and the Early Solar System II*, (ed. D. S. Lauretta and H. Y. McSween, Jr.), The University of Arizona Press, 853-867.
- Bland P. A., Howard L. E., Prior D. J., Wheeler J., Hough R. M. and Dyl K. A. (2011) Earliest rock fabric formed in the Solar System preserved in a chondrule rim. *Nature Geoscience*, 4(4), 244-247.
- Bland P. A., Muxworthy A. R., Collins G. S., Moore J., Davison T. M., Prior D. J., Wheeler J., Ciesla F. J. and Dyl K. A. (2012) Effect of low intensity impacts on chondrite matrix. *43<sup>th</sup> Lunar and Planetary Science Conference*, abstract# 2005.
- Bogard D. D., Clark R. S., Keith J. E. and Reynolds M. A. (1971) Noble gases and radionuclides in Lost City and other recently fallen meteorites. *Journal of Geophysical Research*, 76(17), 4076-4083.
- Bogard D. D. and Cressy Jr. P. J. (1973) Spallation production of  $^3\text{He}$ ,  $^{21}\text{Ne}$ , and  $^{38}\text{Ar}$  from target elements in the Bruderheim chondrite. *Geochimica et Cosmochimica Acta*, 37(3), 527-546.
- Bogard D. D. (2011) K–Ar ages of meteorites: Clues to parent-body thermal histories. *Chemie der Erde-Geochemistry*, 71(3), 207-226.
- Bonal L., Quirico E., Bourot-Denise M. and Montagnac G. (2006) Determination of the petrologic type of CV3 chondrites by Raman spectroscopy of included organic matter. *Geochimica et Cosmochimica Acta*, 70(7), 1849-1863.
- Bonal L., Huss G. R., Krot A. N. and Nagashima K. (2010) Chondritic lithic clasts in the CB/CH-like meteorite Isheyevo: Fragments of previously unsampled parent bodies. *Geochimica et Cosmochimica Acta*, 74(8), 2500-2522.
- Bouvier A., Wadhwa M., and Janney P. (2008)  $^{26}\text{Al}$ - $^{26}\text{Mg}$  and  $^{207}\text{Pb}$ - $^{206}\text{Pb}$  Systematics in an Allende inclusion. *71<sup>st</sup> Meeting Meteoritical Society*, abstract #5299.
- Bowen N. L. (1928) *The evolution of the igneous rocks*. Princeton University Press.
- Brearley A. J. and Jones R. H. (1998) Chondritic meteorites. In *Planetary materials*, (ed. J. J. Papike), Mineralogical Society of America, *Reviews in mineralogy*, 36, pp. 3-1 to 3-398.
- Browning L. B., McSween Jr. H. Y. and Zolensky M. E. (1996) Correlated alteration effects in CM carbonaceous chondrites. *Geochimica et Cosmochimica Acta*, 60(14), 2621-2633.
- Busemann H., Baur H. and Wieler R. (2000) Primordial noble gases in "phase Q" in carbonaceous and ordinary chondrites studied by closed-system stepped etching. *Meteoritics & Planetary Science*, 35(5), 949-973.
- Caffee M. W., Goswami J. N., Hohenberg C. M., Swindle T. D. (1983) Cosmogenic neon from precompaction irradiation of Kapoeta and Murchison. *14<sup>th</sup> Lunar and Planetary Science Conference*, *Journal Geophysical Research*, 88, B267–B273.
- Caffee M. W., Goswami J. N., Hohenberg C. M., and Swindle T. D. (1986) Pre-compaction irradiation of meteorite grains. *17<sup>th</sup> Lunar and Planetary Science Conference*, pp. 99-100.

- Caffee M., Goswami J. N., Hohenberg C. M., and Swindle T. W. (1987) Solar flare irradiation records in meteorites provides evidence for an early active sun. *4<sup>th</sup> International Conference on Cosmic Rays*, pp. 299-302.
- Caffee M. W., Reedy R. C., Goswami J. N., Hohenberg C. M. and Marti K. (1988) Irradiation records in meteorites. In *Meteorites and the Early Solar System*, (ed. J. F. Kerridge and M. S. Matthews), University Arizona Press, Tucson, pp. 205-245.
- Carporzen L., Weiss B. P., Elkins-Tanton L. T., Shuster D. L., Ebel D. and Gattacceca J. (2011) Magnetic evidence for a partially differentiated carbonaceous chondrite parent body. *Proceedings of the National Academy of Sciences*, *108*(16), 6386-6389.
- Cartwright J. A., Ott U., Mittlefehldt D. W., Herrin J. S., Herrmann S., Mertzman S. A., Mertzman K. R., Peng Z. X. and Quinn J. E. (2013) The quest for regolithic howardites. Part 1: Two trends uncovered using noble gases. *Geochimica et Cosmochimica Acta*, *105*, 395-421.
- Charles C. R. J. and Davis D. W. (2010) ( $^{207}\text{Pb}/^{206}\text{Pb}$ )\* ID-TIMS ages of NWA 801 chondrules and Mokoia CAls by a progressive stepwise dissolution. *74<sup>th</sup> Meeting Meteoritical Society*, #5391.
- Chaussidon M. and Gounelle M. (2006) Irradiation processes in the Early Solar System. In *Meteorites and the Early Solar System II*, (ed. D. S. Lauretta and H. Y. McSween Jr.), The University of Arizona Press, Tucson, 323-339.
- Chmeleff J., von Blanckenburg F., Kossert K., and Jakob D. (2010) Determination of the  $^{10}\text{Be}$  half-life by multicollector ICP-MS and liquid scintillation counting. *Nuclear Instruments and Methods in Physics Research Section B: Beam Interactions with Materials and Atoms*, *263*(2), 192-199.
- Clarke R. S. Jr. (1970) The Allende, Mexico meteorite: Strewnfield and specimen morphology. *Meteoritics*, *5*, 189.
- Connelly J. N., Amelin, Y., Krot, A. N. and Bizzarro, M. (2007) Difference in Pb Isotopic Ages of Chondrules and Ca, Al-rich Inclusions from the CV Carbonaceous Chondrite Allende. *LPI Contribution*, *1374*, 46-47.
- Connelly J. N., Amelin Y., Krot A. N. and Bizzarro M. (2008) Chronology of the Solar System's oldest solids. *The Astrophysical Journal Letters*, *675*(2), L121.
- Connelly Jr. J. N., Bizzarro M., Krot A. N., Nordlund Å., Wielandt D. and Ivanova M. A. (2012) The absolute chronology and thermal processing of solids in the solar protoplanetary disk. *Science*, *338*(6107), 651-655.
- Connolly H. C. (2012) Chondrules: Their role in early solar system history. *Meteoritics & Planetary Science*, *47*(7), 1105-1107.
- Crabb J. and Anders E. (1981) Noble gases in E-chondrites. *Geochimica et Cosmochimica Acta*, *45*(12), 2443-2464.
- Cressy Jr. P. J. and Bogard D. D. (1976) On the calculation of cosmic-ray exposure ages of stone meteorites. *Geochimica et Cosmochimica Acta*, *40*(7), 749-762.
- Cristarella T. C. and Sears D. W. (2011) Classifying chondrules based on cathodoluminescence. *42<sup>nd</sup> Lunar and Planetary Science Conference*, abstract #1225.
- Cuzzi J. N., Dobrovolskis A. R. and Hogan R. C. (1996) Turbulence, chondrules and planetesimals. In *Chondrules and the Protoplanetary Disk*, (ed. R. H. Hewins, R. H. Jones and E. R. D. Scott), Cambridge University Press, Cambridge, pp. 35-44.
- Cuzzi J. N., Hogan R. C., Paque J. M. and Dobrovolskis A. R. (2001) Size-selective concentration of chondrules and other small particles in protoplanetary nebula turbulence. *The Astrophysical Journal*, *546*(1), 496-508.
- Cuzzi J. N. (2004) Blowing in the wind: III. Accretion of dust rims by chondrule-sized particles in a turbulent protoplanetary nebula. *Icarus*, *168*(2), 484-497.
- Cuzzi J. N. and Alexander M.O'D. (2006) Chondrule formation in particle-rich nebular regions at least hundreds of kilometres across. *Nature*, *441*(7092), 483-485.
- Cuzzi J. (2011) Gathering dust. *Nature Geoscience*, *4*, 219-220.
- Das J. P. and Murty S. V. S. (2009) Cosmogenic and trapped noble gases in individual chondrules: Clues to chondrule formation. *Meteoritics & Planetary Science*, *44*(11), 1797-1818.
- Das J. P., Goswami J. N., Pravdivtseva O. V., Meshik A. P., and Hohenberg C. M. (2010) Cosmogenic neon in individual chondrule fragments: Records of pre-compaction exposure, *41<sup>st</sup> Lunar and Planetary Science Conference*, abstract #1961.

- Das J. P., Goswami J. N., Pravdivtseva O. V., Meshik A. P. and Hohenberg C. M. (2012) Cosmogenic neon in grains separated from individual chondrules: Evidence of precompaction exposure in chondrules. *Meteoritics & Planetary Science*, 47(11), 1869-1883.
- Desch S. J. and Cuzzi J. N. (2000) The generation of lightning in the solar nebula. *Icarus*, 143(1), 87-105.
- Desch S. J., Morris M. A., Connolly Jr. H. C. and Boss A. P. (2012) The importance of experiments: Constraints on chondrule formation models. *Meteoritics & Planetary Science*, 47(7), 1139-1156.
- Dixon L., Herd R. K., Samson C. and Hunt P. A. (2009) A detailed investigation of the mineralogy and textures of the L4 ordinary chondrite Saratov. 40<sup>th</sup> *Lunar and Planetary Science Conference*, abstract #1465.
- Dodd R. T. (1971) The petrology of chondrules in the Sharps meteorite. *Contributions to Mineralogy and Petrology*, 31(3), 201-227.
- Dodd R. T. (1973) Minor element abundances in olivines of the Sharps (H-3) chondrite. *Contributions to Mineralogy and Petrology*, 42(2), 159-167.
- Dodd R. T. (1978a) The composition and origin of large microporphyritic chondrules in the Manych (L-3) chondrite. *Earth and Planetary Science Letters*, 39(1), 52-66.
- Dodd R. T. (1978b) Compositions of droplet chondrules in the Manych (L-3) chondrite and the origin of chondrules. *Earth and Planetary Science Letters*, 40(1), 71-82.
- Dodd R. T. (1981) *Meteorites - A petrologic-chemical synthesis*. Cambridge University Press, 377 p.
- Ebel D. S. and Grossman L. (2000) Condensation in dust-enriched systems. *Geochimica et Cosmochimica Acta*, 64(2), 339-366.
- Ebel D. S., Weisberg M. K., Hertz J. and Campbell A. J. (2008) Shape, metal abundance, chemistry, and origin of chondrules in the Renazzo (CR) chondrite. *Meteoritics & Planetary Science*, 43(10), 1725-1740.
- Eberhardt P., Eugster O. and Marti K. (1965) A redetermination of the isotopic composition of atmospheric neon. *Zeitschrift für Naturforschung*, 20a, 623-624.
- Eikenberg J., Signer P. and Wieler R. (1993) U-Xe, U-Kr, and U-Pb systematics for dating uranium minerals and investigations of the production of nucleogenic neon and argon. *Geochimica et Cosmochimica Acta*, 57(5), 1053-1069.
- Elkins-Tanton L. T., Weiss B. P. and Zuber M. T. (2011) Chondrites as samples of differentiated planetesimals. *Earth and Planetary Science Letters*, 305(1-2), 1-10.
- Eugster O. (1988) Cosmic-ray production rates for <sup>3</sup>He, <sup>21</sup>Ne, <sup>38</sup>Ar, <sup>83</sup>Kr, and <sup>126</sup>Xe in chondrites based on <sup>81</sup>Kr-Kr exposure ages. *Geochimica et Cosmochimica Acta*, 52(6), 1649-1662.
- Eugster O., Michel Th., Niedermann S., Wang D. and Yi W. (1993) The record of cosmogenic, radiogenic, fissiogenic, and trapped noble gases in recently recovered Chinese and other chondrites. *Geochimica et Cosmochimica Acta*, 57(5), 1115-1142.
- Eugster O. and Michel T. (1995) Common asteroid break-up events of eucrites, diogenites, and howardites and cosmic-ray production rates for noble gases in achondrites. *Geochimica et Cosmochimica Acta*, 59(1), 177-199.
- Eugster O., Herzog, G. F., Marti K. and Caffee M. W. (2006) Irradiation records, cosmic-ray exposure ages, and transfer times of meteorites. In *Meteorites and the Early Solar System II*, (ed. D. S. Lauretta and H. Y. McSween Jr.), The University of Arizona Press, Tucson, 829-851.
- Eugster O., Lorenzetti S., Krahenbühl U. and Marti K. (2007) Comparison of cosmic-ray exposure ages and trapped noble gases in chondrule and matrix samples of ordinary, enstatite, and carbonaceous chondrites. *Meteoritics & Planetary Science*, 42 (7/8), 1351-1371.
- Evans J. C., Reeves J. H. and Reedy R. C. (1987) Solar cosmic ray produced radionuclides in the Salem meteorite, 18<sup>th</sup> *Lunar and Planetary Science Conference*, 271-272.
- Farley K. A., Hurowitz J. A., Asimow P. D., Jacobson N. S. and Cartwright J. A. (2013) A double-spike method for K-Ar measurement: A technique for high precision in situ dating on Mars and other planetary surfaces. *Geochimica et Cosmochimica Acta*, 110, 1-12.
- Fireman E. L. and Goebel R. (1970) Argon 37 and argon 39 in recently fallen meteorites and cosmic-ray variations. *Journal of Geophysical Research*, 75(11), 2115-2124.

- Floss C. and Stadermann F. J. (2009a) Auger Nanoprobe analysis of presolar ferromagnesian silicate grains from primitive CR chondrites QUE 99177 and MET 00426. *Geochimica et Cosmochimica Acta*, 73(8), 2415-2440.
- Floss C. and Stadermann F. J. (2009b) High abundances of circumstellar and interstellar C-anomalous phases in the primitive CR3 chondrites QUE 99177 and MET 00426. *The Astrophysical Journal*, 697, 1242-1255.
- Formisano V., Bellucci G. and Mastracci F. (1993) The Renazzo meteorite. *Il Nuovo Cimento*, 16C(6), 775-781.
- Freundel M., Schultz L. and Reedy R. C. (1986) Terrestrial  $^{81}\text{Kr}$ -Kr ages of Antarctic meteorites. *Geochimica et Cosmochimica Acta*, 50(12), 2663-2673.
- Gao S., Luo T.-C., Zhang B.-R., Zhang H.-F., Han Y.-w., Zhao Z.-D. and Hu Y.-K. (1998) Chemical composition of the continental crust as revealed by studies in East China. *Geochimica et Cosmochimica Acta*, 62(11), 1959-1975.
- Garrison D., Rao M. and Bogard D. (1995) Solar-proton-produced neon in shergottite meteorites and implications for their origin. *Meteoritics*, 30(6), 738-747.
- Gattacceca J., Weiss B. P., Gounelle M., Lima E. A. and Rochette P. (2013) More Evidence for a Partially Differentiated CV Parent Body from the Meteorite Kaba. *44<sup>th</sup> Lunar and Planetary Science Conference*, abstract # 1721.
- Geiger T. and Bischoff A. (1992) Mineralogy of carbonaceous chondrites and Acfer 217 from the Sahara. *Meteoritics*, 27, p. 223.
- Gooding J. L. and Keil K. (1981) Relative abundances of chondrule primary textural types in ordinary chondrites and their bearing on conditions of chondrule formation. *Meteoritics*, 16(1), 17-43.
- Grady M. M. and Wright I. (2006) Types of extraterrestrial material available for study. In *Meteorites and the Early Solar System II*, (ed. D. S. Lauretta and H. Y. McSween, Jr.), The University of Arizona Press. Tucson, 3-18.
- Graf Th., Signer P., Wieler R., Herpers U., Sarafin R., Vogt S., Fieni Ch., Pellas P., Bonani G., Suter M. and Wölfli W. (1990) Cosmogenic nuclides and nuclear tracks in the chondrite Knyahinya. *Geochimica et Cosmochimica Acta*, 54(9), 2511-2520.
- Graham, D. W.. (2002) Noble gas isotope geochemistry of Mid-ocean ridge and Ocean island basalts: Characterization of mantle source reservoirs. In: *Noble Gases in Geochemistry and Cosmochemistry*, (ed. D. Porcelli, C. J. Ballentine. and R. Wieler), Geochemical Society & Mineralogical Society of America, *Reviews in Mineralogy and Geochemistry*, 47, 247-317.
- Greenberg R. R., Bode P. and De Nadai Fernandes E. A. (2011) Neutron activation analysis: A primary method of measurement. *Spectrochimica Acta Part B: Atomic Spectroscopy*, 66(3), 193-241.
- Greshake A. (1997) The primitive matrix components of the unique carbonaceous chondrite Acfer 094: A TEM study. *Geochimica et Cosmochimica Acta*, 61(2), 437-452.
- Grossman J. N., Rubin A. E., Nagahara H. and King E. A. (1988) Properties of chondrules. In *Meteorites and the Early Solar System I*, (ed. J. F. Kerridge and M. S. Matthews), The University of Arizona Press, 619-679.
- Grossman J. F. and Brearley A. J. (2005) The onset of metamorphism in ordinary and carbonaceous chondrites. *Meteoritics & Planetary Science*, 40(1), 87-122.
- Grossman L. (2010a) Vapor-condensed phase processes in the early solar system. *Meteoritics & Planetary Science*, 45(1), 7-20.
- Grossman L. (2010b) *personal communication*
- Haisch Jr. K. E., Lada E. A. and Lada C. J. (2001) Disk frequencies and lifetimes in young clusters. *The Astrophysical Journal Letters*, 553(2), L153-156.
- Hanon P., Robert F. and Chaussidon M. (1998) High carbon concentrations in meteoritic chondrules: A record of metal-silicate differentiation. *Geochimica et Cosmochimica Acta*, 62(5), 903-913.
- Heber V. S., Wieler R., Baur H., Olinger C., Friedmann T. A. and Burnett D. S. (2009) Noble gas composition of the solar wind as collected by the Genesis mission. *Geochimica et Cosmochimica Acta*, 73(24), 7414-7432.

- Heber V. S., Baur H., Bochsler P., McKeegan K. D., Neugebauer M., Reisenfeld D. B., Wieler R. and Wiens R. C. (2012) Isotopic mass fractionation of solar wind: Evidence from fast and slow solar wind collected by the Genesis mission. *The Astrophysical Journal*, 759(2), 121-134.
- Herd R. K., Dixon L., Samson C. and Hunt P. A. (2009) A new classification scheme for chondrules based on very detailed study of Saratov. 72<sup>nd</sup> *Meteoritical Society Conference*, abstract #5420.
- Herd R. K., Samson C., Dixon L., Cooke A. and Hunt P. A. (2010) Testing and extending a new classification scheme for chondrules. 41<sup>st</sup> *Lunar & Planetary Science Conference*, abstract #2026.
- Hewins R. (1997) Chondrules. *Annual Review of Earth and Planetary Sciences*, 25(1), 61-83.
- Hewins R., Connolly Jr. H. C., Lofgren G. E. and Libourel G. (2005) Experimental constraints on chondrule formation. In *Chondrites and the protoplanetary disk*, (eds. A. N. Krot, E. R. D. Scott and B. Reipurth), ASP Conference Series Vol. 341, 286-316.
- Hewins R. H. and Zanda B. (2012) Chondrules: Precursors and interactions with the nebular gas. *Meteoritics & Planetary Science*, 47(7), 1120-1138.
- Hezel D. C. and Palme H. (2007) The conditions of chondrule formation, Part I: Closed system. *Geochimica et Cosmochimica Acta*, 71(16), 4092-4107.
- Hezel D. and Palme H. (2010) The chemical relationship between chondrules and matrix and the chondrule matrix complementarity. *Earth and Planetary Science Letters*, 294(1-2), 85-93.
- Hintenberger H., König H., Schultz L. and Wänke H. (1964) Radiogene, spallogene und primordiale Edelgase in Steinmeteoriten. *Zeitschrift Naturforschung Teil A*, 19, 327.
- Hörandel J. R., Antoni T., Apel W. D., Badea F., Bekk K., Bercuci A., Blümer H., Bollmann E., Bozdog H., Brancus I. M., Büttner C., Chilingarian A., Daumiller K., Doll P., Engler J., Feßler F., Gils H. J., Glasstetter R., Haeusler R., Haungs A., Heck D., Holst T., Iwan A., Kampert K-H., Klages H. O., Knapp J., Maier G., Mathes H. J., Mayer H. J., Milke J., Müller M., Obenland R., Oehlschläger J., Petcu M., Rebel H., Risse M., Roth M., Schatz G., Schieler H., Scholz J., Thouw T., Ulrich H., Vulpesu B., Weber J. H., Wentz J., Wochele J. and Zabierowski J. (2002) On the onset of the knee – air shower measurements with KASCADE. *Nuclear Physics Proceedings Supplements*, 110:453–456.
- Hörandel J. R. (2013) The composition of cosmic rays at the knee. *AIP Conference Proceedings*, 1516, 185-194.
- Hörz F. and Schaal R. B. (1981) Asteroidal agglutinate formation and implications for asteroidal surfaces. *Icarus*, 46(3), 337-353.
- Hohenberg C. M., Marti K., Podosek F. A., Reedy R. C. and Shirck J. R. (1978) Comparisons between observed and predicted cosmogenic noble gases in lunar samples, 9<sup>th</sup> *Lunar and Planetary Science Conference*, 2311-2344.
- Hohenberg C. M., Nichols Jr. R. H., Olinger C. T., and Goswami J. N. (1990) Cosmogenic neon from individual grains of CM meteorites: Extremely long pre-compaction exposure histories or an enhanced early particle flux. *Geochimica et Cosmochimica Acta*, 54(7), 2133-2140.
- Hong D. C., Quinn P. V. and Luding S. (2001) Reverse Brazil nut problem: Competition between percolation and condensation. *Physical Review Letters*, 86(15), 3423.
- Hopp J., Trierloff M., Ott U., Korochantseva E. V. and Buykin A. I. (2014) <sup>39</sup>Ar-<sup>40</sup>Ar chronology of the enstatite chondrite parent bodies. *Meteoritics & Planetary Science*, 49(3), 358-372.
- Housen K. R., Wilkening L. L., Chapman C. R. and Greenberg R. (1979) Asteroidal regoliths. *Icarus*, 39(3), 317-351.
- Housen K. R. and Wilkening L. L. (1982) Regoliths on small bodies in the solar system. *Annual Review of Earth and Planetary Sciences*, 10(1), 355-376.
- Housen K. R. (1992) Crater ejecta velocities for impacts on rocky bodies. *Lunar and Planetary Science Conference*, XXII, 555-556.
- Howard K. T. and Alexander C. M. O'D. (2013) A new classification scheme for aqueously altered carbonaceous chondrites based on total phyllosilicate abundance. 44<sup>th</sup> *Lunar and Planetary Science Conference*, abstract #2598.
- Huber L., Metzler K., Maden C., Vogel N., and Wieler R. (2012) Cosmic ray irradiation history of individual Murchison chondrules analyzed by UV-laser ablation, 43<sup>th</sup> *Lunar and Planetary Science Conference*, abstract #1420.

- Huerta D. A. and Ruiz-Suárez J. C. (2004) Vibration-induced granular segregation: A phenomenon driven by three mechanisms. *Physical Review Letters*, 92(11), 114301.
- Hurt S. M., Rubin A. E. and Wasson J. T. (2012) Fractionated matrix composition in CV3 Vigarano and alteration processes on the CV parent asteroid. *Meteoritics & Planetary Science*, 47(6), 1035-1048.
- Huss G. R. and Lewis R. S. (1994) Noble gases in presolar diamonds I: Three distinct components and their implications for diamond origins. *Meteoritics*, 29, 791-810.
- Huss G. R., Rubin A. E. and Grossman J. N. (2006) Thermal metamorphism in chondrites. In *Meteorites and the Early Solar System II*, (ed. D. S. Lauretta and H. Y. McSween Jr.), The University of Arizona Press, 567-586.
- Hutcheon I. D., Marhas K. K., Krot A. N., Goswami J. N. and Jones R. H. (2009)  $^{26}\text{Al}$  in plagioclase-rich chondrules in carbonaceous chondrites: Evidence for an extended duration of chondrule formation. *Geochimica et Cosmochimica Acta*, 73: 5080-5099.
- Imamura M., Nishiizumi K., Nitoh O., Yanagita S. and Honda M. (1979) Complex cosmic ray records found in some meteorites. *16<sup>th</sup> International Cosmic Ray Conference*, pp. 321-323.
- Ishii H. A., Bradley J. P., Bonal L., Krot A. N., Huss G. R., Nagashima K., Hutcheon I. D. and Teslich N. (2009) Transmission electron microscopy on highly  $^{15}\text{N}$ -enriched chondritic clasts in the Isheyevo meteorite. *40<sup>th</sup> Lunar and Planetary Science Conference*, abstract #2467.
- Itoh S. and Yurimoto H. (2003) Contemporaneous formation of chondrules and refractory inclusions in the early Solar System. *Nature*, 423(6941), 728-731.
- Ivanova M. A., Nazarov M. A., Kononkova N. N. and Brandstaetter F. (2005) Isheyevo: A new CB chondrite. *68<sup>th</sup> Meeting Meteoritical Society*, abstract #5073.
- Ivanova M. A., Kononkova N. N., Krot A. N., Greenwood R. C., Franchi I. A., Verchovsky A. B., Trieloff M., Korochantseva E. V. and Brandstätter F. (2008) The Isheyevo meteorite: Mineralogy, petrology, bulk chemistry, oxygen, nitrogen, carbon isotopic compositions, and  $^{40}\text{Ar}$ - $^{39}\text{Ar}$  ages. *Meteoritics & Planetary Science*, 43(5), 915-940.
- Jacobsen B., Yin Q.-z., Moynier F., Amelin Y., Krot A. N., Nagashima K., Hutcheon I. D. and Palme H. (2008)  $^{26}\text{Al}$ - $^{26}\text{Mg}$  and  $^{207}\text{Pb}$ - $^{206}\text{Pb}$  systematics of Allende CAIs: Canonical solar initial  $^{26}\text{Al}/^{27}\text{Al}$  ratio reinstated. *Earth and Planetary Science Letters*, 272(1), 353-364.
- Jones R. H. and Scott E. R. D. (1989) Petrology and thermal history of type IA chondrules in the Semarkona (LL3.0) chondrite. In *Lunar and Planetary Science Conference Proceedings*, pp. 523-536.
- Jones R. H. (1990) Petrology and mineralogy of type II, FeO-rich chondrules in Semarkona (LL3.0): Origin by closed-system fractional crystallization, with evidence for supercooling. *Geochimica et Cosmochimica Acta*, 54(6), 1785-1802.
- Jones R. H. (1992a) Classification of porphyritic, pyroxene-rich chondrules in the Semarkona ordinary chondrite. *Lunar and Planetary Science Conference*, XXIII, 629-630.
- Jones R. H. (1992b) Petrology of FeO-poor, Porphyritic Pyroxene Chondrules in the Semarkona Ordinary Chondrite. *Lunar and Planetary Science Conference*, XXIII, 631-632.
- Jones R. H. (1994) Petrology of FeO-poor, porphyritic pyroxene chondrules in the Semarkona chondrite. *Geochimica et Cosmochimica Acta*, 58(23), 5325-5340.
- Jones R. H. (1996) FeO-rich, porphyritic pyroxene chondrules in unequilibrated ordinary chondrites. *Geochimica et Cosmochimica Acta*, 60(16), 3115-3138.
- Jones R. H., Grossman J. N. and Rubin A. E. (2005) Chemical, mineralogical and isotopic properties of chondrules: Clues to their origin. In *Chondrites and the Protoplanetary Disk*, (eds. A. N. Krot, E. R. D. Scott and B. Reipurth), ASP Conference Series Vol. 341, pp. 251-285.
- Jones R. H. (2012) Petrographic constraints on the diversity of chondrule reservoirs in the protoplanetary disk. *Meteoritics & Planetary Science*, 47(7), 1176-1190.
- Kallemeyn G. W. and Wasson J. T. (1981) The compositional classification of chondrites - I. The carbonaceous chondrite groups. *Geochimica et Cosmochimica Acta*, 45(7), 1217-1230.
- Kallemeyn G. W. and Wasson J. T. (1982) The compositional classification of chondrites: III. Ungrouped carbonaceous chondrites. *Geochimica et Cosmochimica Acta*, 46(11), 2217-2228.
- Keil K. (2000) Thermal alteration of asteroids: Evidence from meteorites. *Planetary and Space Science*, 48(10), 887-903.
- Kieffer, S. W. (1975) Droplet chondrules. *Science*, 189, 333-340.

- Kim, J. S. and Marti, K. (1994) Distribution of some highly volatile elements in chondrules. *Meteoritics* 29(4), 482.
- King E. A. Jr., Schonfeld E., Richardson K. A. and Eldridge J. S. (1969) Meteorite fall at Pueblito de Allende, Chihuahua, Mexico: Preliminary information. *Science*, 163(3870), 928-929.
- King E. A. (1983) Reduction, partial evaporation, and spattering - Possible chemical and physical processes in fluid drop chondrule formation. In: *Chondrules and their origins*, p. 180-187.
- Kita N. T., Nagahara H., Togashi S. and Morishita Y. (2000) A short duration of chondrule formation in the solar nebula: evidence from  $^{26}\text{Al}$  in Semarkona ferromagnesian chondrules. *Geochimica et Cosmochimica Acta*, 64(22), 3913-3922.
- Kita N. T., Huss G., Tachibana S., Amelin Y., Nyquist L. and Hutcheon I. (2005) Constraints on the origin of chondrules and CAIs from short-lived and long-lived radionuclides. In *Chondrites and the protoplanetary disk*, (eds. A. N. Krot, E. R. D. Scott and B. Reipurth), ASP Conference Series Vol. 341, pp. 558.
- Kita N. T. and Ushikubo T. (2012) Evolution of protoplanetary disk inferred from  $^{26}\text{Al}$  chronology of individual chondrules. *Meteoritics and Planetary Science*, 47(7), 1108-1119.
- Klerner S. and Palme H. (1999) Origin of chondrules and matrix in the Renazzo meteorite. 62<sup>nd</sup> Meeting Meteoritical Society, abstract #5174.
- Kong P. and Palme H. (1999) Compositional and genetic relationship between chondrules, chondrule rims, metal, and matrix in the Renazzo chondrite. *Geochimica et Cosmochimica Acta*, 63(21), 3673-3682.
- Korschinek G., Bergmaier A., Faestermann T., Gerstmann U. C., Knie K., Rugel G., Wallner A., Dillmann I., Dollinger G. and von Gostomski Ch. L. (2010) A new value for the half-life of  $^{10}\text{Be}$  by heavy-ion elastic recoil detection and liquid scintillation counting. *Nuclear Instruments and Methods in Physics Research Section B: Beam Interactions with Materials and Atoms*, 268(2), 187-191.
- Krot A. N. and Wasson J. T. (1995) Igneous rims on low-FeO and high-FeO chondrules in ordinary chondrites. *Geochimica et Cosmochimica Acta*, 59(23), 4951-4966.
- Krot A. N., Rubin A. E., Keil K. and Wasson J. T. (1997) Microchondrules in ordinary chondrites: Implications for chondrule formation. *Geochimica et Cosmochimica Acta*, 61(2), 463-473.
- Krot A. N., Meibom A., Petaev M. I., Keil K., Zolensky M. E., Saito A., Mukai M. and Ohsumi K. (2000a) Ferrous silicate spherules with euhedral iron-nickel metal grains from CH carbonaceous chondrites: Evidence for supercooling and condensation under oxidizing conditions. *Meteoritics & Planetary Science*, 35(6), 1249-1258.
- Krot A. N., Meibom A. and Keil K. (2000b) A clast of Bali-like oxidized CV material in the reduced CV chondrite breccia Vigarano. *Meteoritics & Planetary Science*, 35(4), 817-825.
- Krot A. N., Meibom A., Weisberg M. K. and Keil K. (2002) The CR chondrite clan: Implications for early solar system processes. *Meteoritics & Planetary Science*, 37(11), 1451-1490.
- Krot A. N., Amelin Y., Cassen P. and Meibom A. (2005) Young chondrules in CB chondrites from a giant impact in the early solar system. *Nature*, 436(7053), 989-992.
- Krot A. N., Keil K., Goodrich C. A. and Scott E. R. D. (2007a): Classification of meteorites. In *Meteorites, Comets and Planets, Treatise on Geochemistry*, vol. 1 (ed. A.M. Davis) (executive eds. H. D. Holland and K. K. Turekian). Elsevier, Oxford, pp. 83-128.
- Krot A. N., Ivanova M. A. and Ulyanov A. A. (2007b) Chondrules in the CB/CH-like carbonaceous chondrite Isheyevo: Evidence for various chondrule-forming mechanisms and multiple chondrule generations. *Chemie der Erde-Geochemistry*, 67(4), 283-300.
- Kudrolli A. (2004) Size separation in vibrated granular matter. *Reports on progress in Physics*, 67(3), 209.
- Kunihiro T., Rubin A. E., McKeegan K. D., and Wasson J. T. (2004) Initial  $^{26}\text{Al}/^{27}\text{Al}$  in carbonaceous-chondrite chondrules: too little  $^{26}\text{Al}$  to melt asteroids. *Geochimica et Cosmochimica Acta*, 68(13), 2947-2957.
- Kurahashi E., Kita N. T., Nagahara H. and Morishita Y. (2004) Contemporaneous formation of chondrules in the  $^{26}\text{Al}$ - $^{26}\text{Mg}$  system for ordinary and CO chondrites. 35<sup>th</sup> Lunar and Planetary Science Conference, abstract #1476.
- Kurahashi E., Nagashima K., Krot A. N. and Russell S. S. (2011) Young  $^{26}\text{Al}$ - $^{26}\text{Mg}$  ages of chondrules in the LL3.1 chondrite Bishunpur: Evidence for thermal processing on asteroidal body? 74<sup>th</sup> Meeting Meteoritical Society, abstract #5257.



- Lal D., Rajan R. S. and Venkatavaradan V. S. (1967) Nuclear effects of "solar" and "galactic" cosmic-ray particles in near-surface regions of meteorites. *Geochimica et Cosmochimica Acta*, 31(10), 1859-1869.
- Langevin Y. and Maurette M. (1980) A model for small body regolith evolution: The critical parameters. *Lunar and Planetary Science Conference*, XI, 602-604.
- Langevin Y. (1982) Evolution of an asteroidal regolith: Granulometry, mixing and maturity. In *Lunar Breccias and Soils and their Meteoritic Analogs*, (eds. G. J. Taylor L. L. Wilkening), The Lunar and Planetary Institute, Houston, 87-93.
- Lauretta D. S., Nagahara, H. and Alexander C. M. O'D. (2006) Petrology and origin of ferromagnesian silicate chondrules. In *Meteorites and the Early Solar System II*, (ed. D. S. Lauretta and H. Y. McSween, Jr.), The University of Arizona Press, 431-459.
- Leitner J., Hoppe P., Vollmer C. and Zipfel J. (2010) The inventory of presolar grains in primitive meteorites: a NanoSIMS study of C-, N-, and O-isotopes in NWA 852. *Proc. Symp. Nuclei Cosmos XI*, 144.
- Leitner J., Metzler K., Vollmer C. and Hoppe P. (2013) Search for presolar grains in fine-grained chondrule rims: First results from CM chondrites and Acfer 094. *44<sup>th</sup> Lunar and Planetary Science Conference*, abstract # 2273.
- Levi-Donati G. R., Nelen J. and Fredriksson K. (1977) The Vigarano chondrite - A reevaluation. *Meteoritics*, 12, 287-290.
- Levsky L. K. (1972) New data on the isotopic content of rare gases of stony meteorites. *Meteoritika*, 31, 149-150.
- Lewis R. S., Srinivasan B. and Anders E. (1975) Host phase of a strange xenon component in Allende. *Science*, 190, 1251-1262.
- Lewis R. S., Amari S., and Anders E. (1994) Interstellar grains in meteorites: II. SiC and its noble gases. *Geochimica et Cosmochimica Acta*, 58(1), 471-494.
- Leya I., Lange H., Neumann S., Wieler R. and Michel R. (2000) The production of cosmogenic nuclides in stony meteoroids by galactic cosmic-ray particles. *Meteoritics and Planetary Science*, 35(2), 259-286.
- Leya I., Neumann S., Wieler R. and Michel R. (2001) The production of cosmogenic nuclides by galactic cosmic-ray particles for 2 $\pi$  exposure geometries. *Meteoritics & Planetary Science*, 36(11), 1547-1561.
- Leya I. and Masarik J. (2009) Cosmogenic nuclides in stony meteorites revisited. *Meteoritics and Planetary Science*, 44(7), 1061-1086.
- Liffman K. (2005) Chondrule and metal grain size sorting from jet flows. *Meteoritics & Planetary Science*, 40(1), 123-138.
- Lin B. E., Weisberg M. K. and Ebel, D. S. (2011) Refractory inclusions in MET 00426, a CR3 chondrite. *42<sup>nd</sup> Lunar and Planetary Science Conference*, abstract #1297.
- Lingenfelter R. E. and Higdon J. C. (2007) The composition of cosmic rays and the mixing of the interstellar medium. *Space Science Reviews*, 130(1-4), 465-473.
- Lodders K. (2003) Solar system abundances and condensation temperatures of the elements. *The Astrophysical Journal*, 591(2), 1220.
- Lofgren G. E. and Dehart J. M. (1995) Some observations on the petrology of enstatite chondrites PCA91020 and EET87746 with Implications for chondrite forming processes. *26<sup>th</sup> Lunar and Planetary Science Conference*, abstract #855.
- Lorin J. C. and Pellas P. (1979) Preirradiation history of Djermaia (H) chondritic breccia. *Icarus*, 40(3), 502-509.
- Macke R. J., Consolmagno G. J. and Britt D. T. (2011) Density, porosity, and magnetic susceptibility of carbonaceous chondrites. *Meteoritics & Planetary Science*, 46(12), 1842-1862.
- MacPherson G. J. and Krot A. N. (2002) Distribution of Ca-Fe-silicates in CV3 chondrites: Possible controls by parent-body compaction. *65<sup>th</sup> Meeting Meteoritical Society*, abstract #5227.
- Manuel O. K., Wright R. J., Miller D. K. and Kuroda P. K. (1972) Isotopic compositions of rare gases in the carbonaceous chondrites Mokoia and Allende. *Geochimica et Cosmochimica Acta*, 36(9), 961-983.

- Marti K. and Graf T. (1992) Cosmic-ray exposure history of ordinary chondrites. *Annual Review of Earth and Planetary Sciences*, 20, 221-243.
- Masarik J., Nishiizumi K. and Reedy R. C. (2001) Production rates of cosmogenic helium-3, neon-21, and neon-22 in ordinary chondrites and the lunar surface. *Meteoritics & Planetary Science*, 36(5), 643-650.
- Mason B. and Wiik H. B. (1962) The Renazzo meteorite. *Amer. Mus. Novitates*, 2106, 1–11.
- Mason B. (1971) The carbonaceous chondrites - A selective review. *Meteoritics*, 6(2), 59-70.
- Matsuda J.-I., Lewis R. S., Takahashi H. and Anders E. (1980) Isotopic anomalies of noble gases in meteorites and their origins--VII. C3V carbonaceous chondrites. *Geochimica et Cosmochimica Acta*, 44(11), 1861-1874.
- Matsuda S., Nakashima D., Iio H., Bajo K. and Nagao K. (2009) Laser microprobe noble gas analysis of chondrules in the NWA 801 CR2 chondrite. *40<sup>th</sup> Lunar and Planetary Science Conference*, abstract #1628.
- Matsuda S., Nakashima, D. and Nagao, K. (2010) Detection of primordial argon-rich noble gas in the Parnallee LL 3.6 chondrite by laser microscope ablation method *Antarctic Meteorites*, 33, 49-50.
- Mazor E., Heymann D. and Anders E. (1970) Noble gases in carbonaceous chondrites. *Geochimica et Cosmochimica Acta*, 34, 781-824.
- McKay D. S., Swindle T. D. and Greenberg R. (1989) Asteroidal regoliths – What do we know. In *Asteroids II*. (ed. R. P. Binzel, T. Gehrels and M. S. Matthews), The University of Arizona Press, pp. 921-945.
- McKeegan K. D., Greenwood J. P., Leshin L. A. and Cosarinsky M. (2000) Abundance of <sup>26</sup>Al in ferromagnesian chondrules of unequilibrated ordinary chondrites. *31<sup>st</sup> Lunar and Planetary Science Conference*, abstract #2009.
- McSween H. Y. Jr (1977a) Chemical and petrographic constraints on the origin of chondrules and inclusions in carbonaceous chondrites. *Geochimica et Cosmochimica Acta*, 41(12), 1843-1860.
- McSween H. Y. Jr (1977b) Petrographic variations among carbonaceous chondrites of the Vigarano type. *Geochimica et Cosmochimica Acta*, 41(12), 1777-1790.
- McSween H. Y. Jr and Richardson S. M. (1977) The composition of carbonaceous chondrite matrix. *Geochimica et Cosmochimica Acta*, 41(8), 1145-1161.
- McSween H. Y. Jr (1979) Are carbonaceous chondrites primitive or processed? A review. *Reviews of Geophysics*, 17(5), 1059-1078.
- McSween H. Y. Jr, Fronabarger A. K. and Driese S. G. (1983) Ferromagnesian chondrules in carbonaceous chondrites. In: *Chondrules and their origins*, p. 195-210.
- McSween H. Y. Jr. and Huss G. R. (2010) *Cosmochemistry*, Cambridge University Press, Cambridge, 549 pp.
- Merchel S. (1998) Über die Wechselwirkungen der kosmischen Strahlung mit extraterrestrischer Materie: Radiochemische Bestimmung der Produktionsraten von kosmogenen langlebigen Radionukliden in Meteoriten. Universität zu Köln, Köln. Ph.D. Thesis. pp. 1-231.
- Merchel S., Smith T., Ott U., Beyersdorf-Kuis U., Herrmann S., Leya I., Akhmadaliev S., Rugel G., Pavetich S, Ziegenrucker R., Wallner A., Fifield L. K., Tims S., Fimiani L. and Korschinek G. (2014): Bedtime stories from space: History of meteorites and cosmic radiation told by cosmogenic nuclides. *Abstract submitted to 13<sup>th</sup> Int. Conf. on Acceleration Mass Spectrometry*.
- Merrill G. P. (1920) On chondrules and chondritic structure in meteorites. *Proceedings of the National Academy of Sciences of the United States of America*, 6(8), 449-472.
- Metzger M. J., Remy B. and Glasser B. J. (2011) All the Brazil nuts are not on top: Vibration induced granular size segregation of binary, ternary and multi-sized mixtures. *Powder technology*, 205(1), 42-51.
- Metzler K., Bischoff A. and Stöffler D. (1992) Accretionary dust mantles in CM chondrites: Evidence for solar nebula processes. *Geochimica et Cosmochimica Acta*, 56(7), 2873-2897.
- Metzler K. (1997) Preirradiated Olivines in CM Chondrites. *Meteoritics & Planetary Science*, 32(4), A91.
- Metzler K. (2004) Formation of accretionary dust mantles in the solar nebula: Evidence from preirradiated olivines in CM chondrites. *Meteoritics & Planetary Science*, 39(8), 1307-1319.

- Metzler K., Ott U., Welten K., Caffee M. W. and Franke L. (2008) The L3-6 regolith breccia Northwest Africa 869: Petrology, noble gases, and cosmogenic radionuclides. *34<sup>th</sup> Lunar and Planetary Science Conference*, abstract #1120.
- Metzler K. (2012) Ultrarapid chondrite formation by hot chondrule accretion? Evidence from unequilibrated ordinary chondrites. *Meteoritics & Planetary Science*, 47(12), 2193-2217.
- Michel R., Dragovitsch P., Englert P., Peiffer F., Stück R., Theis S., Begemann F., Weber H., Signer P., Wieler R., Filges D. and Cloth P. (1986) On the depth dependence of spallation reactions in a spherical thick diorite target homogeneously irradiated by 600 MeV protons: Simulation of production of cosmogenic nuclides in small meteorites. *Nuclear Instruments and Methods in Physics Research Section B: Beam Interactions with Materials and Atoms*, 16(1), 61-82.
- Michel R., Leya I. and Borges L. (1996) Production of cosmogenic nuclides in meteoroids: accelerator experiments and model calculations to decipher the cosmic ray record in extraterrestrial matter. *Nuclear Instruments and Methods in Physics Research*, B16, 113(1), 434-444.
- Mittlefehldt, D. (2001) *Antarctic Meteorite Newsletter*, 24(2), 1-24.
- Miura Y. N. and Nagao K. (1997) Noble gas compositions in individual chondrules of the Allende CV3 chondrite. *Antarctic Meteorites*, XXII, 118-120 (Natl. Inst. Polar Res., Tokyo).
- Miyamoto H., Yano H., Scheeres D. J., Abe S., Barnouin-Jha O., Cheng A. F., Demura H., Gaskell R. W., Hirata N., Ishiguro M., Michikami T., Nakamura A. M., Nakamura R., Saito J. and Sasaki S. (2007) Regolith migration and sorting on asteroid Itokawa. *Science*, 316(5827), 1011-1014.
- Möbius M. E., Lauderdale B. E., Nagel S. R. and Jaeger H. M. (2001) Brazil-nut effect: Size separation of granular particles. *Nature*, 414(6861), 270-270.
- Morris M. A. and Desch S. J. (2010) Thermal histories of chondrules in solar nebula shocks. *The Astrophysical Journal*, 722(2): 1474-1494.
- Morris M. A. and Garvie L. (2013) New constraints on the formation of igneous rims around chondrules. *44<sup>th</sup> Lunar and Planetary Science Conference*, abstract #2852.
- Morris M. A. and Desch S. J. (2014) A re-evaluation of chondrule formation in large-scale shocks. *45<sup>th</sup> Lunar and Planetary Science Conference*, abstract #2577.
- Murdoch N., Rozitis B., Green S. F., Michel P., de Lophem T.-L. and Losert W. (2013) Simulating regoliths in microgravity. *Monthly Notices of the Royal Astronomical Society*, 433(1), 506-514.
- Murrie R. P., Quinton J. S. and Popelka-Filcoff R. S. (2013) Determination of the f parameter for  $k_0$ -neutron activation analysis at the Australian 20 MW OPAL research reactor. *Journal of Radioanalytical and Nuclear Chemistry*, 298(1), 77-86.
- Nagao K., Okazaki R., Nakamura T., Miura Y. N., Osawa T., Bajo K.-i., Matsuda S., Ebihara M., Ireland T. R., Kitajima F., Naraoka H., Noguchi T., Tsuchiyama A., Yurimoto H., Zolensky M. E., Uesugi M., Shirai K., Abe M., Yada T., Ishibashi Y., Fujimura A., Mukai T., Ueno M., Okada T., Yoshikawa M. and Kawaguchi J. (2011) Irradiation history of Itokawa regolith material deduced from noble gases in the Hayabusa samples. *Science*, 333(6046), 1128-1131.
- Nakamura T., Nagao K. and Takaoka N. (1999) Microdistribution of primordial noble gases in CM chondrites determined by in situ laser microprobe analysis: Decipherment of nebular processes. *Geochimica et Cosmochimica Acta*, 63(2), 241-255.
- Nakashima D., Matsuda S., Iio H., Bajo K., Ebisawa N. and Nagao K. (2009a) Noble gases in the NWA 852/801 CR2 chondrites. *40<sup>th</sup> Lunar and Planetary Science Conference*, abstract #1661.
- Nakashima D., Matsuda S., Iio H., Bajo K. and Nagao K. (2009b) Solar wind like noble gases in a chondrule in the NWA 852 CR2 chondrite. *40<sup>th</sup> Lunar and Planetary Science Conference*, abstract #1674.
- Natta A., Testi L., Calvet N., Henning T., Waters R. and Wilner D. (2006) Dust in proto-planetary disks: Properties and evolution. In *Protostars and Planets V*, (ed. B. Reipurth, D. Jewitt, K. Keil), The University Arizona Press, pp. 767-781.
- Newton J., Bischoff A., Arden J. W., Franchi I. A., Geiger T., Greshake A. and Pillinger C. T. (1995) Acfer 094, a uniquely primitive carbonaceous chondrite from the Sahara. *Meteoritics*, 30, 47-56.
- Nguyen A. N., Alexander C. M. O'D. and Nittler L. R. (2008) An abundant mix of presolar matter in the highly primitive CR chondrite QUE 99177. *71<sup>st</sup> Meteoritical Society*, abstract #5277.
- Nguyen A. N., Keller L. P., Rahman Z. and Messenger S. (2013) Crystal structure and chemical composition of a presolar silicate from the Queen Elizabeth Range 99177 meteorite. *44<sup>th</sup> Lunar and Planetary Science Conference*, abstract #2853.

- Nishiizumi K., Regnier S. and Marti K. (1980) Cosmic ray exposure ages of chondrites, pre-irradiation and constancy of cosmic ray flux in the past. *Earth and Planetary Science Letters*, 50(1), 156-170.
- Nishiizumi K., Nagai H., Imamura M., Honda M., Kobayashi K., Kubik P. W., Sharma P., Wieler R., Signer P., Goswami J. N., Sinha N., Reedy R. C. and Arnold J. R. (1990) Solar cosmic ray produced nuclides in the Salem meteorite. *Meteoritics*, 25, 392-393.
- Nishiizumi K., Arnold J. R., Fink D., Klein J. and Middleton R. (1991)  $^{41}\text{Ca}$  production profile in the Allende meteorite. *Meteoritics*, 26, 379.
- Okazaki R., Takaoka N., Nagao K., Sekiya M. and Nakamura T. (2001) Noble-gas-rich chondrules in an enstatite meteorite. *Nature*, 412(6849), 795-798.
- Okazaki R., Takaoka N., Nagao K. and Nakamura T. (2010) Noble gases in enstatite chondrites released by stepped crushing and heating. *Meteoritics and Planetary Science*, 45(3), 339-360.
- Ormel C. W., Cuzzi J. N. and Tielens A. G. G. M. (2008) Co-accretion of chondrules and dust in the solar nebula. *The Astrophysical Journal*, 679(2), 1588-1610.
- Ott U. and Begemann F. (2000) Spallation recoil and age of presolar grains in meteorites. *Meteoritics and Planetary Science*, 35(1), 53-64.
- Ott U. (2002) Noble gases in meteorites - trapped components. In: Noble Gases in Geochemistry and Cosmochemistry, (ed. D. Porcelli, C. J. Ballentine. and R. Wieler), Geochemical Society & Mineralogical Society of America, *Reviews in Mineralogy and Geochemistry*, 47, 71-100.
- Ott U., Heck P. R., Gyngard F., Wieler R., Wrobel F., Amari S. and Zinner E. (2009) He and Ne ages of large presolar silicon carbide grains: Solving the recoil problem. *Publications of the Astronomical Society of Australia*, 26(03), 297-302.
- Ott U., Haubold R., Herrmann S. and Sudek C. (2010) Ureilite noble gases measured by multiple ion counting mass spectrometry. *Meteoritics and Planetary Science Supplement* 73, 5096.
- Ott U., Wieler R. and Huber L. (2013) Comment on "Cosmogenic neon in grains separated from individual chondrules: Evidence of precompaction exposure in chondrules" by J. P. Das, J. N. Goswami, O. V. Pravdivtseva, A. P. Meshik, and C. M. Hohenberg. *Meteoritics & Planetary Science*, 48(8), 1524-1528.
- Ott U., Merchel S., Beyersdorf-Kuis U., Akhmadaliev S., Pavetich S., Rugel G. and Ziegenrucker R. (2014) Ancient and recent exposure history of chondrule from two highly primitive meteorites. *Abstract submitted to 13<sup>th</sup> Int. Conf. on Acceleration Mass Spectrometry*.
- Ozima M. and Podosek F. A. (2002) Noble gas geochemistry, 2<sup>nd</sup> ed. Cambridge University Press, pp. 300
- Padia J. T. and Rao M. N. (1989) Neon isotope studies of Fayetteville and Kapoeta meteorites and clues to ancient solar activity. *Geochimica et Cosmochimica Acta*, 53(6), 1461-1467.
- Paque J. M. and Cuzzi J. N. (1997) Physical characteristics of chondrules and rims, and aerodynamic sorting in the solar nebula. 28<sup>th</sup> Lunar and Planetary Science Conference, abstract #1189.
- Patzer A. and Schultz L. (2001) Noble gases in enstatite chondrites I: Exposure ages, pairing, and weathering effects. *Meteoritics & Planetary Science*, 36(7), 947-961.
- Pedroni A., Baur H., Wieler R., and Signer P. (1988) T-Tauri irradiation of Kapoeta grains? 19<sup>th</sup> Lunar and Planetary Science Conference, pp. 913-914.
- Pedroni A. (1991) Precompaction irradiation of the howarditic regolith breccia Kapoeta. 22<sup>nd</sup> Lunar and Planetary Science Conference, pp. 1047-1048.
- Pepin R. O. (1969) private communication to Mazar et al. (1970).
- Polnau E., Eugster O., Krähenbühl U. and Marti K. (1999) Evidence for a precompaction exposure to cosmic rays in a chondrule from the H6 chondrite ALH76008. *Geochimica et Cosmochimica Acta*, 63(6), 925-933.
- Polnau E., Eugster O., Burger M., Krähenbühl U. and Marti K. (2001) Precompaction exposure of chondrules and implications. *Geochimica et Cosmochimica Acta*, 65(11), 1849-1866.
- Porcelli D. Ballentine C. J. Wieler R. (2002) An overview of noble gas geochemistry and cosmochemistry, In: Noble Gases in Geochemistry and Cosmochemistry, (ed. D. Porcelli, C. J. Ballentine. and R. Wieler), Geochemical Society & Mineralogical Society of America, *Reviews in Mineralogy and Geochemistry*, 47, 1-19.

- Prinz M., Weisberg M. K., Nehru C. E. and Delaney J. S. (1985) Chondrules of the Renazzo and Al Rais carbonaceous chondrites: Layering and accretionary growth as part of the chondrule-forming process. *16<sup>th</sup> Lunar and Planetary Science Conference*, pp. 677-678.
- Prior G. T. (1916) On the genetic relationship and classification of meteorites. *Mineralogical Magazine*, 18(83), 26-44.
- Prior G. T. (1920) The classification of meteorites. *Mineralogical Magazine*, 19(90), 51-63.
- Pun A., Keil K., Taylor G. J. and Wieler R. (1998) The Kapoeta howardite: Implications for the regolith evolution of the howardite-eucrite-diogenite parent body. *Meteoritics & Planetary Science*, 33(4), 835-851.
- Reedy R. C. (1989) Cosmogenic-nuclide production rates in interstellar grains. *20<sup>th</sup> Lunar and Planetary Science Conference*, pp. 888-889.
- Reedy R. C. (1992) Solar-proton production of neon and argon. *23<sup>rd</sup> Lunar and Planetary Science Conference*, 1133-1134.
- Reichenbach C. von (1860) Meteorite in Meteoriten. *Ann. Phys. Lpz.*, CXI, pp. 353-386
- Renne P. R., Mundil R., Balco G., Min K. and Ludwig K. R. (2010) Joint determination of  $^{40}\text{K}$  decay constants and  $^{40}\text{Ar}^*/^{40}\text{K}$  for the Fish Canyon sanidine standard, and improved accuracy for  $^{40}\text{Ar}/^{39}\text{Ar}$  geochronology. *Geochimica et Cosmochimica Acta*, 74(18), 5349.
- Reynolds J. H. and Turner G. (1964) Rare gases in the chondrite Renazzo. *Journal of Geophysical Research*, 69(15), 3263-3281.
- Rosato A., Strandburg K. J., Prinz F. and Swendsen R. H. (1987) Why the Brazil nuts are on top: Size segregation of particulate matter by shaking. *Physical Review Letters*, 58(10), 1038.
- Rosato A. D., Blackmore D. L., Zhang N. and Lan Y. (2002) A perspective on vibration-induced size segregation of granular materials. *Chemical Engineering Science*, 57(2), 265-275.
- Rose G. (1864) Beschreibung und Einteilung der Meteoriten auf Grund der Sammlung im Mineralogischen Museum zu Berlin. Königliche Akademie der Wissenschaften, Berlin.
- Roth A. S. G., Baur H., Heber V. S., Reusser E., and Wieler R. (2008) Exposure ages of chondrules in Allende and Murchison. *71<sup>st</sup> Meteoritical Society*, abstract #5217.
- Roth A. S. G., Baur H., Heber V. S., Reusser E. and Wieler R. (2009) Cosmic-ray-produced helium and neon in chondrules in Allende and Murchison, *40<sup>th</sup> Lunar and Planetary Science Conference*, abstract #1838.
- Roth A. S. G., Baur H., Heber V. S., Reusser E. and Wieler R. (2011) Cosmogenic helium and neon in individual chondrules from Allende and Murchison: Implications for the precompaction exposure history of chondrules. *Meteoritics & Planetary Science*, 46(7), 989-1006.
- Rubin A. E. (1984) Coarse-grained chondrule rims in type 3 chondrites. *Geochimica et Cosmochimica Acta*, 48(9), 1779-1789.
- Rubin A. E. and Wasson J. T. (1987) Chondrules, matrix and coarse-grained chondrule rims in the Allende meteorite: Origin, interrelationships and possible precursor components. *Geochimica et Cosmochimica Acta*, 51(7), 1923-1937.
- Rubin A. E., Scott E. R. D. and Keil K. (1997) Shock metamorphism of enstatite chondrites. *Geochimica et Cosmochimica Acta*, 61(4), 847-858.
- Rubin A. E., Trigo-Rodríguez J. M., Huber H. and Wasson J. T. (2007) Progressive aqueous alteration of CM carbonaceous chondrites. *Geochimica et Cosmochimica Acta*, 71(9), 2361-2382.
- Rubin A. E. (2010) Physical properties of chondrules in different chondrite groups: Implications for multiple melting events in dusty environments. *Geochimica et Cosmochimica Acta*, 74, 4807-4828.
- Russell S. S., Srinivasan G., Huss G. R., Wasserburg G. J., and MacPherson G. J. (1996) Evidence for widespread  $^{26}\text{Al}$  in the solar nebula and constraints for nebula time scales. *Science*, 273(5276), 757-762.
- Russell S. S., Zipfel J., Grossman J. N. and Grady M. M. (2002) The Meteoritical Bulletin, No. 86. *Meteoritics & Planetary Science*, 37(S5), A157-A184.
- Russell S. S., Zolensky M., Righter K., Folco L., Jones R., Connolly Jr. H. C., Grady M. M. and Grossman J. N. (2005) The Meteoritical Bulletin, No. 89. *Meteoritics & Planetary Science*, 40(9), A201-A263.

- Russell S. S., Armytage R., Bodenan J.-D., Franchi I. A., Jeffries T., Spratt J. and Starkey N. A. (2013) Relationship between CAIs and chondrules: What we can learn from a chondrule-CAI hybrid from the Allende CV3 meteorite. *44<sup>th</sup> Lunar and Planetary Science Conference, abstract #2062*.
- Sanders I. S. and Scott E. R. D. (2012) The origin of chondrules and chondrites: Debris from low-velocity impacts between molten planetesimals? *Meteoritics & Planetary Science, 47(12)*, 2170-2192.
- Scherer P., Schultz L. and Weber H. (1997a) Comparative noble gas study of CK, CV, and some unusual carbonaceous chondrites. *Meteoritics and Planetary Science, 32*, A115.
- Scherer P., Schultz L., Neupert U., Knauer M., Neumann S., Leya I., Michel R., Mokoš J., Lipschutz M. E., Metzler K., Suter M. and Kubik P. W. (1997b) Allan Hills 88019: An Antarctic H-chondrite with a very long terrestrial age. *Meteoritics & Planetary Science, 32(6)*, 769-773.
- Scherer P., Herrmann S. and Schultz L. (1998) Noble gases in twenty-one Saharan LL-chondrites: Exposure ages and possible pairings. *Meteoritics & Planetary Science, 33(2)*, 259-265.
- Scherer P. and Schultz L. (2000) Noble gas record, collisional history, and pairing of CV, CO, CK, and other carbonaceous chondrites. *Meteoritics & Planetary Science, 35(1)*, 145-153.
- Schneider D. M., Symes S. J. K., Benoit P. H. and Sears D. W. G. (2002) Properties of chondrules in EL3 chondrites, comparison with EH3 chondrites, and the implications for the formation of enstatite chondrites. *Meteoritics and Planetary Science, 37*, 1401-1416.
- Schrader D. L., Franchi I. A., Connolly Jr. H. C., Greenwood R. C., Lauretta D. S. and Gibson J. M. (2011) The formation and alteration of the Renazzo-like carbonaceous chondrites I: Implications of bulk-oxygen isotopic composition. *Geochimica et Cosmochimica Acta, 75(1)*, 308-325.
- Schrader D. L., Nagashima K. and Krot A. N. (2013) Variations in oxygen-isotope compositions of the gaseous reservoir during formation of type-I and type-II chondrules in CR carbonaceous chondrites. *44<sup>th</sup> Lunar and Planetary Science Conference, abstract #2616*.
- Schultz L., Signer P., Lorin J. C. and Pellas P. (1972) Complex irradiation history of the Weston chondrite. *Earth and Planetary Science Letters, 15(4)*, 403-410.
- Schultz L. and Signer P. (1973) *private communication*, cited in Schultz and Franke (2004).
- Schultz L. and Signer P. (1976) Depth dependence of spallogenic helium, neon, and argon in the St. Severin chondrite. *Earth and Planetary Science Letters, 30(2)*, 191-199.
- Schultz L. and Signer P. (1977) Noble gases in the St. Mesmin chondrite: Implications to the irradiation history of a brecciated meteorite. *Earth and Planetary Science Letters, 36(3)*, 363-371.
- Schultz L. and Freundel M. (1985) On the production rate of <sup>21</sup>Ne in ordinary chondrites. In *Isotopic ratios in the solar system* (ed. Centre National d'Etudes Spatiales), pp. 27-33.
- Schultz L., Weber H. W. and Begemann F. (1991) Noble gases in H-chondrites and potential differences between Antarctic and non-Antarctic meteorites. *Geochimica et Cosmochimica Acta, 55(1)*, 59-66.
- Schultz L. and Franke L. (2004) Helium, neon, and argon in meteorites: A data collection. *Meteoritics & Planetary Science, 39(11)*, 1889-1890.
- Schultz P. H. and Gault D. E. (1975) Seismic effects from major basin formations on the Moon and Mercury. *The Moon, 12(2)*, 159-177.
- Schwenzer S. P., Herrmann S., Mohapatra R. K. and Ott U. (2007) Noble gases in mineral separates from three shergottites: Shergotty, Zagami, and EETA79001. *Meteoritics & Planetary Science, 42(3)*, 387-412.
- Scott E. R. D. and Taylor G. J. (1983) Chondrules and other components in C, O, and E chondrites: similarities in their properties and origins. *Journal of Geophysical Research, 88*, B275 - B286.
- Scott E. R. D., Keil K. and Stöfler D. (1992) Shock metamorphism of carbonaceous chondrites. *Geochimica et Cosmochimica Acta, 56(12)*, 4281-4293.
- Scott E. R. D. (2007) Chondrites and the protoplanetary disk, *Annu. Rev. Earth Planet. Sci.*, 35, 577-620.
- Sears D. W. G. and Dodd R. T. (1988) Overview and classification of meteorites. In *Meteorites and the Early Solar System I*, (ed. J. F. Kerridge and M. S. Matthews), The University of Arizona Press, pp. 3-31.
- Sears D. W. G., Jie L., Benoit P. H., Dehart J. M. and Lofgren G. E. (1992) A compositional classification scheme for meteoritic chondrules. *Nature, 357*, 207-210.

- Sears D. W. G., Shaoxiong H. and Benoit P. H. (1995) Chondrule formation, metamorphism, brecciation, an important new primary chondrule group, and the classification of chondrules. *Earth and Planetary Science Letters*, 131(1), 27-39.
- Sears D. W. G. (2004) The origin of chondrules and chondrites. Cambridge University Press, pp. 209.
- Shinbrot T. and Muzzio F. J. (1998) Reverse buoyancy in shaken granular beds. *Physical Review Letters*, 81(20), 4365-4368.
- Shinbrot T. (2004) Granular materials: The brazil nut effect - in reverse. *Nature*, 429(6990), 352-353.
- Shu F. H., Shang H. and Lee T. (1996) Toward an astrophysical theory of chondrites. *Science*, 271(5255), 1545-1552.
- Shu F. H., Shang H., Glassgold A. E. and Lee T. (1997) X-rays and fluctuating X-winds from protostars. *Science*, 277(5331), 1475-1479.
- Shu F. H., Shang H., Gounelle M., Glassgold A. E. and Lee T. (2001) The origin of chondrules and refractory inclusions in chondritic meteorites. *The Astrophysical Journal*, 548(2), 1029-1050.
- Smith S. P., Huneke J. C., Rajan R. S. and Wasserburg G. J. (1977) Neon and argon in the Allende meteorite. *Geochimica et Cosmochimica Acta*, 41(5), 627-647.
- Stracke A., Palme H., Gellissen M., Münker C., Kleine T., Birbaum K., Günther D., Bourdon B. and Zipfel J. (2012) Refractory element fractionation in the Allende meteorite: Implications for solar nebula condensation and the chondritic composition of planetary bodies. *Geochimica et Cosmochimica Acta*, 85, 114-141.
- Strashnov I. and Gilmour J. D. (2012) Cosmic ray exposure history of individual chondrules from Allegan H5 ordinary chondrite probed by  $^{81}\text{Kr}$ -Kr chronometer. *43<sup>th</sup> Lunar and Planetary Science Conference*, abstract #1820.
- Stöffler D., Keil K. and Scott E. R. D. (1991) Shock metamorphism of ordinary chondrites. *Geochimica et Cosmochimica Acta*, 55, 3845-3867.
- Tachibana S. and Huss G. R. (2005) Sulfur isotope composition of putative primary troilite in chondrules from Bishunpur and Semarkona. *Geochimica et Cosmochimica Acta*, 69(12), 3075-3097.
- Takahashi H., Janssens M.-J., Morgan J. W., and Anders E. (1978) Further studies of trace elements in C3 chondrites. *Geochimica et Cosmochimica Acta*, 42(1), 97-106.
- Tancredi G., Maciel A., Heredia L., Richeri P. and Nesmachnow S. (2012) Granular physics in low-gravity environments using discrete element method. *Monthly Notices of the Royal Astronomical Society*, 420(4), 3368-3380.
- Tenner T. J., Nakashima D., Ushikubo T., Kita N. T. and Weisberg M. K. (2011) Oxygen isotope ratios in chondrules from primitive CR chondrite MET 00426: a correlation with chondrule Mg#. *74<sup>th</sup> Meteoritical Society*, abstract #5366.
- Tenner T. J., Nakashima D., Ushikubo T., Kita N. T. and Weisberg M. K. (2012) Oxygen isotopes of chondrules in the Queen Alexandra Range 99177 CR3 chondrite: Further evidence for systematic relationships between chondrule Mg# and  $\Delta^{17}\text{O}$  and the role of ice during chondrule formation. *43<sup>d</sup> Lunar and Planetary Science Conference*, abstract #2127.
- Tonui E., Zolensky M., Lipschutz M. and Okudaira K. (2001) Petrographic and chemical evidence of thermal metamorphism in new carbonaceous chondrites. *Meteoritics and Planetary Science*, 36, Supplement, A207.
- Tomeoka K. and Tanimura I. (2000) Phyllosilicate-rich chondrule rims in the Vigarano CV3 chondrite: Evidence for parent-body processes. *Geochimica et Cosmochimica Acta*, 64(11), 1971-1988.
- Trappitsch R. and Leya I. (2013) Cosmogenic production rates and recoil loss effects in micrometeorites and interplanetary dust particles. *Meteoritics & Planetary Science*, 48(2), 195-210.
- Trigo-Rodriguez J. M., Rubin A. E. and Wasson J. T. (2006) Non-nebular origin of dark mantles around chondrules and inclusions in CM chondrites. *Geochimica et Cosmochimica Acta*, 70(5), 1271-1290.
- Trieloff M., Falter M., Buikin A. I., Korochantseva E. V., Jessberger E. K. and Altherr R. (2005) Argon isotope fractionation induced by stepwise heating. *Geochimica et Cosmochimica Acta*, 69(5), 1253-1264.
- Tschermak G. (1885) Die mikroskopische Beschaffenheit der Meteoriten. *Smithsonian Contributions to Astrophysics*, 4, 137-239 (1964, translated by J. A. Wood and E. M. Wood).

- Ushikubo T., Kimura M., Nakashima D. and Kita N. T. (2010) A combined study of the Al-Mg systematics and O isotope ratios of chondrules from the primitive carbonaceous chondrite Acfer 094. *41<sup>th</sup> Lunar and Planetary Science Conference, abstract #1491*.
- Ushikubo T., Kimura M., Kita N. T. and Valley J. W. (2012) Primordial oxygen isotope reservoirs of the solar nebula recorded in chondrules in Acfer 094 carbonaceous chondrite. *Geochimica et Cosmochimica Acta*, 90, 242-264.
- Van Schmus W. R. and Wood J. A. (1967) A chemical-petrologic classification for the chondritic meteorites. *Geochimica et Cosmochimica Acta*, 31, 747-765.
- Varela M. E., Zinner E., Kurat G., and Magnelli D. (2011) Acfer 182 Chondrules Give Evidence for Direct Condensation of Enstatite-Rich Liquids from the Solar Nebula. *42<sup>nd</sup> Lunar and Planetary Science Conference, abstract #1497*.
- Vogel N., Wieler R., Bischoff A. and Baur H. (2003) Microdistribution of primordial Ne and Ar in fine-grained rims, matrices, and dark inclusions of unequilibrated chondrites - Clues on nebular processes. *Meteoritics & Planetary Science*, 38(9), 1399-1418.
- Vogel N., Leya I., Bischoff A., Baur H., and Wieler R. (2004) Noble gases in chondrules and associated metal-sulfide-rich samples: Clues on chondrule formation and the behavior of noble gas carrier phases. *Meteoritics & Planetary Science*, 39(1), 117-135.
- Vogel N., Baur H., Bischoff A., Leya I., Roszjar J. and Wieler R. (2009) <sup>81</sup>Kr-Kr dating to detect pre-irradiation effects in CAIs: Feasibility and first results. *72<sup>nd</sup> Meeting Meteoritical Society, abstract #5320*.
- Vollmer C., Hoppe P., Stadermann F. J., Floss C. and Brenker F. E. (2009) NanoSIMS analysis and Auger electron spectroscopy of silicate and oxide stardust from the carbonaceous chondrite Acfer 094. *Geochimica et Cosmochimica Acta*, 73(23), 7127-7149.
- Wasson J. T. (1974) Meteorites. Classification and properties. Springer-Verlag New York, pp. 327.
- Wasson J. T. and Kallemeyn G. W. (1988) Compositions of chondrites. *Philosophical Transactions of the Royal Society of London. Series A, Mathematical and Physical Sciences*, 325(1587), 535-544.
- Wasson J. T. (1993) Constraints on chondrule origins. *Meteoritics*, 28(1), 14-28.
- Wasson J. T., Krot A. N., Lee M. S. and Rubin A. E. (1995) Compound chondrules. *Geochimica et Cosmochimica Acta*, 59(9), 1847-1869.
- Wasson J. T., Kallemeyn G. W. and Rubin A. E. (2000) Chondrules in the LEW85332 ungrouped carbonaceous chondrite: Fractionation processes in the solar nebula. *Geochimica et Cosmochimica Acta*, 64(7), 1279-1290.
- Wasson J. T. and Rubin A. E. (2010) Matrix and whole-rock fractionations in the Acfer 094 type 3.0 ungrouped carbonaceous chondrite. *Meteoritics & Planetary Science*, 45(1), 73-90.
- Weidenschilling S. J. (1977) Aerodynamics of solid bodies in the solar nebula. *Monthly Notices of the Royal Astronomical Society*, 180, 57-70.
- Weinbruch S., Styrsa V. and Müller W. F. (2003) Exsolution and coarsening in iron-free clinopyroxene during isothermal annealing. *Geochimica et Cosmochimica Acta*, 67(24), 5071-5082.
- Weisberg M. K., Prinz M. and Nehru C. E. (1988) Macrochondrules in ordinary chondrites: Constraints on chondrule forming processes. *Meteoritics*, 23, 309-310.
- Weisberg M. and Prinz M. (1991) El Djouf 001: A new CR2 chondrite. *Meteoritics*, 26, 406.
- Weisberg M. K., Prinz M., Clayton R. N. and Mayeda T. K. (1993) The CR (Renazzo-type) carbonaceous chondrite group and its implications. *Geochimica et Cosmochimica Acta*, 57(7), 1567-1586.
- Weisberg M. K., Prinz M., Clayton R. N., Mayeda T. K., Grady M. M., Franchi I., Pillinger C. T. and Kallemeyn G. W. (1996) The K (Kakangari) chondrite grouplet. *Geochimica et Cosmochimica Acta*, 60(21), 4253-4263.
- Weisberg M. K., Prinz M., Clayton R. and Mayeda T. (1997) CV3 chondrites: Three subgroups, not two. *Meteoritics and Planetary Science*, 32, Supplement, A138.
- Weisberg M. K. and Prinz M. (2000) The Grosvenor Mountains 95577 CR1 chondrite and hydration of the CR chondrites. *Meteoritics and Planetary Science*, 35, Supplement, A168.
- Weisberg M. K. (2001) Sahara 00182, the first CR3 chondrite and formation of multi-layered chondrules. *Meteoritics and Planetary Science*, 36, Supplement, A222.



- Weisberg, M. K., McCoy, T. J. and Krot, A. N. (2006) Systematics and evaluation of meteorite classification. In *Meteorites and the Early Solar System II*, (ed. D. S. Lauretta and H. Y. McSween, Jr.), The University of Arizona Press, pp. 19-52.
- Welten K. C., Alderliesten C., van der Borg K., Lindner L., Loeken T. and Schultz L. (1997) Lewis Cliff 86360: An Antarctic L-chondrite with a terrestrial age of 2.35 million years. *Meteoritics & Planetary Science*, 32(6), 775-780.
- Wetherill G. W. (1954) Variations in the isotopic abundances of neon and argon extracted from radioactive minerals. *Physical Review*, 96(3), 679-683.
- Weyrauch M. and Bischoff A. (2012) Macrochondrules in chondrites—Formation by melting of mega-sized dust aggregates and/or by rapid collisions at high temperatures? *Meteoritics & Planetary Science*, 47(12), 2237-2250.
- Wiedenbeck M. E. (2013) Elemental and isotopic composition measurements of galactic cosmic rays. *AIP Conference Proceedings*, 1516, 150-155.
- Wieler R., Graf Th. and Signer P. (1986) Pre-exposure of clasts in Fayetteville's progenitor asteroidal regolith. 17<sup>th</sup> *Lunar and Planetary Science Conference*, pp. 600.
- Wieler R., Graf Th., Pedroni A., Signer P., Pellas P., Fieni C., Suter M., Vogt S., Clayton R. N. and Laul J. C. (1989) Exposure history of the regolithic chondrite Fayetteville: II. Solar-gas-free light inclusions. *Geochimica et Cosmochimica Acta*, 53(6), 1449-1459.
- Wieler R., Pedroni A. and Leya I. (2000) Cosmogenic neon in mineral separates from Kapoeta: No evidence for an irradiation of its parent body regolith by an early active Sun. *Meteoritics & Planetary Science*, 35(2), 251-257.
- Wieler R. (2002a) Noble gases in the Solar System. In *Noble Gases in Geochemistry and Cosmochemistry*, (ed. Porcelli D., Ballentine C. J. and Wieler R.), Geochemical Society & Mineralogical Society of America, *Reviews in Mineralogy and Geochemistry*, 47, 21-70.
- Wieler R. (2002b) Cosmic ray-produced noble gases in meteorites. In *Noble Gases in Geochemistry and Cosmochemistry*, (ed. Porcelli D., Ballentine C. J. and Wieler R.), Geochemical Society & Mineralogical Society of America, *Reviews in Mineralogy and Geochemistry*, 47, 125-170.
- Wlotzka F. (1991) The Meteoritical Bulletin, No. 71 (*Meteoritics*, 26, 255-262)
- Wlotzka F. (1993) A weathering scale for the ordinary chondrites. *Meteoritics*, 28, 460.
- Wood J. A. (1962) Metamorphism in chondrites. *Geochimica et Cosmochimica Acta*, 26(7), 739-749.
- Wood, J. A. (1996) Unresolved issues in the formation of chondrules and chondrites. In *Chondrules and the Protoplanetary Disk*, (ed. R.H. Hewins, R.H. Jones, E.R.D. Scott), Cambridge University Press, Cambridge, pp. 55–69.
- Woolum D. S. and Hohenberg C. (1993) Energetic particle environment in the early solar system—extremely long pre-compaction meteoritic ages or an enhanced early particle flux. In *Protostars and Planets III*, (ed. E. H. Levy, J. I. Lunine, M. A. Reynolds and D. D. Bogard), The University of Arizona Press, pp. 903-919.
- Yano H., Kubota T., Miyamoto H., Okada T., Scheeres D., Takagi Y., Yoshida K., Abe M., Abe S., Barnouin-Jha O., Fujiwara F, Hasegawa S., Hashimoto T., Ishiguro M., Kato, M. Kawaguchi J., Mukai T., Saito J., Sasaki S and Yoshikada M. (2006) Touchdown of the Hayabusa spacecraft at the Muses Sea on Itokawa. *Science*, 312(5778), 1350-1353.
- Zanda B., Bourot-Denise M., Hewins R. H., Cohen B. A., Delaney J. S., Humayun M. and Campbell A. J. (2002) Accretion textures, iron evaporation and re-condensation in Renazzo chondrules, 33<sup>rd</sup> *Lunar and Planetary Science Conference*, abstract#1852.
- Zanda B. (2004) Chondrules. *Earth and Planetary Science Letters*, 224(1-2), 1-17.
- Ziegler J. F. (2004) SRIM-2003. *Nuclear Instruments and Methods in Physics Research Section B: Beam Interactions with Materials and Atoms*, 219-220, 1027-1036.

## Appendix

Appendix 1: Target element abundances used for calculation of production of cosmogenic noble gases of all matrix (mat) and chondrule (ch) samples. ....	145
Appendix 2: Additional elemental abundances of all matrix (mat) and chondrule (ch) samples.....	147
Appendix 3: Concentrations of $^{22}\text{Ne}$ , $^{20}\text{Ne}_{\text{tr}}$ , $^{21}\text{Ne}_{\text{c}}$ , $^{20}\text{Ne}/^{22}\text{Ne}$ , $^{21}\text{Ne}/^{22}\text{Ne}$ and shielding parameters $(^{22}\text{Ne}/^{21}\text{Ne})_{\text{c}}$ of all matrix (mat) and chondrule (ch) samples. ....	148
Appendix 4: Concentrations of $^3\text{He}$ , $^4\text{He}$ and $^3\text{He}/^4\text{He}$ of all matrix (mat) and chondrule (ch) samples. ....	149
Appendix 5: Concentrations of $^{40}\text{Ar}$ , $^{36}\text{Ar}_{\text{tr}}$ , $^{38}\text{Ar}_{\text{c}}$ , $^{38}\text{Ar}/^{36}\text{Ar}$ and $^{40}\text{Ar}/^{36}\text{Ar}$ of all matrix (mat) and chondrule (ch) samples. ....	150

**Appendix 1: Target element abundances used for calculation of production of cosmogenic noble gases of all matrix (mat) and chondrule (ch) samples.**

	weight	Mg	Al	Si min <sup>a</sup>	Si max <sup>a</sup>	Ca	Fe	Ni	Mn	Cr	Ti	K
<i>CR2 chondrites</i>												
Re-mat	13.2	9.45(3)	1.06(4)	17.3(1.1)	21.0(1.1)	1.53(9)	26.1(9)	1.49(17)	0.134(5)	0.260(9)	0.018	0.159
Re-ch1	0.07	11.5(4)	1.03(4)	16.2(1.2)	19.9(1.2)	1.66(17)	26.4(13)	1.17(29)	0.160	0.326(17)	0.078	0.112
Re-ch2	1.52	12.5(4)	1.21(8)	15.9(1.1)	19.5(1.1)	1.12(9)	25.4(9)	1.43(20)	0.168	0.395(14)	0.042	0.248
El-mat	13.0	8.87(47)	1.06(4)	15.9(1.1)	20.0(1.1)	1.18(9)	28.6(1.0)	1.87(17)	0.156(5)	0.311(12)	1.394(50)	0.132(7)
El-ch2	1.70	13.7(5)	1.08(4)	18.0(1.1)	21.0(1.1)	1.18(7)	22.2(8)	0.19	0.092(3)	0.371(13)	0.075	0.009(1)
El-ch3	17.0	22.4(8)	1.16(4)	19.2(1.1)	20.3(1.1)	1.12(10)	8.43(30)	0.45	0.156(5)	0.508(18)	0.099(11)	0.024(2)
El-ch4	7.80	19.3(7)	1.81(6)	17.0(1.1)	18.9(1.1)	2.45(12)	13.5(5)	0.79(18)	0.137(5)	0.372(13)	0.100(12)	0.012(1)
El-ch5	6.62	19.7(7)	2.31(8)	18.1(1.1)	19.6(1.1)	2.20(10)	11.0(4)	0.14	0.129(5)	0.369(13)	0.111(13)	0.130
El-ch6	1.43	18.3(7)	1.29(5)	20.3(1.1)	21.8(1.1)	1.39(12)	10.4(4)	0.46	0.462(16)	0.466(17)	0.081	0.101(7)
El-ch7	4.63	16.0(6)	1.10(4)	18.6(1.1)	21.1(1.1)	1.02(6)	17.1(6)	1.05(15)	0.138(5)	0.435(15)	0.057(12)	0.147
El-ch8	5.05	14.1(5)	4.25(15)	23.5(1.0)	24.8(1.0)	4.28(22)	9.28(35)	0.21	0.085(3)	0.329(12)	0.252(28)	0.123
El-ch9	7.85	18.3(6)	1.45(5)	16.5(1.1)	18.9(1.1)	1.75(8)	16.7(6)	0.96(13)	0.096(3)	0.412(15)	0.094(10)	0.022(2)
El-ch10	4.80	14.6(0)	1.17(4)	18.0(1.0)	20.7(1.0)	1.53(8)	19.4(7)	1.10(17)	0.172(7)	0.467(17)	0.063(11)	0.020(1)
El-ch11a	1.51	13.0(5)	1.26(4)	18.1(1.2)	21.0(1.1)	1.21(10)	21.3(8)	0.64	0.318(11)	0.468(16)	0.044	0.358
El-ch11b	1.90	13.7(5)	1.40(5)	17.4(1.2)	20.3(1.2)	1.59(9)	20.8(7)	0.49	0.342(12)	0.497(17)	0.028	0.426
NWA-mat	10.7	8.35(30)	0.92(3)	14.8(1.1)	19.5(1.1)	0.83(8)	33.2(1.2)	1.85(21)	0.145(5)	0.278(10)	0.023	0.174
NWA-ch1	3.18	18.3(6)	1.38(5)	11.8(1.1)	15.3(1.1)	1.29(7)	23.8(8)	2.10(19)	0.100(4)	0.389(14)	0.084(13)	0.250
NWA-ch2	4.13	17.9(6)	0.05(3)	9.85(1.2)	14.1(1.1)	1.06(6)	29.7(1.0)	2.21(15)	0.106(4)	0.381(13)	0.065(11)	0.245
<i>CR3 chondrites</i>												
MET-mat	17.1	10.8(4)	1.06(4)	19.6(1.1)	22.6(1.1)	1.30(8)	21.9(8)	0.56	0.163(6)	0.299(11)	0.070(13)	0.478
MET-ch1	0.81	0.11(1)	0.01(0)	0.0	0.00	0.00	95.5(3.4)	5.44(19)	0.005(0)	0.249(9)	0.005	0.020
MET-ch2	1.26	18.6(7)	2.34(8)	15.8(1.1)	18.0(1.1)	1.72(11)	15.8(6)	1.24(14)	0.123(4)	0.362(13)	0.092(23)	0.187
MET-ch3	4.03	17.1(6)	1.41(5)	11.5(1.1)	15.2(1.1)	1.63(7)	25.8(9)	1.76(9)	0.082(3)	0.454(16)	0.076(11)	0.004
MET-ch4	2.17	15.3(5)	1.06(4)	14.9(1.1)	18.3(1.1)	0.98(8)	24.0(8)	1.36(16)	0.139(5)	0.433(15)	0.029	0.307
MET-ch5	2.26	16.7(6)	1.48(5)	17.6(1.1)	20.0(1.1)	1.43(8)	16.9(6)	1.10(14)	0.120(4)	0.440(15)	0.083(16)	0.243
MET-ch6	8.39	15.8(6)	1.41(5)	15.3(1.1)	18.4(1.1)	1.26(14)	21.7(8)	1.22(17)	0.189(7)	0.427(15)	0.080(12)	0.359
QUE-mat	20.3	9.33(33)	0.93(3)	16.3(1.1)	20.5(1.1)	0.91(9)	29.5(1.1)	1.41(21)	0.129(5)	0.268(10)	0.053(11)	0.365
QUE-ch1	1.01	16.6(6)	1.43(5)	13.3(1.1)	16.7(1.1)	1.27(12)	24.2(1.1)	1.43(12)	0.177(6)	0.507(18)	0.041	0.014(2)
QUE-ch2	0.72	19.9(7)	1.46(5)	17.1(1.1)	19.0(1.1)	1.59(13)	12.5(1.0)	1.30	0.435(15)	0.587(21)	0.054	0.083(5)
QUE-ch3	4.56	17.5(6)	1.41(5)	14.7(1.1)	17.6(1.1)	1.27(6)	20.1(7)	1.34(15)	0.336(12)	0.541(19)	0.075(15)	0.347

QUE-ch4	3.90	19.1(7)	1.72(6)	17.2(1.1)	19.2(1.1)	2.04(11)	13.6(5)	0.92(17)	0.118(4)	0.404(14)	0.096(14)	0.265
QUE-ch5	1.67	17.1(6)	1.24(4)	19.7(1.1)	21.5(1.0)	1.47(14)	12.5(5)	0.98	0.328(11)	0.413(15)	0.040	0.618
QUE-ch6	9.99	15.6(5)	1.49(5)	16.0(1.1)	18.9(1.1)	1.53(7)	20.2(7)	1.36(14)	0.215(8)	0.469(17)	0.090(12)	0.312
<i>CV3 chondrites</i>												
Al-mat	38.7	13.3(7)	1.24(4)	15.5(1.1)	21.6(1.1)	1.38(6)	25.1(9)	1.39(11)	0.150(5)	0.334(12)	0.060(8)	0.021(3)
Al-ch3	5.28	20.6(5)	1.94(7)	14.8(1.1)	19.6(1.1)	1.09(8)	15.9(6)	1.38(11)	0.067(2)	0.408(14)	0.108(12)	0.035(4)
Al-ch6	1.30	19.6(7)	2.20(8)	14.6(1.1)	19.5(1.1)	2.05(10)	16.0(6)	1.12(23)	0.117(4)	0.497(17)	0.095(16)	0.035(4)
Vi-mat	21.6	13.9(9)	1.74(6)	15.7(1.1)	18.7(1.1)	2.17(9)	21.3(8)	1.25(26)	0.149(5)	0.321(11)	1.038(38)	0.031(6)
Vi-ch1	0.58	17.7(3)	1.66(6)	23.1(1.0)	23.9(1.0)	2.05(11)	6.49(30)	0.13	0.104(4)	0.288(12)	0.150(28)	0.035(3)
Vi-ch2	1.31	11.2(6)	1.24(4)	19.0(1.1)	21.8(1.1)	2.76(13)	20.4(9)	0.19	0.144(5)	0.304(12)	0.072(15)	0.086(9)
Vi-ch3	0.37	24.8(4)	1.15(4)	14.3(1.1)	16.2(1.1)	1.42(7)	12.8(5)	0.45(7)	0.063(2)	0.392(14)	0.079(9)	0.003
A82-mat	20.0	10.8(4)	2.16(8)	17.0(1.1)	20.3(1.1)	2.58(15)	23.2(8)	1.24(29)	0.133(5)	0.264(10)	0.066(14)	0.181
A82-ch1	0.38	25.0(4)	0.81(8)	15.9(1.1)	17.4(1.1)	1.43(15)	10.5(8)	0.98(29)	0.080(5)	0.384(10)	0.036	0.021
A82-ch2	2.60	20.0(7)	1.32(5)	17.7(1.1)	19.6(1.1)	1.19(6)	13.5(6)	0.71(8)	0.102(4)	0.399(14)	0.117(14)	0.030(4)
A82-ch3	4.18	17.4(6)	1.02(4)	14.5(1.1)	17.6(1.1)	0.98(6)	22.5(8)	1.13(17)	0.104(4)	0.398(14)	0.061(10)	0.221
<i>Ungrouped 3 chondrite</i>												
A94-mat	7.43	7.91(28)	1.22(4)	20.2(1.1)	23.6(1.1)	1.54(10)	24.4(9)	0.59	0.162(6)	0.241(9)	0.019	0.443
A94-ch1	0.47	12.1(4)	1.46(7)	16.9(1.1)	20.1(1.1)	1.89(13)	23.9(1.0)	0.56	0.246(9)	0.374(14)	0.052	0.445

Sample weights are given in mg, abundances in wt%. <sup>3</sup>Si was calculated by converting the major elements into oxides, and assuming the remainder to be SiO<sub>2</sub>. Iron is a special case, since it also occurs as metal and sulfide. For “Si minimal” Fe is assumed as being completely oxidized in silicates as FeO, for “Si maximal” Fe is assumed to be present exclusively as metal and sulfide. Uncertainties (1 s. d.) are given in parenthesis. Where values are marked in gray, concentrations were below the detection limit; the listed values (also used in calculating production rates) are 1/2 the detection limit.

**Appendix 2: Additional elemental abundances of all matrix (mat) and chondrule (ch) samples.**

	Cl	Na	V	Co	Au
<i>CR2 chondrites</i>					
Re-mat	2292(86)	10770(386)	58.91(2.30)	811.7(36.2)	0.207(13)
Re-ch1	306.3(36.4)	469.3(18.3)	58.90(5.05)	634.2(23.5)	0.077
Re-ch2	171.2(18.1)	1055(44)	65.57(2.86)	681.8(25.7)	0.202(16)
El-mat	412.9(22.0)	1265(67)	667.4(23.6)	884.8(48.2)	0.236(75)
El-ch2	76.62(9.81)	371.4(14.1)	70.81(2.98)	605.8(22.3)	0.013
El-ch3	35.76	487.3(18.7)	94.95(3.44)	200.7(7.2)	0.023
El-ch4	33.61	266.8(9.5)	106.5(3.9)	351.3(12.6)	0.031(4)
El-ch5	868.4(55.1)	384.6(22.4)	118.4(4.4)	321.4(16.4)	0.013
El-ch6	4838(177)	4322(170)	90.69(3.98)	151.9(8.2)	0.016
El-ch7	920.7(39.4)	657.0(34)	79.30(2.96)	480.4(29.3)	0.056(8)
El-ch8	1336(67)	1551(63)	150.3(5.5)	251.1(14.9)	0.432
El-ch9	536.1(26.5)	1013(39)	97.60(3.77)	472.3(26.4)	0.028(4)
El-ch10	1362(65)	1246(66)	75.43(2.82)	522.4(26.5)	0.055(6)
El-ch11a	321.5(51.3)	2905(130)	84.64(3.44)	491.8(18.5)	0.024
El-ch11b	154.5(25.9)	3526(156)	88.74(3.71)	454.2(18.3)	0.019
NWA-mat	1231(55)	1400(60)	63.26(2.93)	881.6(35.8)	0.093(15)
NWA-ch1	32.33	621.8(29.0)	109.7(4.1)	945.6(34.3)	0.036
NWA-ch2	113.2(13.9)	314.1(17.0)	99.76(3.65)	977.7(36.7)	0.090(13)
<i>CR3 chondrites</i>					
MET-mat	2928(114)	5025(184)	64.60(2.47)	504.6(24.4)	0.121
MET-ch1	63.90(3.49)	9.72(1.14)	14.79(0.69)	2600(92)	0.365(29)
MET-ch2	75.03(10.72)	973(46)	128.7(5.0)	495.7(19.3)	0.102(18)
MET-ch3	68.49(7.83)	1084(39)	97.84(3.62)	809.8(33.4)	0.079(7)
MET-ch4	74.66(16.65)	700.7(40.5)	82.45(3.54)	543.3(36.4)	0.112(18)
MET-ch5	36.46	389.9(32.2)	105.3(4.0)	563.7(21.0)	0.057(13)
MET-ch6	76.57(15.89)	1272(63)	88.58(3.24)	672.8(24.2)	0.042
QUE-mat	1701(69)	2150(88)	56.82(2.17)	758.5(26.8)	0.079
QUE-ch1	139.9(13.6)	332.7(11.7)	75.68(3.41)	738.1(27.3)	0.076(9)
QUE-ch2	192.1(40.8)	3883(139)	104.3(4.9)	126.1(9.2)	0.040
QUE-ch3	64.3	2128(86)	88.86(3.31)	577.5(21.1)	0.123(12)
QUE-ch4	36.1	313.4(23.7)	100.2(3.7)	399.2(15.8)	0.169
QUE-ch5	86.1	2682(122)	84.57(3.49)	329.8(16.6)	0.207
QUE-ch6	37.6	1180(49)	80.03(3.03)	608.9(21.9)	0.085(13)
<i>CV3 chondrites</i>					
Al-mat	164.7(15.8)	1851(69)	71.91(2.59)	712.7(34.7)	0.153(9)
Al-ch3	217.7(15.7)	3735(139)	128.1(4.7)	651.1(23.2)	0.109(15)
Al-ch6	180.1(17.2)	4292(154)	117.3(4.4)	594.7(20.9)	0.064(15)
Vi-mat	866.2(38.6)	3129(41)	544.7(19.2)	631.1(40.4)	0.185(98)
Vi-ch1	6179(222)	3737(138)	71.6(3.2)	239.1(13.6)	0.075(14)
Vi-ch2	26950(947)	13420(502)	74.5(2.9)	539.9(40.2)	0.137(13)
Vi-ch3	94.2(9.0)	1142(41)	105.4(4.1)	409.6(15.6)	0.020
A82-mat	674.0(36.5)	1297(55)	102.4(4.1)	506.0(26.2)	0.267(27)
A82-ch1	213.2(17.6)	1018(40)	91.9(3.7)	343.4(14.9)	0.024
A82-ch2	99.5(11.5)	2052(77)	114.0(4.2)	342.6(14.9)	0.017
A82-ch3	160.4(13.6)	321.9(17.2)	89.3(3.3)	643.2(25.6)	0.186(13)
<i>Ungrouped 3 chondrite</i>					
A94-mat	2134(99)	3287(138)	67.0(2.6)	650.0(25.4)	0.664(72)
A94-ch1	63.9	877.9(41.1)	86.5(4.4)	646.6(39.2)	119.2

Abundances are given in mg/kg. Uncertainties (1 s. d.) are given in parenthesis. Where values are marked in gray, concentrations were below the detection limit; the listed values are 1/2 the detection limit.

**Appendix 3: Concentrations of  $^{22}\text{Ne}$ ,  $^{20}\text{Ne}_{\text{tr}}$ ,  $^{21}\text{Ne}_{\text{c}}$ ,  $^{20}\text{Ne}/^{22}\text{Ne}$ ,  $^{21}\text{Ne}/^{22}\text{Ne}$  and shielding parameters ( $^{22}\text{Ne}/^{21}\text{Ne}$ )<sub>c</sub> of all matrix (mat) and chondrule (ch) samples.**

	$^{22}\text{Ne}$	$^{20}\text{Ne}/^{22}\text{Ne}$	$^{21}\text{Ne}/^{22}\text{Ne}$	$^{20}\text{Ne}_{\text{tr}}$	$^{21}\text{Ne}_{\text{c}}$	( $^{22}\text{Ne}/^{21}\text{Ne}$ ) <sub>c</sub>
<i>CR2 chondrites</i>						
Re-mat	1.849(123)	3.947(24)	0.468(10)	6.402(606)	0.838(59)	1.286(126)
Re-ch1	2.264(236)	5.163(450)	0.111(67)	11.38(1.64)	0.205(164)	<sup>a</sup>
Re-ch2	2.135(152)	3.104(47)	0.575(11)	5.377(540)	1.207(90)	1.250(115)
El-mat	16.70(53)	10.70(9)	0.0800(1)	178.1(11.4)	0.834(46)	<sup>a</sup>
El-ch2	1.826(100)	2.347(34)	0.701(11)	3.053(0.280)	1.268(73)	1.171(66)
El-ch3	3.012(160)	2.063(21)	0.775(11)	4.067(370)	2.319(128)	1.115(26)
El-ch4	2.891(114)	2.164(14)	0.743(7)	4.249(360)	2.131(87)	1.135(55)
El-ch5	2.720(154)	1.216(19)	0.810(12)	1.158(169)	2.199(129)	1.178(23)
El-ch6	2.301(145)	1.170(22)	0.827(17)	0.862(140)	1.902(127)	1.161(30)
El-ch7	3.462(186)	4.382(44)	0.572(12)	13.43(1.10)	1.937(112)	1.081(66)
El-ch8	2.335(132)	2.355(35)	0.697(11)	3.923(366)	1.611(95)	1.179(68)
El-ch9	3.171(176)	3.386(50)	0.645(10)	8.874(743)	2.017(118)	1.113(63)
El-ch10	1.979(115)	1.414(22)	0.785(12)	1.275(150)	1.549(94)	1.185(29)
El-ch11a	1.818(141)	1.557(30)	0.770(13)	1.456(184)	1.395(110)	1.187(30)
NWA-mat	10.34(65)	12.04(18)	0.054(1)	124.2(10.0)	0.240(27)	<sup>a</sup>
NWA-ch1	16.23(1.25)	3.281(49)	0.657(10)	43.54(4.46)	10.53(83)	1.111(28)
NWA-ch2	20.35(1.57)	3.779(56)	0.619(10)	65.37(6.68)	12.34(97)	1.125(35)
<i>CR3 chondrites</i>						
MET-mat	39.99(4.51)	11.38(19)	0.081(2)	453.4(57.7)	2.033(252)	<sup>a</sup>
MET-ch1	0.550(31)	8.283(159)	0.347(10)	4.416(362)	0.178(11)	<sup>a</sup>
MET-ch2	22.62(1.18)	10.89(16)	0.131(2)	244.5(19.1)	2.308(144)	1.045(151)
MET-ch3	5.049(259)	7.742(111)	0.284(4)	37.95(2.97)	1.315(73)	<sup>a</sup>
MET-ch4	87.61(6.83)	12.02(18)	0.056(1)	1051(105)	2.157(268)	<sup>a</sup>
MET-ch5	14.43(1.10)	10.52(15)	0.119(3)	150.7(14.7)	1.305(111)	<sup>a</sup>
MET-ch6	30.38(3.33)	10.68(11)	0.179(1)	321.0(39.5)	4.595(530)	<sup>a</sup>
QUE-mat	3.287(376)	6.543(95)	0.210(5)	20.84(2.75)	0.609(72)	<sup>a</sup>
QUE-ch1	2.339(154)	4.460(71)	0.441(8)	9.408(0.884)	0.994(68)	1.241(148)
QUE-ch2	1.702(114)	1.377(41)	0.724(14)	1.035(200)	1.228(86)	1.285(42)
QUE-ch3	2.218(146)	2.262(35)	0.647(11)	3.523(356)	1.421(97)	1.266(54)
QUE-ch4	0.963(78)	3.690(58)	0.501(11)	3.057(325)	0.470(39)	1.275(52)
QUE-ch5	5.473(433)	4.366(456)	0.499(10)	21.45(3.13)	2.649(217)	1.116(135)
QUE-ch6	2.629(300)	3.619(40)	0.512(10)	8.138(1.082)	1.311(153)	1.267(57)
<i>CV3 chondrites</i>						
Al-mat	2.426(81)	2.211(21)	0.785(11)	3.662(298)	1.893(27)	1.084(27)
Al-ch3	2.834(108)	0.955(13)	0.930(10)	0.417(462)	2.635(65)	1.058(24)
Al-ch6	2.630(111)	0.867(50)	0.934(13)	0.106(156)	2.457(109)	1.066(17)
Vi-mat1	2.822(151)	4.399(23)	0.544(5)	11.02(92)	1.498(80)	1.118(88)
Vi-mat2	3.185(217)	4.391(23)	0.539(8)	12.43(1.17)	1.674(117)	1.118(67)
Vi-ch1	2.628(261)	1.174(46)	0.917(20)	0.990(187)	2.406(247)	1.050(25)
Vi-ch2	3.248(208)	4.747(57)	0.500(11)	13.95(1.27)	1.576(105)	1.124(111)
Vi-ch3	2.559(121)	1.422(345)	0.909(18)	1.653(2.099)	2.321(116)	1.013(59)
A82-mat	0.684(46)	5.397(37)	0.454(19)	3.421(313)	0.300(21)	1.095(73)
A82-ch1	1.159(81)	1.137(255)	0.901(21)	0.388(328)	1.043(75)	1.074(33)
A82-ch2	0.875(68)	1.036(92)	0.883(16)	0.197(96)	0.771(53)	1.107(24)
A82-ch3	0.068(7)	3.130(169)	0.680(26)	0.173(22)	0.046(5)	1.065(72)
<i>Ungrouped 3 chondrite</i>						
A94-mat	7.402(495)	7.980(50)	0.093(2)	58.57(5.38)	0.460(37)	<sup>a</sup>
A94-ch1	8.789(683)	8.246(123)	0.099(2)	71.87(7.14)	0.609(58)	<sup>a</sup>

Uncertainties (1 s. d.) are given in parenthesis. Abundances of  $^{22}\text{Ne}$ ,  $^{20}\text{Ne}_{\text{tr}}$  and  $^{21}\text{Ne}_{\text{c}}$  in units of  $10^{-8}$  cc/g. <sup>a</sup>Large uncertainties because of large dominant trapped component or Ne-E contribution (Re-ch1)

**Appendix 4: Concentrations of  $^3\text{He}$ ,  $^4\text{He}$  and  $^3\text{He}/^4\text{He}$  of all matrix (mat) and chondrule (ch) samples.**

	$^3\text{He}$	$^4\text{He}$	$(^3\text{He}/^4\text{He}) [10^{-4}]$
<i>CR2 chondrites</i>			
Re-mat	3.942(159)	2321(95)	16.95(23)
Re-ch1	1.251(625)	3474(223)	3.601(3.071)
Re-ch2	6.333(162)	2083(60)	24.59(3.01)
EI-mat	18.94(32) <sup>a</sup>	49217(1194)	3.873(93)
EI-ch2	6.498(121)	1286(24)	50.24(74)
EI-ch3	10.85(19)	2142(37)	50.40(45)
EI-ch4	9.854(193)	2768(71)	35.58(99)
EI-ch5	9.779(187)	2580(57)	37.51(69)
EI-ch6	8.978(202)	1039(20)	86.37(1.02)
EI-ch7	9.609(236)	4471(96)	21.49(25)
EI-ch8	7.837(153)	3837(84)	20.01(46)
EI-ch9	8.317(144)	3100(55)	26.57(45)
EI-ch10	7.754(149)	1326(35)	57.04(1.61)
EI-ch11a	7.029(654)	1121(108)	63.71(1.49)
NWA-mat	322.8(18.0) <sup>c</sup>	889472(52675)	3.637(51)
NWA-ch1	42.13(2.50)	21180(1277)	19.93(32)
NWA-ch2	49.32(2.94)	28577(1794)	17.29(26)
<i>CR2 chondrites</i>			
MET-mat	66.49(2.51) <sup>a</sup>	152807(9864)	4.322(78)
MET-ch1	11.48(67)	1508(89)	76.16(1.55)
MET-ch2	40.91(3.30)	81795(6656)	4.999(73)
MET-ch3	13.84(35)	12089(333)	11.42(18)
MET-ch4	103.3(6.6) <sup>a</sup>	244704(15263)	4.223(63)
MET-ch5	26.86(1.47) <sup>a</sup>	49642(2570)	5.411(93)
MET-ch6	62.90(3.09)	113770(8008)	5.471(219)
QUE-mat	4.545(177) <sup>a</sup>	3127(206)	14.50(27)
QUE-ch1	7.403(366)	2345(118)	31.83(65)
QUE-ch2	9.456(963)	1659(178)	57.56(2.14)
QUE-ch3	10.27(34)	2001(72)	51.42(89)
QUE-ch4	3.879(234)	773.5(40.5)	50.90(1.87)
QUE-ch5	16.29(92)	5425(281)	30.03(67)
QUE-ch6	9.914(403)	2448(163)	40.07(70)
<i>CV3 chondrites</i>			
AI-mat	8.574(158)	2479(67)	34.66(76)
AI-ch3	9.440(295)	3234(104)	29.24(81)
AI-ch6	9.170(404)	3061(98)	29.75(1.56)
Vi-mat1	<i>not measured</i>		
Vi-mat2	5.968(264)	2859(151)	20.81(24)
Vi-ch1	7.979(555)	2066(140)	38.61(62)
Vi-ch2	5.604(210)	2291(85)	25.68(44)
Vi-ch3	7.564(358)	1622(34)	47.70(2.18)
A82-mat	0.986(40)	310.3(12.6)	31.79(49)
A82-ch1	1.551(233)	96.51(15.03)	160.7(28.3)
A82-ch2	1.425(50)	71.24(2.73)	199.9(6.9)
A82-ch3	0.117(14)	4.817(937)	243.6(62.8)
<i>Ungrouped 3 chondrite</i>			
A94-mat	2.365(98)	4390(175)	5.342(81)
A94-ch1	3.499(680)	6075(1046)	5.910(1.056)

Uncertainties (1 s. d.) are given in parenthesis. Abundances of  $^3\text{He}$  and  $^4\text{He}$  in units of  $10^8$  cc/g. In most cases  $^3\text{He}$  is given as it was measured; only in a few cases  $^3\text{He}$  was calculated from  $^4\text{He}$  and  $^3\text{He}/^4\text{He}$  because of the smaller error. <sup>a</sup>Includes significant amounts of trapped solar wind  $^3\text{He}$ .

**Appendix 5: Concentrations of  $^{40}\text{Ar}$ ,  $^{36}\text{Ar}_{\text{tr}}$ ,  $^{38}\text{Ar}_{\text{c}}$ ,  $^{38}\text{Ar}/^{36}\text{Ar}$  and  $^{40}\text{Ar}/^{36}\text{Ar}$  of all matrix (mat) and chondrule (ch) samples.**

	$^{40}\text{Ar}$	$^{36}\text{Ar}$	$^{38}\text{Ar}/^{36}\text{Ar}$	$^{40}\text{Ar}/^{36}\text{Ar}$	$^{38}\text{Ar}_{\text{c}}$	$^{36}\text{Ar}_{\text{tr}}$
<i>CR2 chondrites</i>						
Re-mat	546.9(9.5)	18.78(40)	0.190(2)	29.12(80)	<sup>a</sup>	18.78(40)
Re-ch1	<sup>a</sup>	39.91(2.53)	0.186(4)	<sup>a</sup>	<sup>a</sup>	39.91(2.53)
Re-ch2	771.1(69.8)	18.36(1.77)	0.197(4)	42.00(5.56)	0.173(84)	18.36(1.77)
El-mat	334.6(14.9)	375.2(13.7)	0.189(1)	0.894(51)	<sup>a</sup>	375.2(13.7)
El-ch2	103.4(24.0)	34.19(1.99)	0.192(2)	3.025(723)	<sup>a</sup>	34.19(1.99)
El-ch3	180.7(7.0)	18.96(1.11)	0.194(2)	9.532(668)	0.117(60)	18.96(1.11)
El-ch5	150.1(11.0)	8.569(140)	0.206(3)	17.52(1.32)	0.171(32)	8.569(140)
El-ch6	3795(208)	14.87(1.15)	0.196(3)	255.2(24.2)	0.135(56)	14.87(1.15)
El-ch7	174.5(17.5)	32.61(2.05)	0.191(2)	5.349(634)	<sup>a</sup>	32.61(2.05)
El-ch8	179.3(14.4)	30.86(51)	0.198(2)	5.808(478)	0.352(101)	30.86(51)
El-ch9	1120(17)	31.05(45)	0.193(2)	36.06(751)	<sup>a</sup>	31.05(45)
El-ch10	103.1(15.0)	10.83(23)	0.198(4)	9.522(1.405)	0.117(50)	10.83(23)
El-ch11a	2501(84)	13.27(38)	0.197(4)	188.5(8.3)	0.136(61)	13.27(38)
NWA-mat	58859(1996)	165.4(4.9)	0.191(2)	355.9(16.1)	<sup>a</sup>	165.4(4.9)
NWA-ch1	87.29(8.13)	13.49(39)	0.241(4)	6.470(631)	0.833(71)	13.49(39)
NWA-ch2	305.0(9.6)	46.74(1.35)	0.204(2)	6.525(279)	0.828(161)	46.74(1.35)
<i>CR3 chondrites</i>						
MET-mat	2251(129)	197.9(10.2)	0.189(2)	11.37(88)	<sup>a</sup>	197.9(10.2)
MET-ch1	21.16(32.47)	2.209(110)	0.388(9)	9.582(14.706)	0.588(31)	2.209(110)
MET-ch2	281(22)	83.37(1.98)	0.191(2)	3.373(278)	<sup>a</sup>	83.37(1.98)
MET-ch3	157.9(7.4)	61.59(1.37)	0.191(2)	2.564(134)	<sup>a</sup>	61.59(1.37)
MET-ch4	438.3(25.7)	158.7(8.0)	0.189(2)	2.761(214)	<sup>a</sup>	158.7(8.0)
MET-ch5	191.1(15.2)	99.56(5.04)	0.189(2)	1.919(181)	<sup>a</sup>	99.56(5.04)
MET-ch6	833.4(47.0)	144.0(7.3)	0.191(2)	5.789(439)	<sup>a</sup>	144.0(7.3)
QUE-mat	459.0(22.6)	184.4(9.3)	0.188(2)	2.489(175)	<sup>a</sup>	184.4(9.3)
QUE-ch1	161.9(35.0)	85.46(2.25)	0.190(2)	1.895(413)	<sup>a</sup>	85.46(2.25)
QUE-ch2	4428(108)	10.08(27)	0.200(4)	439.2(16.0)	0.130(49)	10.08(27)
QUE-ch3	2520(53)	24.72(61)	0.193(2)	102.0(3.3)	<sup>a</sup>	24.72(61)
QUE-ch4	1306(80)	30.77(1.69)	0.191(2)	42.45(3.50)	<sup>a</sup>	30.77(1.69)
QUE-ch5	207.4(20.1)	167.0(8.5)	0.189(2)	1.241(136)	<sup>a</sup>	167.0(8.5)
QUE-ch6	825.5(46.5)	61.48(3.11)	0.192(2)	13.43(1.02)	0.217(199)	61.48(3.11)
<i>CV3 chondrites</i>						
Al-mat	2062(112)	18.38(65)	0.207(2)	112.2(7.3)	0.384(56)	18.38(65)
Al-ch3	187.7(6.4)	1.478(34)	0.297(5)	127.0(5.2)	0.220(11)	1.478(34)
Al-ch6	3148(81)	1.198(50)	0.363(10)	2628(129)	0.274(17)	1.198(50)
Vi-mat1	198.4(7.0)	95.65(48)	0.189(2)	2.074(74)	<sup>a</sup>	95.65(48)
Vi-mat2	32.07(3.27)	0.860(20)	0.184(2)	37.30(3.90)	<sup>a</sup>	0.860(20)
Vi-ch1	423.9(128.8)	0.163(77)	0.309(20)	2599(1464)	0.163(77)	1.63(77)
Vi-ch2	1188(167)	613.5(78.4)	0.189(2)	1.936(367)	<sup>a</sup>	613.5(78.4)
Vi-ch3	348.7(108.8)	30.78(1.85)	0.193(2)	11.33(3.61)	0.151(103)	30.78(1.85)
A82-mat	89.79(1.77)	9.227(205)	0.194(2)	9.732(290)	0.061(30)	9.227(205)
A82-ch1	507.7(69.4)	1.083(154)	0.254(7)	468.9(92.4)	0.085(13)	1.083(154)
A82-ch2	369.3(13.8)	0.480(28)	0.318(8)	769.0(53.0)	0.078(4)	0.480(28)
A82-ch3	237.1(7.4)	4.964(99)	0.197(3)	47.75(1.77)	0.048(21)	4.964(99)
<i>Ungrouped 3 chondrite</i>						
A94-mat	379.0(8.0)	545.8(12.35)	0.188(2)	0.694(21)	<sup>a</sup>	545.8(12.35)
A94-ch1	457.4(49.1)	706.6(35.92)	0.188(2)	0.647(77)	<sup>a</sup>	706.6(35.92)

Uncertainties (1 s. d.) are given in parenthesis. Abundances of  $^{40}\text{Ar}_{\text{tr}}$ ,  $^{38}\text{Ar}_{\text{c}}$  and  $^{36}\text{Ar}_{\text{tr}}$  in units of  $10^8$  cc/g.  $P_{38}$  and  $T_{38}$  are given in  $10^8$  cc/(g Ma) and Ma, respectively. <sup>a</sup>Large uncertainties because of large dominant trapped component.



## Danksagung

An dieser Stelle möchte ich mich bei allen bedanken, die mich während meiner Dissertationszeit arbeitstechnisch und moralisch unterstützt haben:

Zuerst möchte ich mich bei *Prof. Dr. Mario Trieloff* für die Vergabe des Projektes sowie die stete und verlässliche Betreuung bedanken.

Mein besonderer Dank gilt *PD Dr. habil. Ulrich Ott*. Er führte mich an die Themen extraterrestrische Materie und Edelgase heran, lässt mir jedoch genug Freiheit, um eigene Ideen zu verfolgen. Mit viel Geduld und einfachen Worten kann er komplizierte Sachverhalte erklären. Seine Ideen halfen mir stets weiter.

*Dr. Julia Cartwright* danke ich für die fachliche und moralische Unterstützung. Sie zeigte mir, wie Proben vorbereitet und Edelgasmessungen durchgeführt werden. Außerdem gab sie mir zahlreiche Denkanstöße, die meine Sichtweise auf das Thema erweiterten und mir auch bei Vorträgen halfen.

*Siegfried Herrmann* möchte ich für das Erlernen der Edelgasmessungen und die Hilfe bei der Auswertung der Messergebnisse danken. Ohne sein Engagement und seinen Einfallsreichtum wäre der Messbetrieb in einem Edelgaslabor nicht so reibungslos abgelaufen. *Christa Sudek* danke ich für die Durchführung einiger Arbeit zur Probenaufbereitung. Zudem gilt mein Dank den anderen ehemaligen Kollegen der Arbeitsgruppe Kosmochemie am Max-Planck-Institut für Chemie in Mainz wie etwa *Bastian Baecker* und *Dr. Reinhard Haubold*.

Ganz herzlich möchte ich mich bei *Massimo Guglielmino* für die Durchführung und Hilfe bei der Auswertung der SEM-Analysen bedanken. Ihm habe ich es zu verdanken, dass die Mineralogie für mich kein "Buch mit sieben Siegeln" ist.

Ebenso bedanken möchte ich mich außerdem bei *Dr. Jan Leitner* für die Hinweise zur Chondrenseparation, *Maik Biegler* für die Präparation der Proben, *Dr. John Bennett* und *Dr. Attila Stopic* für die Durchführung der INAA sowie *Julia Weinauer* für die Bereitstellung der Fotos von einigen Chondren.

Der *Deutschen Forschungsgemeinschaft* möchte ich für die finanzielle Förderung danken. Diese Arbeit wurde im Rahmen des Schwerpunktprogrammes "The first 10 Million Years of the Solar System – a Planetary Materials Approach" angefertigt.

Nicht zuletzt möchte ich meiner Familie und meinen Freunden für ihre Unterstützung danken. Ohne sie wäre diese nicht gelungen.



**Eidesstattliche Versicherung gemäß § 8 der Promotionsordnung  
der Naturwissenschaftlich-Mathematischen Gesamtfakultät  
der Universität Heidelberg**

1. Bei der eingereichten Dissertation zu dem Thema

Pre-irradiation of chondrules in the Early Solar System

---

---

---

handelt es sich um meine eigenständig erbrachte Leistung.

2. Ich habe nur die angegebenen Quellen und Hilfsmittel benutzt und mich keiner unzulässigen Hilfe Dritter bedient. Insbesondere habe ich wörtlich oder sinngemäß aus anderen Werken übernommene Inhalte als solche kenntlich gemacht.

3. Die Arbeit oder Teile davon habe ich ~~wie folgt~~ bislang nicht<sup>1)</sup> an einer Hochschule des In- oder Auslands als Bestandteil einer Prüfungs- oder Qualifikationsleistung vorgelegt.

Titel der Arbeit: \_\_\_\_\_

---

Hochschule und Jahr: \_\_\_\_\_

Art der Prüfungs- oder Qualifikationsleistung: \_\_\_\_\_

4. Die Richtigkeit der vorstehenden Erklärungen bestätige ich.

5. Die Bedeutung der eidesstattlichen Versicherung und die strafrechtlichen Folgen einer unrichtigen oder unvollständigen eidesstattlichen Versicherung sind mir bekannt.

Ich versichere an Eides statt, dass ich nach bestem Wissen die reine Wahrheit erklärt und nichts verschwiegen habe.

Heidelberg, 8.05.2014  
Ort und Datum

Ma. Spendorf-Kreis  
Unterschrift

<sup>1)</sup> Nicht Zutreffendes streichen. Bei Bejahung sind anzugeben: der Titel der andernorts vorgelegten Arbeit, die Hochschule, das Jahr der Vorlage und die Art der Prüfungs- oder Qualifikationsleistung.